SQUARAINE DYES FOR NON-LINEAR OPTICS AND ORGANIC ELECTRONICS

A Dissertation
Presented to
The Academic Faculty

By

Yanrong Shi

In Partial Fulfillment
Of the Requirements for the Degree
Doctor of Philosophy in the School of
Chemistry and Biochemistry

Georgia Institute of Technology

August 2011

SQUARAINE DYES FOR NON-LINEAR OPTICS AND ORGANIC ELECTRONICS

Approved By:

Dr. Seth R. Marder, Advisor
School of Chemistry and Biochemistry
Georgia Institute of Technology

Dr. Jean-Luc Brédas
School of Chemistry and Biochemistry
Georgia Institute of Technology

Dr. Laren Tolbert
School of Chemistry and Biochemistry
Georgia Institute of Technology

Dr. Joseph W. Perry
School of Chemistry and Biochemistry
Georgia Institute of Technology

Dr. Elsa Reichmanis
School of Chemical and Biomolecular Engineering
Georgia Institute of Technology

Date Approved: May 2, 2011

致我敬爱的父母和亲爱的黄春
To my Parents and Chun

ACKNOWLEDGEMENTS

I still remember, as an undergraduate student of nobody, it was Seth's prompt reply to my email, from which I saw his trust, faith, and confidence in me as he is in the later days, made me finally decide to come to Georgia Tech. Look back to the five years, Professor Marder is always being supportive and understanding as my research advisor. I would like to express my sincerest appreciation to Seth, for his guidance, encouragement on me. What I have learned from Seth in these years is not only about performing chemistry experiments, thinking critically and logically, but also for surviving in the unfamiliar environment as a foreigner and refining my personality. No matter where I will be and what type of job I will take in the future, Seth's impact on me will never gone and will guide me to go further. I would also like to thank all of my committee members for providing their valuable suggestions to this thesis.

I appreciate the help from Dr. Stephen Barlow and Dr. Mariacristina Rumi for their mentorship these years. For every step towards Ph.D, they support me with the insightful suggestions in chemical physics for my presentation and qualification. Besides research advices, Seth, Steve and Cristina set good examples for my English and teach me how to tell a story of my ideas and research. I would like to give my especial thanks to Steve who spent a tremendous amount of time proofreading my thesis. I am also grateful to the time and effort provided by Cristina and Mr. Anthony Giordano in proofreading and editing parts of this thesis.

Without collaboration from several other research groups, this thesis would not been accomplished. I appreciate Dr. Joseph Perry and his group members, including Dr. Joel Hales, Dr. Jochen, Campo, Dr. Sarah Chi, Dr. Matthew Sartin, and Mr. Anselmo

Kim for their efforts on the nonlinear optical characterization and the helpful discussions. I am thankful to Dr. Michael Grätzel and his group members, Ms. Rebecca (Mitchell) Hill, Dr. Yum Jun Ho, Dualeh Amalie, and Dr. Mdkhaja K. Nazeeruddin at École Polytechnique Fédérale de Lausanne in Switzerland for dye-sensitized solar cell device fabrications. I would like to thank Dr. Bernard Kippelen and his group members, Dr. Yinhua Zhou, Dr. William Postcavage *Jr*. and Dr. Shree Tiwari for solar cell and transistor test. Last but not least, I thank Dr. Eric Van Stryland and Dr. David Hagan and the group members such as Dr. Scott Webster, Dr. Lazaro Padilha, Mr. Davorin Peceli and Mr. Honghua Hu at University of Central Florida for their contribution in studying the metal complexes.

I would like to show my appreciation for the friendly research environment provided by the Marder family including the previous and current members. Especially, I thank Dr. Samy Elangovan who guided me to start my lab work and trained me to form the good habit. I thank Dr. Benjamin Wunsch and Mr. Anthony Giordano for some AFM analysis, Dr. Chun Huang for TGA, DSC and some GPC measurements, Dr. Yadong Zhang, Dr. Jonathan Matichak, Dr. Hsin-Chieh Lin and Dr. Nam Nantalaksakul for providing some starting materials. I also want to thank Ms. Marsha D. Lamb, Ms. Carmen Rivera, and Miss Veronique Brédas; they make my life in the Marder group much easier.

One of the biggest wealth I gained in Atlanta is the friendship with Feifei Zhang, whom I also see as a little sister from the first day of her arrival. We spent a lot of unforgettable time together and can always tell each other's mind. My old friends and

friends forever, including Chong He, Kuang He, Xiaomu Guan, Yaling, Zhu, Ping He, Xin Chen and many others are always there whenever I need a hug.

I would like to give my deepest appreciation to my parents for not only giving life to me, but also raise me up with their warmest hearts loving me and softest hands protecting me. I would like to give this thesis as a gift to my greatest mother in the world, for every wrinkle on her face and every white hair on her head. At the end, I have nothing to say but thank you to the man, Chun, who taught me hand-by-hand to set-up the first reaction at Georgia Tech, who cooks the most delicious food, who is always there when I need a shoulder to cry, who locks my heart with the ring and makes me the happiest woman in the world.

TABLE OF CONTENTS

Chapter 3. Synthesis, Photophysical and Electronic Properties of Squaraine Dimers and Oligomers

Chapter 4. Synthesis, Photophysical and Organic Photovoltaic Properties of Phthalocyanine- and Squaraine-based Platinum and Gold Complexes

LIST OF TABLES

LIST OF FIGURES

LIST OF SCHEMES

LIST OF ABBREVIATIONS

1PA	One-Photon Absorption
2PA	Two-Photon Absorption
AFM	Atomic Force Microscopy
C_p	Cyclopentadienyl, C_5H_5
DMF	Dimethylformamide
DPP	Double Pump-probe
DSC	Differential Scanning Calorimetry
DSSC	Dye-sensitized Solar Cell
EA	Electron Affinity
GPC	Gel Permeation Chromatography
HOMO	Highest Occupied Molecular Orbital
HRMS	High Resolution Mass Spectrometry
IC	Internal Conversion
ISC	Intersystem Crossing
IP	Ionization Potential
IPCE	Incident Photon-to-current Conversion Efficiency
LUMO	Lowest Unoccupied Molecular Orbital
M_n	Number-average molecular weight
M_w	Weight-average molecular weight
MPc	Metallophthalocyanine
NIR	Near Infrared
NLO	Nonlinear Optical
NMR	Nuclear Magnetic Resonance
OD	Optical Density
OPL	Optical-power Limiting
Pc	Phthalocyanine
PCBM	Phenyl-C61-butyric acid methyl ester
PCE	Power Conversion Efficiency
PEDOT:PSS	Poly(3,4-ethylenedioxythiophene):poly(styrenesulfonate)
PPh_3	Triphenylphosphine
TGA	Thermogravimetric Analysis
THF	Tetrahydrofuran
TLC	Thin-layer Chromatography
TPIF	Two-photon induced fluorescence
UV-Vis	Ultraviolet-Visible

Other abbreviations and symbols are explained in the text.

SUMMARY

This dissertation describes the investigation of the synthesis and characterization of new squaraine-based photonic and electronic materials. In the first part of this thesis, squaraine dyes with large conjugation systems, including extended squaraines consisting of bis(donor)substituted vinylene-heterocycles and bis(indolinylenemethyl)squaraine-based oligomers linking through different π-bridges were designed, synthesized and characterized to achieve strong two-photon absorption (2PA) for optical-power limiting applications in the near-infrared (NIR). It was found that using strong π-donating amine donor and alternate vinylene and heterocycle bridges, the extended squaraine exhibited strong 2PA band in the NIR region and in some cases the 2PA bands cover a broad spectrum window. Utilizing some of these dyes, strong optical suppressions for nanosecond and femtosecond laser pulses at selected wavelengths were obtained. It is worth noting that one of the dendronized squaraine forms smooth and high optical quality films with large NIR transparency which makes it promising candidate for practical OPL and other 2PA-induced applications. The oligomers approach achieved materials with large 2PA cross-sections at the wavelength close to one-photon resonance. Use these oligomers as light harvesting donors in organic solar cells revealed enhanced photovoltaic performance with larger oligomers. In the second part of this thesis, a series of squaraine- and phthalocyanine-acetylide ligands were coordinated to platinum and gold, and the photophysical properties of these complexes were studied. Despite of the presence of heavy atom(s), these dyes did not exhibit impressive triplet quantum yields but with surprisingly high fluorescence quantum yields observed in the monomeric

squaraine-platinum and gold complexes. The low triplet quantum and unchanged redox potentials in comparison to the ligand of these dyes indicate possible poor electronic coupling between the metal d-orbital and the ligand π-system. However, using these compounds in organic solar cells showed significant enhancement compared with their metal-free counterparts. In Chapter 5, an effective approach on optimizing bis(indolinylenemethyl)-based squaraine sensitizers with various surface anchor groups and π-linkers, achieved high power conversion efficiencies (PCEs) of 6.7% in liquid dye-sensitized solar cells (DSSCs) and 2.7% in solid-state DSSCs, which stand out all the previous reported squaraine-based sensitizers, as does the very broad range over wavelengths over which high incident-photon-to-current efficiencies (IPCEs) were obtained.

Chapter 1: Introduction to Squaraines

1.1 General introduction to squaraine dyes

Squarylium dyes (also often called squaraines) are a class of cyanine-like dyes with delocalized electronic structure that can be represented by several zwitterionic forms consisting of a conjugated scaffold linking two donor end groups to an electron-deficient central four-membered ring (Figure 1.1). The electronic distribution in cyanine π-system extended from one end to the other, however, squaraines are often characterized as donor-acceptor-donor (D-A-D) structures.[1,2] Another significant difference between squaraines and many cyanines is that typical cyanine chromophores are charged whereas squaraine dyes are typically neutral. The synthesis of squaraine dyes was reported as early as 1965.[3] These dyes are typically the condensation products of electron-rich aromatic or heterocyclic compounds,[4-6] such as *N,N*-dialkylanilines, benzothiazoles, phenols, azulenes and pyrroles, with squaric acid. The electronic structures of squaraines are quite analogous to cyanine dyes, which lead a characteristic narrow absorption band with a high molar extinction coefficient ($\varepsilon > 10^5\ M^{-1}cm^{-1}$) in the visible or near infrared (IR) region of the spectrum in solution. Squaraines are usually fluorescent with small Stokes shifts and can be highly photo-stable.[7-9] The absorption bands of squaraines are generally broadened in the solid state and there is significant quenching of the emission as a consequence of strong intermolecular charge-transfer interactions resulting in a

tendency to aggregate.[1,10] There is a wide structural diversity of squaraine dyes due to the choice of different donors and/or the possibility for both symmetrical and unsymmetrical architectures. Squaraines with tunable optical and electronic properties have been extensively studied for various applications including photodynamic therapy,[11,12] second-order nonlinear optics,[10,13] biological labeling,[14] optical imaging,[15] ion sensing,[16,17] photovoltaics,[18-21] and light-emitting field-effect transistors.[22,23] Furthermore, it has been shown that some squaraines can behave as highly efficient two-photon absorption (2PA) dyes.[24,25]

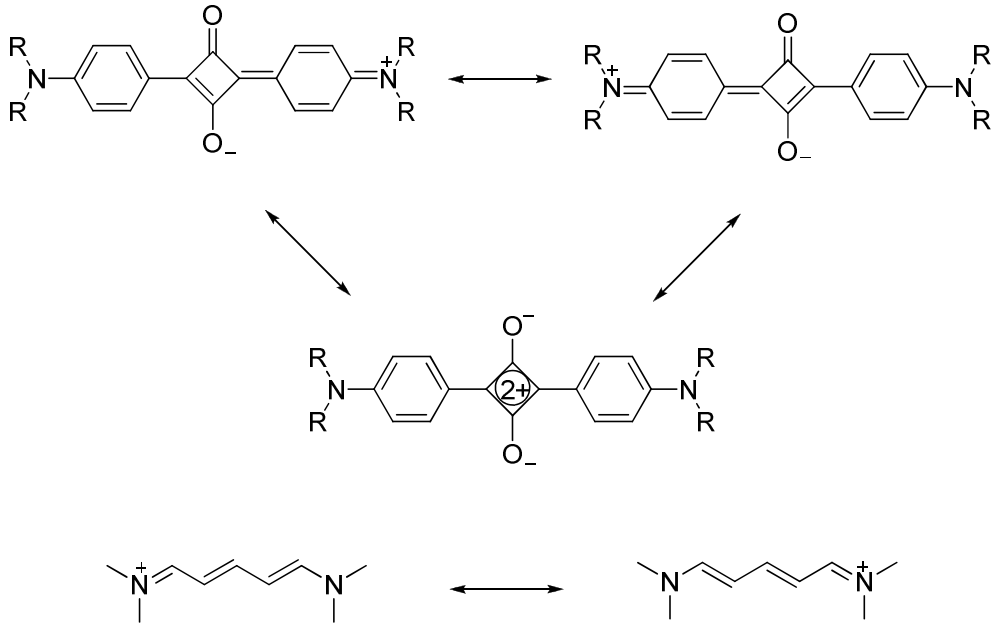

Figure 1.1: Representative resonance structures for squaraines and cyanines.

1.2 Synthesis of squaraines

1.2.1 Early stage synthesis of squaric acid and its symmetrical derivatives

3,4-Dihydroxycyclobut-3-ene-1,2-dione, often called squaric acid, was first synthesized by Cohen and coworkers in 1959.[26] The original synthesis started from 1-chloro-1,2,2-trifluoroethylene, which dimerized to perfluorocyclobutene on dechlorination with zinc. This compound was converted to 1,2-diethoxy-3,3,4,4-tetrafluoro-1-cyclobutene with ethanol and then finally hydrolyzed with strong acid to give squaric acid. Squaric acid is a colorless, crystalline compound having a decomposition temperature about 293 °C. Its high acidity (p$K_a \approx 1$ for the first proton and a p$K_a = 2.2$ for the second), is attributable to resonance stabilization of the anion.[27,28]

The condensation between squaric acid and active α-unsubstituted pyrroles in ethanol with catalytic amounts of perchloric acid gave the red-violet dye **1** in 65% yield. In cases where both the 2 and 5 positions of the pyrrole ring are unoccupied, mixtures of readily variable blue to blue-green insoluble dyes were obtained, which were assumed to be polymeric structures. In acetic acid, the reaction between squaric acid and 1,3,5-trihydroxybenzene gave compound **2** with 67% yield. These were the first squaraines in literature that were reported by Treib and Jakob.[3]

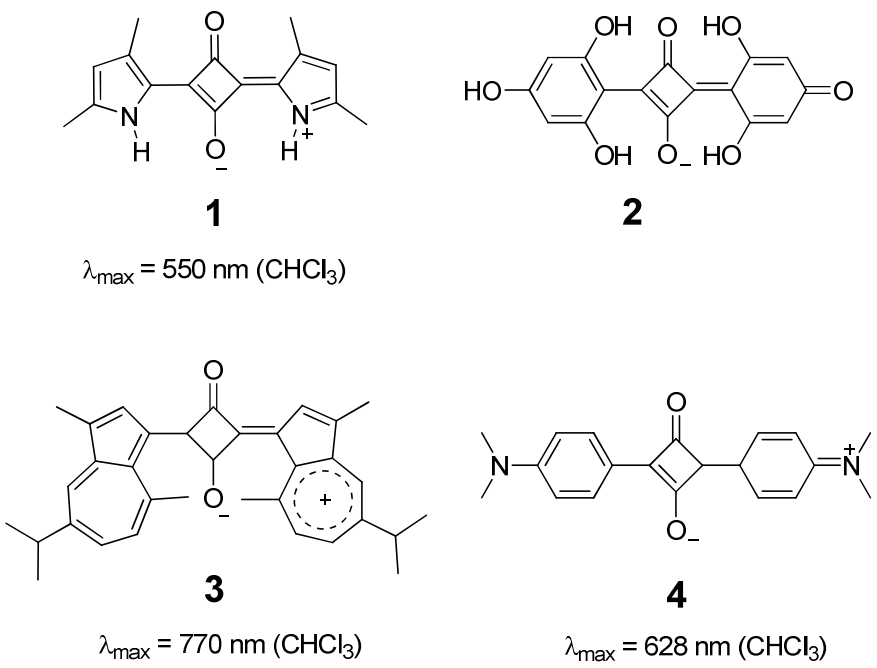

Figure 1.2: Chemical structures of the early squaraines.[3,29,30]

Immediately following the first report of the aforementioned squaraines, Ziegenbein and Sprenger readily obtained the condensation products of squaric acid with azulene[29] (**3**) and dialkylaniline[30] (**4**) in a refluxing butanol/benzene mixture, to azeotropically distill water formed in reaction, thereby enable them to drive the condensation to completion. The compounds are a deep blue to green color for **3** and green in the case of **4**. Since then, mixtures of butanol (or isopropanol) and benzene (or toluene) have been widely employed in squaraine synthesis. The mechanism for condensation reactions were proposed by Sprenger and Ziegenbein in their later reviews[31] (as shown in Scheme 1.1). The condensation involves preliminary activation of the squaric acid by the formation of monobutyl squarate followed by nucleophilic attack of the aromatic compound (Ar-H) at the carbon where butoxy group resides. The monoaryl

squaric acid is then presumably obtained as an intermediate by removal of the alcohol. Another aromatic compound subsequently attacks the electron deficient carbonyl carbon; subsequent dehydration forms the squaraine dye.

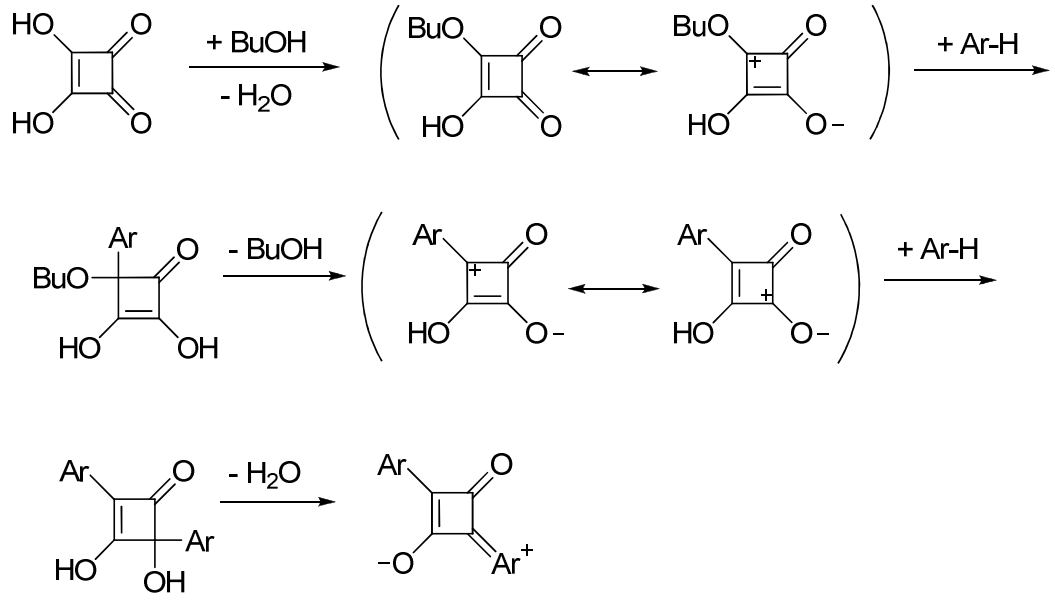

Scheme 1.1: Proposed reaction mechanism for squaraine formation.[31]

The synthesis for another major type of symmetrical squaraines involves the condensation between 2 molar equivalents of nucleophilic heterocyclic compounds with active methyl groups such as 2-methyl-substituted quinolinium, benzothiazolium, and benzoselenazolium iodide, which can transformed to enamine structures under basic conditions. First reported by Sprenger and Ziegenbein,[32] squaraines of this class were obtained in butanol and benzene mixtures with a small amount of quinoline to neutralize the HI formed and to convert the quaternary heterocyclic salts to the corresponding enamine form. When reacted with more electron rich 2-methylindolium substrates, the reaction went to completion in high yields without the addition of base. Those squaraines

are generally stable, high-melting compounds with a metallic sheen, which give intensely colored solutions and dissolve with difficulty in alcohols or ether but more readily in dichloromethane, benzonitrile, or dimethylformamide (DMF). The absorption maxima and isolated yields for some example dyes (**5**-**7**) are listed in Table 1.1.

It is worth noting that if dialkyl squarate was employed, instead of squaric acid, only 3,4-disubstituted 1,2-dioxocyclobut-3-enes were obtained (Scheme 1.2). These 1,2-substituted dyes adopt merocyanine-like structures, which are as not strongly colored as 1,3-substituted counterpart and exhibit blue-shifted absorption spectra, because the intramolecular cross-conjugation from the aromatic (or heterocyclic) moieties to the central cyclobutenedione disturbs extensive π-electron resonance over the whole molecule. It should be noted that these types of compounds are sometimes obtained as byproducts in squaraine synthesis, probably due to the esterification of squaric acid by butanol as might be expected from the proposed mechanism. When addition of the second equivalent of electron-rich component to the semisquaraine occurs, it is not completely regio-selective and a certain amount of the 1,2-condensation product can be formed. Due to their more twisted conformation, those 1,2-condensed compounds are generally much more soluble in organic solvents than their 1,3-analogues. The 1,3-substituted products are usually isolated simply by filtration from the cooled reaction mixture. These two compounds are also differentiable by thin-layer chromatography (TLC).

Table 1.1: 1,3-substituted symmetrical and unsymmetrical squaraines 5 to 10

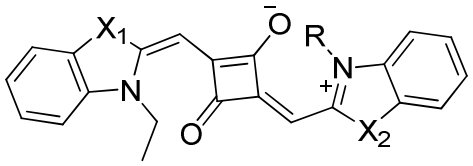

Compound	X, R	λ_{max} (log ε)	Yield(%)
5[24]	$X_1 = X_2 = C(CH_3)_2$, R = Et	635 ($CHCl_3$) (5.47)	83
6[32]	$X_1 = X_2$ = S, R = Et	670 ($CHCl_3$)	80
7[32]	$X_1 = X_2$ = Se, R = Et	678 (DMF)	42
8[33]	X_1 = S, $X_2 = C(CH_3)_2$, R = Me	649 ($CHCl_3$) (5.20)	77
9[33]	X_1 = Se, $X_2 = C(CH_3)_2$, R = Me	657 ($CHCl_3$) (5.03)	88
10[33]	X_1 = S, X_2 = Se, R = Et	677 ($CHCl_3$) (5.03)	36

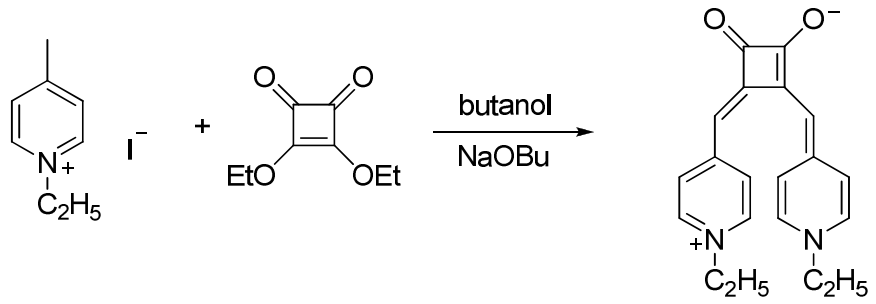

Scheme 1.2: Example of 1,2-substititued squaraine.[32]

It also should be noted that a more pronounced electron-rich nature for the activated aromatic or heterocyclic compounds generally result in forming the corresponding squaraines in relatively higher yields. The condensation between squaric acid and 2,4-dimethylpyrrole, which is a particularly active reagent, can be conducted in refluxing ethanol,[3] while no reaction occurs at all with thiophene, unless substituted with

strong electron donating groups.[34]

1.2.2. Synthesis of unsymmetrical squaraines

Synthesis of squaraines with unsymmetrical structures can provide structural variability leading to tunable electronic and physicochemical properties which could extend applicability of these dyes in many fields. According to the proposed mechanism for squaraine formation, one rational strategy to prepare unsymmetrical derivatives is to isolate the semisquaraine intermediate from the reaction of squaric acid with an aromatic or heterocyclic component, and subsequently performing the condensation with a different activated reactant. However, chromatographic purification can often be inefficient and tedious if semisquaraine is formed in the presence of a large excess of squaric acid.

Law and coworkers developed a method for the synthesis of semisquaraine without employing squaric acid.[35] Here, the four-membered ring could be accessed through [2 + 2] cycloaddition reaction between (*p*-methoxyphenyl)acetyl chloride and freshly prepared tetraethoxyethylene in the presence of triethylamine followed by treatment with basic alumina and subsequent acid hydrolysis (reaction for compound **11**). This method has not been widely used after the advent of readily available commercial sources of high quality squaric acid.

Green and Neuse first reported the Friedel-Crafts type reaction, in the presence of

$AlCl_3$, in benzene with 3,4-dichlorocyclobut-3-ene-1,2-dione, which was available from the chlorination of squaric acid with thionyl chloride.[36] Later, it was found that condensation reactions using electron-rich aromatic and heterocyclic compounds (reactions for compounds **12**, **13**, **14**) could be conducted under mild conditions without $AlCl_3$ (in CH_2Cl_2, at rt).[37] A similar preparation of semisquarates from strong electron-rich heterocycles such as 1,2-dimethylpyrrole, 1,2,3,3-tetramethylindolium, benzothiazolium and benzoselenazolium salt, with 3,4-diethoxycyclobut-3-ene-1,2-dione proved to be successful in obtaining the corresponding semisquarates (reactions for compounds **15**, **16**, **17**).[33] Hydrolysis of both the semichloride and semisquarate under basic or acidic conditions conveniently afforded the corresponding semisquaraines. A selection of semisquaraine syntheses is shown in Scheme 1.3.

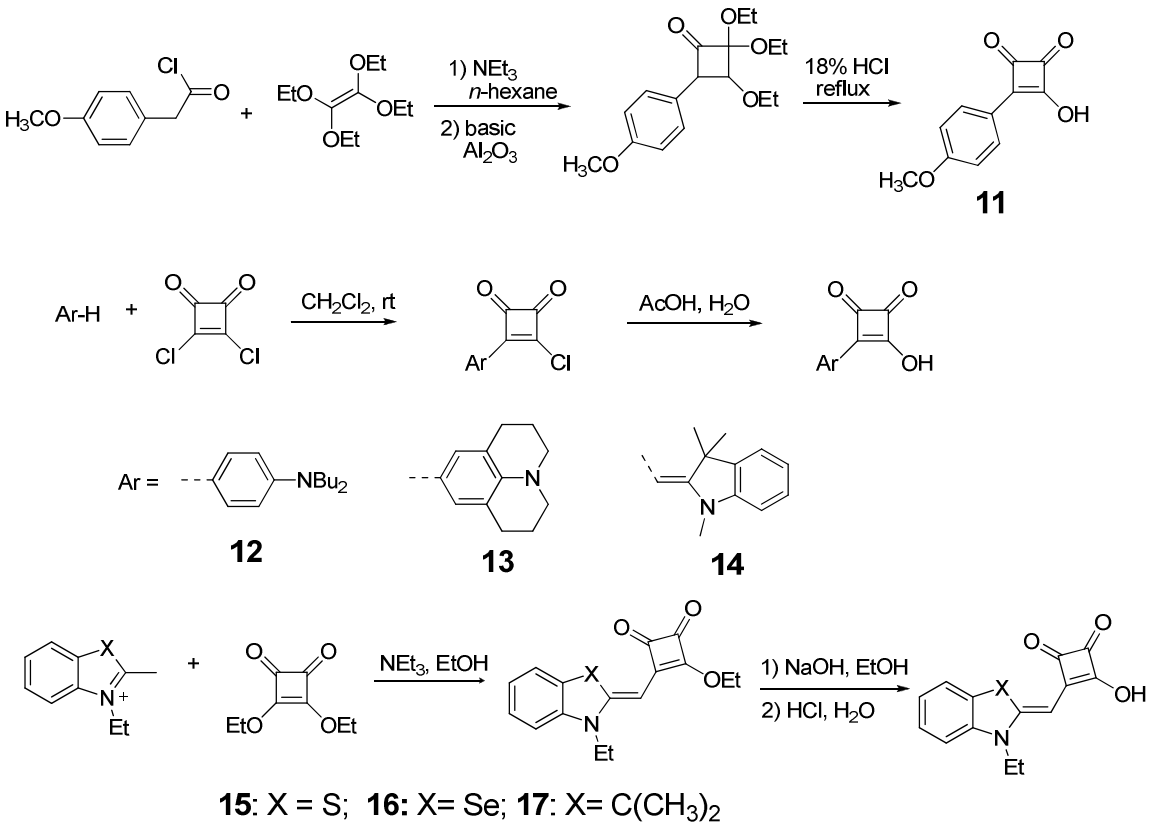

Scheme 1.3: Examples of semisquaraine synthesis. [35,37,33]

A semisquaraine condensing with the second equivalent of an electron-rich compound can be done under two general conditions. For arene derivatives, as reported by Law,[35] use of 2-propanol containing a small amount of tributyl orthoformate gave better yields and reduced the side reactions of forming undesired polymers, while in the case of active heterocycles, unsymmetrical squaraines could be achieved by refluxing the mixture in either butanol/toluene or isopropanol/benzene mixture with the addition of a base such as quinoline or imidazole (in some cases, base is not necessary), as shown in Scheme 1.4.

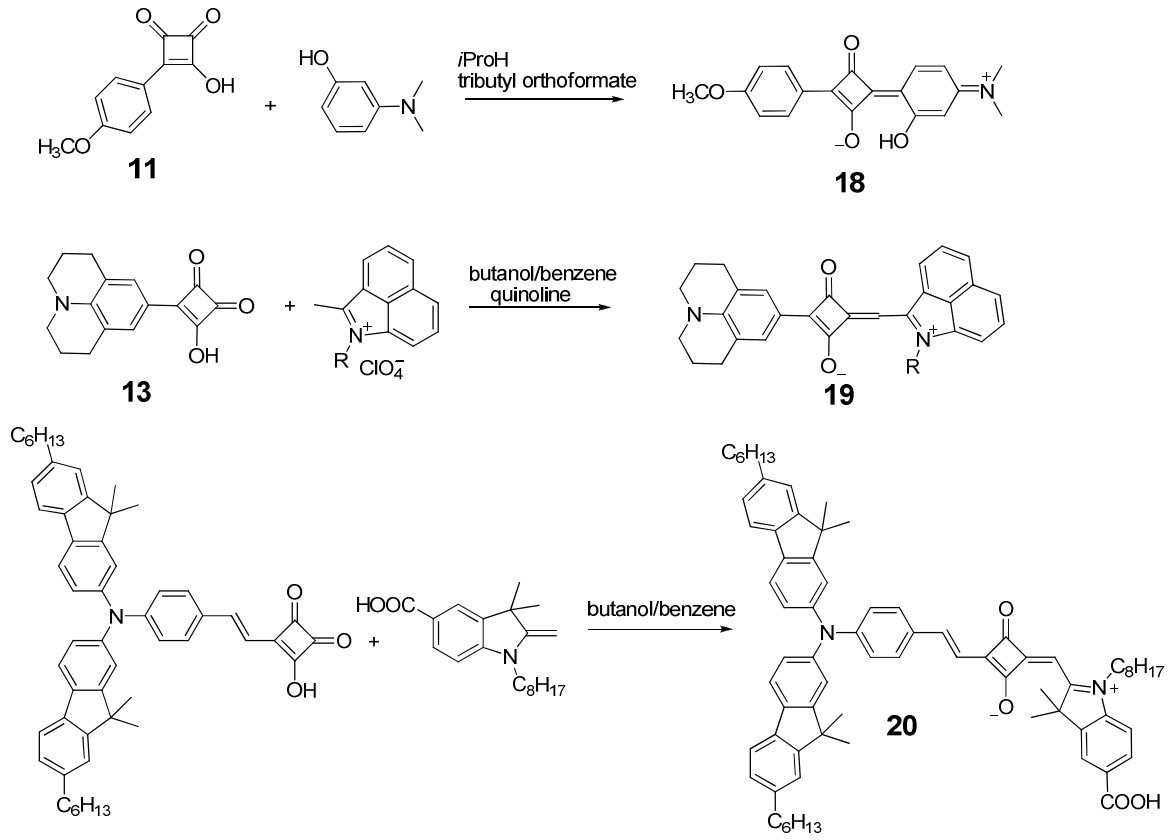

Scheme 1.4: Examples of unsymmetrical squaraine synthesis. [35,37,38]

The core-substituted squaraine derivatives, where the modification can be done at the semisquarate stage with methylene bases to give semisquaraine derivatives functionalized with an electron acceptor on the squaric core, have been well discussed by Beverina.[4] There are also several reviews available in literature on polysquaraines.[5,6,39]

1.3 Physicochemical properties and applications of squaraine dyes

1.3.1 Linear optical properties of squaraines

One of the characteristics of squaraine dye is its intense and sharp absorption peak in solution with molar extinction coefficients on the order of 10^5 $M^{-1}mol^{-1}$. The

absorption maxima vary from the visible to near-IR region depending on the chemical structures of the substituents. As summarized in Table 1.1, the heterocyclic base substituted squaraine show increasing red-shifted absorption from indolium to benzoselenazole derivatives[33] which correlates to the more π-donating nature in the order of Se > S > CR_2.

These symmetric squaraine derivatives could be general classified as donor-acceptor-donor (D-A-D) type molecules where charges are extensive delocalized along the squaraine backbone. In the early theoretical paper by Bigelow and Freund[40] on a NMe_2 substituted squaraine, it was claimed that charge transfer during the electronic transition between the ground state (S_0) and the first excited state (S_1) is mostly confined within the central C_4O_2 core and the amino group nitrogen donates very little charge. In most cases, the absorption maxima of symmetrical squaraines show bathochromic-shift if π-conjugation in the donor is extended or substituted with more electron-rich component.[41,42] However, the study of the structure-property relationships between conjugation length and optical gap on a series of donor-substituted bis(stilbenyl)squaraines found that similar to the observation on other stilbenoid like donor-acceptor systems, there was a dramatic red shift of around 300 nm first, which became blue shifted with longer conjugation. This is probably because of the less efficient electron coupling of the end-capping donating group with the electron withdrawing squarylium core.[43]

In organic solvents, squaraines often form solute-solvent complexes, the equilibrium constant of which is dependent on D-A-D charge-transfer character of the squaraines.[44] Owing to the significant intermolecular charge-transfer interactions and tendency to aggregate, squaraines exhibit an absorption that cover a broad range of the visible or near-IR spectrum in the solid state as a consequence (the absorption is often broader and red-shifted compared to that in solution), as shown in Figure 1.3.

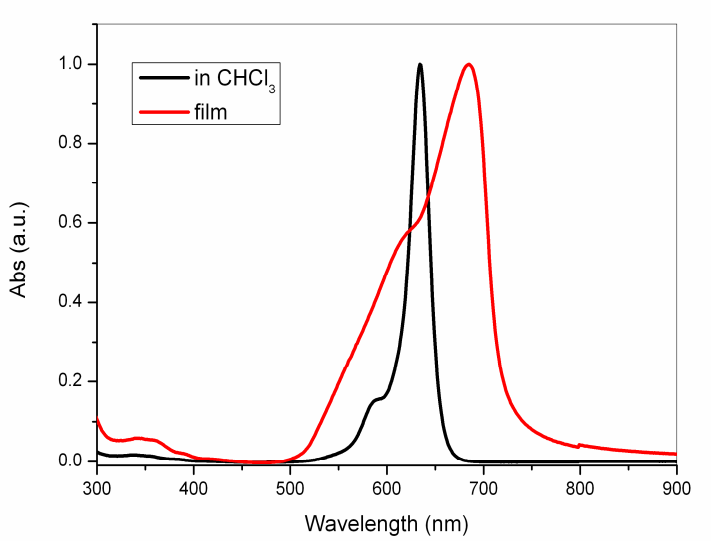

Figure 1.3: Absorption spectra of 5 in $CHCl_3$ solution and spin-coated film.

In general, the emission spectra of squaraines are mirror images of the absorption spectra with variable fluorescence quantum yields depending on the structure and the environment. The excitation spectra are generally similar to the absorption spectrum and are independent of the monitoring wavelengths.[45]

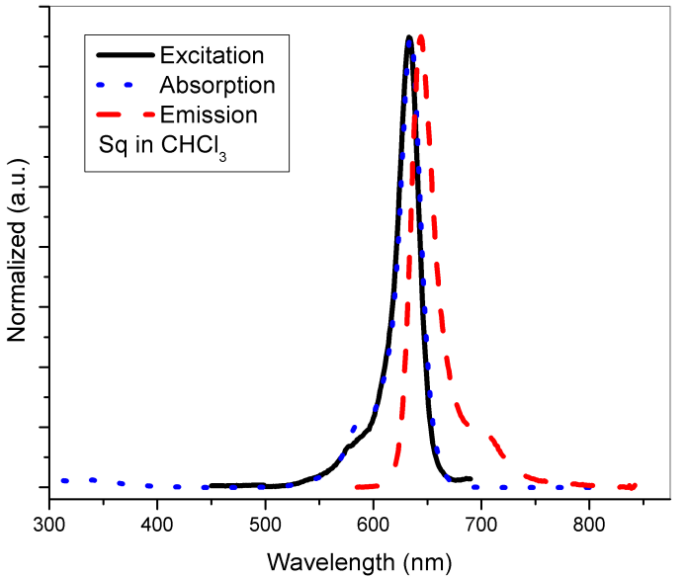

Figure 1.4: Absorption, excitation and emission spectra of 5 in $CHCl_3$.

1.3.2 Squaraines with large two-photon absorption (2PA) cross-sections

Two-photon absorption is defined as the electronic excitation of a molecule by simultaneous absorption of two photons of the same or different energy. The energy gap involved in a 2PA process is the sum of the energies of the two photons, thus, 2PA can often take place at much longer wavelength than the one-photon absorption. The phenomenon was first predicted by Göppert-Mayer[46] in 1931, who calculated the transition probability for a two quantum absorption process. With the development of lasers, this phenomenon was first demonstrated experimentally 30 years later in 1961.[47] Organic materials exhibiting large 2PA cross-sections (δ) are of interest for applications including photodynamic therapy, optical pulse suppression, two-photon fluorescence microscopy, 3D microfabrication, and 3D optical data storage, which have been reviewed

in depth in literature.[48-51]

For one-photon absorption, according to the Beer-Lambert law, the attenuation of a beam is given by Equation (1), where σ is one-photon absorption cross-section, N_{GS} is the number of molecules at ground state per unit volume, and I is the intensity of light. With the equivalent assumption, Equation (2) can be written for two-photon absorption, where one molecule interacts with two photons at a time and the absorption is proportional to the light intensity squared. δ is the 2PA cross-section, usually expressed in units of Göppert-Mayers (1 GM is 10^{-50} cm^4 s photon^{-1}). As moving away from the focus by distance of z, the intensity of a laser beam decreases proportional to z^2. Hence, the probability of 2PA excitation is proportional to z^{-4}, which gave 2PA induced process with high spatial resolution in three dimensions.

$$\frac{dN_{1PA}}{dt} = \sigma \times N \times I \qquad (1)$$

$$\frac{dN_{2PA}}{dt} = \frac{1}{2}\,\delta \times N \times I^2 \qquad (2)$$

For centrosymmetric molecules, as illustrated in Figure 1.5, the three "essential" states involved in degenerate 2PA process (two photons of the same energy) usually have alternating symmetry. Both the ground state (g) and the higher excited state (e') wave-functions are *gerade* (symmetric with respect to the center of inversion), whereas the lowest excited state (e) is *ungerade* (antisymmetric with respect to the center of inversion). According to the selection rule,[52,53] the electric-dipole-allowed transitions are different for 1PA and 2PA, where transitions from a state with inverted symmetry (g to e

and e to e') are allowed for 1PA. In the case of 2PA, the lowest accessible electronic state e' which has the same symmetry as the ground state g usually lies higher than the 1PA-allowed state e. The selection rule for noncentrosymmetric chromophores are not mutually exclusive, some of the excited states can be reached by either 1PA or 2PA. After excitation by 1PA or 2PA, a molecule typically undergoes internal conversion on the picosecond timescale to the lowest excited state and relaxes back to its ground state by radiative decay (ea. fluorescence) or non-radiative decay. In addition, energy transfer, electron transfer or other reactions may take place to release the energy.

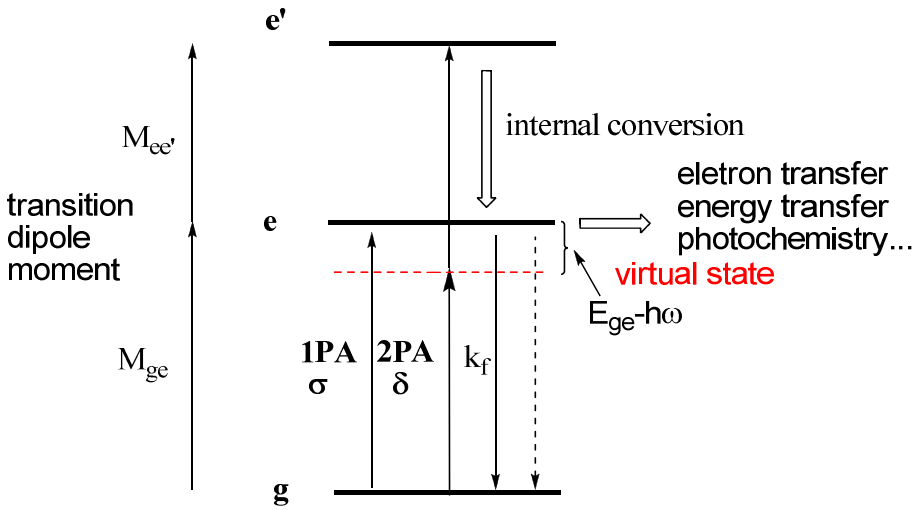

Figure 1.5: Jablonski diagrams illustrating the process of one-photon absorption (1PA) and two-photon absorption (2PA).

According to perturbation theory, restricting the sum-over-states equations,[54] to only include the three states described above for a quadrupolar molecule, the maximum 2PA cross-section can be expressed as follow[55,56]:

$$\delta_{max} = f(\omega, n)\frac{M_{ge}^2 M_{ee'}^2}{(E_{ge} - \hbar\omega)^2 \Gamma_{ge'}} \qquad (3)$$

where M_{ge} and $M_{ee'}$ are the transition dipole moment beweent the state g and e and between e and e', respectively. E_{ge} is the energy gap between state g and e, $\hbar\omega$ is the excitation photon energy at 2PA resonance. The term $E_{ge} - \hbar\omega$ is often called detuning energy. $\Gamma_{ge'}$ is an energy damping term for the transiton of g to e' and is related to the natural line width of transition. Compounds characterized with large values of M_{ge} and/or $M_{ee'}$ are expected to have large δ_{max}. One of the design strategies that has been employed to develop π-conjugated molecules with large δ is to use structure with D-A-D motifs where the incorporation terminal electron-rich groups have been shown to correlate with enhancements the transition moment $M_{ee'}$.[49,57,58] The apparent value of the 2PA cross-section δ strongly depends on the measurement techniques. The most commonly used techniques are two-photon induced fluorescence (TPIF) and *z*-scan.[50,51] By comparing one- and two-photon induced fluorescence excitation spectra to a reference compound with a known 2PA spectrum under identical conditions, 2PA spectra can be obtained from TPIF. For the *z*-scan technique, by moving the sample along the axis of laser beam, the intensity of light reaching the detector is changing as a function of sample position respect to the focus. The 2PA cross-section can be extracted from intensity-dependent transmission when the detector is at an open-aperture setup. For detailed description of the techniques, one can refer to a recent review by Rumi and Perry.[59]

Squaraines can be considered examples of D-A-D chromophores, which usually have small detuning energy that have been investigated for 2PA performance. Two

indolic squaraines **22a** and **22b** with short conjugation were reported by Pagani and Beverina[60] to exhibit 2PA in 700–800 nm spectra region with peak cross-section around 450 GM, measured by TPIF. Using these materials, significant optical-power suppressions were observed by measuring the non-linear transmittance in the region of 690 to 730 nm for nanosecond pulse.

Marder *et al*.[25] synthesized a series of π-extended bis(donor)-substituted squaraine chromophores exhibiting large 2PA cross-sections (δ_{max} as high as 33 000 GM, measure by fs *z*-scan) in the near-IR region with peak performances at photon wavelengths of ca. 1 μm. The conjugations in these molecules extend from the central squarylium acceptor to the donor terminal groups through vinylene and electron-rich heterocycles. For such large π-systems of these chromophores, even if one calculate δ_{max} *per* π*-electron* (ca. 300 GM for **24a**, **26**, **27**; ca. 600 GM for **23** and **25**), values obtained are among the highest reported for organic molecules to date. The high 2PA efficiency could be attributable to the combination of large transition dipole moment and small detuning energy. In many cases, at very small detuning energy, it is not possible to measure a 2PA process due to the overlap of 1PA onset. Since squaraines generally have very sharp absorption peak in solution and the probe wavelength can be rather close to the edge of 1PA.

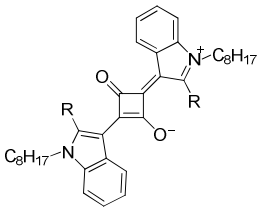

22a: R = H, δ_{max} = 450 GM at 730 nm (TPIF)
22b: R = CH_3, δ_{max} = 220 GM at 750 nm (TPIF)

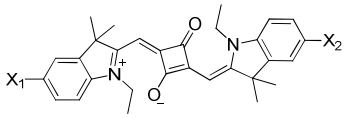

28a: X_1 = H, X_2 = H, δ_{max} = 200 GM at 820 nm (TPIF)
28b: X_1 = H, X_2 =  , δ_{max} = 900 GM at 867 nm (TPIF)
28c: X_1 =  , X_2 =  , δ_{max} = 5 100 GM at 898 nm (TPIF)

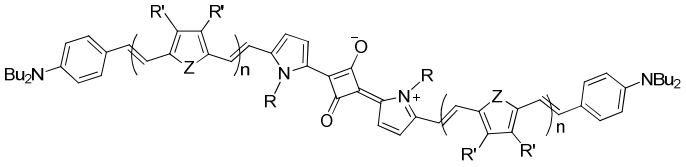

23: R = ^{n}hex, n = 0, δ_{max} = 27 000 GM at 960 nm (z-scan)
24a: R = ^{n}hex, n = 1, Z = S, R' = O^{n}Bu, δ_{max} = 18 000 GM at 1100 nm (z-scan)
24b: R = $CH_2CH(n\text{-}C_{10}H_{21})\text{-}n\text{-}C_{12}H_{25}$, n = 1, Z = S, R' = O^{n}Bu
25: R = ^{n}hex, n = 1, Z = N^{n}hex, R' = H, δ_{max} = 33 000 GM at 1050 nm (z-scan)

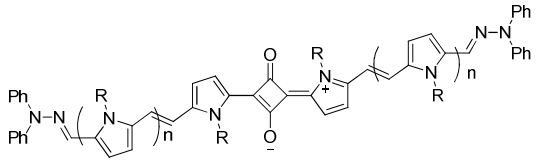

26: R = $(CH_2CH_2O)_3Me$, n = 0, δ_{max} = 9 500 GM at 850 nm (z-scan)
27: R = $(CH_2CH_2O)_3Me$, n = 1, δ_{max} = 14 000 GM at 1040 nm (z-scan)

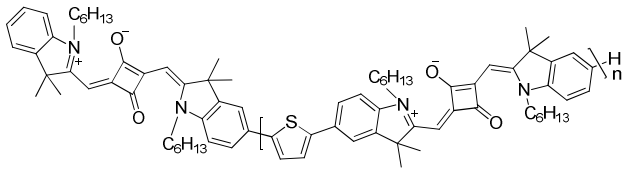

29a: n = 1, δ_{max} = 4 700 GM at 1038 nm (TPIF)
29b: n = 2, δ_{max} = 13 000 GM at 1064 nm (TPIF)
29c: n = 3, δ_{max} = 18 000 GM at 1074 nm (TPIF)
29d: n = 4, δ_{max} = 25 000 GM at 1078 nm (TPIF)

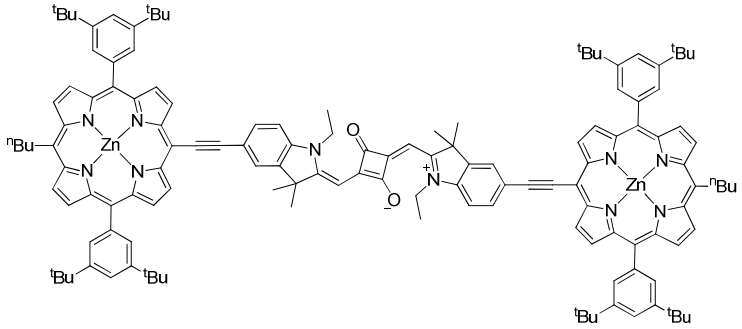

30, δ_{max} = 11 000 GM at 1060 nm (TPIF)

Figure 1.6: Chemical structures of squaraines with large 2PA cross-sections.[24,25,60,63]

The 2PA behavior of the bis(indolinylenemethyl) based squaraines bearing a variety of substituents and the respective conjugated oligomers were studied by Scherer *et al.*[24] As the conjugation extended from **28a** to **28c** with thiophene substituents, the maximum linear absorption wavelength red shifted with concurrent increase of oscillator strengths. The 2PA cross-section increases with longer conjugation as well. There were two 2PA bands observed using TPIF technique, E_2 peak with δ_{max} of 200 to 500 GM at transition energy around 2.0 to 2.1 eV and E_3 peak at around 2.7 to 3.3 eV with δ_{max} ranged from 300 to 5 000 GM (Figure 1.7). The first 2PA peak at transition energies close to those of the lowest energy one-photon electronic transitions, exactly at the same energy as the vibronic shoulder of the absorption band (peak 2 in Figure 1.8), were also observed in other squaraine systems.[25,61,62] The author proposed that it could be explained as exciting the molecule into a vibrational sublevel of the one-photon absorption (1PA) state, which was subsequent corroborated using theoretical calculation.[61]

As illustrated in Figure 1.8, for squaraine with indolinylenemethyl donors, there are no low-lying electronic states that are symmetry-allowed for 2PA. It has been shown that the 2PA-allowed $2A_g$ state has the same electronic nature as the 1PA $1B_u$ state but coupling through b_u vibrational modes. In the case of squaraine with diarylamino donors, peak 2 corresponds to excitation of the molecule through purely electronic channels to the lowest 2PA active electronic state, which is close in energy to the $1B_u$. The presence of the E_3 peak (peak 3 in Figure 1.8) with a higher transition energy, which was predicted

by calculations[40] and observed in this work, could be assigned to the excitation to a high lying electronic state ($3A_g$) with appropriate symmetry for 2PA.

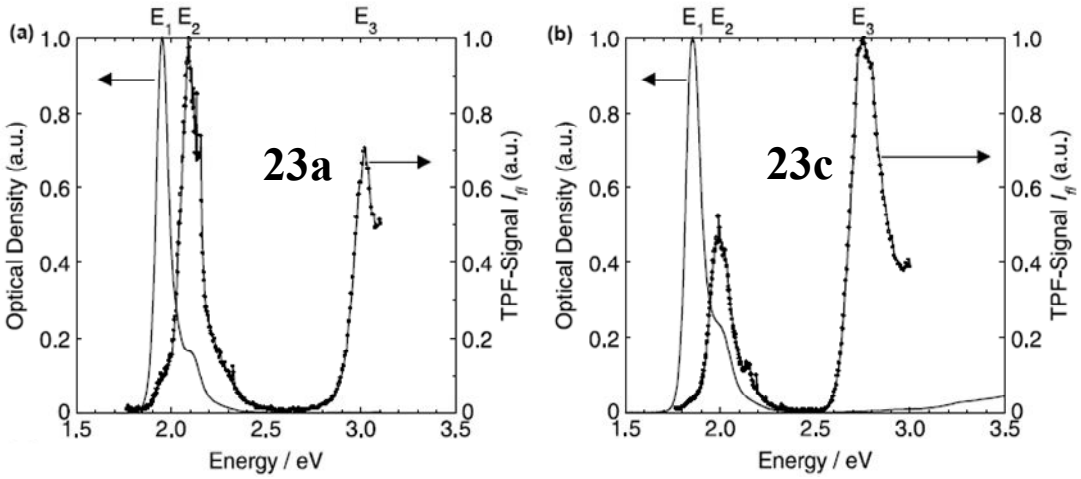

Figure 1.7: Two-photon excitation scans (dots) and linear absorption spectra (line) for 23a and 23c. The normalized fluorescence emission signal I_{fl} is plotted versus the doubled excitation energy.[24] Reprinted with permission from ref 24. Copyright Elsevier.

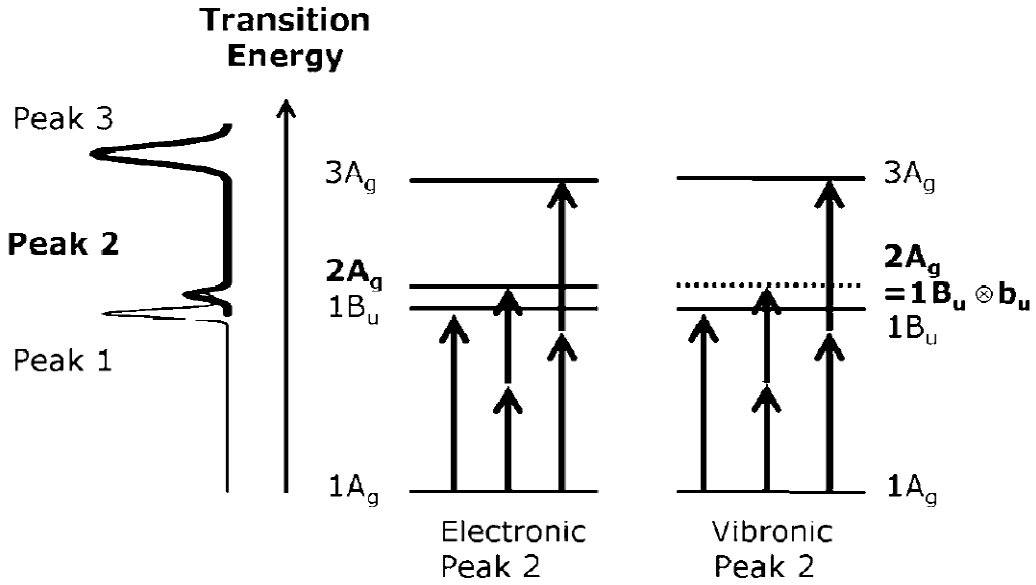

Figure 1.8: Illustration of the one-photon (light line) and two-photon (bold line) absorption processes in squaraines. Left: Sketch of the absorption spectra of squaraines. Middle: peak 2 is purely electronic. Right: peak 2 has the same electronic nature as the 1Bu state.[61] Reprinted with permission from ref 61. Copyright Wiley-VCH.

As demonstrated in many studies, increasing the conjugation length of the chromophores can have a large effect on 2PA spectrum. Since 2PA cross-sections are molecular quantities, linking together two chromophores in a way that results in no electronic delocalization will simply double the 2PA cross-section. However, if the π-systems are strongly electronically coupled, the transition dipole moment may be significantly increased, which may result in considerably enhanced 2PA. A good example of this is the porphyrin oligomers.[64-66] A 500-fold cooperative enhancement in 2PA cross-section was observed, when going from porphyrin monomer to acetylene-linked dimer.[64]

As conjugation in squaraine oligomers were extended through thiophene linkage, reported in Scherer's work,[24] the linear absorption spectrum of each longer oligomer overlapped that of the shorter oligomer and is slightly red shifted. The δ_{max} increases dramatically as the number of the monomeric subunits increase from 1 to 5 with that for **24d** up to 24 000 GM. This nonlinear increase for δ_{max} is correlated with the increase of the transition dipole moment (M_{ge}).

Recently, a bis(porphyrin)-substituted squaraine triad (Por-Sq-Por**,** **30**) was synthesized by Odom and Marder *et al*.[62,63] The lowest-energy absorption band of **30** red-shifted compared to that in squaraine **28a** about 100 nm. The δ_{max} measured by TPIF method for **30** is 11 000 GM at 1060 nm, which is similar in magnitude to those for several other porphyrin dimers.[64,65] It is worth noting that the 2PA band of **30**, with δ_{max} > 780 GM, covers over a 750 nm-wide wavelength range including the telecommunication

wavelengthes (1300–1500 nm) (Figure 1.9). Calculations using density functional theory (DFT) optimized geometries suggested that the frontier orbitals are significantly delocalized across the whole molecular backbone, where the broad 2PA spectrum is likely to arise from the overlap of several transitions.

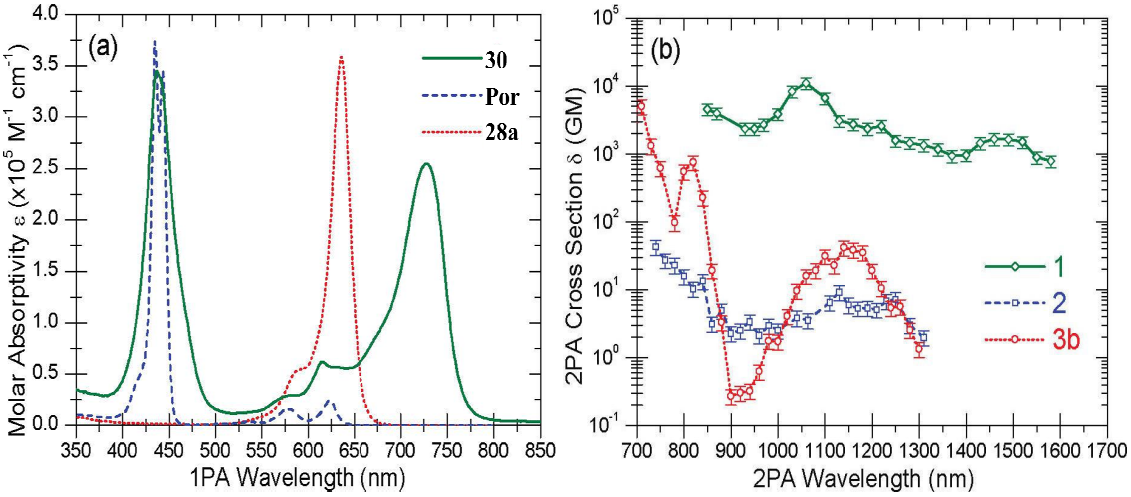

Figure 1.9: (a) 1PA and (b) semilogarithmic 2PA spectra of 30, Por, and 28a in CH_2Cl_2 with 1% pyridine. The spectra are plotted so the transition wavelengths can be directly compared (i.e. with the 2PA excitation wavelengths twice those of the 1PA wavelengths).[63] Reprinted with permission from ref 63. Copyright 2009 American Chemical Society.

1.3.3 Application of squaraine dyes in organic bulk-heterojunction solar cells

Energy remains one of the greatest global issues, particularly with the continued depletion of fossil fuels resources. Over the decades, researchers have endeavored to develop new, innovative materials that can provide inexpensive renewable energy resources and to improve the technologies for higher energy conversion. Solar energy is expected to be one of the clean alternative energy sources to fossil fuels in the near future. Photovoltaic cells using organic materials as the active layer are potentially a

flexible, cost-effective, and lightweight solar energy conversion platform as compared to their inorganic counterparts.[67-71] Among various device architectures, the bulk-heterojunction organic photovoltaic cells (BHJ-OPV) and dye-sensitized solar cells (DSSC, also called Grätzel cells), are two of the most promising candidates for organic material based systems. The solar irradiance (Figure 1.10) arrives at the surface of the earth at approximately 33% in the red to near-IR region (650–1000 nm), while the UV-visible radiation (350–650 nm) accounts for about 40%. To utilize more of the solar spectrum, development of red and near-IR absorbing molecules are highly desirable in order to achieve higher efficiency. Squaraines with their intense visible to near-IR absorption, reversible redox behavior and high thermal stability are attracting research interest as active materials for both types of solar cells.

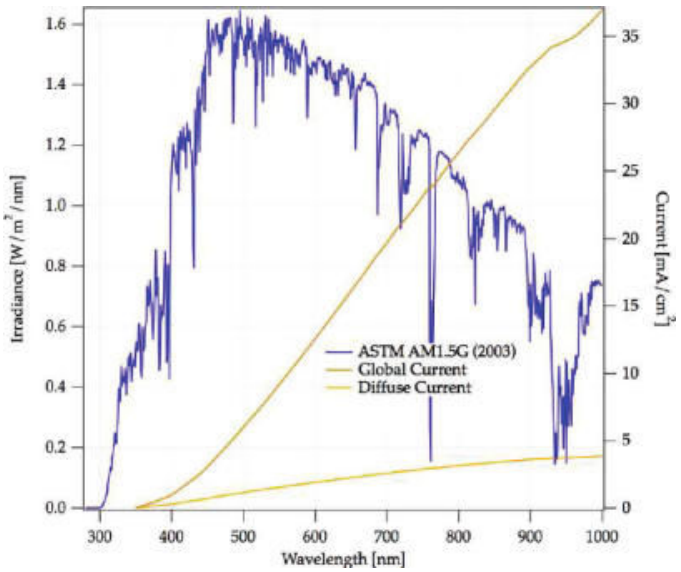

Figure 1.10: (Blue curve) Spectral distribution of the intensity for AM 1.5 solar radiation. (Yellow curves) short circuit current (*J*sc) values for a device converting all incident photons below the absorption onset wavelength into electric current.[72] Reprinted with permission from ref 72. Copyright 2009 American Chemical Society.

In BHJ solar cells, the photovoltaic process in D/A blend can be schematically described by the following steps, illustrated in Figure 1.11:[67,73-75]

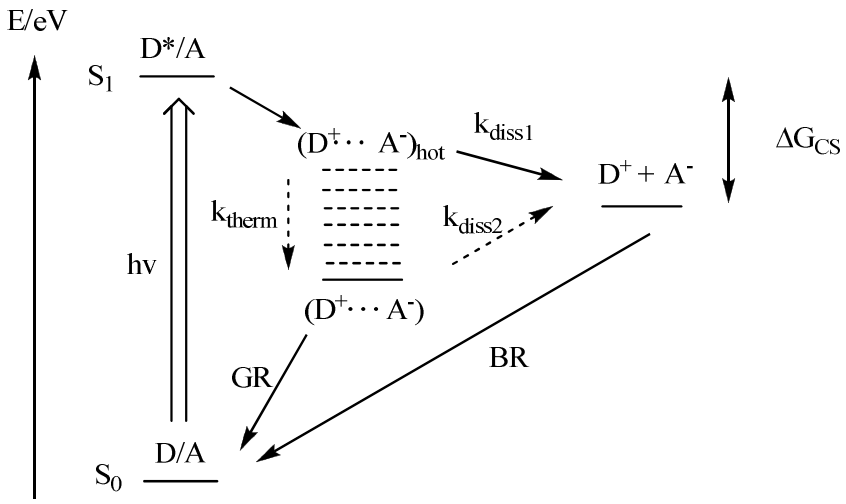

Figure 1.11. Energy state diagram for free charge formation in a donor/acceptor (D/A) system via a bound CT state following photo-excitation.

1) Photo excitation of either donor or acceptor component followed by exciton diffusion to the D/A interface followed by the formation of the ($D^+\cdots A^-$) charge transfer (CT) state. For the case of common donor/fullerene systems, the donor excited state is usually generated because of its superior light harvesting ability than fullerene derivatives.

2) The initially formed bound $(D^+\cdots A^-)_{hot}$ CT state can either undergo thermalisation (k_{therm}) to lower energy ($D^+\cdots A^-$) CT states or dissociation (k_{diss1}) into the charge-separated (CS) state $D^+ + A^-$ with free hole and electron. However, the ($D^+\cdots A^-$) CT states and $D^+ + A^-$ CS state can also undergo geminate (GR) and bimolecular (BR) charge recombination respectively to get back to the ground state.[67,73]

3) Free charge carriers transport within the active layer to the respective

electrodes for charge-carrier collection to form current in devices, which is actually not described on Figure 1.11.

Hence, detail of the photovoltaic process is actually much more complicated than is often schematically described in literature using only estimates of the frontier molecular orbital energies of the donor and acceptor and is still far from fully understood.[67] It should be noted that the energy difference, ΔG_{CS}, between the CS state and the donor first excited singlet-state (S_1) as shown in Figure 1.11, is generally considered the driving force for charge-separation, which is correlated to the free energy loss in the photovoltaic process and plays an important role in the efficiency of photo-induced charge separation as well as solar cell performance for many D/A blends. In depth discussion about this issue can be found in literature.[73-75]

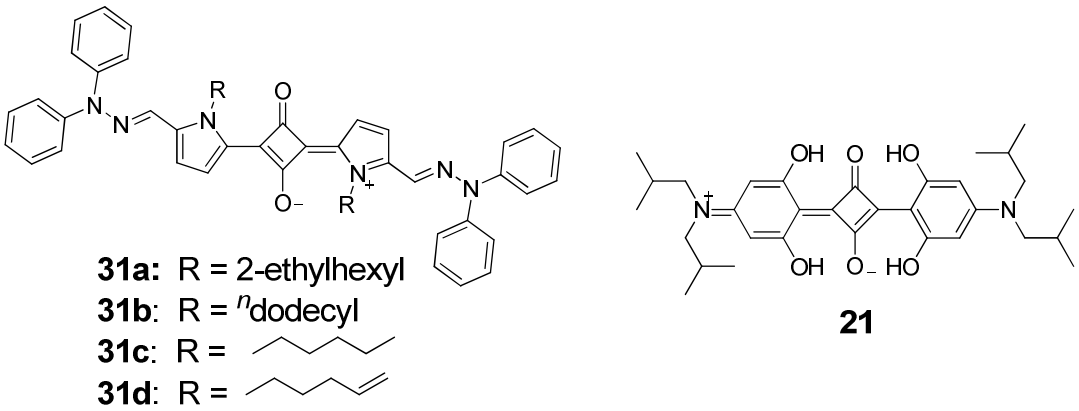

Figure 1.12: Chemical structures of squaraine used as donor in BHJ-OPV.[18,20,21]

As early as in the 1970s, squaraines were utilized as active components in single-layer OPVs, affording power conversion efficiencies (PCE) of ~0.02%.[76] Recently, Silvestri *et al*[20] reported the hydrazone end capped squaraines **31a** and **31b** in solution-

processed BHJ-OPV consisting of a mixture of a squaraine donor and **PCBM** acceptor. Linear and branched alkyl chain substituents were chosen to impart improved solubility and vary the film morphology. Figure 1.10 shows the normalized spectra of **31a** and **31b** in solution and in spin-cast film along with the frontier orbital energy level relative to **PCBM**. A broad absorption spectra in the solid states along with a relatively energy level matching gave the solar cells with a maximum PCE of 1.2% using a blend of **31a**:**PCBM** at 1:3 weight ratio with short circuit current (J_{SC}) of 5.70 mA/cm^2.

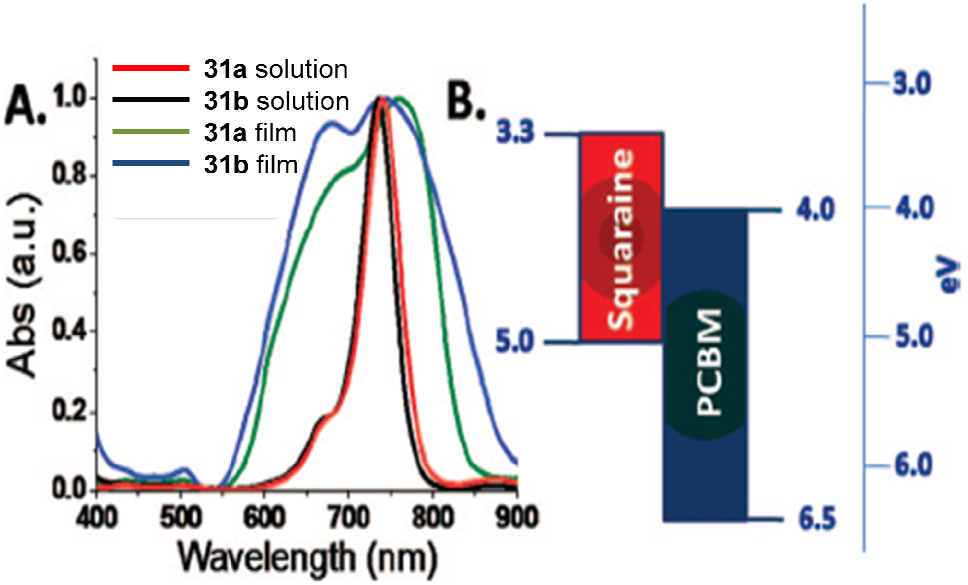

Figure 1.13: (A) Normalized optical absorption spectra: 31a (red line) and 31b (black line) as solutions in $CHCl_3$; 31a (green line) and 31b (blue line) as films from $CHCl_3$. (B) HOMO/LUMO levels for 31a and 31b vs PCBM.[20] Reprinted with permission from ref 20. Copyright 2008 American Chemical Society.

Later, with a minor change of the structure by using *n*-hexyl (**31c**) or *n*-hexenyl (**31d**) substituents at the pyrrolic nitrogen, the data reveal a much enhanced OPV performance.[18] From the crystal structure, it was found that there was a smaller minimum

interplane distance (3.138 Å, which is smaller than the sum of C–C van der Waals radii (3.4 Å)[77]) and minimum interstack distance between cores of **31d** than that of **31c** indicative of a more densely packed bulk film. The highest efficiency of ~2% was obtained from solar cells using a blended film of **31d:PC$_{71}$BM** ([6,6]-phenyl-C$_{71}$-butyric acid methyl ester) with 1:3 weight ratio and annealed at 50 °C for 30 min, this is more than 40% improvement comparing with that of the corresponding devices using **31c:PC$_{71}$BM** blends. The major reason could be attributed to higher hole mobilities for **31d** than **31c** tested in thin-film transistors ($(1.2 \pm 0.2) \times 10^{-4}$ and $(2.7 \pm 1.8) \times 10^{-5}$ cm^{2}V^{-1}s^{-1} respectively), since the film morphologies of the two blends are practically identical, as determined by atomic force microscopy (AFM) images.

Wang and Thompson[21] investigated the OPV performance as a function of thickness of squaraine **21** in heterojunction cells deposited by vacuum thermal evaporation. Devices with the following architecture ITO / **21**(x) / C$_{60}$(400 Å) / BCP(100 Å) / Al(1000 Å), x = 65, 110, 150 and 200 Å, were fabricated to give the highest average PCEs on the order of 3.2 ± 0.2%. The V_{oc} of these cells ranged from 0.75 to 0.84 V which is around 300 mV greater than that observed for device with copper phthalocyanine (CuPc) in place of the squaraine. The solution-processed BHJ cells were also tested in the same group using the blend of **21** and **PC$_{70}$BM** with a different weight ratio.[78] By incoporation of a MoO_3 buffer layer, the device using the mixture of **21:PC$_{70}$BM** = 1: 6 results in the best cells with a PCE of ca. 2.7 %, J_{SC} of ca. 8.85 mA/cm^2, and V_{OC} of ca.

0.89 V under global AM 1.5G simulated solar irridiation. The relatively high V_{OC} could be attributted to the buffer layer which reduced the dark current arising from electron leakage to the anode.[79] However, in comparison to a planar heterojuction **21**/$\mathbf{C_{60}}$ cell control with an efficiency of ca. 4.1% under similar conditions, the lower efficiencies of devices using these solution-processed **21:**$\mathbf{PC_{70}BM}$ blends was claimed to result from unbalanced electron and hole transport. The morphology study of these blends from spin-coating suggested nonuniform distribution of squariane domains throughout the whole film, which caused relatively low hole mobilities.

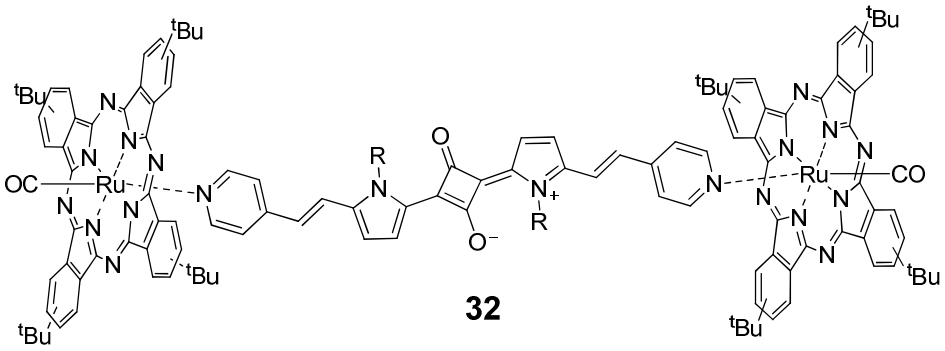

32

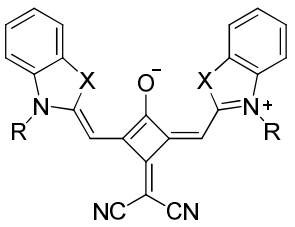

33a: X = $C(CH_3)_2$, R = *i*Pr
33b: X = S, R = *n*BuOH

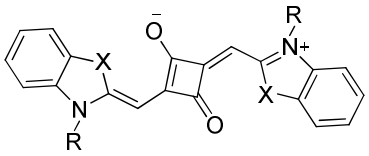

34a: X = $C(CH_3)_2$, R = *i*Pr
34b: X = S, R = *n*BuOH

Figure 1.14: Chemical structures of squaraine derivatives as donor in BHJ solar cells.[19,80]

A supramolecular phthalocyanine-squaraine ensemble (Pc-Sq-Pc, **32)** was synthesized and used as donor material in solution-processed BHJ-OPVs by Silvestri and

Torres.[80] By employing the supramolecular architecture, they were able to achieve optical absorption with more coverage of the visible spectrum than the sum of individual squaraine and phthalocyanine. The preliminary device PCEs of ca. 0.3 % was obtained at **32:PCBM** = 1:4 weight ratio, attributable to a low short-circuit current. It was also suggested that rationally tailoring the redox properties of the bridging squaraine could allow a further enhancement of these parameters.

Squaraine devaritives with modification at the squaric core have also been investigated for BHJ solar cells.[19] The compound **33b** bearing an additonal dicyovinyl acceptor moiety at the center ring afforded BHJ-solar cells with PCEs of up to 1.79% as blended with **PCBM**, comparing with the unsubstituted counterpart **34b**, the PCE of which was only 0.07%. It is worth noting that with intense absorption in the highly desirable near-IR range, a high J_{SC} of ca. 12.6 $mAcm^{-2}$ was achieved upon thermal annealing at 110 °C for 15 min. X-ray analysis of a single crystal of **34b** indicates an almost planar π-skeleton with only 9° twisted angle between the dicyanovinyl unit and the squaraine ring, which could benefit charge-carrier mobilities in thin films. The absorption of the densely packed chromophore shows a red shift and band broadening upon annealing along with the hole mobility increasing from $\mu_h = 1.5 \times 10^{-5}$ $cm^2V^{-1}s^{-1}$ to a respectible 1.3×10^{-3} $cm^2V^{-1}s^{-1}$.

1.3.4 Application of squaraine dyes in dye-sensitized solar cells (DSSCs)

The first dye-sensitized solar cells (DSSCs) were invented by Michael Grätzel and Brian O'Regan at the École Polytechnique Fédérale de Lausanne in 1991[81] and are also known as Grätzel cells. Different from conventional photovoltaic cells, dye-sensitized solar cells separate the two functions of light harvesting and charge-carrier transport, which makes DSSC promising candidates for having high conversion efficiency and low cost fabrication for alternative clean energy sources.

The schematic illustration of the operating principles of DSSCs is given in Figure 1.15. Sunlight is harvested by a sensitizer which is attached to the surface of nanocrystalline large band-gap semiconductor, typically a film constituted with TiO_2, although alternative wide band gap oxides such as ZnO and Nb_2O_5 have also been investigated. Photo excitation of the sensitizer results in the injection of an electron into the conduction band of the oxide. An organic hole conductor or electrolyte, usually the iodide/triiodide couple as a redox shuttle for the latter case, donates electron to regenerate the sensitizer. Other mediators such as cobalt(II/III) complexes[82] or the 2,2,6,6-tetramethyl-1-piperidinyloxy (TEMPO)/$TEMPO^+$ redox couple[83] have also been developed recently as an alternative to the I^-/I_3^- system. The iodide is restored by reducing triiodide in turn at the counter-electrode, where the electrons are supplied via migration through the external load to complete the cycle without suffering any permanent chemical transformation. The voltage generated under illumination is related

to the difference between the Fermi level that the electrons attain in the TiO_2 nanoparticles and the redox potential of the electrolyte, in the absence of any other parasitic losses.

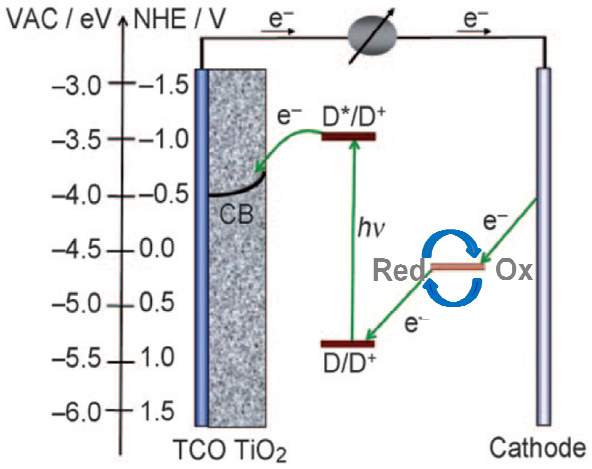

Figure 1.15: Principle of operation and energy level scheme of the dye-sensitized nanocrystalline solar cell. Modified with permission from ref 8. Copyright 2009 WILEY-VCH.

An essential requirement for an ideal sensitizer to have efficient conversion of solar energy is a good spectral match of the sensitizer absorption to the solar spectrum. The sensitizer must also have an anchor group such as carboxylate or phosphonate to firmly attach it to the semiconductor oxide surface and to facilitate efficient charge transfer. In order to inject electrons efficiently into the TiO_2 conduction band, the excited-state ionization potential (IP) of the dye should be less than the electron affinity (EA, is defined as positive that $EA = E_{initial} - E_{final}$) of the conduction band of the TiO_2, so that the electron transfer process is exergonic. However, this process should not be too strongly exergonic as this more energy is being lost unnecessarily. In addition the IP of

the sensitizer should be sufficiently high that it can be regenerated via electron donation from electrolyte or hole conductor (Figure 1.15). To efficiently prevent charge recombination between the dye cation and TiO_2, the driving force for near-quantitative reduction of the oxidized sensitizer by oxidation of iodide to triioide has been empirically estimated to be at least 0.2–0.3 eV.[72] Moreover, photo- and thermo-stability to sustain about 10^8 turnover cycles are required, which is rather demanding for many organic dyes.[84]

In these DSSCs, the most efficient charge-transfer sensitizers studied to date have been ruthenium polypyridyl complexes, in which solar-to-electric PCE under AM 1.5G simulated solar irradiation efficiencies up to 11% have been reported.[85-87] However, the main drawbacks of ruthenium complexes are their relatively high cost of ruthenium, along with their lack of absorption in the red region of the visible spectrum and their low molar absorption coefficients ($\varepsilon \leq 20000$ $M^{-1}cm^{-1}$ for the longest wavelength metal-to-ligand charge transfer transition). Squaraines, have been investigated as sensitizers as a class of cyanine dyes with low optical gaps and strong absorption in the visible and near-IR, extremely high molar absorptivity, high thermal and photo-stability in general.[8,9]

One of first studies using squaraines as sensitizers in DSSCs were reported in the late 1990s by Xiao and co-workers.[88] Symmetric bis(indolinylenemethyl)-based squaraines were utilized to give a PCE of ca. 2.17% for **35** and a maximum IPCE of ca. 6.2% at 650 nm for the dye of highest adsorption ability among the three dyes have been

investigated. Doping *cis*-Ru[4,4'-(LL)]$_2$(NCS)$_2$ (L = 2,2'-bipyridyl-4,4'-dicarboxylate) with 1% molar ratio of **35** as photosensitizer, lead to a panchromic absorption, with a 12% increase in PCE compared to that of pure *cis*-Ru[4,4'-(LL)]$_2$(NCS)$_2$, owing to the complementary light-harvesting capacity by **35**.

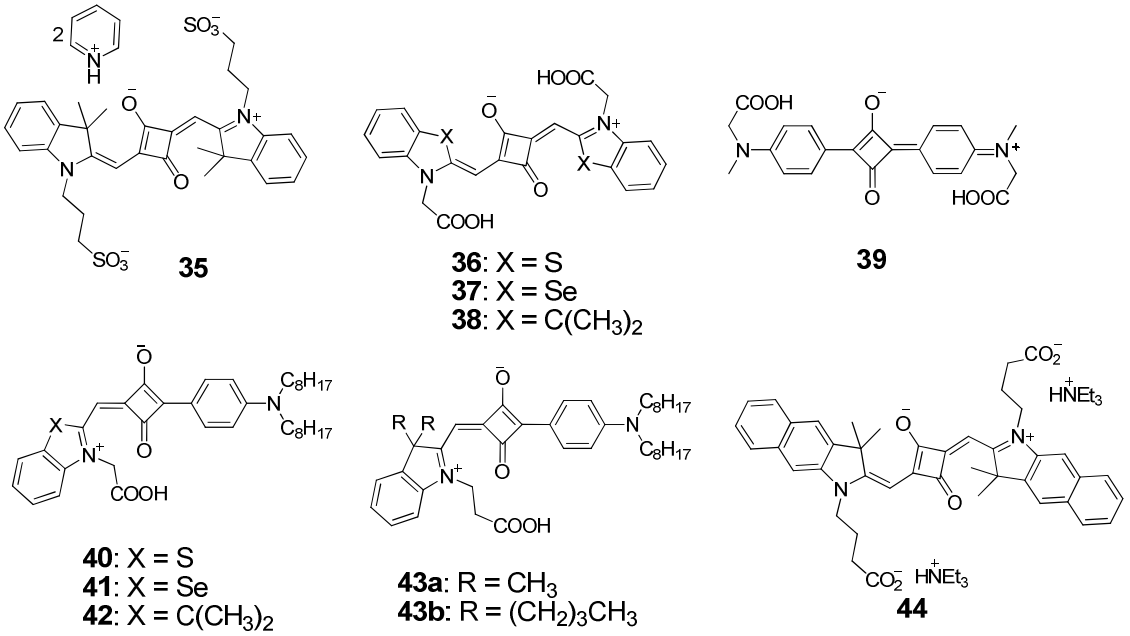

Figure 1.16: Structure of squaraines with non-conjugated anchor groups as sensitizers for DSSCs.[88-91]

Das and co-workers characterized a series of symmetrical and unsymmetrical squaraine dyes (**36–42**) possessing a non-conjugated –COOH anchoring group enabling the stable grafting of the dye on the titania surface.[89] Figure 1.17 shows the calculated molecular structures and the electron distribution of the HOMO and LUMO levels of **36**, **39**, **40**, indicating a clear shift of electron density from one end of the molecule to the other end with the anchor group for the unsymmetrical squaraine **40**, which could facilitate the charge transfer from the dye to the conduction band of TiO_2. The cells with

unsymmetrical squaraines also showed higher V_{oc} and J_{sc} compared to symmetrical squaraines with the highest PCE for **42** of ca. 2%.

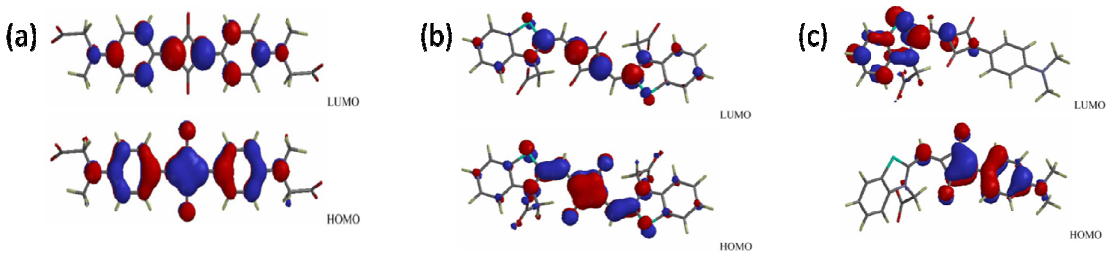

Figure 1.17: Frontier molecular orbital of the anionic form of 36 (left), 39 (middle), 40 (right).[89] Reprinted with permission from ref 89. Copyright Elsevier.

It has been shown that efficient light to photocurrent conversion by the self-assembled dyes on TiO_2 facilitated by charge displacement from a region of the dye distant from the TiO_2 surface in the ground state to the part of the dye in close proximity to the semiconductor surface in the excited state. Photochemically robust and thermal stable D-π-A dyes have been developed with high PCEs,[92-94] where the electron density of the HOMO is mainly localized on the donor part, while the LUMO is centered at the acceptor (anchoring group) part. Hence, within a simple one electron approximation, during light excitation, electrons are transferred from the donor through the π bridge to the surface-bound acceptor. As a consequence of strong coupling between the excited-state of the dye and the TiO_2 conduction band, rapid and efficient electron injection can be achieved. On the other hand, back charge transfer from TiO_2 to the HOMO of the dyes can be reduced by spatially separating the HOMO of the dye from TiO_2, since the HOMO mainly locate in the donor part of the dye.[72]

Das concluded from his work that aggregation of symmetrical dyes on the TiO_2 surface results in significant decrease in their sensitization efficiency.[89] Another study on similar unsymmetrical squaraine dyes (**43a** and **43b**) sensitized ZnO with an aggregation breaking agent, deoxycholic acid (**DCA**), showed more than 60% improvement in PCEs by suppressing the molecular aggregation.[90] It was found that the decreased aggregation contributes not only to the increase of J_{SC} but also to the increase of V_{OC}, which is likely due to the reduced back electron transfer in the presence of **DCA**.[95]

The dye aggregates may lead to broad absorption and better light harvesting, however, they may also cause strong intermolecular quenching of the excited-states of the dyes and lower electron injection efficiency. As a result, lower J_{SC} and consequently poor photovoltaic performance are observed.[8,72,96] A recent report on organic photosensitizer having orderly conjugated ethylenedioxythiophene and dithienosilole (**DTS**) blocks sets a new benchmark of ca. 10% efficiency measured at the AM 1.5G conditions with non-ruthenium dyes.[94] One of the possible reasons for the high PCE is the introduction of dihexyl-substituted **DTS** featuring a tetrahedral silicon center which might significantly reduce the π-π stacking of dye molecules on nanocrystals without interference to the planarity of π-conjugated spacer.

Burke and Grätzel demonstrated later that, in the presence of chenodeoxycholic acid (**CDCA**) to prevent aggregation, even symmetrical squaraines can efficiently perform when the dye was adsorbed as the corresponding ammonium salt **44**.[91] With broad near-IR

absorption of **44** sensitized TiO_2, PCEs as high as 3.7% was achieved.

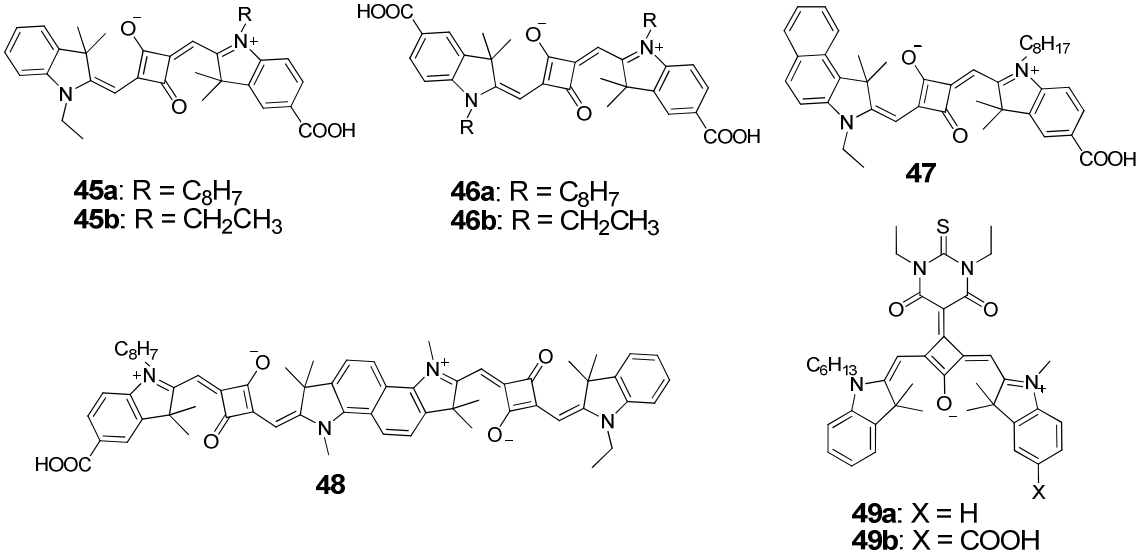

Figure 1.18: Structure of squaraines with conjugated anchor groups as sensitizers for DSSCs.[97-101]

By introducing the carboxyl docking group directly on the squaraine main conjugation, Nüesch and co-workers significantly improved the efficiency up to 4.5% with J_{sc} = 10.50 ± 0.20 mA/cm^2, V_{oc} = 603 ± 30 mV, and FF = 0.71 ± 0.03 using **45a** (with **CDCA**).[97] They attributed the high efficiencies to the strong electronic coupling of the π-system of the dye to the conduction band of TiO_2 through the conjugated linked carboxylic group, along with reduced surface aggregation and self-quenching of the excited state in the presence of an octyl chain on one of the indoline unit. Utilizing the same dye, an inorganic and organic hybrid poly-3(hexylthiophene) (**P3HT**) based heterojucntion solid state DSSCs were fabricated by Grimes and co-workers.[102] With electron transporting in TiO_2 nanotube arrays, which is sensitized with red and near-IR light absorbing squaraine **45a**, along with hole transporting and visible light absorbing regioregular **P3HT**, device efficiencies of ca.

3.2% were achieved. Figure 1.19 illustrates the structure of the cell and the relative energy level positions. A recently published paper reported on both symmetrical and unsymmetrical squaraine derivatives with structures similar to that of **45a**.[101] Replacing the octyl group by an ethyl group, the PCEs of **45b** sensitized cells decreased to 2.43%. With the symmetrical analogs **46a** and **46b**, even lower efficiencies were obtained, 2.09% (3.15% with **CDCA**) and 1.46% (2.49% with **CDCA**) for **46a** and **46b**, respectively.

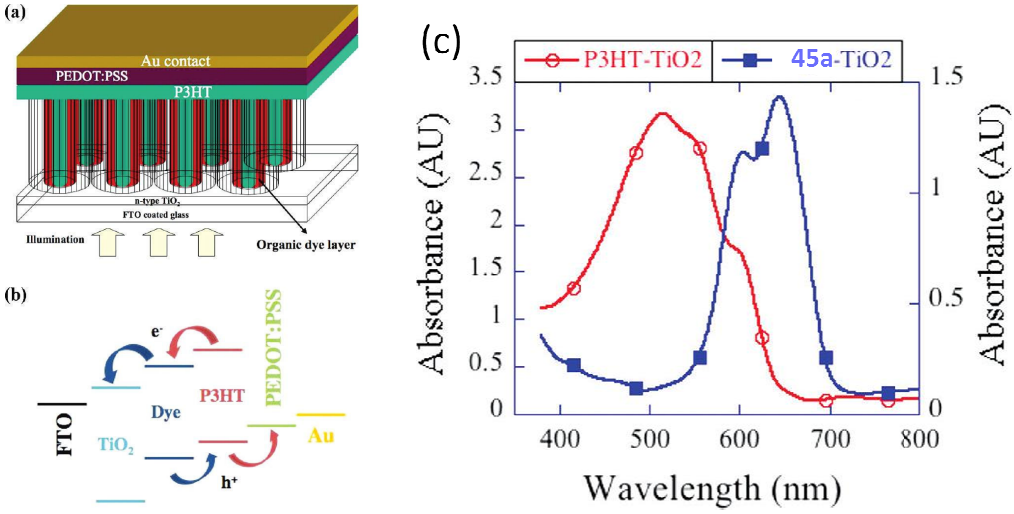

Figure 1.19: (a) Depiction of hybrid solid-state solar cell. Dye sensitization and polymer intercalation between the nanotubes is not shown to maintain clarity of the drawing. (b) Depiction of energy level positions and charge transfer processes of the constituent layers of the described hybrid solar cell. (c) Absorption of 45a sensitized TiO_2 nanotube arrays and P3HT intercalated nanotube arrays without dye sensitization.[102] Reprinted with permission from ref 102. Copyright 2009 American Chemical Society.

A molecular design in which the structure of **45a** is changed slightly with extended π framework to **47** resulted in an efficiency increase of approximately 20%.[98] The higher PCEs were attributed to the bathochromic shift of the absorption maximum, the higher molar absorption coefficient, and the stronger electronic coupling between the excited-state

of the dye and the TiO_2 conduction band, providing a faster electron injection and preventing non-radiative recombination. Another recent report on molecular engineering of the unsymmetrical squaraine by varying the donor moiety with fluorene-based amino donor (**20**) gave a comparable efficiency of 4.9% (with **CDCA**).[38] It was further increased to 5.2% by coating an Al_2O_3 layer between the sensitizer and electrolyte. This was demonstrated to be an effective methods to reduce the interface charge recombination losses.[103,104] Further extending the conjugation of the unsymmetrical squaraine to a dimer **48** pushes the absorption to the near-IR with an 85 nm red shift at the maximum compared with **45a** and covers the 500–800 nm spectral region.[99] However, the preliminary DSSC proof-of-concept device revealed a relatively low efficiency of 1.3%, which the authors claimed might due to aggregate formation.

It should also be noted that although squaraines possess intense near-IR absorption, the rather weak absorption in the high energy region of the visible spectra (300 – 500 nm) limits their light harvesting capability. Functionalization of the squaraine core with an electron-withdrawing conjugated residue was reported by Beverina and co-workers.[100] With the diethylthiobarbiturate group, the squaraine is in its *cis* conformation and possesses a second high-energy band in the absorption spectrum which helps to harvest more sun light. A similar performance in DSSC using **49b** was obtained as compared to that of **45a** with efficiency of ca. 4.7%, despite the broader absorption. This was attributed to the *cis* configuration of **49b** forcing unfavorable adsorption geometry on the TiO_2 surface, which

consequently increases the rate of parasite back-electron-transfer process.

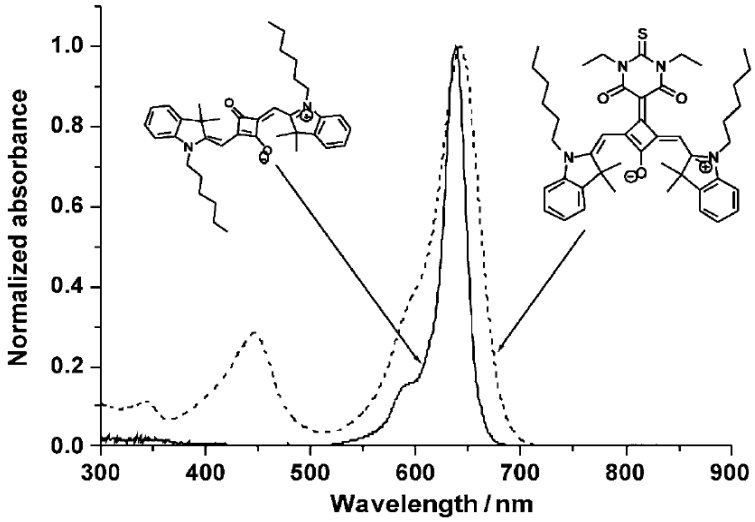

Figure 1.20: Absorption spectra of symmetrical squaraine and the core-substituted squaraine 49a.[100] Reprinted with permission from ref 100. Copyright 2009 WILEY-VCH.

1.3.5 Other applications of squaraines

Squaraines have also been widely studied for applications such as ion probes, bio-labeling and imaging, low-band gap polymers, and photodynamic therapy. Only a few examples are given here. For more extensive compilations of various applications, readers are referred to literature reviews.[4-6,14,15,39,105]

Organic functional dyes have been attracting intense research attention with respect to the applications as chemosensory, bio-labeling, and imaging for important analytes in the fields of chemistry, biology, medicine, and environmental studies. Squaraines with their unique optical properties, which can be tuned by formation of

aggregates, temperature, polarity of solvents, and metal ions, have been used as probes for the detection of various analytes, and fluorescent label for proteins. The change in the absorption, emission or redox potentials can be monitored through the binding of substrates either to the oxygen atoms of the cyclobutene ring or a recognition site integrated to the squaraine dyes.

With squaraine tethered bichromophoric podands (**50a-f**), Arunkumar and coworkers successfully demonstrated that the bichromophoric podands have higher selectivity to alkaline earth metal cations, especially Ca^{2+} and Mg^{2+}, in changing of absorption spectra but no response to alkali metal ions.[106] Compared with the mono-squaraine based analogous (**51a-c**), which showed no change in the optical properties to alkaline earth metal cations, it was proposed that the squaraines formed a 2:1 sandwich type foldamer with Ca^{2+} as the chelating center.[107]

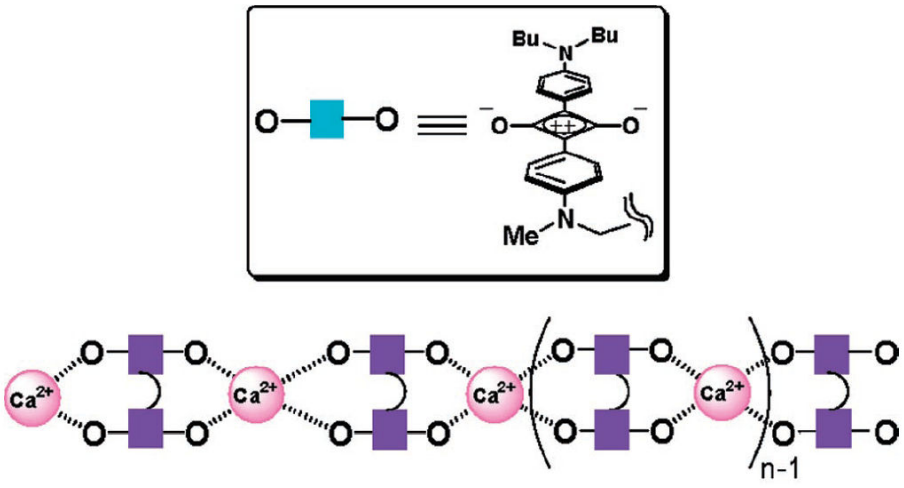

Figure 1.21: Schematic illustration of the possible structure of the metalosupramolecular architecture of 50 with Ca^{2+}.[108] Reprinted with permission from ref 108. Copyright 2007 American Chemical Society.

In the absence of a podand chain, Yagi and co-workers investigated a bis-squaraine connected with a polymethylene chain (**52a-c**), which could form folded H-type aggregates in the presence of Ca^{2+}.[108] It was suggested that the Ca^{2+} was first weakly bonded to the oxygen of the squaric core to form a 1:1 complex which further facilitated the formation of an extended metallo-supramolecular arrays through alternative chelation of negative charged oxygen from the folded H-type squaraine dimers to Ca^{2+} as shown in Figure 1.21.

Fluorescence labeling of proteins such as human serum albumin (HSA) and bovine serum albumin (BSA) by a bis-squaraine dyes **53** (linked by thiophene) and **54** (linked by pyrene) have been studied by Nakazumi and co-workers.[109] The fluorescence of these dyes exhibited large enhancement when bonded to HSA and BSA in the form of 1:1 dye-protein complexes as noncovalent labeling probes in the near-IR region in aqueous solution. Dye **54** gave the most notable result, where the fluorescence quantum yield was about 14 times higher for dye-BSA than that for the free dye.

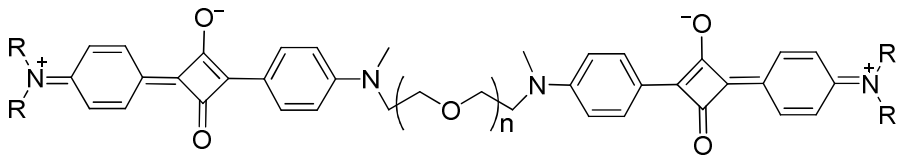

50a: n = 1, R = C_4H_9; **50b**: n = 2, R = C_4H_9; **50c**: n = 3, R = CH_3;
50d: n = 4, R = CH_3; **50e**: n = 5, R = CH_3; **50f**: n = 6, R = CH_3.

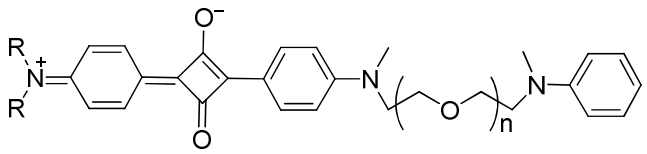

51a: n = 1, R = C_4H_9; **51b**: n = 2, R = C_4H_9; **51c**: n = 3, R = CH_3.

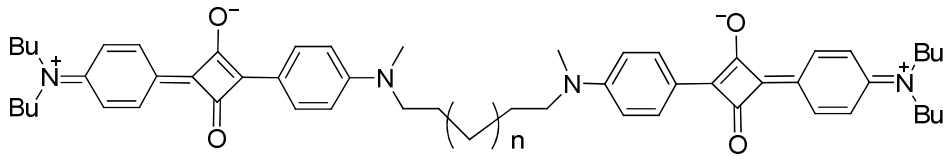

52a: n = 2; **52b**: n = 3; **52c**: n = 4

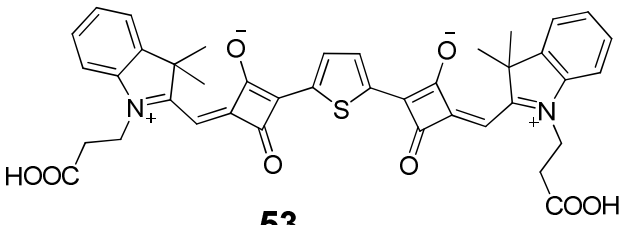

53

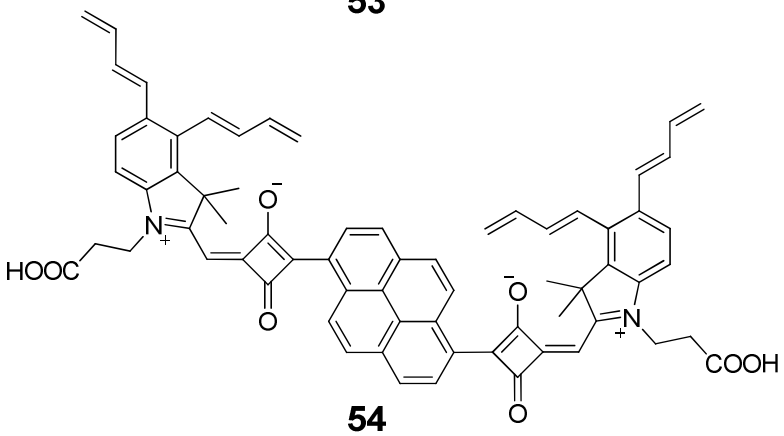

54

Figure 1.22: Chemical structures of squaraines used as ion probe or biolabling. [106-109]

Designs of semiconducting π-conjugated polymers with low optical gaps are important for their applications in molecular electronics.[110-112] An approach to extremely low optical-gap polysquaraines with intense near-IR absorption and high intrinsic conductivity can be achieved by an A-B type copolymerization of squaric acid and a bifunctional monomer with two reactive end groups that are connected to an electron-rich conjugated bridging unit which results in zwitterionic polysquaraines with resonance stabilized quinoid structures. Polycondensation of bispyrroles with squaric acid resulted in the formation of polysquaraines **57-60** (Scheme 1.5), which intensely absorb in the near-IR region with spectra broadening (Figure 1.23).[113-115] Calculated from the onset of the absorption bands, the optical band-gap of the polymers are estimated to be 0.7−1.1 eV. The conductivities of the polysquaraines vary with the length of the side chains, in the order of 10^{-7} to 10^{-4} S cm^{-1}, where the compounds with short side chains exhibited higher conductivity. It was attributed to the close inter-chain packing and inter-layer π-π stacking which facilitates electron hopping.

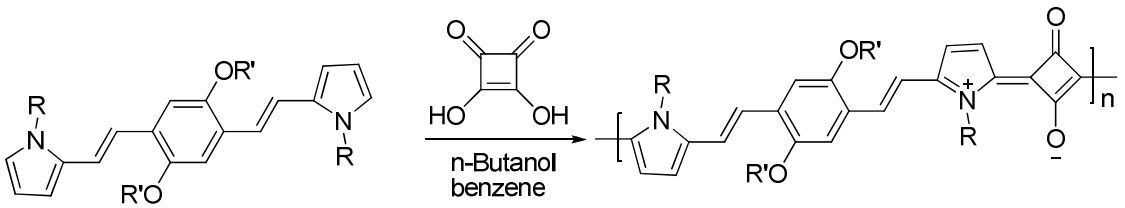

55-58

55: R = CH_3; R' = C_4H_9
56: R = CH_3; R'=C_8H_{17}
57: R = $C_{12}H_{25}$; R' = $C_{12}H_{25}$
58: R = $C_{12}H_{25}$; R'=CH_3

Scheme 1.5: Examples of polysquaraine synthesis.[5]

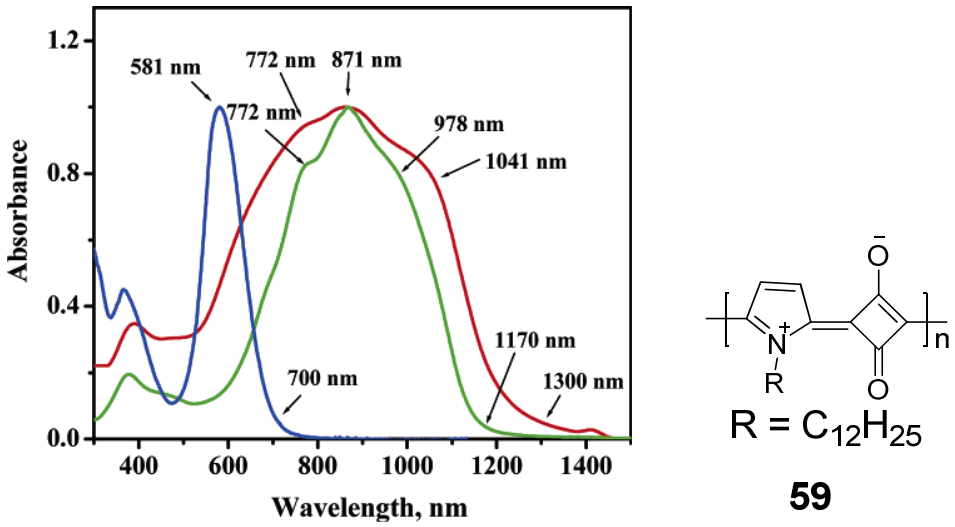

Figure 1.23: Absorption spectra of polysquaraines 59 (blue), 55 (red), and 58 (green).[6] Reprinted with permission from ref 6. Copyright 2005 American Chemical Society.

Photodynamic therapy (PDT) was developed as a new medical technology from the 1980s and use a photosensitizer to generate an excited singlet-state oxygen molecule which induces cell damage through direct and indirect cytotoxicity for cancer treatment.[116,117] When exposed to visible or near-IR light, the photosensitizer is excited from ground state to an excited singlet-state, which can be followed by intersystem crossing to a longer-lived excited triplet-state. Energy transfer can take place when the molecular oxygen is in close proximity to create excited singlet oxygen. The photosensitizers are required to have high absorption at long wavelengths where tissue is much more transparent and allow the light to penetrate deeper. A high singlet oxygen quantum yield is needed along with, low photo-bleaching, high chemical stability, and low dark toxicity. Squaraines are promising candidates for this application that have been extensively studied.[118-121] Recently, Webster and co-workers demonstrated near-unity

quantum yields for intersystem crossing and singlet oxygen generation experimentally, using a squaraine derivative **60** where the oxygen atoms of the cyclobutene ring were replaced by sulfur atoms.[122] This substitution significantly lowers the energy of an n-π* transition which leads to an inversion of the energetic order of the lowest singlet π-π* electronic transition by n-π* (Figure 1.24). Hence, the intersystem crossing is much enhanced without the use of "heavy atoms" due to effectively reduced energy difference between singlet and triplet states. The largest 2PA cross-section of ca. 7000 GM (*z*-scan) for **60** was observed at 760 nm which indicates this dye is potentially useful for two-photon induced photodynamic therapy.

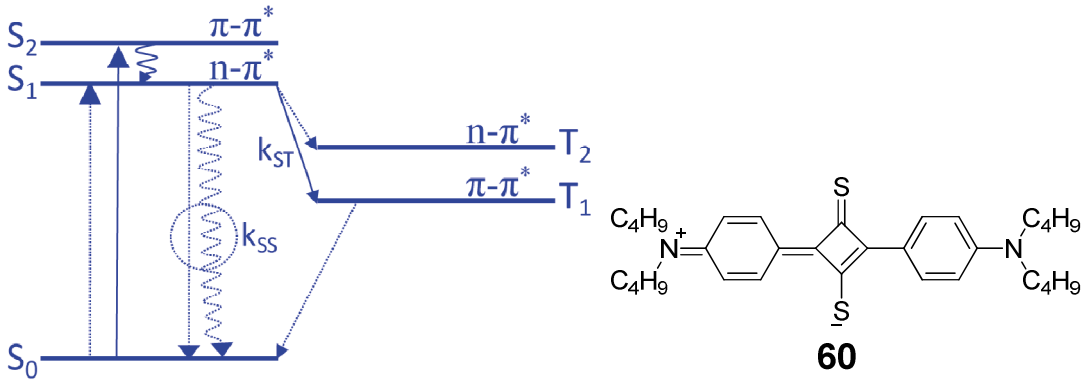

Figure 1.24: Schematic of energy level structures and the nature of transitions and chemical structure for 60.[122] Reprinted with permission from ref 122. Copyright 2010 American Chemical Society.

1.4 Research goals and organization of the thesis

1.4.1 Research goals and Design strategy

In summary, squaraine dyes with their unique optical and electronic properties are promising candidates for many applications as described above. The goal of the research described in the remainder of this thesis is to develop new squaraine-based photonic and electronic materials and understand their structure-property relationship to better meet the needs for optical applications such as optical limiting and 2PA-based all-optical switching as well as organic electronics.

2PA related applications, such as 2PA-induced optical limiting and 2PA-based all optical switching, require materials that have a large 2PA cross-section and can be integrated into high optical quality films. We are particularly interested in the near-IR spectral region (800 – 1600 nm), which includes the telecommunication wavelength (1300 – 1550 nm). In the first part of this thesis, squaraines with extended conjugation through vinylene-heterocycle donor arms or in the form of oligomers were designed in order to achieve large transition dipole moments and small detuning energy to realize large 2PA coefficients. By utilizing different heterocycles (thiophenes and pyrroles) and adjusting the length of the bridge, it may allow for the tuning of various properties of the squaraine dyes. It may help achieve larger transition dipole moments and bathochromically shift the absorption bands by using the less aromatic heterocycles. Incorporation of pyrrole rings with long alkyl chains into the bridge may improve the solubility of the squaraine dyes and also modify the absorption spectra due to the greater electron-richness and lower aromaticity of pyrrole vs. thiophene. The use of a Fréchet-

type phenol-based dendron as the side-chain, may help to improve the film forming properties and miscibility with polymers to achieve high optical quality films.[123-125] The oligomer approach may largely increase the 2PA efficiency but maintain the narrow and solution-like absorption in the solid states. It may also allow us to have an insight understanding of the photo-physical properties of squaraines.

For reverse saturable absorption induced optical limiting, squaraine and phthalocyanine-based metal complexes were designed. It is well known that heavy-metal effect facilitates the spin–orbit coupling to enhance the intersystem crossing (ISC) from the excited singlet-state (S_1) to the excited triplet-state (T_1), and significantly increase the optical limiting response. Phthalocyanine and squaraine dyes, with their wide transparency window and large nonlinear polarizability, and strong excited-state absorption, were built into architectures in which heavy-atom(s), platinum or gold, were coordinated to the chromophore through acetylide ligands. The optical limiting performance of these materials was investigated.

For heterojuction organic solar cells, one of the possible reasons for the relatively low efficiencies of devices using squaraine-based donor is the imbalance in hole and electron mobilities. The presence of platinum in the squaraine conjugated framework may facilitate charge transport, and consequently promote the overall performance of the device.[126-128] The heavy atom(s) containing squaraines described above could also serve as low optical-gap donors in solar cells with their high molar absorptivities in the near-IR

region. For mesoscopic cells, unsymmetrical donor-acceptor type squaraines have shown promising results. As reviewed earlier in this chapter, changing the acceptor position can significant affect charge transfer from the excited-states of squaraines to TiO_2 conduction band, where breaking aggregation of the dye is also a crucial point to improve the power conversion efficiency. A series of unsymmetrical indolium-based squaraines were developed. A variety of acceptors were explored with different linker groups in order to improve the performance and better understand the process of charge transfer from the excited-state of the dyes to TiO_2 conduction band through different bonding and path length and also to influence their aggregation behavior.

1.4.2 Thesis organization

In this chapter, general chemical and physical properties of squaraines have been reviewed along with their two-photon absorption properties and applications in bulk heterojuction and dye-sensitized solar cells.

Chapter 2 focuses on squaraines with extended conjugation through vinylene heterocycles bridges, their 2PA properties, and optical-limiting performance. A squaraine with a Fréchet-type dendron attached is also explored as an analog for creating better optical films.

Chapter 3 discusses the synthesis and structure-property relationships of squaraine-based dimers with different linkers, oligomers, and their application for organic optics and electronics.

Chapter 4 studies heavy-atom containing squaraine and phthalocyanine dyes for reverse satuarable absorption based optical-limiting and electronic applications such as organic photovoltaic cells

Chapter 5 explores unsymmetrical donor-acceptor type squaraines with various acceptors (anchor groups) through different linkage for dye-sensitized solar cells.

Chapter 6 summarizes the major findings from the research described in this thesis and suggests future directions that may lead to further improvement in solar cells and optical-limiting materials with squaraine moieties.

1.5 References

(1) Law, K.-Y. *Chem. Rev.* **1993**, *93*, 449.

(2) Yagi, S.; Nakazumi, H. *Functional Dyes*; 1st ed.; Elsevier: Oxford, UK, 2006.

(3) Treibs, A.; Jacob, K. *Angew. Chem. Int. Ed.* **1965**, *4*, 694.

(4) Beverina, L.; Salice, P. *Eur. J. Org. Chem.* **2010**, 1207.

(5) Sreejith, S.; Carol, P.; Chithra, P.; Ajayaghosh, A. *J. Mater. Chem.* **2008**, *18*, 264.

(6) Ajayaghosh, A. *Acc. Chem. Res.* **2005**, *38*, 449.

(7) Yasui, S.; Matsuoka, M.; Kitao, T. *Dyes and Pigments* **1988**, *10*.

(8) Mishra, A.; Fischer, M. K. R.; Bäuerle, P. *Angew. Chem. Int. Ed.* **2009**, *48*, 2474.

(9) Terpetschnig, E.; Szmacinski, H.; Lakowicz, J. R. *Anal. Chim. Acta* **1993**, *282*, 633.

(10) Meyers, F.; Chen, C. T.; Marder, S. R.; Brédas, J. L. *Chem. Eur. J.* **1997**, *3*, 530.

(11) Devia, D. G.; Cibina, T. R.; Ramaiahb, D.; Abraham, A. *J. Photochem. Photobiol. B: Biology* **2008**, *92*, 153.

(12) Jisha, V. S.; Arun, K. T.; Hariharan, M.; Ramaiah, D. *J. Phys. Chem. B* **2010**, *114*, 5912.

(13) Chen, C. T.; Marder, S. R.; Cheng, L. T. *J. Am. Chem. Soc.* **1994**, *116*, 3117.

(14) Sameiro, M.; Gonçalves, T. *Chem. Rev.* **2009**, *109*, 190.

(15) Escobedo, J. O.; Rusin, O.; Lim, S.; Strongin, R. M. *Curr. Opin. Chem. Biol.* **2010**, *14*, 64.

(16) Sreejith, S.; Divya, K. P.; Ajayaghosh, A. *Angew. Chem. Int. Ed.* **2008**, *47*, 7883.

(17) Ajayaghosh, A.; Chithra, P.; Varghese, R. *Angew. Chem. Int. Ed.* **2007**, *46*, 230.

(18) Bagnis, D.; Beverina, L.; Huang, H.; Silvestri, F.; Yao, Y.; Yan, H.; Pagani, G. A.; Marks, T. J.; Facchetti, A. *J. Am. Chem. Soc.* **2010**, *132*, 4074.

(19) Mayerhöffer, U.; Deing, K.; Gruß, K.; Braunschweig, H.; Meerholz, K.; Würthner, F. *Angew. Chem. Int. Ed.* **2009**, *48*, 8776.

(20) Silvestri, F.; Irwin, M. D.; Beverina, L.; Facchetti, A.; Pagani, G. A.; Marks, T. J. *J. Am. Chem. Soc.* **2008**, *130*, 17640.

(21) Wang, S.; Mayo, E. I.; Perez, M. D.; Griffe, L.; Wei, G.; Djurovich, P. I.; Forrest, S. R.; Thompson, M. E. *Appl. Phys. Lett.* **2009**, *94*, 233304.

(22) Woobkenberg, P. H.; Labram, J. G.; Swiecicki, J.-M.; Parkhomenko, K.; Sredojevic, D.; Gisselbrecht, J.-P.; Leeuw, D. M. d.; Bradley, D. D. C.; Djukic, J.-P.; Anthopoulos, T. D. *J. Mater. Chem.* **2010**, *20*, 3673.

(23) Smits, E. C. P.; Setayesh, S.; Anthopoulos, T. D.; Buechel, M.; Nijssen, W.; Coehoorn, R.; Blom, P. W. M.; de Boer, B.; de Leeuw, D. M. *Adv. Mater.* **2007**, *19*, 734.

(24) Scherer, D.; Dorfler, R.; Feldner, A.; Vogtmann, T.; Schwoerer, M.; Lawrentz, U.; Grahn, W.; Lambert, C. *Chem. Phys.* **2002**, 179.

(25) Chung, S.-J.; Zheng, S.; Odani, T.; Beverina, L.; Fu, J.; Padilha, L. A.; Biesso, A.; Hales, J. M.; Zhan, X.; Schmidt, K.; Ye, A.; Zojer, E.; Barlow, S.; Hagan, D. J. W.; Van Stryland, E.; Yi, Y.; Shuai, Z.; Pagani, G. A.; Brédas, J.-L.; Perry, J. W.; Marder, S. R. *J. Am. Chem. Soc.* **2006**, *128*, 14444.

(26) Cohen, S.; Lacher, J. R.; Park, J. D. *J. Am. Chem. Soc.* **1959**, *81*, 3480.

(27) West, R.; Niu, H. Y.; Powell, D. L.; Evans, M. V. *J. Am. Chem. Soc.* **1960**, *82*, 6204.

(28) Ito, M.; West, R. *J. Am. Chem. Soc.* **1963**, *85*, 2580.

(29) Ziegenbein, W.; Sprenger, H. E. *Angew. Chem. Int. Ed.* **1966**, *5*, 893.

(30) Sprenger, H. E.; Ziegenbein, W. *Angew. Chem. Int. Ed.* **1966**, *5*, 894.

(31) Sprenger, H. E.; Ziegenbein, W. *Angew. Chem. Int. Ed.* **1968**, *7*, 530.
(32) Sprenger, H. E.; Ziegenbein, W. *Angew. Chem. Int. Ed.* **1967**, *6*, 553.
(33) Terpetschnig, E.; Lakowicz, J. R. *Dyes and Pigments* **1993**, *21*, 227.
(34) Keil, D.; Hartmann, H. *Dyes and Pigments* **2001**, *49*, 161.
(35) Law, K.-Y.; Bailey, F. C. *J. Org. Chem.* **1992**, *57*, 3278.
(36) Green, B. R.; Neuse, E. W. *Synthesis* **1974**, 46.
(37) Yagi, S.; Hyodo, Y.; Matsumoto, S.; Takahashi, N.; Kono, H.; Nakazumi, H. *J. Chem. Soc., Perkin Trans. 1* **2000**, 599.
(38) Choi, H.; Kim, J.-J.; Song, K.; Ko, J.; Nazeeruddinc, M. K.; Grätzel, M. *J. Mater. Chem.* **2010**, *20*, 3280.
(39) Ajayaghosh, A. *Chem. Soc. Rev.* **2003**, *32*, 181.
(40) Bigelow, R. W.; Freund, H. J. *Chem. Phys.* **1986**, *107*, 159.
(41) Meier, H.; Dullweber, U. *J. Org. Chem.* **1997**, *62*, 4821.
(42) Meier, H.; Dullweber, U. *Tetrahedron Lett.* **1996**, *37*, 1191.
(43) Meier, H.; Petermann, R.; Gerold, J. *Chem. Commun.* **1999**, 977.
(44) Kamat, P. V.; Das, S.; Thomas, K. G.; Georg, M. V. *J. Phys. Chem.* **1992**, *96*, 195.
(45) Law, K.-Y. *J. Phys. Chem.* **1995**, *99*, 9818.
(46) Göppert-Mayer, M. *Ann. Phys.* **1931**, *401*, 273.
(47) Kaiser, W.; Garrett, C. G. B. *Phys. Rev. Lett.* **1961**, *7*, 229.
(48) Terenziani, F.; Katan, C.; Badaeva, E.; Tretiak, S.; Blanchard-Desce, M. *Adv. Mater.* **2008**, *20*, 4641.
(49) Rumi, M.; Barlow, S.; Wang, J.; Perry, J. W.; Marder, S. R. *Adv. Polym. Sci.* **2008**, *213*, 1.
(50) He, G. S.; Tan, L.-S.; Zheng, Q.; Prasad, P. N. *Chem. Rev.* **2008**, *108*, 1245.
(51) Pawlicki, M.; Collins, H. A.; Denning, R. G.; Anderson, H. L. *Angew. Chem. Int. Ed.* **2009**, *48*, 3244.
(52) Peticolas, W. L. *Annu. Rev. Phys. Chem.* **1967**, *18*, 233.
(53) McClain, W. M. *Acc. Chem. Res.* **1974**, *7*, 129.
(54) Orr, B. J.; Ward, J. F. *Mol. Phys.* **1971**, *20*, 513.
(55) Kogej, T.; Beljonne, D.; Meyers, F.; Perry, J. W.; Marder, S. R.; Brédas, J. L. *Chem. Phys. Lett.* **1998**, *298*, 1.
(56) Rumi, M.; Ehrlich, J. E.; Heikal, A. A.; Perry, J. W.; Barlow, S.; Hu, Z.; McCord-Maughon, D.; Parker, T. C.; Roöckel, H.; Thayumanavan, S.; Marder, S. R.; Beljonne, D.; Brédas, J.-L. *J. Am. Chem. Soc.* **2000**, *122*, 9500.
(57) Albota, M.; Beljonne, D.; Brédas, J.-L.; Ehrlich, J. E.; Fu, J.-Y.; Heikal, A. A.; Hess, S. E.; Kogej, T.; Levin, M. D.; Marder, S. R.; McCord-Maughon, D.; Perry, J. W.; Röckel, H.; Rumi, M.; Subramaniam, G.; Webb, W. W.; Wu, X.-L.; Xu, C. *Science* **1998**, *281*, 1653.

(58) Zojer, E.; Beljonne, D.; Kogej, T.; Vogel, H.; Marder, S. R.; Perry, J. W.; Brédas, J. L. *J. Chem. Phys* **2002**, *116*, 3646.

(59) Rumi, M.; Perry, J. W. *Adv. Opt. Photonics* **2010**, *2*, 451.

(60) Beverina, L.; Crippa, M.; Salice, P.; Ruffo, R.; Ferrante, C.; Fortunati, I.; Signorini, R.; Mari, C. M.; Bozio, R.; Facchetti, A.; Pagani, G. A. *Chem. Mater.* **2008**, *20*, 3242.

(61) Ohira, S.; Rudra, I.; Schmidt, K.; Barlow, S.; Chung, S.-J.; Zhang, Q.; Matichak, J.; Marder, S. R.; Brédas, J.-L. *Chem. Eur. J.* **2008**, *14*, 11082.

(62) Webster, S.; Odom, S. A.; Padilha, L. A.; Przhonska, O. V.; Peceli, D.; Hu, H.; Nootz, G.; Kachkovski, A. D.; Matichak, J.; Barlow, S.; Anderson, H. L.; Marder, S. R.; Hagan, D. J.; Van Stryland, E. W. *J. Phys. Chem. B* **2009**, *113*, 14854.

(63) Odom, S. A.; Webster, S.; Padilha, L. A.; Peceli, D.; Hu, H.; Nootz, G.; Chung, S.-J.; Ohira, S.; Matichak, J. D.; Przhonska, O. V.; Kachkovski, A. D.; Barlow, S.; Brédas, J.-L.; Anderson, H. L.; Hagan, D. J.; Van Stryland, E. W.; Marder, S. R. *J. Am. Chem. Soc.* **2009**, *131*, 7510.

(64) Drobizhev, M.; Stepanenko, Y.; Dzenis, Y.; Karotki, A.; Rebane, A.; Taylor, P. N.; Anderson, H. L. *J. Am. Chem. Soc.* **2004**, *126*, 15352.

(65) Drobizhev, M.; Stepanenko, Y.; Dzenis, Y.; Karotki, A.; Rebane, A.; Taylor, P. N.; Anderson, H. L. *J. Phys. Chem. B* **2005**, *109*, 7223.

(66) Drobizhev, M.; Stepanenko, Y.; Rebane, A.; Wilson, C. J.; Screen, T. E. O.; Anderson, H. L. *J. Am. Chem. Soc.* **2006**, *128*, 12432.

(67) Kippelen, B.; Brédas, J. L. *Energy Environ. Sci.* **2009**, *2*, 251.

(68) Zhan, X.; Zhu, D. *Polym. Chem.* **2010**, *1*, 409.

(69) Günes, S.; Neugebauer, H.; Sariciftci, N. S. *Chem. Rev.* **2007**, *107*, 1324.

(70) Thompson, B. C.; Fréchet, J. M. J. *Angew. Chem. Int. Ed.* **2008**, *47*, 58.

(71) Darling, S. B. *Energy Environ. Sci.* **2009**, *2*, 1266.

(72) Grätzel, M. *Acc. Chem. Res.* **2009**, *42*, 1788.

(73) Ohkita, H.; Cook, S.; Astuti, Y.; Duffy, W.; Tierney, S.; Zhang, W.; Heeney, M.; McCulloch, I.; Nelson, J.; Bradley, D. D. C.; Durrant, J. R. *J. Am. Chem. Soc.* **2008**, *130*, 3030.

(74) Shoaee, S.; Clarke, T. M.; Huang, C.; Barlow, S.; Marder, S. R.; Heeney, M.; McCulloch, I.; Durrant, J. R. *J. Am. Chem. Soc.* **2010**, *132*, 12919.

(75) Shoaee, S.; An, Z. S.; Zhang, X.; Barlow, S.; Marder, S. R.; Duffy, W.; Heeney, M.; McCulloch, I.; Durrant, J. R. *Chem Commun* **2009**, 5445.

(76) Merritt, V. Y.; Hovel, H. J. *Appl. Phys. Lett.* **1976**, *29*, 414.

(77) Bondi, A. *J. Phys. Chem.* **1964**, *68*, 441.

(78) Wei, G.; Wang, S.; Renshaw, K.; Thompson, M. E.; Forrest, S. R. *ACS Nano* **2010**, *4*, 1927.

(79) Li, N.; Lassiter, B. E.; Lunt, R. R.; Wei, G. D.; Forrest, S. R. *Appl. Phys. Lett.* **2009**, *94*, 023307.

(80) Silvestri, F.; López-Duarte, I.; Seitz, W.; Beverina, L.; Martıínez-Díaz, M. V.; Marks, T. J.; Guldi, D. M.; Pagani, G. A.; Torres, T. *Chem. Commun.* **2009**, 4500.

(81) O'Regan, B.; Grätzel, M. *Nature* **1991**, *353*, 737.

(82) Nusbaumer, H.; Zakeeruddin, S. M.; Moser, J.-E.; Grätzel, M. *Chem. Eur. J.* **2003**, *9*, 3756.

(83) Zhang, Z.; Chen, P.; Murakami, T. N.; Zakeeruddin, S. M.; Grätzel, M. *Adv. Funct. Mater.* **2008**, *18*, 341.

(84) Grätzel, M. *J. Photochem. Photobiol. C: Photochem. Rev.* **2003**, *4*, 145.

(85) Chiba Y, I. A., Wanatabe Y, Komiya R, Koide N, Han L. *Jpn. J. Appl. Phys.* **2006**, *45*, 638.

(86) Cao, Y.; Bai, Y.; Yu, Q.; Cheng, Y.; Liu, S.; Shi, D.; Gao, F.; Wang, P. *J. Phys. Chem. C* **2009**, *113*, 6290.

(87) Hagfeldt, A.; Boschloo, G.; Sun, L.; Kloo, L.; Pettersson, H. *Chem. Rev.* **2010**, *110*, 6595.

(88) Zhao, W.; Hou, Y. J.; Wang, X. S.; Zhang, B. W.; Cao, Y.; Yang, R.; Wang, W. B.; Xiao, X. R. *Sol. Energ. Mat. Sol. C* **1999**, *58*, 173.

(89) Alex, S.; Santhosh, U.; Das, S. *J. Photochem. Photobiol. A: Chemistry* **2005**, *172*, 63.

(90) Otsuka, A.; Funabiki, K.; Sugiyama, N.; Yoshida, T.; Minoura, H.; Matsui, M. *Chem. Lett.* **2006**, *35*, 666.

(91) Burke, A.; Schmidt-Mende, L.; Ito, S.; Grätzel, M. *Chem. Commun.* **2007**, 234.

(92) Zhang, G.; Bala, H.; Cheng, Y.; Shi, D.; Lv, X.; Yu, Q.; Wang, P. *Chem. Commun.* **2009**, 2198.

(93) Choi, H.; Baik, C.; Kang, S. O.; Ko, J.; Kang, M.-S.; Nazeeruddin, M. K.; Grätzel, M. *Angew. Chem. Int. Ed.* **2008**, *47*, 327.

(94) Zeng, W.; Cao, Y.; Bai, Y.; Wang, Y.; Shi, Y.; Zhang, M.; Wang, F.; Pan, C.; Wang, P. *Chem. Mater.* **2010**, *22*, 1915.

(95) Hara, K.; Dan-oh, Y.; Kasada, C.; Ohga, Y.; Shinpo, A.; Suga, S.; Sayama, K.; Arakawa, H. *Langmuir* **2004**, *20*, 4205.

(96) Ning, Z.; Fu, Y.; Tian, H. *Energy Environ. Sci.* **2010**, *3*, 1170.

(97) Yum, J.-H.; Walter, P.; Huber, S.; Rentsch, D.; Geiger, T.; Nüesch, F.; Angelis, F. D.; Grätzel, M.; Nazeeruddin, M. K. *J. Am. Chem. Soc.* **2007**, *129*, 10320.

(98) Geiger, T.; Kuster, S.; Yum, J.-H.; Moon, S.-J.; Nazeeruddin, M. K.; Grätzel, M.; Nüesch, F. *Adv. Funct. Mater.* **2009**, *19*, 2720.

(99) Kuster, S.; Sauvage, F.; Nazeeruddin, M. K.; Grätzel, M.; Nüesch, F. A.; Geiger, T. *Dyes and Pigments* **2010**, *87*, 30.

(100) Beverina, L.; Ruffo, R.; Mari, C. M.; Pagani, G. A.; Sassi, M.; Angelis, F. D.; Fantacci, S.; Yum, J.-H.; Grätzel, M.; Nazeeruddin, M. K. *Chemsuschem* **2009**, *2*, 621.

(101) Inouea, T.; Pandeya, S. S.; Fujikawaa, N.; Yamaguchib, Y.; Hayasea, S. *J. Photochem. Photobiol. A: Chemistry* **2010**, *213*, 23.

(102) Mor, G. K.; Kim, S.; Paulose, M.; Varghese, O. K.; Shankar, K.; Basham, J.; Grimes, C. A. *Nano Lett.* **2009**, *9*, 4250.

(103) Choi, H.; Kim, S.; Kang, S. O.; Ko, J.; Kang, M.-S.; Clifford, J. N.; Forneli, A.; Palomares, E.; Nazeeruddin, M. K.; Grätzel, M. *Angew. Chem. Int. Ed.* **2008**, *47*, 8259.

(104) Clifford, J. N.; Palomares, E.; Nazeeruddin, M. K.; Thampi, R.; Grätzel, M.; Durrant, J. R. *J. Am. Chem. Soc.* **2004**, *126*, 5670.

(105) McEwen, J. J.; Wallace, K. J. *Chem. Commun.* **2009**, 6339.

(106) Ajayaghosh, A.; Arunkumar, E.; Daub, J. *Angew. Chem. Int. Ed.* **2002**, *41*, 1766.

(107) Arunkumar, E.; Chithra, P.; Ajayaghosh, A. *J. Am. Chem. Soc.* **2004**, *126*, 6590.

(108) Yagi, S.; Hyodo, Y.; Hirose, M.; Nakazumi, H.; Sakurai, Y.; Ajayaghosh, A. *Org. Lett.* **2007**, *9*, 1999.

(109) Nakazumi, H.; Ohta, T.; Etoh, H.; Uno, T.; Colyer, C. L.; Hyodo, Y.; Yagi, S. *Synt. Met.* **2005**, *153*, 33.

(110) Brédas, J. L.; Street, G. B. *Acc. Chem. Res.* **1985**, *18*, 309.

(111) Roncali, J. *Chem. Rev.* **1997**, *97*, 173.

(112) Van Mullekom, H. A. M.; Vekeman, J. A. J. M.; Havinga, E. E.; W., M. E. *Mater. Sci. Eng.* **2001**, *32*, 1.

(113) Eldo, J.; Arunkumar, E.; Ajayaghosh, A. *Tetrahedron Lett.* **2000**, *41*, 6241.

(114) Ajayaghosh, A.; Eldo, J. *Org. Lett.* **2001**, *3*, 2595.

(115) Eldo, J.; Ajayaghosh, A. *Chem. Mater.* **2002**, *14*, 410.

(116) Huang, Z. *Technol. Cancer Res. Treat.* **2005**, *4*, 283.

(117) Wilson, B. C.; Patterson, M. S. *Phys. Med. Biol.* **2008**, *53*, R61.

(118) Santos, P. F.; Reis, L. V.; Duarte, I.; Serrano, J. P.; Almeida, P.; Oliveira, A. S.; Ferreira, L. F. V. *HeIv. Chim. Acta* **2005**, *88*, 1135.

(119) Arunkumar, E.; Sudeep, P. K.; Kamat, P. V.; Noll, B. C.; Smith, B. D. *New J. Chem.* **2007**, *31*, 677.

(120) Santos, P. F.; Reis, L. V.; Almeida, P.; Serrano, J. P.; Oliveira, A. S.; Vieira Ferreira, L. F. *J. Photochem. Photobiol., A* **2004**, *163*, 267.

(121) Santos, P. F.; Reis, L. V.; Almeida, P.; Oliveira, A. S.; Vieira Ferreira, L. F. *J. Photochem. Photobiol., A* **2003**, *160*, 159.

(122) Webster, S.; Peceli, D.; Hu, H.; Padilha, L. A.; Przhonska, O. V.; Masunov, A. E.; Gerasov, A. O.; Kachkovski, A. D.; Slominsky, Y. L.; Tolmachev, A. I.; Kurdyukov, V. V.; Viniychuk, O. O.; Barrasso, E.; Lepkowicz, R.; Hagan, D. J.; Van Stryland, E. W. *J. Phys. Chem. Lett.* **2010**, *1*, 2354.

(123) Bosman, A. W.; Janssen, H. M.; Meijer, E. W. *Chem. Rev.* **1999**, *99*, 1665.

(124) Hecht, S.; Fréchet, J. M. J. *Angew. Chem. Int. Ed.* **2001**, *40*, 74.

(125) Grayson, S. M.; Fréchet, J. M. J. *Chem. Rev.* **2001**, *101*, 3819.

(126) Wong, W.-Y.; Ho, C.-L. *Acc. Chem. Res.* **2010**, *43*, 1246.

(127) Wong, W.-Y.; Harvey, P. D. *Macromol. Rapid Commun.* **2010**, *31*, 671.
(128) Eloi, J.-C.; Chabanne, L.; Whittell, G. R.; Manners, I. *Materials Today* **2008**, *11*, 28.

Chapter 2: Synthesis, Two-photon Absorption and Optical-power Limiting Properties of Squaraines with Extended Conjugation

2.1 Introduction

Since the development of high-intensity laser light sources in 1960s,[1] rapid advances in related technology have resulted in the ubiquitous use of lasers in everyday life, for example, in CD players, inventory scanners, and laser pointers. The materials and techniques to protect optical sensors, photoelectric devices, and human eyes (the maximum permissible exposure for human eyes to nanosecond pulses in the visible region is less than 0.2 $\mu J)^2$ against high intensity lasers including those applied in laboratory research and military laser weapons,[3] are highly desirable. An optical-power limiter is a device that employs materials that are transparent under ordinary ambient light, but strongly attenuate intense laser beams and limit the transmittance under high-intensity illumination, as illustrated in Figure 2.1. The nonlinear behavior of optical-power limiting (OPL) materials originates from their intrinsic photophysical properties, rather than from any external electronic or mechanical control mechanism. Inorganic nanoparticles,[4-6] carbon nanotubes and nanotube composites,[7,8] fullerenes,[9,10] organometallic complexes,[11-13] and organic molecules with highly delocalized π-electron systems such as porphyrin and phthalocyanine derivatives[2,14-17] have been shown to exhibit excellent OPL responses at certain wavelengths.

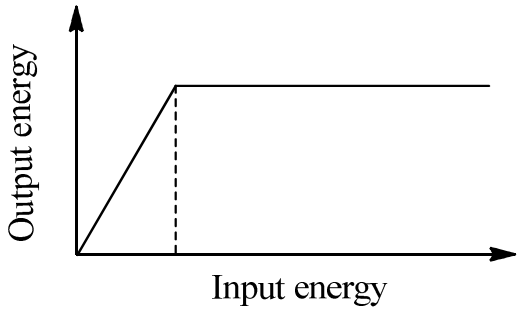

Figure 2.1: Ideal behavior of an optical-power limiter.

Nonlinear absorption is one of the main mechanisms for OPL. Optical limiters based on organic conjugated materials utilizing the nonlinear absorption mechanism can exhibit fast response times. In addition, they utilize materials that can potentially be processing, and are amenable to structural modifications, allowing them to be tuned for use in different wavelength ranges.[2,14,18,19] One-photon absorption (1PA) and two-photon absorption (2PA) initiated excited-state absorption (ESA) form the basis of many approaches for nonlinear absorption mechanism for optical-power suppression. Under illumination, a molecule in its ground singlet-state S_0 is excited by absorbing a photon (1PA in Figure 2.2) to a high vibrational level of excited singlet-state S_1 or absorbing two photons (2PA in Figure 2.2) to a higher excited singlet-state S_n. The molecule at higher excited-states can quickly relax back to its lowest excited-state via internal conversion (IC), which may undergo intersystem crossing to the lower energy triplet-state T_1. Another photon at the same wavelength may be absorbed by the molecule from S_1 to S_n, or from T_1 to T_n. If a significant population has been accumulated at the excited-state and the ESA cross-section (σ_{ex}) is larger than the ground-state absorption cross-section (σ_0), the molecular effective absorption coefficient increases. This effect, where the transmittance of the materials decreases at high intensity of light, is known as reverse

saturable absorption (RSA). This process is illustrated in Figure 2.2[21]

Thus, the ratio of effective cross-section σ_{ex}/σ_0 is a very important parameter to evaluate RSA materials. Since the transmittance change for a material and damage to optical devices are fluence (Jcm^{-2}) dependent, the threshold fluence is also used in many cases to quantify and compare OPL efficiency, which is defined as the fluence at which the transmission decreases to half of its linear value. Other parameters such as saturation fluence and figure-of-merit (the ratio of linear transmittance to final transmittance) are sometimes reported in literature as well.[2]

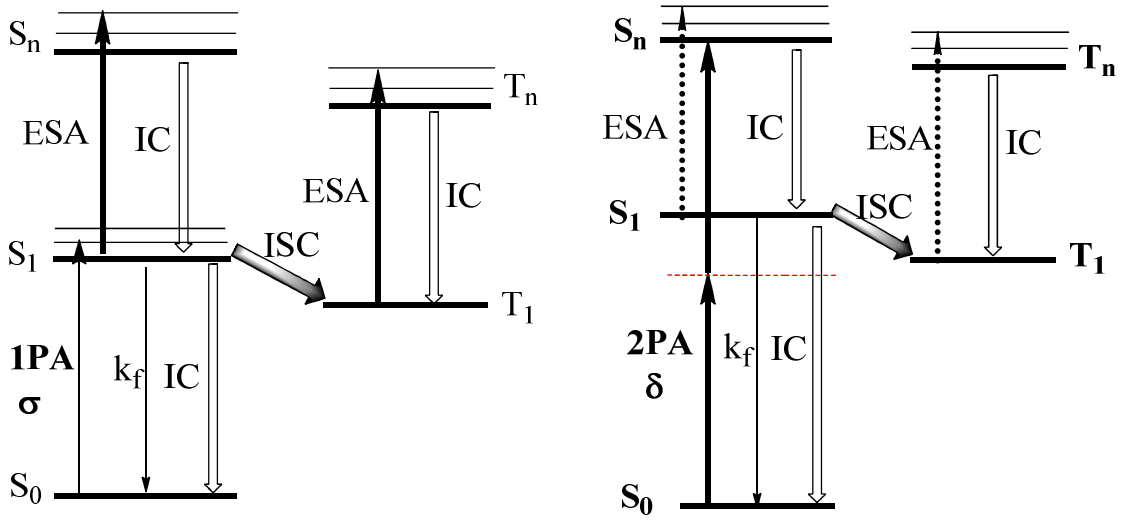

Figure 2.2: Simplified Jablonski diagram for optical-power limiting (OPL) by either 1PA or 2PA. Shown are the excited-state absorption (ESA), internal conversion (IC), and intersystem crossing (ISC).

The criteria for a good optical limiter include limiting over a wide wavelength range with good transparency to ambient light to maintain high beam quality. For one-photon induced RSA, significant ground-state absorption is required to lead to a sufficient excited-state population from which further absorption can occur. Hence, 2PA appears an attractive mechanism to give excellent transparency since no linear absorption

is required. Although, 2PA itself is a nonlinear absorption process, at present, the 2PA cross-sections of materials are not sufficient large to give a high effective absorption coefficient and low limiting threshold. The combination of 2PA and subsequent ESA is more practical in that further suppression could be realized by cycling between ESA and internal conversion after a 2PA process. To achieve efficient OPL, some important features need to be fulfilled as following: large 2PA cross-section, small 1PA cross-section at 2PA wavelength, large excited-state cross-section at the same wavelength, long-lived excited-state species compared to the pulse width. For longer pulse lengths, use of excited-state triplet-triplet absorption is an attractive approach for optical limiting. This approach requires a high triplet quantum yield (facilitated by fast intersystem crossing (ISC) from S_1 to T_1 than IC from S_1 to S_0), and long triplet lifetime (slow ISC from T_1 to S_0). Other criteria that also need to be taken into consideration for practical applications include fast response times, broad spectral bandwidth for limiting, and a high damage threshold as well as facile process of the materials into high optical quality films.

Many 2PA dyes exhibit strong ESA at similar photon wavelength to their 2PA peaks which are quite promising for OPL. Prasad and co-workers investigated the OPL behavior of several organic compounds in solution at 602 nm with 0.5 ps laser pulse and their two-photon absorption properties.[22] Based on the assumption that 2PA is the only predominant mechanism response for the OPL without considering induced scattering, refraction and thermal lens effects, the transmittance can be expressed as in Equation (1)[22]

$$T = I / I_0 = [\ln(1 + I_0 L\beta)]/I_0 L\beta \qquad (1)$$

where I_0 is the incident intensity, L is the path length of the beam through the sample, β is the 2PA coefficient. The molecular 2PA cross-section δ (in units of cm^4/GW) can be calculated from the 2PA coefficient β (in units of cm/GW) with Equation (2)[23]

$$\delta = \frac{1000\beta}{N_A C} \qquad (2)$$

where N_A is Avogadro's number, C is the sample concentration (in units of mol/L).

Perry and co-workers studied the nonlinear absorption of 4,4'-bis(di-*n*-butylamino)stilbene (DBBAS) and 4,4'-bis(diphenylamino)stilbene (DBPAS) in the nanosecond regime and found that it is a two-step processes of an initial 2PA followed by ESA.[23] The substantial pulse-width dependence of 2PA was much smaller for picosecond pulses than nanosecond pulses and further picosecond pump-probe measurements and nanosecond transient absorption measurements confirmed the presence of two-photon-induced ESA. Even so, for OPL experiments in nanosecond regime, approximate fitting with an effective 2PA coefficient β_{eff} or 2PA cross-section δ_{eff} have been adopted in many practical cases.[24-27]

2.2 Motivation and molecule design

Large 2PA cross-sections in the near infrared (IR) region have been achieved with a series of π-extended bis(donor)-substituted squaraine chromophores with peak performances at photon wavelengths of ca. 1 μm, shown in Figure 2.3.[28] From the central squarylium acceptor, the conjugation was extended through alternating vinylene unites and electron-rich heterocycles.

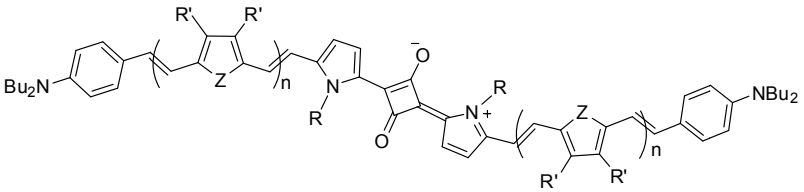

1: R = ^{n}hex, n = 0, δ_{max} = 27 000 GM at 960 nm
2a: R = ^{n}hex, n = 1, Z = S, R' = O^{n}Bu, δ_{max} = 18 000 GM at 1100 nm
2b: R = $CH_2CH(n\text{-}C_{10}H_{21})\text{-}n\text{-}C_{12}H_{25}$, n = 1, Z = S, R' = O^{n}Bu
3: R = ^{n}hex, n = 1, Z = N^{n}hex, R' = H, δ_{max} = 33 000 GM at 1050 nm

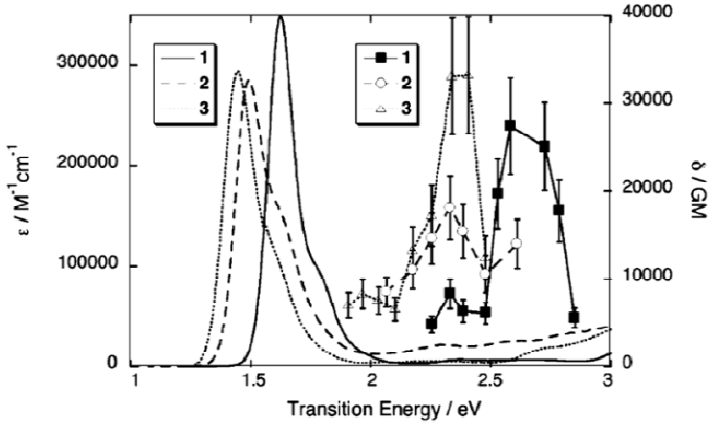

Figure 2.3: Chemical structures, 1PA (lines) and degenerate (z-scan) 2PA (data points and lines) spectra for 1 in CH_2Cl_2 and for 2a and 3 in THF.[28] Reprinted with permission from ref 28. Copyright 2006 American Chemical Society.

These squaraine derivatives could be potentially useful for OPL in the near-IR region including the telecommunication wavelength (1300 to 1550 nm). We are particularly interested in protection from high-intensity light-source damage in this region, for sensor protection and telecommunication applications. One of the most commonly used lasers, the Nd:YAG, operate within this region, at a wavelength of 1064 nm and is used in various applications.

To synthesize squaraines with large 2PA cross-sections and good processability which can be used at high concentration solutions or solid-phase materials are the research targets in this chapter. Squaraine **1** to **4** with extended conjugation, as shown in Figure 2.4, were developed. **Sq1** was designed based on a previously made molecule but

in the hope of achieving better processability, i.e. better solubility and film forming properties, with long alkyl chains incorporated into the pyrrole bridge. **Sq2**, as reported in Chung's work[28] is a viscous liquid, which can be integrated into high number density optical quality films for OPL devices, was prepared in relatively large quantity for OPL investigation. Exchanging phenyl rings with less aromatic heterocycles (the resonance energies for benzene, thiophene, and pyrrole are 36, 28.2, and 22.8 kcal/mol, respectively[29]), may allow the tuning of various properties of the squaraine dyes. It may help achieve larger transition dipole moments and bathochromically shift absorption bands by using the less aromatic heterocycles. Previous research on bis(donor)-terminated[30] bis(heterocycles)vinylene have shown that the molecules with bis(pyrrole)vinylene bridge have larger calculated transition dipole moments and smaller detuning energies than the corresponding pyrrole-vinylene bridged chromophores. By studying the electron-transfer-donor strengths and π-donor strengths of various amines, Marder *et. al.*[31] concluded that among the donors investigated, the 4-[bis(4-methoxyphenyl)amino]phenyl groups combines high stability and a reasonably high π-donor strength, while 2-(5-diarylamino)thienyl group is the strongest π-donor, which could be attributed to the reduced aromaticity of thiophene relative to benzene. Bearing these literature evidences on mind, **Sq3** and **Sq4** with bis(pyrrole)vinylene bridge in each donor arm were designed and synthesized. The combination of different donor and bridges were attempeted but the dyes were not obtained with sufficient purity and quantaties due to the stabilities of the precusors and purification difficulties. For example, the dialkylaminothiophene was expected to be a stronger donor but the corresponding phosphonate could not be synthesized under the typical condition as described below.

The attempts to employ π-bridge with three pyrrole-vinylene unit in each donor arm were not succufful due to the highly electron-rich nature of this compound that results in light-sensitivity and low thermal-stablility.

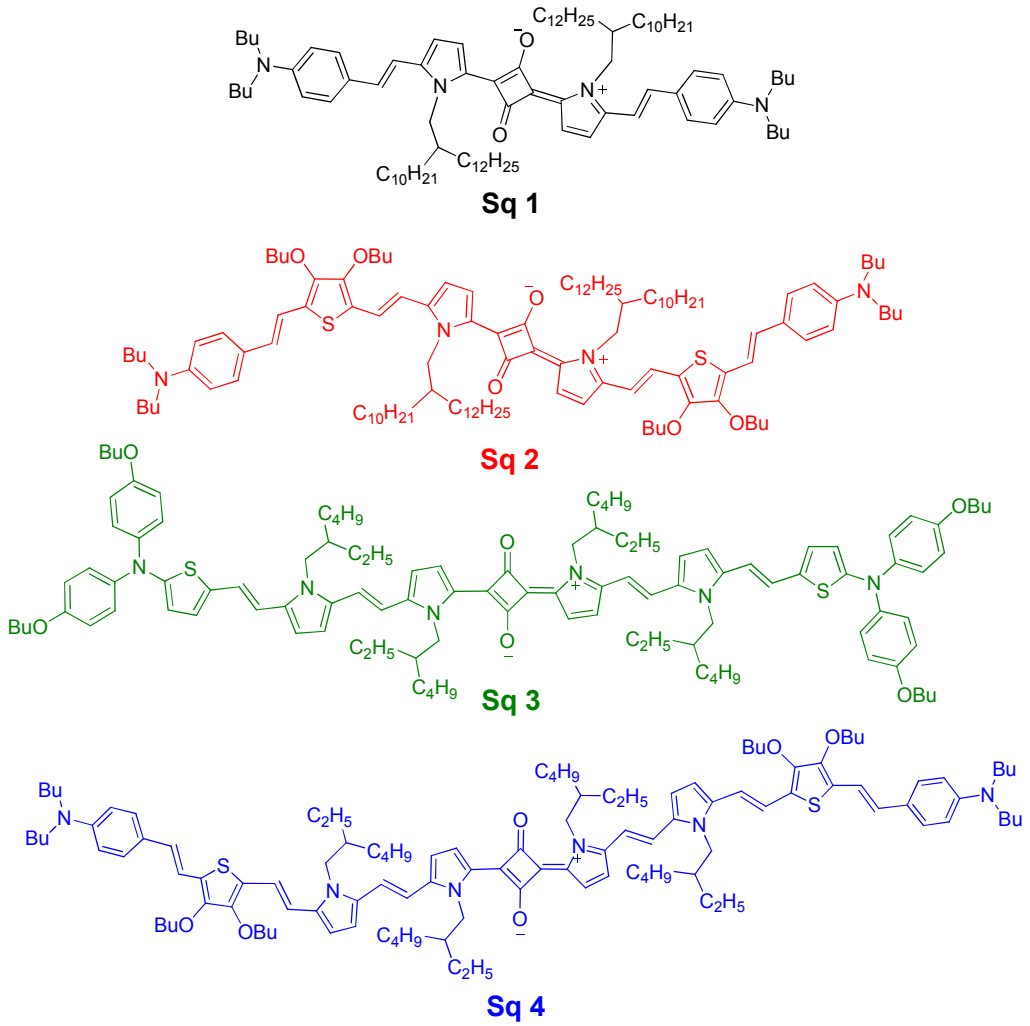

Figure 2.4: Chemical structures of extended squaraines 1 to 4.

For practical applications, high quality optical films with large molecule number densities are required. However, pure materials are often crystalline and aggregate at high concentrations. Scattering and aggregation can broaden the linear absorption bands which lead to a loss of transparency. Blends are a possible solution, but phase separation may occur. One promising approach is to incorporate bulky units into the chromophores that

the steric hindrance limits intermolecular interaction between neighboring molecules.[32,33] As the molecular weight increases of the dendritic generation, the intrinsic viscosity increases,[34] which may allow preparation of thicker films. Here, **G2Sq1** was obtained as an analog of **Sq1** by introducing the second-generation Fréchet type polyether dendron[34] onto the pyrrole nitrogen without interfering with the conjugated backbone as shown in Figure 2.5.

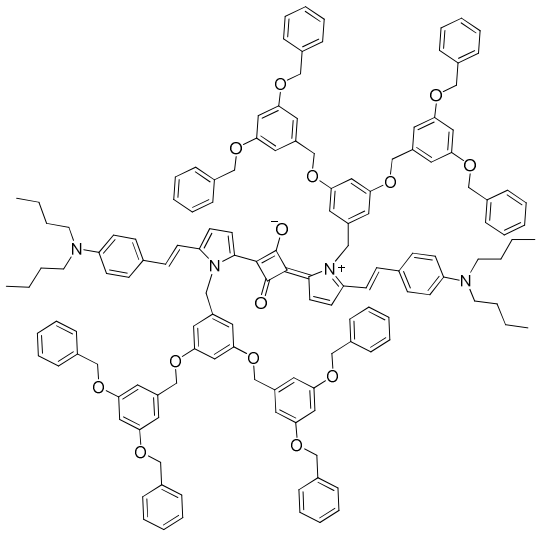

Figure 2.5: Chemical structure of G2Sq1.

2.3 Synthesis of squaraines with extended conjugation

The synthesis of the π-extended squaraines can be divided into three stages: synthesis of the donor phosphonate (Scheme 2.1), formation of the (pyrrole)vinylene bridge (Scheme 2.2), and the final condensation of squaric acid with donor arms (Scheme 2.3).

The donor phosphonate synthesis started from Vilsmeier formylation[35,36] of *N*,*N*-dibutylaniline with dimethylformamide (DMF) and phosphorus oxychloride, followed by reduction with sodium borohydride. Under the modified Arbuzov reaction conditions,[37]

by treatment with triethyl phosphite and one equivalent of iodine at low temperature, the electron-rich benzylic alcohols were converted to the corresponding phosphonate esters in one pot. The conjugated bridge could be further extended by Horner–Wadsworth–Emmons condensation[38,39] with aldehydes. The phosphonate-stabilized carbanions are more nucleophilic than phosphonium ylides,[39] and the phosphate salt by-product is easily removed by aqueous extraction. Since this type of reaction is known to give predominantly *E* isomers,[40] especially for aromatic aldehydes, the double-bonds formed are expected to be in *E* configuration as shown in Figure 2.4, 2.5 and Scheme 2.1, 2.3. The coupling constant of the proton on the vinylene bridge are typically around 15 – 16 Hz in ^{1}H NMR and no evidence of more than one isomer for all the products from this type of reaction were observed in ^{13}C NMR spectra, suggesting that *E*, *Z* and *Z*, *Z* isomers are only present in negligible quantities (< 5%) if at all.

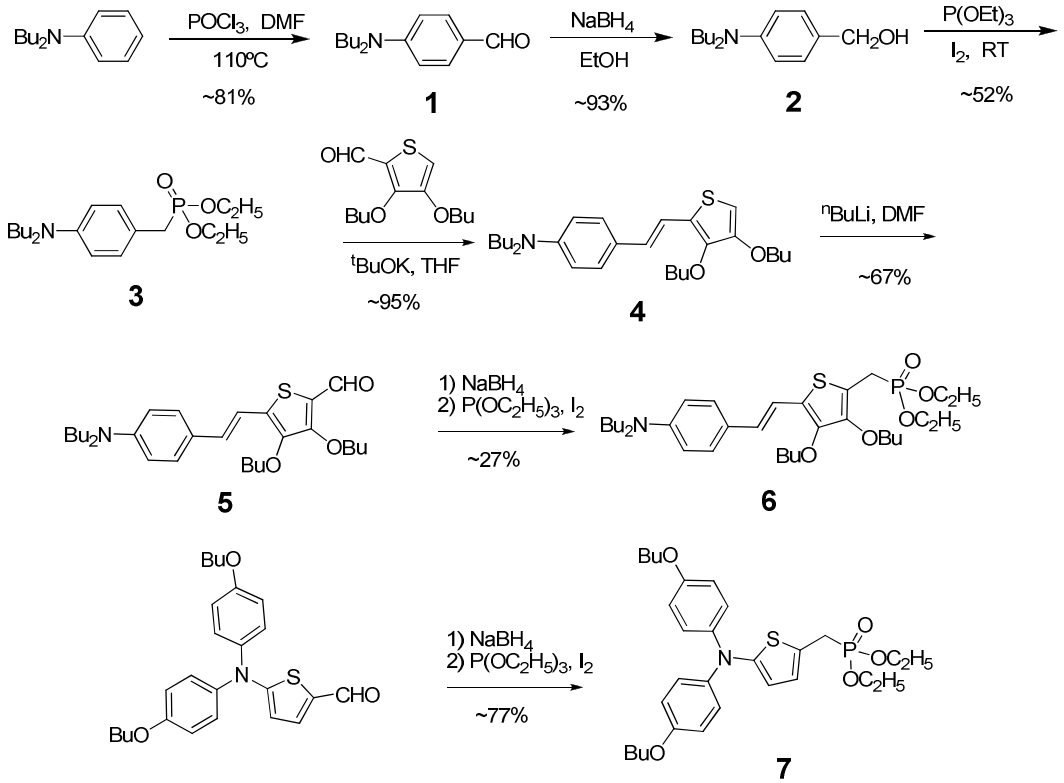

Scheme 2.1: The synthesis of the donor phosphonates.

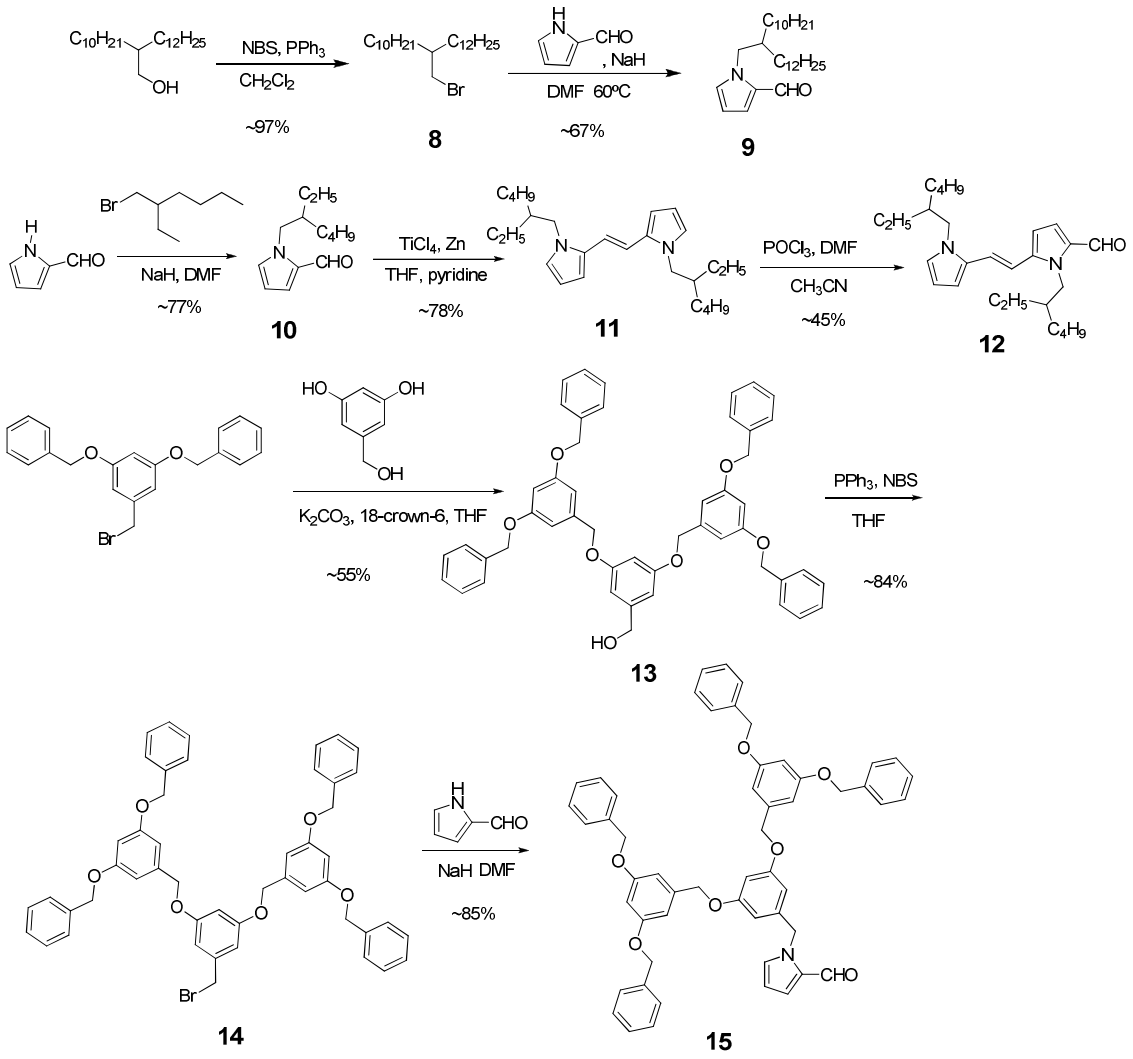

Scheme 2.2: The synthesis of the pyrrole bridges.

The pyrrole-containing bridges were synthesized following the procedure shown in Scheme 2.2. The pyrrole-2-carboxaldehyde **9** and **10** could be simply obtained by alkylation with the corresponding branched alkyl bromide. The McMurry coupling reaction[41] was then applied to afford the vinylene-bridged dipyrrole, which was further formylated to a mono-aldehyde using the Vilsmeier reaction. It was noted that the ratio of the dipyrrole substrate to phosphorus oxychloride and the reaction time are crucial for forming mono-aldehyde instead of the di-aldehyde by-product (the highest yield of ca. 56% for isolated mono-aldehyde was obtained at the ratio of compound **11** : $POCl_3$ = 1 : 0.9

with 1.5 h reaction time). In the case of the dipyrrole with longer decyl-tetradecyl substituents, more than 90% of the dipyrrole was converted to the corresponding di-aldehyde. For **15**, the second-generation dendron was synthesized under the typical conditions in literature[34,42] and then attached to a pyrrole-2-carboxaldehyde.

The condensation to prepare the squaraine dyes were carried out in two-step synthesis as shown in Scheme 2.3. The intermediate compounds are light sensitive and easily oxidized due to their highly electron-rich nature and unprotected pyrrole α-position, resulting in purification challenges. Typically, after flash silica-gel column chromatography, the isolated heterocycle-vinylene compounds were used for condensation with squaric acid directly, during which period water was azeotropically removed by a Dean-Stark trap set-up to push the reaction to completion. The squaraines were then purified by careful column chromatography and, in some cases, recrystallizations from ethanol. In case of squaraine **G2Sq1** with dendrons, the yield was relatively low, which is likely due to the steric hindrance of the bulky substituents that prevent the nucleophilic addition of the pyrrole ring to the carbonyl group of squaric acid.

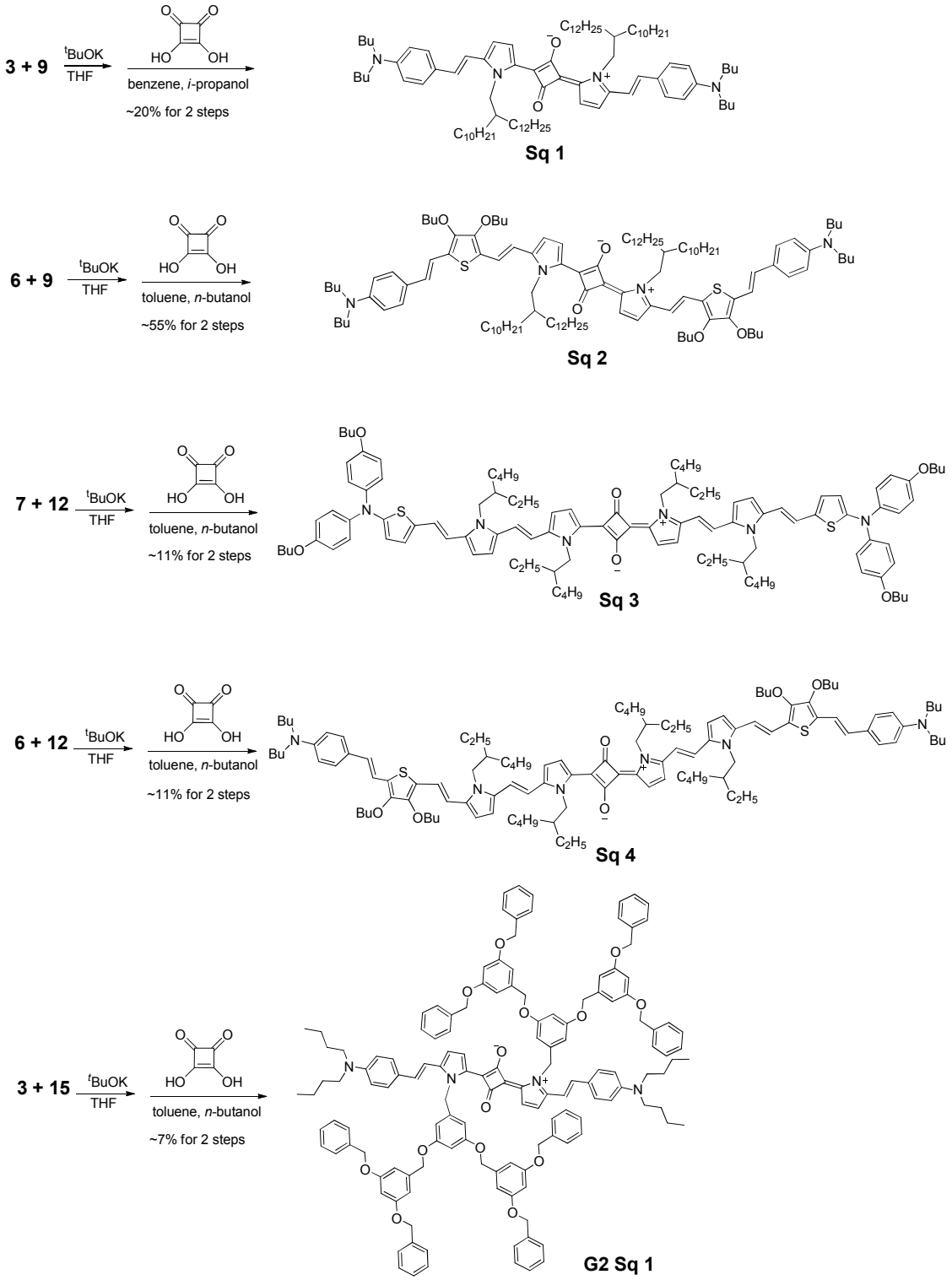

Scheme 2.3: The synthesis of the extended squaraines.

2.4 Optical properties of the squaraines

2.4.1 Linear absorption spectra of Sq1-4

The UV–vis absorption spectra of the four π-extended squaraines in toluene are shown in Figure 2.6. In general, **Sq1-4** exhibit sharp near-IR absorption peaks with small vibronic shoulders and high extinction coefficients, which are characteristics for squaraine dyes.[43,44] With extended conjugation, **Sq2-4** absorb further into the near-IR region with significant bathochromic-shift compared with **Sq1** and the spectra of **Sq2-4** are also somewhat broader. The absorption maximum of **Sq4** is up to λ_{max} = 873 nm, corresponding to a transition energy of 1.42 eV. The absorption maxima and molar absorptivities, along with the transition dipole moments of the first electronic transition, calculated from the absorption spectra, for the four squaraines are summarized in Table 2.1. Large transition dipole moments M_{ge} from the ground-state to the first 1PA allowed electronic state are observed and they increase with conjugation length as goes from **Sq1** to **Sq4**, but may appear to approaching saturation.

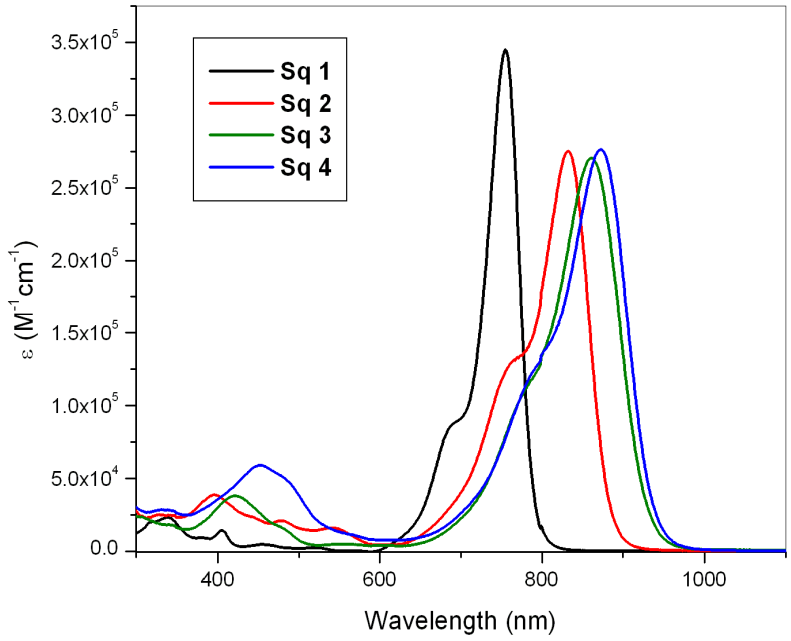

Figure 2.6: Molar absorptivities of Sq1-4 in toluene.

Table 2.1: Optical properties of Sq1-4

	Sq1	Sq2	Sq3	Sq4
λ_{max} (nm)	755	832	861	873
ε_{max} (10^5 $M^{-1}cm^{-1}$)	3.45	2.75	2.70	2.76
M_{ge} (D)	16.8	18.6	19.3	20.0

2.4.2 Two-photon absorption of Sq1-4 and optical-power limiting of Sq1 and Sq2

The non-linear absorption properties of these extended squaraines have been studied in collaboration with the Perry group. The 2PA spectra of **Sq1** were determined by two-photon induced fluorescence (TPIF) in CCl_4 and femtosecond (fs) z-scan measurements in toluene by Dr. Jochen Campo, shown in Figure 2.7. The data obtained from both methods matches resonably well, suggesting a 2PA peak at photon wavelength between 850 – 950 nm, close to the 1PA transition wavelength, with the 2PA cross-section δ over 55 000 GM. The cross-sections obtained here are larger than that reported for an analog of **Sq1** in the previous work,[28] using different solvent could be one of the possible reason that counts for the difference. The high 2PA efficiency could be attributed to the large transition dipole moment M_{ge} and small detuning energy of ca. 0.29 eV, thanks to the sharp linear absorption band that allow the probe window close to the 1PA edge. The other peak, with 2PA cross-section of several hundred GM, locates at photon wavelength around 1400 nm, which assigned to photo-excitation to a state that is close in energy to the 1PA allowed state, as it was predicted by theortical calculation in Chung's work.[28]

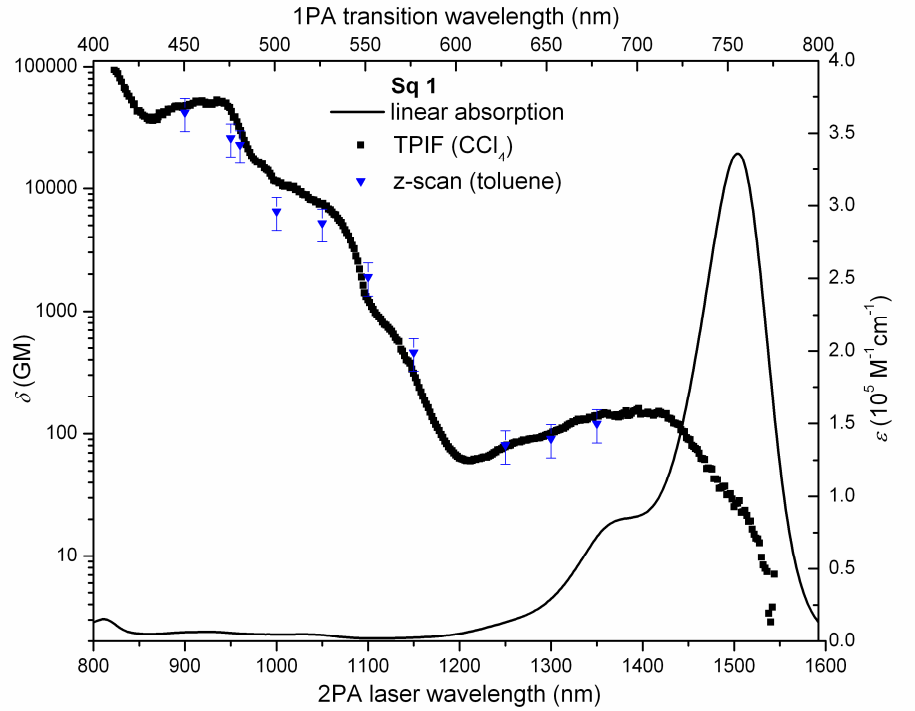

Figure 2.7: 1PA (line), two-photon induced fluorescence (TPIF) excitation spectra (black dots) and degenerate (z-scan) 2PA spectra (blue data points) of Sq1 in solution. (Figure adapted from Dr. Jochen Campo in the Perry group)

The high δ value of **Sq1** in the near-IR especially around the 1PA edge suggests its promising candidacy for OPL in this region. Nanosecond OPL measurements of **Sq1**, in toluene (~3×10^{-2} M), with 1 mm path length show a roughly 4 times suppression (optical suppression determined by (max T_{NL})$^{-1}$) at the excitation wavelength of 850 nm (Figure 2.8). The inset shows the data plotted using the output energy vs. the input energy. This significant deviation from linear response indicates a strong attenuation of the laser beam. However, despite of its long branched side-chain, **Sq1** is a red crystalline solid with metallic luster, which suggests preparation of thick films with sufficient quality may be challenging and thus limits its further application for practical uses.

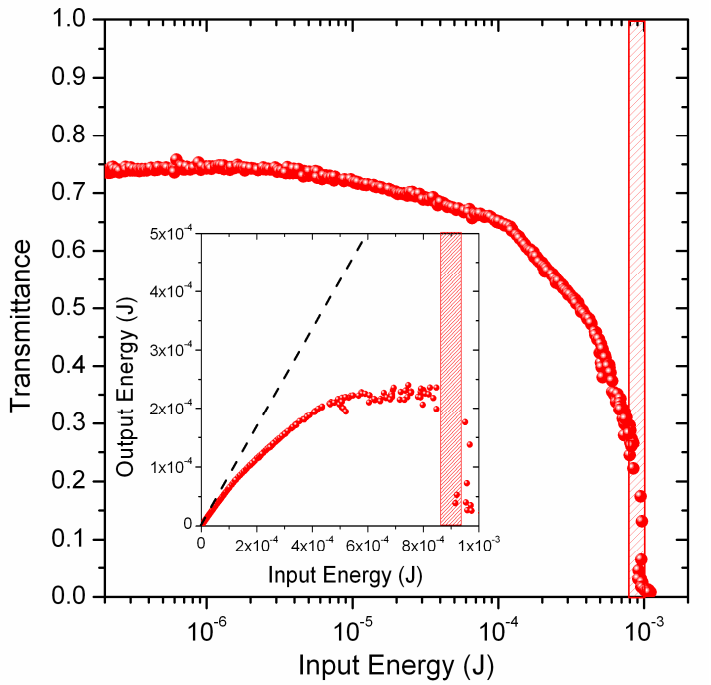

Figure 2.8: Nanosecond optical-power limiting (OPL) of Sq1 in toluene with 1 mm path length at 850 nm. The inset is plot using output energy vs. input energy (the dashed line indicates a linear response). (Figure adapted from Dr. Sarah Chi and Joel Hales in the Perry group)

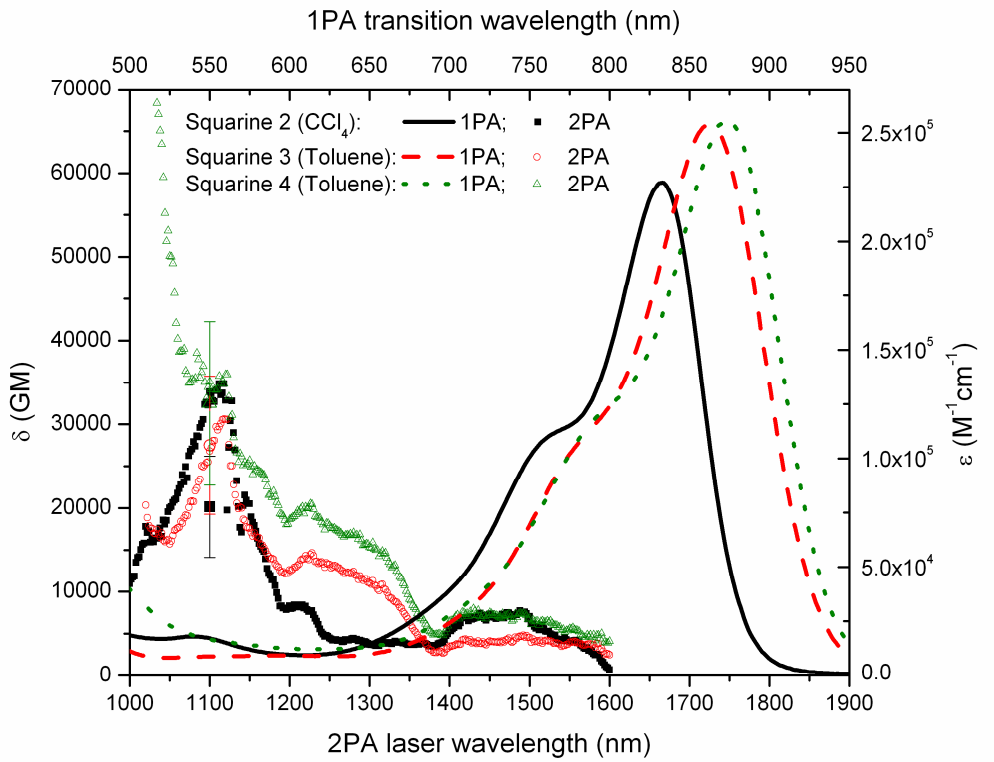

Figure 2.9: 1PA (line), TPIF excitation spectra (data points) and z-scan (data points with error bars) of Sq2-4. (Figure adapted from Dr. Jochen Campo in the Perry group)

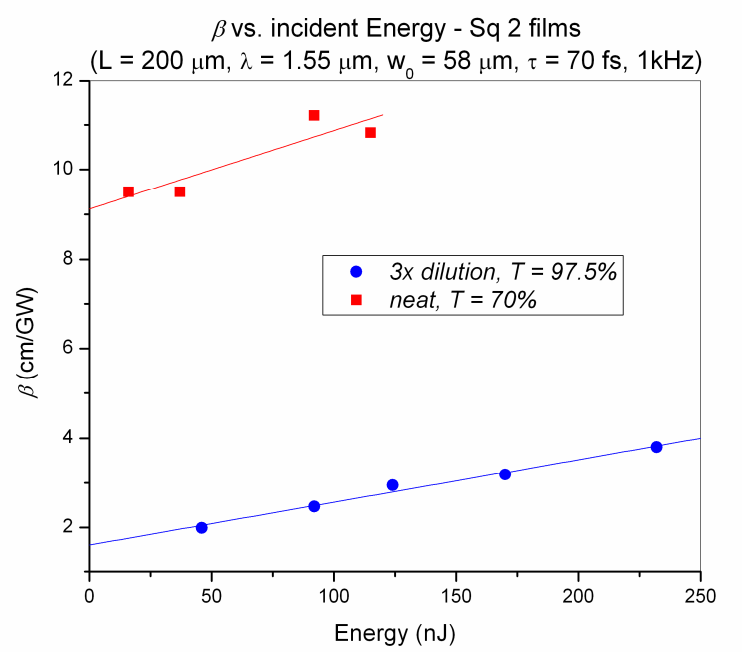

Figure 2.10: Effective 2PA coefficient β measurements (z-scan) of Sq2: 200-μm neat film (~5.6 × 10^{-1} M) and 3 times diluted toluene solution (~1.9 × 10^{-1} M). (Figure adapted from Dr. Sarah Chi and Joel Hales in the Perry group)

Sq2 is a highly soluble, liquid-like squaraine, which permits facile processing of high optical quality films consisting of neat material. The 2PA profile in CCl_4 was explored using TPIF methods with peak performance around 1100 nm, shown in Figure 2.9. The non-linear absorption behavior of **Sq2** films with various thickness and concentrated toluene solutions were further investigated in the telecommunication wavelengths. A 200-μm neat films (concentration was estimated to be ~5.6 × 10^{-1} M) as well as a 200-μm cell consisting of highly concentrated solutions (3 times dilution with toluene, ~1.9 × 10^{-1} M) show good transparency in 1540-1630 nm range. Femtosecond open aperture z-scan measurements at 1550 nm reveal a roughly three times enhancement of 2PA for the 200-μm neat film compared with the 3 times diluted toluene solution, consistent with increase in number density. However, values of the 2PA coefficient β scale linearly with irradiance irrespective of concentration and thickness of **Sq2** samples,

shown in Figure 2.10, suggesting 2PA-induced excited-state absorption. Femtosecond OPL measurements, at a low repetition rate (50 Hz), to reduce thermal effect, on the 200-μm neat film and 3 times diluted solution cell both show more than 10 times suppression at 1550 nm (Figure 2.11). The suppression was as large as 25 times when using a smaller laser spot size. Nanosecond optical limiting measurement was applied on the 200-μm film and 10 mm-path solution as well, however, less significant power suppressions were detected.

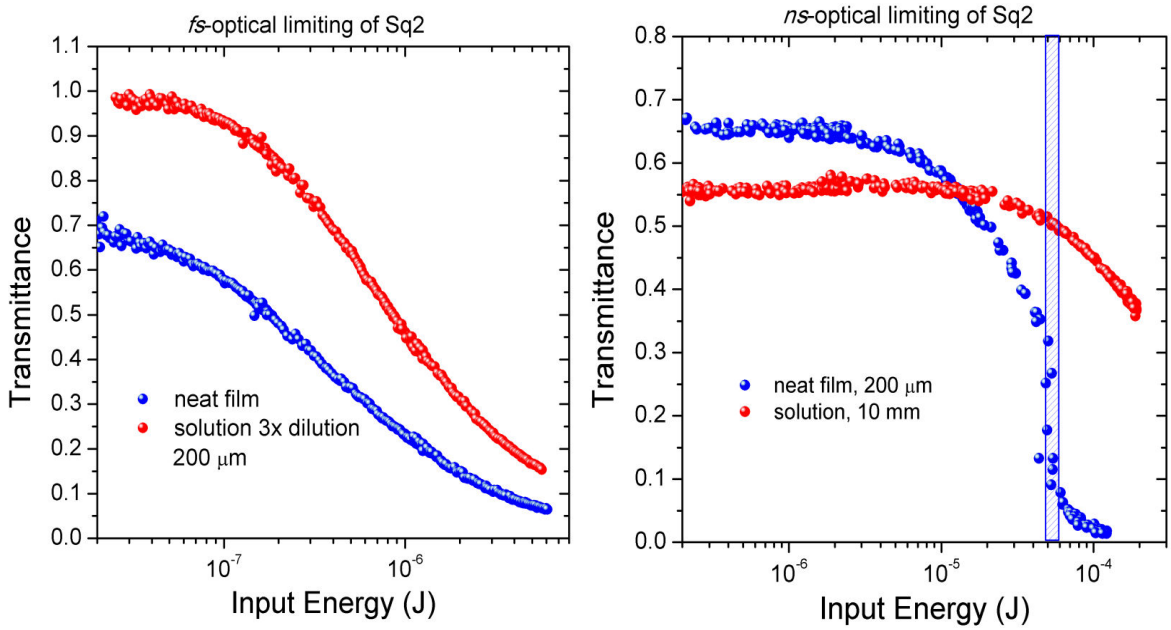

Figure 2.11: Femtosecond and nanosecond optical limiting measurements of Sq2: 200-μm neat film (~5.6 × 10^{-1} M) and 3 times diluted toluene solution (~1.9 × 10^{-1} M). (Figure adapted from Dr. Sarah Chi and Joel Hales in the Perry group)

The 2PA-induced fluorescence excitation spectra of **Sq3** and **Sq4** were measured in toluene solution due to the stability issue in CCl_4. The spectra are quite similar to **Sq2** with 2PA cross-section maxima over 30 000 GM. Z-scan at a single wavelength in the vicinity of the two-photon absorption peak for **Sq3** and **Sq4** gave reasonable agreement with the TPIF data. In the wavelengths between 1100 nm and 1400 nm, the 2PA cross-

sections significantly increase from **Sq2** to **Sq3** and **Sq4**, correlating with extended conjugation length. The high 2PA efficiencies of **Sq3** and **Sq4** over a broad spectrum range indicate these materials may be promising candidates for wide-window optical limiters.

2.4.3 Transient absorption measurements of Sq1-4

Transient absorption spectroscopy was performed on **Sq1-4** toluene solutions by Dr. Jochen Campo in the Perry group to study the photo-induced process and ESA contribution to the OPL response. For all the four compounds, upon pumping at near the linear absorption peak with femtosecond laser pulses, there was no significant signal collected by the detector in the visible region except ground-state bleaching. Signals in Figure 2.12 and Figure 2.13 were generated upon excitation of **Sq1** and **Sq2**, respectively, and collected with a near-IR probe. The transient spectra shortly after photo-excitation (< 180 fs) show the ESA spectrum of **Sq1** centered at around 1240 nm and the spectra at later time intervals show the growth of the peak and decay after around 2 ns with the estimated lifetime of ca. 800 ps. The negative peak at around 900 nm could be attributed to stimulated emission. The negligible ESA at 850 nm, where the OPL measurements were performed, suggests its OPL response may mainly come from pure 2PA contribution. The transient spectra are quite different for **Sq2** with a fast growth of peak at 950 nm and broad transient absorption around 1500 nm along with the ground-state bleaching, which is not seen in the case of **Sq1** because its ground-state absorption is out of the probe range. By calculating sum of the transition energy of the ESA peak at 1550 nm and the ground-state absorption peak, one can expect a 2PA-allowed state with

transition energy corresponding to 2PA photon wavelength of 1100 nm which gives good agreement with the 2PA data obtained from TPIF. The strong transient signals at 1550 nm is consistent with the observed intensity-depended β, suggesting the ESA of **Sq2** is contributing to the OPL response. Unlike the transient peaks of **Sq1**, the signals for **Sq2** rapidly decayed within 100 ps with the excited-state lifetime of ca. 45 ps, which is consistent with its weaker power suppression in nanosecond OPL measurements that the short-lived excited-state absorption does not contribute much to longer time scale laser pulse. Except for a negative peak seen for **Sq3** at 1050 nm, which could due to stimulated emission, **Sq3** and **Sq4** revealed very similar transient signals as that of **Sq2** with comparable lifetimes (30 ps for **Sq3** and 40 ps for **Sq4**, respectively). Consider the combination of strong excited-state absorption and 2PA over a broad range between 1100 nm and 1600 nm, along with their excited-state lifetimes; one would expect significant OPL response to picosecond laser in this wide spectrum region.

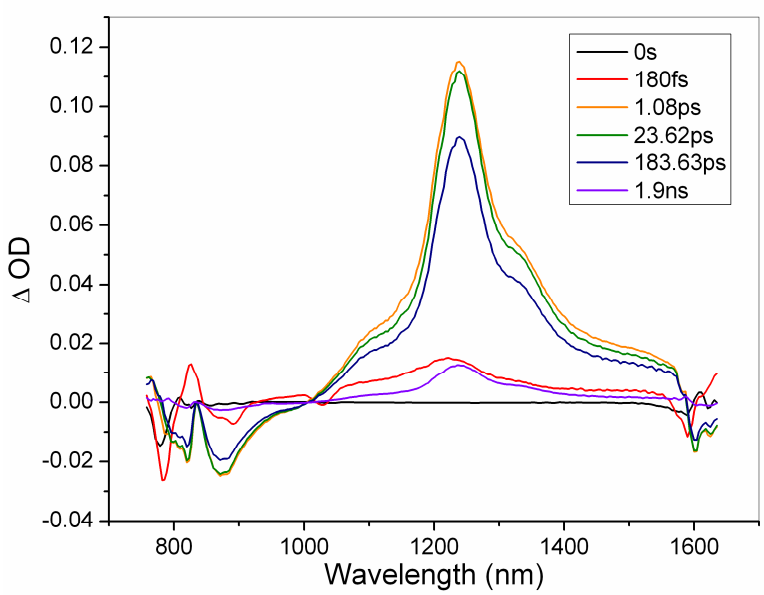

Figure 2.12: Femtosecond transient spectra of Sq1 (Figure adapted from Dr. Jochen Campo in the Perry group)

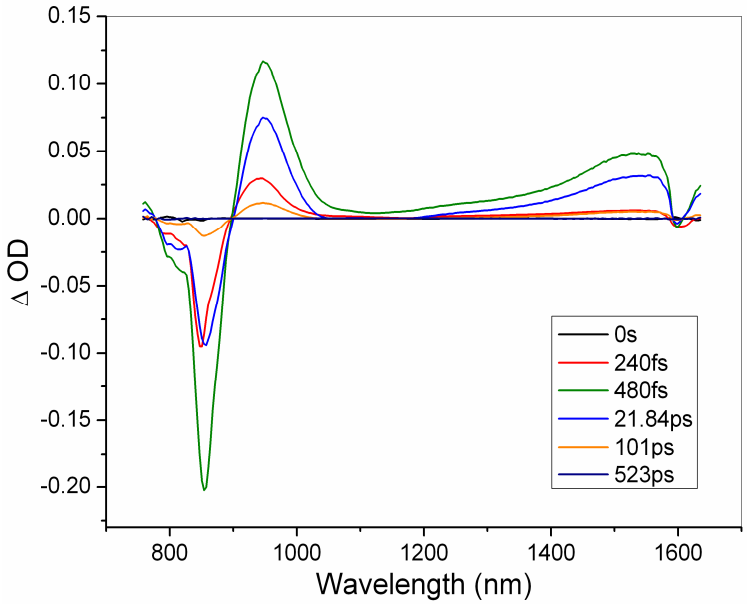

Figure 2.13: Femtosecond transient spectra of Sq2 (Figure adapted from Dr. Jochen Campo in the Perry group)

2.5 Comparison between Sq1 and G2Sq1

The absorption spectrum of **G2Sq1** slightly bathochromically shifted (13 nm, 0.03 eV) compared with **Sq1** as shown in Figure 2.14. The molar absorptivity of **G2Sq1** is much lower than that of **Sq1** (ε_{max} = 223 000 $M^{-1}cm^{-1}$ vs. 345 000 $M^{-1}cm^{-1}$ in toluene, respectively), although the shape of their absorption bands are quite similar. As these compounds spin-coated from the respective trichloroethane solution with amorphous polycarbonate (APC) at 1:1 weight ratio, the **G2Sq1**/APC film showed a narrower absorption peak, suggesting less aggregation between the π-conjugation backbone of squaraine cores than that of **Sq1**. It is worth noting that the less pronounced long-wavelength tail in the absorption spectrum of the **G2Sq1**/APC film gives wide transparency window in the near-IR that the linear absorption loss can be significantly reduced for certain applications that involve signal processing.

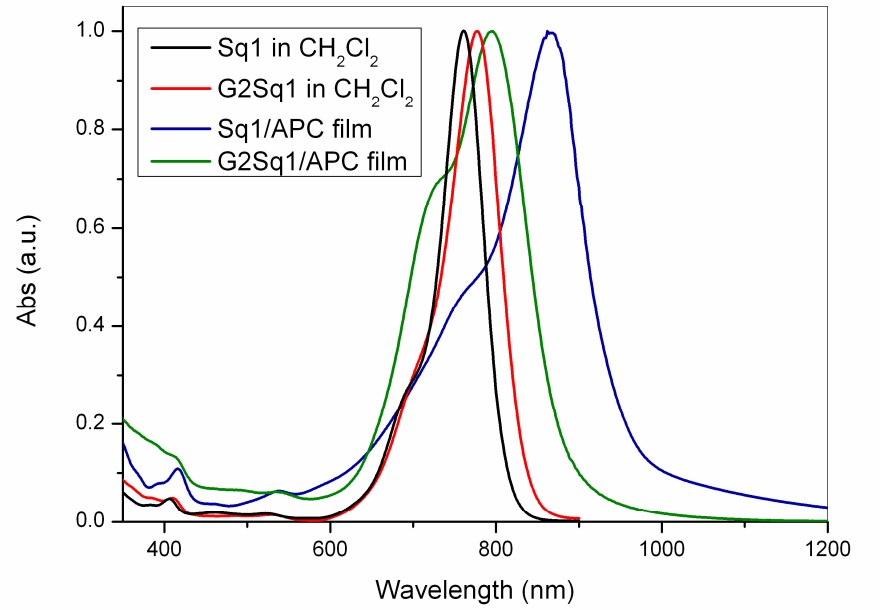

Figure 2.14: Absorption spectra of Sq1 and G2Sq1 in CH_2Cl_2 solution and in blend films with amorphous polycarbonate (APC). (Figure adapted from Dr. Jochen Campo in the Perry group)

Both **Sq1** and **G2Sq1** exhibited good thermal stability with the decomposition temperatures (T_d) above 300 °C, under nitrogen atmosphere, as determined by thermogravimetric analysis (TGA) heating from room temperature to 500 °C at a heating rate of 5 °C/min, and defined as that at which 5% weight loss. With a dendron attached, **G2Sq1** (T_d = 304 °C) is less stable than **Sq1** (T_d = 352 °C). These two dyes are investigated through differential scanning calorimetry (DSC) analysis over the temperature range from -30 to 300 °C under nitrogen atmosphere. The DSC traces of the second heating with a heating rate of 5 °C/min are shown in Figure 2.15 and reveal a melting point of 114 °C for **Sq1**, while there was only a glass transition was observed for **G2Sq1** at T_g = 45 °C, suggesting **G2Sq1** is an amorphous materials while **Sq1** is quite crystalline.

In the solid-state, **Sq1** is a red crystalline compound with metallic luster, while **G2Sq1** is a blue powder-like compound. Spin-coated films prepared from 3 mg/mL

toluene solutions are distinguishable by eye, **Sq1** films are highly scattering whereas **G2Sq1** films are transparent. The atomic force microscopy (AFM) topography images (Figure 2.16) of **Sq1** exhibit a porous, tangled structure; however, the film of **G2Sq1** is much smoother. The high quality optical films of **G2Sq1** may allow further investigation of the dye in OPL devices for practical uses.

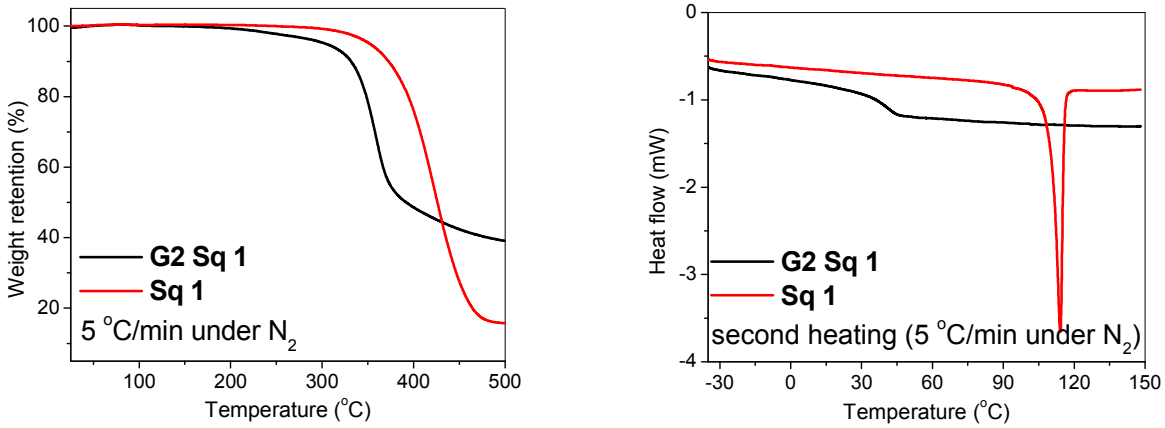

Figure 2.15: Thermogravimetric analysis (TGA, left) and differential scanning calorimetry (DSC, right) traces of Sq1 and G2Sq1. (Data collected by Dr. Chun Huang)

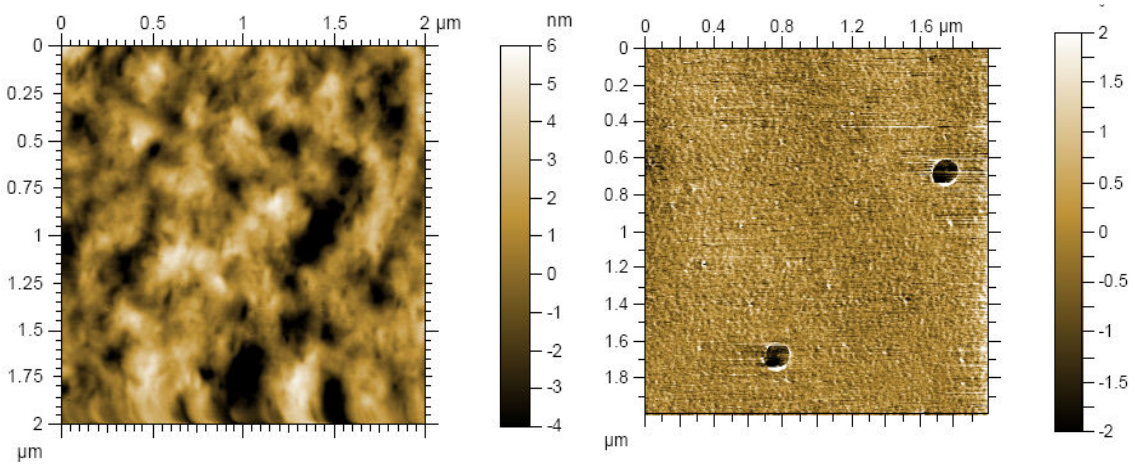

Figure 2.16: Atomic force microscopy (AFM) images (topography) of Sq1 (left) and G2Sq1 (right). (The images were collected by Dr. Benjamin Wunsch)

2.6 Conclusion

In this chapter, a series of squaraine dyes in which conjugation is extended through vinylene-heterocycle bridges to amine donors have been synthesized and characterized. These dyes exhibited intense absorption in the near-IR region and the spectra bathochromically-shifted with longer conjugation. Both two-photon induced fluorescence and z-scan measurements revealed extremely large peak 2PA cross-sections over 50 000 GM for **Sq1**, which results in strong optical-power limiting response at 850 nm for nanosecond laser pulses. However, the crystalline nature of **Sq1** in solid state limits its practical applications in films. A dendronized version **G2Sq1** was synthesized by incorporation of Fréchet type polyether dendron onto the π-conjugation skeleton of **Sq1**. High optical quality and much smoother films were achieved using **G2Sq1** with wide near-IR transparency window compared with **Sq1** which will be further investigated for applications such as 2PA induced all-optical switching. **Sq2** is a sticky fluid which can be processed into high density films with transparency over the telecommunication wavelengths. The intensity-depended 2PA coefficients along with the strong signal obtained from femtosecond transient spectra indicate the excited-state absorption contributes to its OPL performance. Power suppressions as large as 25 times for femtosecond laser pulses were observed using neat **Sq2** film at 1550 nm while less pronounced OPL was obtained for nanosecond laser which could be attributed to its short excited-state lifetime. **Sq3** and **Sq4** showed very broad spectrum response with 2PA value over 10 000 GM and strong transient signals in the same range, which make them promising candidates for future investigation on OPL for picoseconds laser considering their excited-state lifetimes.

2.7 Experimental Section

General: All the chemicals were purchased from commercial sources and used without further purification, unless otherwise indicated. Where necessary, THF, dichloromethane, and toluene were dried using an MBraun solvent purification system. ^{1}H and ^{13}C NMR spectra were collected on a Bruker 400 MHz or 500 MHz or a Varian 300 MHz spectrometer. Mass spectra were measured on a VG Instruments 70-SE using the electron impact (EI) or fast-atom bombardment (FAB) mode and on an Applied Biosystems 4700 Proteomics Analyzer using MALDI mode. Elemental analyses were carried out by Atlantic Microlab using a LECO 932 CHNS elemental analyzer. UV-Vis-NIR absorption spectra were recorded on a Varian Cary 5E spectrophotometer. The absorption spectra of a film on glass slides were recorded using an identical blank glass slide as the baseline. Thermogravimetric analysis (TGA) measurements were performed by Dr. Chun Huang on an NETZSCH STA 449C analyzer under a nitrogen flow of 40 mL/min with heating rate of 5 ^{o}C/min. Differential scanning calorimetry (DSC) measurements were performed by Dr. Chun Huang on a TA Instruments DSC Q200 analyzer under a nitrogen flow of 50 mL/min with heating rate of 5 ^{o}C/min.

Atomic Force Microscopy: Intermediate Contact Atomic Force Microscopy (AC-AFM) was performed by Dr. Benjamin Wunsch using an Agilent Technologies, 5600 SL Scanning Probe Microscope running PicoView 1.6 operating software. MikroMasch, Ultrasharp NSC35/no Al, type B silicon tips were used, with a manufacturer reported force constant of 14 N/m. Height, phase, error signal and deflection data were collected for each scan. AFM data was analyzed using the Digial Surf, PicoImage software package. All height data were line corrected using a line-by-line, 2nd order fit. For

samples in which large particulates caused streaking artifacts, an automatic structure exclusion algorithm in the PicoImage software was used to reduce the distortion of the particulate during leveling. Root mean square height data were obtained using the software, based on the ISO 25178 standard.

Femtosecond transient absorption measurements: The experiments were performed on a commercially available transient absorption spectroscopy system (Helios, Newport), by Dr. Jochen Campo in the Perry group. The excitation source was generated by an optical parametric amplifier (TOPAS, Newport) pumped by a Ti:Sapphire regenerative amplifier (Spitfire, Newport), operating at 500 Hz repetition rate. Approximately 5% of the 800 nm Spitfire output was used to generate the white-light continuum probe beam in a proprietary nonlinear optical crystal, at the wavelengths of 440 – 850 nm using Ti:Sapphire and 800 – 1600 nm using Nd:YAG in a sapphire plate. All squaraines were measured in toluene solution (OD of about 1 in a 2 mm path length cuvette), and were excited at a slightly longer wavelength than their absorption maxima.

Femtosecond z-scan:[46] The experiments were performed by Dr. Jochen Campo and Dr. Sarah Chi in the Perry group at multiple wavelengths for **Sq1** and selected wavelength for **Sq2-4** in toluene solution and films for **Sq2**. A computer tunable ultrafast optical parametric amplifier (TOPAS, Newport) which is pumped in turn by a Ti:Sapphire regenerative amplifier (Spitfire, Newport) was used, at a repetition rate of 1 kHz. The reference, open-aperture and closed-aperture signals are detected simultaneously using large area Germanium photoreceivers (2033, New Focus), and are integrated using Boxcar integrators (SR250, Stanford Research Systems). The integrated signals are acquired using a data acquisition card (6025E, National Instruments) and an in-house

developed Labview program. The final result was obtained by careful extrapolation to zero irradiance.

Two-photon induced fluorescence measurements: The two-photon absorption spectrum of **Sq1-4** was measured by Dr. Jochen Campo in solution using a modified two-arm referential two-photon fluorescence technique,[47] and 2-([3-(2-[4-(Dimethylamino)phenyl]ethenyl)-5,5-dimethyl-2-cyclohexen-1-ylidene]methyl)-3-methylbenzothiazolium (styryl-9M) in chloroform as standard. The output beam of the computer controlled TOPAS is weakly focused in between the sample and reference (both of them being liquids in a 1 cm path length cuvette). A small portion of the beam is split off before the focusing lens and is directed into a monochromator (Horiba, MicroHR) coupled to a sandwich diode photo-detector (DSD2, ThorLabs) to monitor the TOPAS output wavelengths during the two-photon fluorescence measurements, as well as the relative excitation power during measurements of the fluorescence power dependence. The two-photon fluorescence is collected by two aspheric lenses and is sent into an optical fiber (BFB-455-7, Princeton Instruments) connected to a monochromator (SpectraPro-150, Acton). The fluorescence spectra of the sample and reference are then detected as two rows on a CCD (ST-133, Roper Scientific). The measurements are performed by scanning the laser wavelength and simultaneously collecting the two-photon absorption induced fluorescence signals from the two channels. Both setting the wavelength and collecting the data are computer controlled through custom-designed LabView VIs. The different collection geometry and efficiency in the two channels is taken into account by placing the sample in channel one and the reference is in channel two, and then exchanging the positions.

Nanosecond optical-power limiting measurements: The excitation source for OPL was an optical parametric oscillator (Newport) pumped by the third harmonic of a Nd:YAG laser (Newport) with a pulse width of 8 ns. A mechanical shutter reduced the pulse repetition rate to 10 Hz to minimize damage to the sample. The laser was focused into the center of the cuvette using f/5 geometry, and the transmitted light was detected by a photoreceiver (New Focus), sampled using a boxcar averager (Stanford Research Systems), and recorded using an analog to digital converter and computer. A beam splitter placed before the sample redirected part of each pulse to a reference photoreceiver to normalize for fluctuations in the input energy of each pulse.

Synthesis:

1: Phosphorus oxychloride (7.4 mL, 80 mmol) was added to DMF (28 mL) at 0 °C under nitrogen. The mixture was stirred for 40 min, and then *N*,*N*-dibutylaniline (18 mL, 80 mmol) was added dropwise at room temperature. The mixture was stirred at room temperature for 20 min then at 110 °C overnight before it was poured into ice water and neutralized with K_2CO_3. The organic layer was extracted with ethyl acetate (4 × 125 mL), washed with water (2 × 150 mL), 10% K_2CO_3 aqueous solution (100 mL), and then dried over $NaSO_4$. The solvent was removed and the residue was purified using silica gel column chromatography eluting with hexane/ethyl acetate (10 : 1). After removal of the solvent, **1** was obtained as a yellow oil (15.2 g, 81%). ^{1}H NMR (300 MHz, $CDCl_3$): δ 9.67 (s, 1H), 7.67 (d, J = 8.4 Hz, 2H), 6.62 (d, J = 9.0 Hz, 2H), 3.33 (t, J = 7.8 Hz, 4H), 1.58 (m, 4H), 1.35 (sextet, J = 7.8 Hz, 4H), 0.95 (t, J = 6.9 Hz, 6H). The ^{1}H NMR spectrum is consistent with that reported in the literature.[48]

2: **1** (15 g, 65 mmol) was dissolved in ethanol (200 mL). After cooling to 0 °C, sodium borohydride (4.92 g, 130 mmol) was added in portions. The solution was stirred at room temperature for 4 h. Ethanol was removed and the residue was dissolved in hexane (200 mL). The hexane solution was then washed with water (3 × 200 mL) and dried over Na_2SO_4. The solvent was removed to yield **2** as a yellow oil (14.2 g, 93%). ^{1}H NMR (500 MHz, CD_2Cl_2): δ 7.15 (d, J = 9.0 Hz, 2H), 6.61 (d, J = 9.0 Hz, 2H), 4.48 (d, J = 5.5 Hz, 2H), 3.25 (t, J = 8.0 Hz, 4H), 1.55 (m, 4H), 1.45 (br, 1H), 1.35 (sextet, J = 7.5 Hz, 4H), 0.95 (t, J = 7.5 Hz, 6H). The ^{1}H NMR spectrum is consistent with that reported in the literature.[48]

3: To a 100 mL round-bottomed flask, **2** (14.2 g, 60.4 mmol) and triethylphosphite (32.0 mL, 202 mmol) were added. After cooling to 0 °C, iodine (15.3 g, 60.4 mmol) was added to the mixture, which was stirred at room temperature overnight. About 10 mL triethylphosphite was removed by distillation under reduced pressure. The residue was purified by silica gel column chromatography (hexane/ethyl acetate = 5 : 1, then 1 : 1). After removal of the solvent, the residual was pumped overnight to remove the remaining triethylphosphite to give **3** as a yellow oil (11.2 g, 52%). ^{1}H NMR (300 MHz, CD_2Cl_2): δ 7.08 (m, 2H), 6.54 (d, J = 9.0 Hz, 2H), 3.97 (m, 4H), 3.21 (t, J = 7.8 Hz, 4H), 3.01 (d, $J_{H\text{-}P}$ = 20.7 Hz, 2H), 1.52 (m, 4H), 1.31 (m, 4H), 1.22 (t, J = 7.2 Hz, 6H), 0.92 (t, J = 7.5 Hz, 6H). The ^{1}H NMR spectrum is consistent with that reported in the literature.[48]

4: To a solution of **3** (6.38 g, 18.0 mmol) and 3,4-dibutoxylthiophene-2-carboxaldehyde[49] (4.61 g, 18.0 mmol) in anhydrous THF (80 mL) was added ^{t}BuOK (1.0 M in THF, 54 mL, 54 mmol) at 0 °C under nitrogen. The mixture was stirred at 0 °C for 30 min, and then stirred at room temperature for 2 h. The light yellow suspension was washed with

water (2 × 300 mL), extracted with diethyl ether (2 × 200 mL), and dried over anhydrous $MgSO_4$. The solvent was removed, and the residue was purified by column chromatography on silica gel (hexane/ethyl acetate = 10 : 1) to give **4** as a light yellow oil (7.80 g, 95%). ^{1}H NMR (300 MHz, $CDCl_3$): δ 7.30 (d, J = 8.7 Hz, 2H), 6.99 (d, J = 16.2 Hz, 1H), 6.72 (d, J = 16.2 Hz, 1H), 6.58 (d, J = 8.7 Hz, 2H), 5.91 (s, 1H), 4.02 (t, J = 6.6 Hz, 2H), 3.94 (t, J = 6.6 Hz, 2H), 3.26 (t, J = 7.8 Hz, 4H), 1.73 (m, 4H), 1.55 (m, 8H), 1.34 (m, 4H), 0.95 (m, 12H). The ^{1}H NMR spectrum is consistent with that reported in the literature.[28]

5: To a 100 mL three-neck round-bottomed flask, DMF (0.99 g, 13.6 mmol) was added, and deoxygenated with nitrogen for 30 min. Phosphorus oxychloride (2.08 g, 13.6 mmol) was added dropwise in 5 min. The resulting mixture was stirred at room temperature for 1 h to form yellow glassy solid. Anhydrous acetonitrile (10 mL) was added to dissolve the solid. The solution of **4** (4.14 g, 9.05 mmol) in CH_3CN (20 mL)/CH_2Cl_2 (10 mL) was added dropwise to the reaction mixture in 15 min. The resulting solution was stirred at room temperature overnight. The deep red solution was poured into ice water (200 mL), extracted with dichloromethane (200 mL), washed with saturated aqueous $NaHCO_3$ solution (500 mL), and dried over $MgSO_4$. After removal of the solvent, the residue was purified by silica gel column chromatography (hexane/ethyl acetate = 10 : 1) to afford **5** as a red oil, red crystal was formed when standing in fridge (2.94 g, 67%). ^{1}H NMR (300 MHz, $CDCl_3$): δ 9.92 (s, 1H), 7.35 (d, J = 8.7 Hz, 2H), 7.01 (d, J = 3.6 Hz, 2H), 6.64 (d, J = 9.3 Hz, 2H), 4.29 (t, J = 6.6 Hz, 2H), 3.99 (t, J = 6.6 Hz, 2H), 3.29 (t, J = 7.7 Hz, 4H), 1.76 (m, 4H), 1.55 (m, 8H), 1.34 (m, 4H), 0.95 (m, 12H). The ^{1}H NMR spectrum is consistent with that reported in the literature.[28]

6: **5** (1.76 g, 3.64 mmol) was dissolved in ethanol (50 mL). After cooling to 0 °C, sodium borohydride (0.275 g, 7.27 mmol) was added in portions and stirred at room temperature for 2 h. After removal of ethanol, dichloromethane was added to dissolve the residue and the resulting solutions was washed with water. The organic layer was dried over Na_2SO_4 and removed solvent. The resulting alcohol (1.74 g, 3.60 mmol) was used in the next step reaction without further purification. To a solution of the alcohol (1.74 g, 3.60 mmol) in triethylphosphite (10 mL), iodine (1.36 g, 5.36 mmol) was added at 0 °C. The resulting solution was stirred overnight. After removal of excess triethylphosphite, the residue was purified by silica gel column chromatography (dichloromethane/ethyl acetate = 6 : 1) to give **6** as an orange oil (0.60 g, 27%). ^{1}H NMR (CD_2Cl_2, 500 MHz): δ 7.28 (d, J = 16.3 Hz, 1H), 6.94 (d, J = 8.8 Hz, 2H), 6.70 (d, J = 16.2 Hz, 1H), 6.61 (d, J = 8.8 Hz, 2H), 4.08 (m, 4H), 4.00 (m, 4H), 3.28 (t, J = 7.7 Hz, 4H), 3.20 (d, $J_{H\text{-}P}$ = 20.5 Hz, 2H), 1.72 (quintet, J = 8.0 Hz, 4H), 1.54 (m, 8H), 1.35 (sextet, J = 7.5 Hz, 4H), 1.30 (t, J = 7.1 Hz, 6H), 0.97 (m, 12H). The ^{1}H NMR spectrum is consistent with that reported in the literature.[28]

7: 5-(Bis(4-butoxyphenyl)amino)thiophene-2-carbaldehyde[50] (1.95 g, 4.60 mmol) was dissolved in ethanol (50 mL). After cooling to 0 °C, sodium borohydride (0.35 g, 9.2 mmol) was added in portions and stirred at room temperature for 2 h. The reaction mixture was poured into cold water and extracted with diethyl ether. The resulting alcohol from the diethyl ether layer was removed solvent and used in the next step reaction without further purification. To a solution of the alcohol in triethylphosphite (10 mL), iodine (1.17 g, 4.60 mmol) was added at 0 °C. The resulting solution was stirred overnight. After removal of excess triethylphosphite, the residue was purified by silica

gel column chromatography (dichloromethane/ethyl acetate = 2 : 1) to give **7** as an orange oil (1.94 g, 77%). ^{1}H NMR ($CDCl_3$, 300 MHz): δ 7.00 (m, 4H), 6.75 (m, 4H), 6.66 (t, J = 3.9 Hz, 1H), 6.34 (d, J = 3.9 Hz, 1H), 4.06 (m, 4H), 3.89 (t, J = 6.3 Hz, 4H), 3.17 (d, $J_{H\text{-}P}$ = 20.4 Hz, 2H), 1.72 (m, 4H), 1.47 (m, 4H), 1.27 (t, J = 6.9 Hz, 6H), 0.95 (t, J = 7.5 Hz, 6H). ^{13}C{^{1}H} NMR (100 MHz, $CDCl_3$): δ 155.11, 152.38 (d, $J_{C\text{-}P}$ = 4 Hz), 141.47, 125.85 (d, $J_{C\text{-}P}$ = 9 Hz), 124.43 (d, $J_{C\text{-}P}$ = 10 Hz), 124.01, 117.74 (d, $J_{C\text{-}P}$ = 3 Hz), 114.98, 67.94, 62.35 (d, $J_{C\text{-}P}$ = 6 Hz), 31.36, 28.41 (d, $J_{C\text{-}P}$ = 143 Hz), 19.23, 16.39 (d, $J_{C\text{-}P}$ = 6 Hz), 13.84. ^{31}P{^{1}H} NMR (162 MHz, $CDCl_3$): δ 25.15. HRMS (EI) Calcd. for $C_{29}H_{40}NO_5PS$ (M^+): 545.2365; Found: 545.2370. Anal. Calcd. for $C_{29}H_{40}NO_5PS$: C, 63.83; H, 7.39; N, 2.57. Found: C, 63.77; H, 7.29; N, 2.54.

8: To a solution of 2-decyl-tetradecanol (42.0 g, 118 mmol), triphenylphosphine (52.6 g, 200 mmol) in anhydrous dichloromethane (85 mL) at 0 °C, *N*-bromosuccinimide (37.0 g 206 mmol) was added in portions. The mixture was stirred at room temperature overnight. The solvent was removed and hexane (500 mL) was added. The resulting mixture was filtered through a pad of silica gel eluting with hexane. After removal of the solvent, **8** was obtained as a colorless oil (47.8 g, 97%). ^{1}H NMR (500 MHz, $CDCl_3$): δ 3.42 (d, J = 4.5 Hz, 2H), 1.57 (m, 1H), 1.37 – 1.24 (m, 40H), 0.86 (t, J = 7.5 Hz, 6H). The ^{1}H NMR spectrum is consistent with that reported in the literature.[51]

9: To a solution of 1-*H*-pyrrole-2-carbaldehyde (5.82 g, 61.3 mmol) in DMF (150 mL) was added sodium hydride (95%, 1.49 g, 63 mmol) at 0 °C and stirred for 30 min. Compound **8** (25.6 g, 61.3 mmol) in DMF (20 mL) was added slowly to the solution and stirred at 60 °C for 48 h. After it was cooled down, the mixture was poured into water (300 mL) and hexane (3 × 150 mL) was used to extract the product out. Then the organic

layer was washed with water (3 × 150 mL) and dried over $MgSO_4$. After the solvent was removed, the crude product was purified on silica column chromatography eluting with hexane/ethyl acetate (10 : 1) to give **9** as a yellow oil (20.0 g, 76%). ^{1}H NMR (500 MHz, $CDCl_3$): δ 9.51 (s, 1H), 6.89 (m, 2H), 6.18 (m, 1H), 4.16 (d, J = 7.0 Hz, 2H), 1.81 (m, 1H), 1.22 (m, 40H), 0.86 (t, J = 7.0 Hz, 6H). Anal. Cacld. for $C_{29}H_{53}NO$: C, 80.68; H, 12.37; N, 3.24. Found: C, 80.55; H, 12.53; N, 3.30. The ^{1}H NMR spectrum is consistent with that reported in the literature.[28]

10: To a solution of ethylhexyl bromide (20.0 g, 104 mmol) and pyrrole-2-carboxylaldehyde (8.27 g, 87.0 mmol) in DMF (100 mL) was added sodium hydride (60% in mineral oil, 4.16 g, 104 mmol) under nitrogen. The mixture was stirred at 60 °C for 3 d, and then poured into ice cold water (200 mL). The aqueous solution was extracted with diethyl ether (6 × 150 mL). The organic layer was combined and washed with water (4 × 150 mL) and brine, and dried over Na_2SO_4. After removal of the solvent, the residue was purified by silica gel column chromatography (hexane/ethyl acetate = 10 : 1) to yield **10** as a yellow oil (16.2 g, 90%). ^{1}H NMR (300 MHz, $CDCl_3$): δ 9.51 (s, 1H), 6.90 (m, 2H), 6.19 (m, 1H), 4.17 (d, J = 7.5 Hz, 2H), 1.77 (m, 1H), 1.23 (m, 8H), 0.84 (m, 6H). ^{13}C{^{1}H} NMR (100 MHz, C_6D_6): δ 179.24, 131.86, 131.60, 124.80, 109.28, 52.76, 40.40, 30.12, 28.32, 23.41, 22.98, 13.99, 10.39. HRMS (EI) Calcd. for $C_{13}H_{21}NO$ (M^+): 207.1623. Found: 207.1623. Anal. Cacld. for $C_{13}H_{21}NO$: C, 75.32; H, 10.21; N, 6.76. Found: C, 75.15; H, 10.32; N, 6.71.[52]

11: To a mixture of zinc (12.6 g, 193 mmol) in anhydrous THF (200 mL) was added titanium tetrachloride (8.05 g, 96 mol) slowly at 0 °C. The mixture was heated to reflux for 30 min, and cooled to 0 °C. A solution of compound **10** (10 g, 48 mmol), pyridine

(10.0 mL, 125 mmol) in THF (50 mL) was added, and the reaction mixture was heated to reflux for 2 h. After it was cooled down, the mixture was poured onto ice (100 g) and extracted with dichloromethane (200 mL). The organic layer was passed through a pad of Celite and washed with 1N HCl aqueous solution and then dried over $MgSO_4$. After removal of the solvent under reduced pressure, the remaining liquid was purified by silica gel column chromatography (hexane/ethyl acetate/triethylamine = 100 : 10 : 1) to give **11** as a yellow oil (7.82 g, 85%). ^{1}H NMR (300 MHz, C_6D_6): δ 6.96 (s, 2H), 6.73 (d, J = 3.4 Hz, 2H), 6.48 (m, 2H), 6.35 (t, J = 3.1 Hz, 2H), 3.44 (m, 4H), 1.63 (m, 2H), 1.13–1.04 (m, 16H), 0.82 (t, J = 7.3 Hz, 6H), 0.69 (t, J = 7.5 Hz, 6H). ^{13}C{^{1}H} NMR (100 MHz, C_6D_6): δ 132.40, 122.92, 115.28, 108.53, 105.96, 50.72, 41.36, 30.88, 28.84, 24.16, 23.27, 14.19, 10.72. HRMS (EI) Calcd. for $C_{26}H_{42}N_2$ (M^+): 382.3348. Found: 382.3374. Anal. Calcd. for $C_{26}H_{42}N_2$: C, 81.61; H, 11.06; N, 7.32. Found: C, 81.47; H, 11.06; N, 7.27.

12: To a solution of compound **11** (1.03 g, 2.70 mmol) and DMF (0.98 g, 13.5 mmol) in acetonitrile (20 mL), was added phosphrous oxychloride (0.41 g, 2.7 mmol) slowly at 0 °C. The mixture was stirred at 0°C for 1.5 h before pouring into ice water. The resulting mixture was neutralized with K_2CO_3, and then extracted with ethyl acetate. The organic phase was collected and dried over K_2CO_3. After removal of solvents, the remaining was purified by silica gel column chromatography (hexane/ethyl acetate = 15 : 1) to give **12** as a yellow oil (0.62 g, 56%). ^{1}H NMR (500 MHz, C_6D_6): δ 9.52 (s, 1H), 7.00 (d, J = 15.7 Hz, 1H), 6.80 (d, J = 15.8 Hz, 1H), 6.72 (dd, J_1 = 3.7 Hz, J_2 = 1.2 Hz, 1H), 6.65 (d, J = 4.2 Hz, 1H), 6.48 (d, J = 4.2 Hz, 1H), 6.46 (t, J = 2.0 Hz, 1H), 6.29 (t, J = 3.2 Hz, 1H), 4.31 (m, 2H), 3.37 (m, 2H), 1.89 (m, 1H), 1.53 (m, 1H), 1.30–1.10 (m, 16H), 0.82 (t, J = 7.2 Hz, 6H), 0.81 (t, J = 7.2 Hz, 3H), 0.68 (t, J = 7.2 Hz, 3H). ^{13}C{^{1}H} NMR (100 MHz,

C_6D_6): δ 177.95, 142.07, 133.18, 131.22, 125.16, 124.39, 120.97, 112.62, 109.12, 108.10, 106.74, 50.71, 48.77, 31.92, 30.82, 30.78, 28.89, 28.83, 24.13, 23.33, 23.23, 23.01, 14.31, 14.18, 14.16, 11.04, 10.70. HRMS (EI) Calcd. for $C_{27}H_{42}N_2O$ (M^+): 410.3297. Found: 410.3293. Anal. Calcd. for $C_{27}H_{42}N_2O$: C, 78.97; H, 10.31; N, 6.82. Found: C, 79.22; H, 10.48; N, 6.85.

13: (5-(Bromomethyl)-1,3-phenylene)bis(oxy)bis(methylene)dibenzene[53] (8.37 g, 21.9 mmol) and 5-(hydroxymethyl)benzene-1,3-diol (1.50 g, 10.9 mmol), K_2CO_3 (4.51 g, 32.7 mmol), and 18-crown-6 (240 mg, 1.09 mmol) were added to a dried round-bottomed flask in anhydrous THF (150 mL). The mixture was heated to reflux overnight before poured into water after cooling down and extracted with dichloromethane. The organic layer was washed with water and dried over Na_2SO_4. The crude product was purified by a silica gel plug with dichloromethane to yield **13** as a white solid (4.44 g, 55%). ^{1}H NMR (400 MHz, $CDCl_3$): δ 7.30 (m, 20H), 6.66 (d, J = 2.0 Hz, 4H), 6.60 (d, J = 1.6 Hz, 2H), 6.56 (t, J = 2.0 Hz, 2H), 6.50 (d, J = 2.0 Hz, 1H), 5.02 (s, 8H), 4.96 (s, 4H), 4.62 (d, J = 6.0 Hz, 2H). The ^{1}H NMR spectrum is consistent with that reported in the literature.[42]

14: To a solution of compound **13** (4.44 g, 5.90 mmol) in THF (100 mL), triphenylphosphine (1.85 g, 7.08 mmol) and *N*-bromosuccinimide (1.26 g, 7.08 mmol) were added and the mixture was stirred under nitrogen at room temperature for 2 h. After removal of the solvent, the organic layer was extracted with dichloromethane and washed with water. The crude product was purified by silica gel column chromatography with dichloromethane to give **14** as a white solid (4.01 g, 84%). ^{1}H NMR (400 MHz, $CDCl_3$): δ 7.29 (m, 20H), 6.65 (d, J = 1.6 Hz, 4H), 6.60 (d, J = 1.6 Hz, 2H), 6.56 (t, J = 2.0 Hz, 2H), 6.49 (d, J = 1.6 Hz, 1H), 5.02 (s, 8H), 4.95 (s, 4H), 4.39 (s, 2H). The ^{1}H NMR

spectrum is consistent with that reported in the literature.[42]

15: 1-*H*-pyrrole-2-carbaldehyde (293 mg, 3.08 mmol) and compound **14** (2.48 g, 3.08 mmol) were dissolved in DMF (100 mL). To the solution, sodium hydride (57-63% dispersion in mineral oil, 0.160 g, 3.70 mmol) was added at 0 °C. The mixture was then stirred at 60 °C overnight. After it was cooled down, the mixture was poured into water (150 mL) and extracted with ethyl acetate (3 × 50 mL). The organic layer was washed with water (3 × 50 mL) and dried with $MgSO_4$. After the solvent was removed, the crude product was purified by silica gel column chromatography eluting with dichloromethane to give **15** as a white sticky solid (2.13 g, 85%). ^{1}H NMR (400 MHz, $CDCl_3$): δ 9.51 (s, 1H), 7.40–7.31 (m, 20H), 6.92 (m, 2H), 6.62 (m, 4H), 6.54 (t, J = 2.0 Hz, 2H), 6.45 (m, 1H), 6.32 (m, 2H), 6.22 (m, 1H), 5.46 (s, 2H), 5.00 (s, 8H), 4.89 (s, 4H). ^{13}C{^{1}H} NMR (100 MHz, $CDCl_3$): δ 179.53, 160.15, 160.08, 139.98, 139.10, 136.76, 131.49, 128.59, 128.01, 127.57, 124.85, 110.20, 106.41, 106.36, 101.61, 101.15, 70.11, 69.97, 51.87 (One aromatic peak missing probably due to overlap of near coincidental resonances). HRMS (MALDI) Calcd. for $C_{54}H_{47}NO_7Na$ ($M+Na^+$): 844.3250. Found: 844.3207. Anal. Calcd. for $C_{54}H_{47}NO_7$: C, 78.91; H, 5.76; N, 1.70. Found: C, 78.63; H, 5.83; N, 1.66.

Sq 1: To a 100 mL two-neck round-bottomed flask, compound **3** (1.0 g, 2.8 mmol) and compound **9** (1.2 g, 2.8 mmol) were added in anhydrous THF (30 mL). The mixture was stirred at 0 °C under N_2, and ^{t}BuOK (1.0 M in THF, 4.2 mL, 4.2 mmol) was added. The reaction mixture was stirred for 3 h before removal of the solvent. Hexane (80 mL) was used to extract the organic layer and washed with H_2O (2 × 40 mL). After two silica gel columns (hexane/ethyl acetate = 10 : 1) and washing with methanol, a dark yellow oil (1.17 g, 66%) was obtained as desired product and used without further purification. To a

mixture of isopropanol (50 mL) and benzene (50 mL) was added the dark yellow oil (1.17 g, 1.85 mmol) and 3,4-dihydoxy-3-cyclobutene-1,2-dione (0.105 g, 0.92 mmol), the resulting mixture was refluxed for 24 h, during which period water was azeotropically removed. After cooling to room temperature, the solvent was removed under reduced pressure. The residue was purified by silica gel column chromatography eluting with hexane and ethyl acetate (first 10 : 1, then 5 : 1), and then recrystallized from ethanol to give **Sq 1** as a solid with metal copper luster. (1.56 g, 26%). ^{1}H NMR (300 MHz, *d*-acetone): δ 7.74 (m, 2H), 7.50 (d, J = 9 Hz, 4H), 7.40 (d, J = 15.9 Hz, 2H), 7.04 (d, J = 14.1 Hz, 2H), 7.00 (s, 2H), 6.72 (d, J = 8.7 Hz, 4H), 4.92 (m, 4H), 3.41 (t, J = 6.6 Hz, 8H), 1.93 (m, 2H), 1.62 (m, 8H), 1.44 - 1.24 (m, 88H), 0.97 (t, J = 7.2 Hz, 12H), 0.87 (t, J = 6.3 Hz, 12H). ^{13}C{^{1}H} NMR (125 MHz, C_6D_6): δ 177.2, 169.3, 149.0, 146.4, 134.8, 132.2, 129.0, 124.7, 123.6, 113.5, 112.2, 111.2, 50.9, 40.5, 32.4, 30.5, 30.2, 30.17, 29.86, 29.75, 23.12, 20.50, 14.39, 14.37, 14.09 (Fifteen aliphatic peaks missing probably due to overlap of near coincidental resonances). HRMS (MALDI) Calcd. for $C_{92}H_{150}N_4O_2$ (M^+): 1342.1759. Found: 1343.1784. Anal. Cacld. for $C_{92}H_{150}N_4O_2$: C, 82.20; H, 11.25; N, 4.17. Found: C, 82.36; H, 11.52; N, 4.22.

Sq 2: To a solution of compound **6** (0.594 g, 0.980 mmol) and compound **9** (0.640 g, 1.47 mmol) in anhydrous THF (20 mL) was added a solution of ^{t}BuOK (1.0 M in THF, 2.0 mL, 2.0 mmol) at 0 °C. The mixture was stirred for 2 h at room temperature, then poured into water and extracted with ethyl acetate. The organic phase was collected and dried over $MgSO_4$, concentrated and purified by silica gel column chromatography (hexane/ethyl acetate = 15 : 1) to give a red oil. It was used for the next step without further purification. A mixture of the red oil (0.846 g, 1.390 mmol) and 3,4-dihydoxy-3-

cyclobutene-1,2-dione (79.5 mg, 0.680 mmol) in toluene/*n*-butanol (15 mL/7.5mL) was heated to reflux overnight, during which period water was azeotropically removed. After removal of the solvent at reduced pressure, the remaining liquid was purified by silica gel column chromatography (hexane/ethyl acetate, 10 : 1 then 3 : 2) to give **Sq 2** as a black sticky oil (500 mg, 55%). ^{1}H NMR (C_6D_6, 300 MHz) δ 8.42 (br, 2H), 7.54 (d, J = 15.6 Hz, 2H), 7.48 (d, J = 16.4 Hz, 2H), 7.47 (d, J = 8.3 Hz, 4H), 7.26 (d, J = 16.0 Hz, 2H), 6.95 (d, J = 15.9 Hz, 2H), 6.64 (d, J = 4.5 Hz, 2H), 6.59 (d, J = 8.6 Hz, 4H), 4.95 (m, 4H), 4.05 (t, J = 6.5 Hz, 4H), 4.00 (t, J = 6.5 Hz, 4H), 3.01 (t, J = 7.4 Hz, 8H), 2.10 (m, 2H), 1.66 (m, 16H), 1.30 (m, 88H), 1.13 (sextet, J = 7.4 Hz, 8H), 0.87 (m, 36H). The ^{1}H NMR spectrum is consistent with that reported in the literature.[28]

Sq 3: Compound **7** (336 mg, 0.62 mmol) and compound **12** (253 mg, 0.62 mmol) were added to anhydrous THF (10 mL). The solution of ^{t}BuOK in THF (1.0 M in THF, 2.5 mL, 2.5 mmol) was added under nitrogen at 0 ºC. The mixture was stirred for 3 h. After removal of THF, the reaction mixture was worked up with hexane and brine. The hexane layer was dried over Na_2SO_4. After a silica gel column chromatography (hexane/ethyl acetate/triethylamine = 100 : 5 : 1), the yellow oil (413 mg, crude yield 83%) was used in the next step without further purification. The crude product was transferred to a dried flask and 3,4-dihydoxy-3-cyclobutene-1,2-dione (29 mg, 0.25 mmol) was added. The reaction flask was pump-filled with nitrogen 3 times. A mixture of toluene (20 mL) and *n*-butanol (10 mL) was added. The resultant mixture was refluxed for 24 h, during which period water was azeotropically removed. After cooling to room temperature, the solvent was removed under reduced pressure. The residue was purified by silica gel column chromatography eluting with hexane/ethyl acetate (7 : 1, then 3 : 1) to afford the desired

product **Sq 3** as a black solid (46 mg, 11%). ^{1}H NMR (500 MHz, C_6D_6): δ 8.52 (s, 2H), 7.21 (d, J = 9.0 Hz, 8H), 6.97 (m, 4H), 6.83 (m, 4H), 6.76 (d, J = 9.0 Hz, 8H), 6.71 (d, J = 4.5 Hz, 2H), 6.67 (d, J = 16 Hz, 2H), 6.61 (d, J = 4.0 Hz, 4H), 6.39 (d, J = 4.0 Hz, 2H), 4.90 (br, 4H), 3.57 (t, J = 6.5 Hz, 8H), 3.42 (m, 4H), 1.91 (m, 2H), 1.56 (m, 16H), 1.32 (m, 10H), 1.21 (m, 8H), 1.06 (m, 16H), 0.81 (m, 18H), 0.63 (t, J = 7.0 Hz, 6H), 0.40 (m, 12H). ^{13}C{^{1}H} NMR (125 MHz, C_6D_6): δ 177.3, 167.8, 156.6, 153.8, 146.3, 141.3, 136.4, 135.3, 134.0, 133.6, 132.7, 125.9, 125.8, 122.4, 121.7, 115.7, 115.3, 113.7, 113.3, 111.9, 111.0, 109.1, 67.8, 50.8, 46.8, 32.8, 32.5, 30.0, 29.2, 27.0, 24.4, 23.9, 23.5, 23.2, 19.6, 14.5, 14.3, 14.0 (Four aliphatic peaks missing probably due to overlap of near coincidental resonances). HRMS (MALDI) Calcd. for $C_{108}H_{140}N_6S_2O_6$ (M^+): 1681.027. Found: 1681.051. Anal. Cacld. for $C_{108}H_{140}N_6S_2O_6$: C, 77.10; H, 8.39; N, 5.00; S, 3.81. Found: C, 76.88; H, 8.57; N, 4.73; S, 3.58.

Sq 4: Compound **6** (330 mg, 0.540 mmol) and compound **12** (200 mg, 0.490 mmol) were added to anhydrous THF (20 mL). ^{t}BuOK (1.0 M in THF, 2.0 mL, 2.0 mmol) was added under nitrogen at 0 ºC. The mixture was stirred for 2.5 h. After removal of THF, the residue was worked up with hexane and brine, and the hexane layer was dried over Na_2SO_4. After silica gel column chromatography (hexane/ethyl acetate = 10 : 1), the remaining yellow oil was used in the next step without further purification. To a mixture of toluene (10 mL) and *n*-butanol (5 mL) were added the yellow oil (359 mg, 0.430 mmol) and 3,4-dihydoxy-3-cyclobutene-1,2-dione (24 mg, 0.21 mmol), the resulting mixture was refluxed for 36 h, during which period water was azeotropically removed. After cooling to room temperature, the solvent was removed under reduced pressure. The residue was purified with silica gel column chromatography with hexane and ethyl

acetate (first 10 : 1, 5 : 1, then 3 : 1), then it was recrystallized from ethanol to give **Sq 4** as a black solid (90 mg, 20%). ^{1}H NMR(500 MHz, C_6D_6): δ 8.51 (br, 2H), 7.55 (m, 4H), 7.46 (d, J = 8.5 Hz, 4H), 7.29 (m, 2H), 6.99 (m, 4H), 6.84 (m, 4H), 6.77 (s, 2H), 6.76 (s, 2H), 6.59 (s, 2H), 6.57 (s, 2H), 4.90 (m, 4H), 4.07 (m, 8H), 3.59 (m, 4H), 3.01 (t, J = 7.0 Hz, 8H), 1.91 (m, 4H), 1.70 (m, 8H), 1.56–1.32 (m, 24H), 1.29–1.09 (m, 32H), 0.89 (m, 48H). ^{13}C{^{1}H} NMR (125 MHz, C_6D_6): δ 177.3, 167.8, 148.6.0, 148.2, 147.5, 146.4, 136.7, 135.1, 133.9, 123.6, 125.8, 125.4, 124.8, 123.7, 123.5, 121.3, 118.0, 114.4, 113.3, 112.5, 112.1, 111.2, 109.6, 51.1, 50.8, 47.0, 42.4, 42.2, 32.8, 31.3, 31.0, 30.4, 30.0, 29.4, 24.7, 24.5, 23.6, 20.7, 19.8, 19.7, 14.6, 14.5, 14.3, 14.2 (one aromatic and seven aliphatic peaks missing probably due to overlap of near coincidental resonances). HRMS (MALDI) Calcd. for $C_{126}H_{168}N_6S_2O_6$ (M^+):1805.247. Found:1805.256. Anal. Cacld. for $C_{116}H_{168}N_6S_2O_6$: C, 77.11; H, 9.37; N, 4.65. Found: C, 76.88; H, 9.36; N, 4.59.

G2Sq1: **3** (1.14 g, 3.2 mmol) and **15** (2.1 g, 2.7 mmol) were dissolved in anhydrous THF (50 mL). ^{t}BuOK (1.0 M in THF, 13.5 mL, 13.5 mmol) was added under nitrogen at 0 ºC. The mixture was stirred for 2 h. After removal of THF, the residue was worked up with ethyl acetate and brine, and the organic layer was dried over Na_2SO_4. After silica gel column chromatography (hexane/ethyl acetate = 8 : 1), the remaining brown oil was used in the next step without further purification. To a mixture of toluene (20 mL) and *n*-butanol (10 mL) was added the brown oil (1.43 g, 1.39 mmol) and 3,4-dihydoxy-3-cyclobutene-1,2-dione (80 mg, 0.70 mmol), the resulting mixture was refluxed for 24 h under nitrogen, during which period water was azeotropically removed. After it was cooled to room temperature, the solvent was removed, the residue was purified with silica gel column chromatography eluting with hexane and ethyl acetate (first 4:1, 2:1, then 3:2)

to give **G2Sq1** as a blue solid (330 mg, 7%). ^{1}H NMR (400 MHz, CD_2Cl_2): δ 7.77 (m, 2H), 7.32–7.26 (m, 40H), 7.24 (d, J = 7.2 Hz, 4H), 7.12 (d, J = 9.6 Hz, 2H), 6.85 (d, J = 3.2 Hz, 2H), 6.61 (m, 10H), 6.56 (d, J = 6.8 Hz, 4H), 6.50 (t, J = 0.8 Hz, 4H), 6.43 (m, 2H), 6.30 (m, 4H), 6.05 (s, 4H), 4.97 (s, 16H), 4.87 (s, 8H), 3.25 (m, 8H), 1.53 (m, 8H), 1.30 (m, 8H), 0.93 (t, J = 7.2 Hz, 12H). ^{13}C NMR (100 MHz, CD_2Cl_2): δ 165.44, 160.43 (two close peaks), 149.47, 147.77, 141.50, 139.76, 137.39, 136.46, 131.09, 129.23, 128.83, 128.25, 127.97, 123.58, 113.75, 111.91, 109.74, 106.58, 105.38, 101.89, 100.97, 77.91, 70.36, 51.02, 50.20, 29.75, 20.61, 14.10 (Two aromatic peaks missing probably due to overlap of near coincidental resonances). HRMS (MALDI) Calcd. for $C_{142}H_{138}N_4O_{14}$ (M^+): 2123.0210. Found: 2122.9949. Anal. Cacld. for $C_{142}H_{138}N_4O_{14}$: C, 80.27; H, 6.55; N, 2.64. Found: C, 80.09; H, 6.65; N, 2.54.

2.8 References

(1) Maiman, T. H. *Nature* **1960**, *187*, 493.

(2) Torre, G. d. l.; Vázquez, P. n.; Agulló-López, F.; Torres, T. *Chem. Rev.* **2004**, *104*, 3723.

(3) Anderberg, B.; Walbarsht, M. L. *Laser weapons: The dawn of a new military age*; Plenum Press: New York, 1992.

(4) Sun, Y.-P.; Riggs, J. E. *Int. Rev. Phys. Chem.* **1999**, *18*, 43.

(5) Sun, Y.-P.; Riggs, J. E.; Rollins, H. W.; Guduru, R. *J. Phys. Chem. B* **1999**, *103*, 77.

(6) François, L.; Mostafavi, M.; Belloni, J. *J. Phys. Chem. B* **2000**, *104*, 6133.

(7) Wang, J.; Chen, Y.; Blau, W. J. *J. Mater. Chem.* **2009**, *19*, 7425.

(8) Rahman, S.; Mirza, S.; Sarkar, A.; Rayfield, G. W. *J. Nanosci. Nanotechnol.* **2010**, *10*, 4805.

(9) Chi, S.-H.; Hales, J. M.; Cozzuol, M.; Ochoa, C.; Fitzpatrick, M.; Perry, J. W. *Opt. Express* **2009**, *17*, 22062.

(10) Kost, A.; Tutt, L.; Klein, M. B. *Opt. Lett.* **1993**, *18*, 334.

(11) Zhou, G.; Wong, W.-Y.; Poon, S.-Y.; Ye, C.; Lin, Z. *Adv. Funct. Mater.* **2009**, *19*, 531.

(12) Guo, F.; Sun, W. *Inorg. Chem.* **2005**, *44*, 4055.

(13) Zhou, G.-J.; Wong, W.-Y.; Ye, C.; Lin, Z. *Adv. Funct. Mater.* **2007**, *17*, 963.
(14) Zhang, L.; Wang, L. *J. Mater. Sci.* **2008**, *43*, 5692.
(15) Dini, D.; Barthel, M.; Hanack, M. *Eur. J. Org. Chem.* **2001**, 3759.
(16) O'Flaherty, S.; Hold, S.; Cook, M.; Torres, T.; Chen, Y.; Hanack, M.; Blau, W. *Adv. Mater.* **2003**, *15*, 19.
(17) Calvete, M.; Yang, G. Y.; Hanack, M. *Synt. Met.* **2004**, *141*, 231.
(18) Spangler, C. W. *J. Mater. Chem.* **1999**, *9*, 2013.
(19) Tutt, L. W.; Boggess, T. F. *Prog. Quant. Electr.* **1993**, *17*, 299.
(20) Kasha, M. *Discuss. Faraday Soc.* **1952**, *9*, 14.
(21) Pawlicki, M.; Collins, H. A.; Denning, R. G.; Anderson, H. L. *Angew. Chem. Int. Ed.* **2009**, *48*, 3244.
(22) He, G. S.; Xu, G. C.; Prasad, P. N.; Reinhardt, B. A.; Bhatt, J. C.; Dillard, A. G. *Opt. Lett.* **1995**, *20*, 435.
(23) Ehrlich, J. E.; Wu, X. L.; Lee, I.-Y. S.; Hu, Z.-Y.; Röckel, H.; Marder, S. R.; Perry, J. W. *Opt. Lett.* **1997**, *22*, 1843.
(24) Lin, T.-C.; He, G. S.; Prasad, P. N.; Tan, L.-S. *J. Mater. Chem.* **2004**, *14*, 982.
(25) Beverina, L.; Crippa, M.; Salice, P.; Ruffo, R.; Ferrante, C.; Fortunati, I.; Signorini, R.; Mari, C. M.; Bozio, R.; Facchetti, A.; Pagani, G. A. *Chem. Mater.* **2008**, *20*, 3242.
(26) He, G. S.; Zheng, Q.; Lu, C.; Prasad, P. N. *IEEE J. Quantum Electron.* **2005**, *41*, 1037.
(27) He, G. S.; Zheng, Q.; Prasad, P. N.; Helgeson, R.; Wudl, F. *Appl. Opt.* **2005**, *44*, 3560.
(28) Chung, S.-J.; Zheng, S.; Odani, T.; Beverina, L.; Fu, J.; Padilha, L. A.; Biesso, A.; Hales, J. M.; Zhan, X.; Schmidt, K.; Ye, A.; Zojer, E.; Barlow, S.; Hagan, D. J.; Van Stryland, E. W.; Yi, Y.; Shuai, Z.; Pagani, G. A.; Brédas, J.-L.; Perry, J. W.; Marder, S. R. *J. Am. Chem. Soc.* **2006**, *128*, 14444.
(29) Eicher, T.; Hauptmann, S.; Speicher, A. *The chemistry of heterocycles: structure, reactions, syntheses, and applications*; 2 ed.; Wiley-VCH: Germany, 2005.
(30) Zheng, S.; Beverina, L.; Barlow, S.; Zojer, E.; Fu, J.; Padilha, L. A.; Fink, C.; Kwon, O.; Yi, Y.; Shuai, Z.; Van Stryland, E. W.; Hagan, D. J.; Brédas, J.-L.; Marder, S. R. *Chem. Commun.* **2007**, 1372.
(31) Kwon, O.; Barlow, S.; Odom, S. A.; Beverina, L.; Thompson, N. J.; Zojer, E.; Brédas, J.-L.; Marder, S. R. *J. Phys. Chem. A* **2005**, *109*, 9346.
(32) Grayson, S. M.; Fréchet, J. M. J. *Chem. Rev.* **2001**, *101*, 3819.
(33) Bosman, A. W.; Janssen, H. M.; Meijer, E. W. *Chem. Rev.* **1999**, *99*, 1665.
(34) Fréchet, J. M. J. *Science* **1994**, *263*, 1710.
(35) Vilsmeier, A.; Haack, A. *Ber. Dtsch. Chem.* **1927**, *60*, 119.
(36) Campaigne, E.; Archer, W. L. In *Org. Syn., Coll.* 1963; Vol. 4, p 331.
(37) Zheng, S.; Barlow, S.; Parker, T. C.; Marder, S. R. *Tetrahedron Lett.* **2003**, *44*, 7989.
(38) Horner, L.; Hoffmann, H.; Wippel, H. G. *Chem. Ber.* **1958**, *91*, 61.
(39) JR., W. S. W.; Emmons, W. D. *J. Am. Chem. Soc.* **1961**, *83*, 1733.
(40) Boutagy, J.; Thomas, R. *Chem. Rev.* **1974**, *74*, 87.

(41) McMurry, J. E.; Fleming, M. P. *J. Am. Chem. Soc.* **1974**, *96*, 4708.
(42) Hawker, C. J.; Fréchet, J. M. J. *J. AM. Chem. Soc.* **1990**, *112*, 7638.
(43) Beverina, L.; Salice, P. *Eur. J. Org. Chem.* **2010**, 1207.
(44) Sreejith, S.; Carol, P.; Chithra, P.; Ajayaghosh, A. *J. Mater. Chem.* **2008**, *18*, 264.
(45) Ohira, S.; Rudra, I.; Schmidt, K.; Barlow, S.; Chung, S.-J.; Zhang, Q.; Matichak, J.; Marder, S. R.; Brédas, J.-L. *Chem. Eur. J.* **2008**, *14*, 11082.
(46) Sheik-Bahae, M. *IEEE J. Quant. Electr.* **1990**, *26*, 760.
(47) Makarov, N. S.; Drobizhev, M.; Rebane, A. *Opt. Express* **2008**, *16*, 4029.
(48) Marder, S. R.; Perry, J.; Zhou, W.; Kuebler, S. M.; Cammack, J. K. *PCT Int. Appl.* **2002**, WO 2002.
(49) Londergan, T.; Todorova, G. K.; Zhu, J.; Huang, D. *PCT Int. Appl.* **2002**, WO 2001.
(50) Odom, S. A.; Lancaster, K.; Beverina, L.; Lefler, K. M.; Thompson, N. J.; Coropceanu, V.; Brédas, J.-L.; Marder, S. R.; Barlow, S. *Chem. Eur. J.* **2007**, *13*, 9637.
(51) Pisula, W.; Kastler, M.; Wasserfallen, D.; Pakula, T.; Müllen, K. *J. Am. Chem. Soc.* **2004**, *126*, 8074.
(52) Zheng, S.; Marder, S. R. *Unpublished results*.
(53) Cheung, S.-Y.; Chow, H.-F.; Ngai, T.; Wei, X. *Chem. Eur. J.* **2009**, *15*, 2278.

Chapter 3: Synthesis, Photophysical and Electronic Properties of Squaraine Dimers and Oligomers

3.1 Introduction

As already discussed in Chapters 1 and 2, two-photon absorption (2PA) can be used in many fields, including optical-power limiting, 3-D optical memory and fabrication and photodynamic therapy, and materials with large 2PA cross-sections (δ) are essential to enable such applications.[1-3] For quadrupolar 2PA dyes, increasing their conjugation length may enhance the corresponding transition dipole moments which result in a significant increase in 2PA cross-section as well as substantially shift the peak position of 2PA to longer wavelength.[4] According to equation (1)[5,6] based on the so-called "three-state model", the enhancement in transition dipole moments may lead to an increase in maximum 2PA cross-section, δ_{max}:

$$\delta_{max} = f(\omega, n) \frac{M_{ge}^2 M_{ee'}^2}{(E_{ge} - \hbar\omega)^2 \Gamma_{ge'}} \qquad (1)$$

where M_{ge} and $M_{ee'}$ denote the transition dipole moment between the ground-state *g* and the first excited-state *e* and between *e* and a higher-lying excited-state *e*' (transitions into which are two-photon allowed), respectively. E_{ge} is the energy gap between state *g* and *e*, $\hbar\omega$ is the excitation photon energy at the 2PA resonance that the energy gap between state *g* and *e*', $E_{ge'} = 2\hbar\omega$. The quantity $E_{ge} - \hbar\omega$ is often called detuning energy. $\Gamma_{ge'}$ is an energy damping term for the transition of *g* to *e*'.

One approach to increase the conjugation length is to make oligomers and polymers of π-conjugated building blocks. An outstanding example is conjugated porphyrin oligomer and polymer arrays that have been extensively investigated in the

literature.[7-22] Large real and imaginary components of third order nonlinear optical susceptibilities ($\chi^{(3)}$) at 1064 nm have been reported by the Anderson's group,[19,22-24] as measured using the degenerate four-wave mixing method, and the large values of the imaginary component were attributed to strong 2PA. Systematic study of butadiyne-linked porphyrin dimers and oligomers using two-photon induced fluorescence method (TPIF)[11,15,17] revealed a 500-fold cooperative enhancement in 2PA cross-section, when going from the porphyrin monomer to the dimer. The monomeric porphyrin model showed a maximum 2PA cross-section δ_{max} = 20 GM (1 GM is 1×10^{-50} cm^4 s photon^{-1}) at a photon wavelength of ca. 850 nm, while the dimers with various conjugated linkers showed δ_{max} up to 11 000 GM around 890 nm.[17] It was claimed that an increase in $M_{ee'}$ is the most important factor for 2PA enhancement caused by linear extension of the system in these dimers.[17] Moreover, theoretical calculations on the transition dipole moments M_{ge} and $M_{ee'}$ suggested that they are parallel in the dimer, whereas they are probably perpendicular one to the other in the monomer.[15] For these dimers, effective porphyrin–porphyrin core coupling were also suggested by the UV-Vis absorption spectra, in which broadness in B bands and unusually intense red-shifted Q bands were observed.

However, extending the length of the oligomers further did not lead to dramatic changes in the 2PA efficiency for each porphyrin core, which was attributed to a saturation of long oligomers with ineffective conjugation by Anderson and co-workers.[11] For example, the tetramer (5500 GM per porphyrin), octamer (4600 GM per porphyrin), or polymer (6400 GM per porphyrin), as shown in Figure 3.1, exhibit extremely large δ_{max} with 2PA spectra shifted to longer wavelength as the number of units in the chain increases, but the contribution to δ_{max} per porphyrin unit did not change significantly.

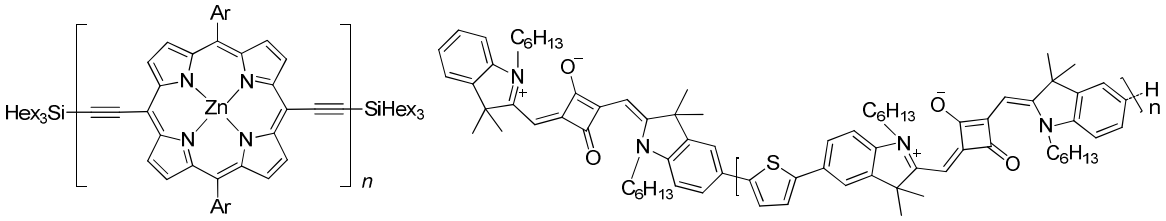

Figure 3.1: Porphyrin and squaraine oligomers with large 2PA cross-sections.

The Anderson's group also studied the effect of various linker groups in porphyrin dimers (Figure 3.2). When changing the central bridge from acetylene to vinylene, a large twisted angle (from crystal structure) between the porphyrin planes disrupts the communication of the two phophyrin π-systems, and significantly reduces the low energy 2PA peak cross-section to 60 GM, comparing to the corresponding 2PA peak of acetylene-linked porphyrin dimer with δ = 255 GM.[14] On the other hand, vinyl linked dimer shows broad one-photon absorption band, which limits the accessible window for TPIF measurement that the maximum 2PA wavelength is unreachable by the probe. Changing the acetylene bridge to a butadiyne unit, which is considered to increase the π-conjugation but might result in larger twisting angle between the porphyrin cores, slightly reduced 2PA cross-section was obtained.[17] Significant efforts have also been devoted to obtaining highly conjugated porphyrin system using a *β-β* double linkage to restrain the rotation of the porphyrin and reduce the dihedral angle,[10,25] or by *meso-β* doubly and meso-meso, *β-β, β-β* triple linkage to form completely fused coplanar systems.[9,13] The conformation of the porphyrin planes could also be controlled by coordination to form double-strand ladder arrays[11,18,26] and changing the length of a "strap" between two macrocycles.[12] Much more enhanced 2PA compared to the corresponding one-site linked "free-move" porphyrin oligomers were observed for the delocalized systems from the studies cited above.

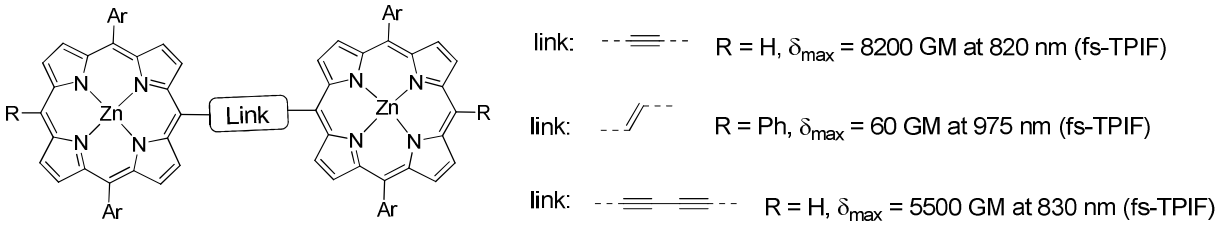

Figure 3.2: Structures and 2PA cross-sections of porphyrin dimers with different linkages.[1]

The one-photon absorption and 2PA behavior of squaraine-based oligomers (structures in Figure 3.1) were investigated by Lambert and co-workers.[27] The molar absorptivity of each higher generation oligomer covers the one of the lower generation oligomer with slightly red-shifted absorption maximum. The peak 2PA cross-section δ, obtained from TPIF measurements, increases nonlinearly with the number of the monomeric subunits n and is correlated with the enhancement of the transition dipole moment M_{ge}. The optical properties of these squaraines are summarized in Table 3.1. According to exciton coupling theory, it was concluded that there was no significant ground-state interaction between the monomeric subunits and the thiophene bridge could be treated as a simple spacer. In the symmetrical monomeric squaraines, two 2PA peaks were observed and assigned to excitation of the molecule to a vibrational sublevel of the one-photon absorption (1PA) state[28] and to a 2PA allowed higher electronic excited-state,[29] respectively.

Table 3.1:Optical properties of squaraine oligomers in the literature[27]

	n = 0	n = 1	n = 2	n = 3	n = 4
λ_{max} (nm)	635	681	708	720	725
ε (10^5 $M^{-1}cm^{-1}$)	2.95	4.18	6.49	6.80	7.52
M_{ge} (D)	12.6	19.8	27.9	29.3	31.1
δ_{max} (10^3 GM)	0.3	4.7	12.9	17.7	24.8

3.2 Motivation and molecule design

Squaraines with sharp intense absorption in the visible to near-IR and unique electronic properties, have been extensively studied for many applications as already described in Chapter 1. In this chapter we will describe a series of squaraine dimers with various π-linkers, a trimer and a benzene centered hexamer (Figure 3.3), which were designed in order to study their structure-property relationships and to achieve large 2PA cross-sections. Here, the monomeric model compound **Sq** was synthesized for comparison. Acetylene, vinylene, and butadiyne linkage were chosen to study the conjugation through different pathway. A non-planar push-pull dimer with [2+2] addition of tetracyanoethylene to the acetylene linker[30] was proposed to investigate the influence of strong electron withdrawing cyano- group on the optical and electronic properties.

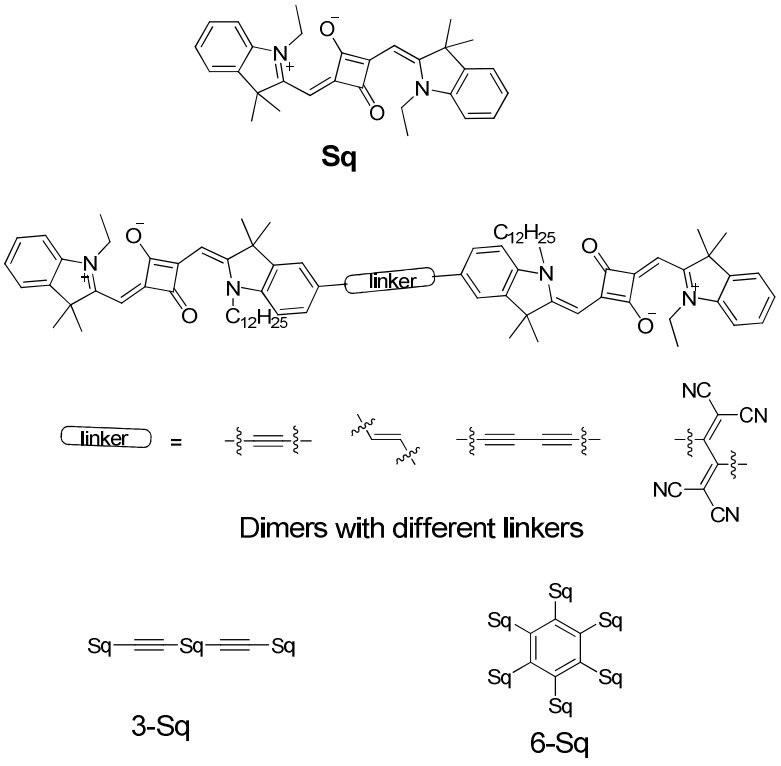

Figure 3.3: Structures of squaraine oligomers.

3.3 Synthesis of the squaraine dimers and oligomers

The symmetrical and unsymmetrical indolium-based squaraines have been synthesized following the conventional procedures as shown in Scheme 3.1 and Scheme 3.2. The bromo functionality was introduced at the stage of Fischer indole synthesis[31] followed by incorporation of a long alkyl chain to ensure good solubility of the squaraine products. It was then condensed with squaric acid under the condition that water is azeotropically removed to give the symmetrical squaraine with di-bromo functionality (**Sq-2Br**). The unsymmetrical squaraine synthesis started from the formation of semisquaraine,[32] as discussed in Chapter 1, and the semisquaraine was subsequently condensed with the bromo-indolium salt to yield **Sq-Br**, as shown in Scheme 3.2.

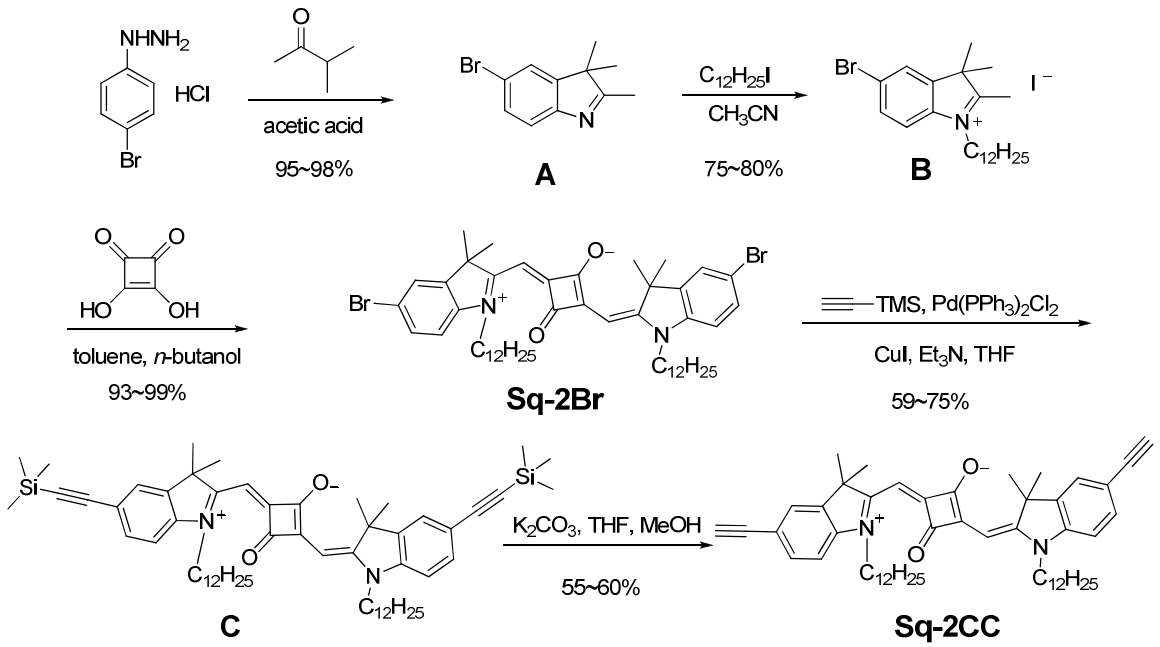

Scheme 3.1: The synthesis of symmetrical squaraine diacetylene.

In the synthesis of **Sq-CC,** the ethynyl substituted squaraine, 2-methylbut-3-yn-2-ol was first chosen as the protected acetylene for the Sonogashira coupling because the hydroxyl group is expected to provide sufficient polarity difference for silica gel column

chromatography purification. However, decomposition of the respective squaraines was observed in the preparation of **Sq-CC,** due to the harsh deprotection conditions such as refluxing with sodium in toluene. Trimethylsilyl protecting group was then selected instead, taking the advantages on its easy deprotection. However, due to the similarity in polarity and molecular size of **Sq-Br**, compound **G**, and **Sq-CC**, the purification was a challenge. In order to have a complete conversion of each starting material, the protection and deprotection reactions were carried out at least overnight. Each compound was purified by flash silica gel column and multiple size-exclusion columns in portions (due to the limited content and length of the column). Similar problems occurred when **Sq-2CC** was synthesized.

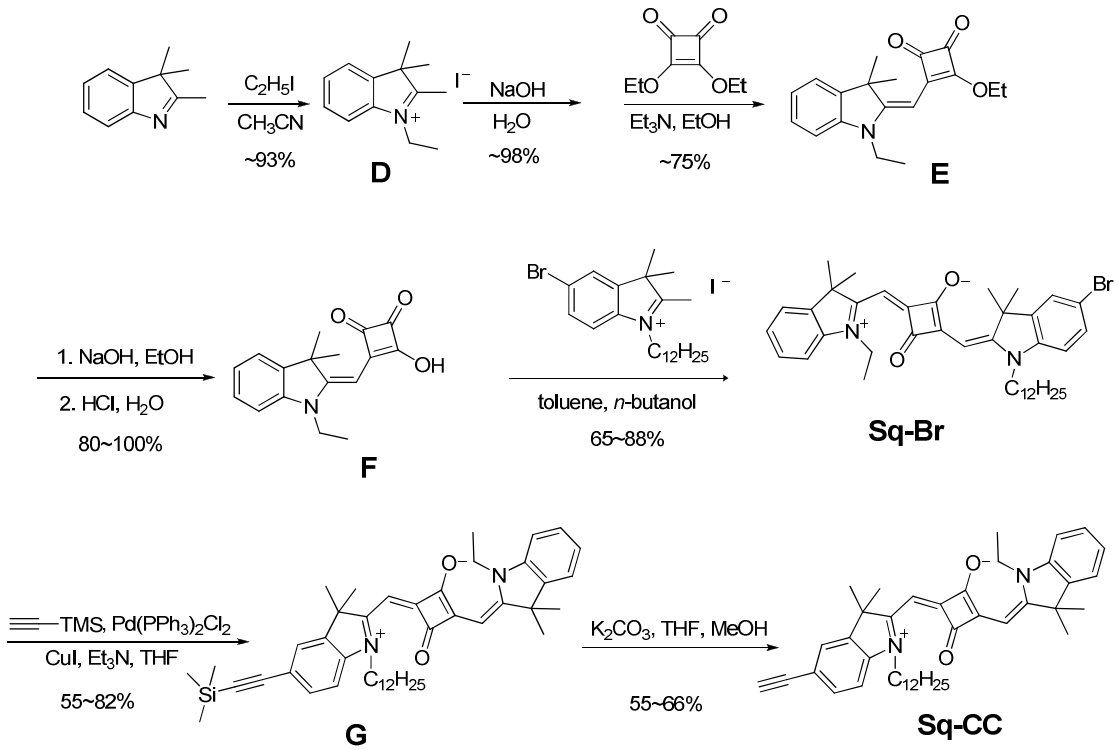

Scheme 3.2: The synthesis of unsymmetrical squaraine mono-acetylene.

It is worth noting that the selection of catalysts for the respective Sonogashira coupling reaction depended upon the substrates (Scheme 3.3). 2-Methylbut-3-yn-2-ol worked well with a Pd [0] catalyst while no coupling occurred with a Pd[II] catalyst when reacted with **Sq-Br**. However, the opposite effects were observed when trimethylsilylacetylene was used.

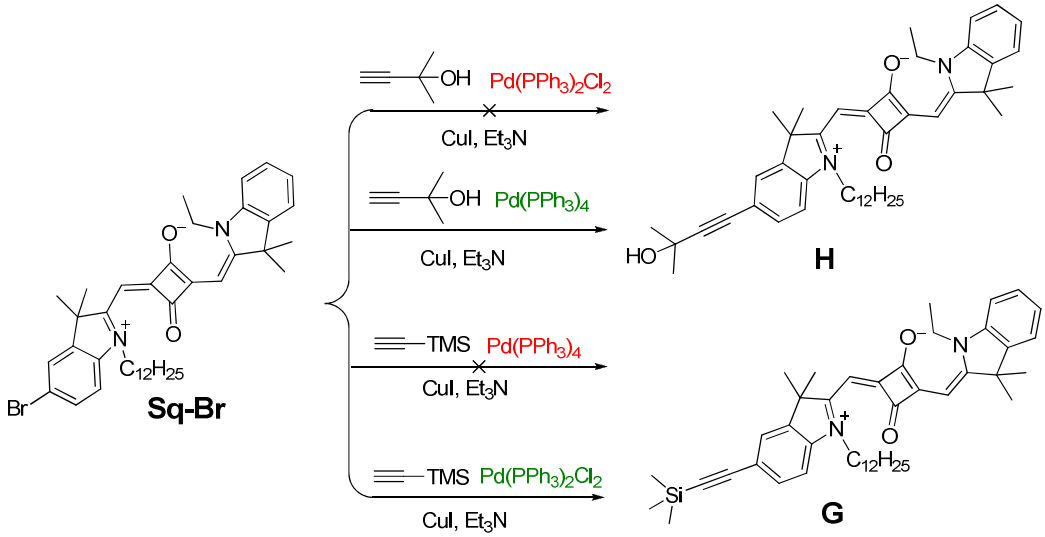

Scheme 3.3: The Sonogashira coupling with different protecting groups.

Acetylene and vinylene linked dimers were synthesized by the microwave-assisted Stille coupling reaction[33] between **Sq-Br** and the corresponding distannyl compounds. However, attempts to make a single-bond linked dimer were not successful with bistributyltin, which might due to the steric hindrance between two squaraines. The dimer with a butadiyne linker, **Sq-CC-CC-Sq**, was obtained in high yield from **Sq-CC** by direct oxidative homo-coupling in the presence of benzoquinone using a literature procedure.[34] As shown in Scheme 3.5, Stille coupling between **Sq-Br** and **Sq-2CC** or **Sq-2Br** and **Sq-CC** gave the trimer, **3Sq**, but with low yields, which could be attributed to the oxidative homo-coupling between the squaraine acetylenes. This was further confirmed by the MALDI mass spectra of the major fractions isolated from the reaction

mixtures. The non-planar push-pull dimer with cyano group on the bridge (**Sq-CN-Sq**) was obtained with high yield by simply treating **Sq-CC-Sq** with tetracyanoethylene (TCNE) in dichloromethane at room temperature.[30,35] A star-shaped molecular architecture with six squaraines (**6-Sq**) was made by $Co_2(CO)_8$ catalyzed trimerization from **Sq-CC-Sq**.[36] All the oligomers have been purified through silica gel column chromatography followed by size-exclusion column chromatography. The chemical structures and purity of the compounds have been confirmed by ^{1}H NMR, ^{13}C NMR, mass spectroscopy and elemental analysis.

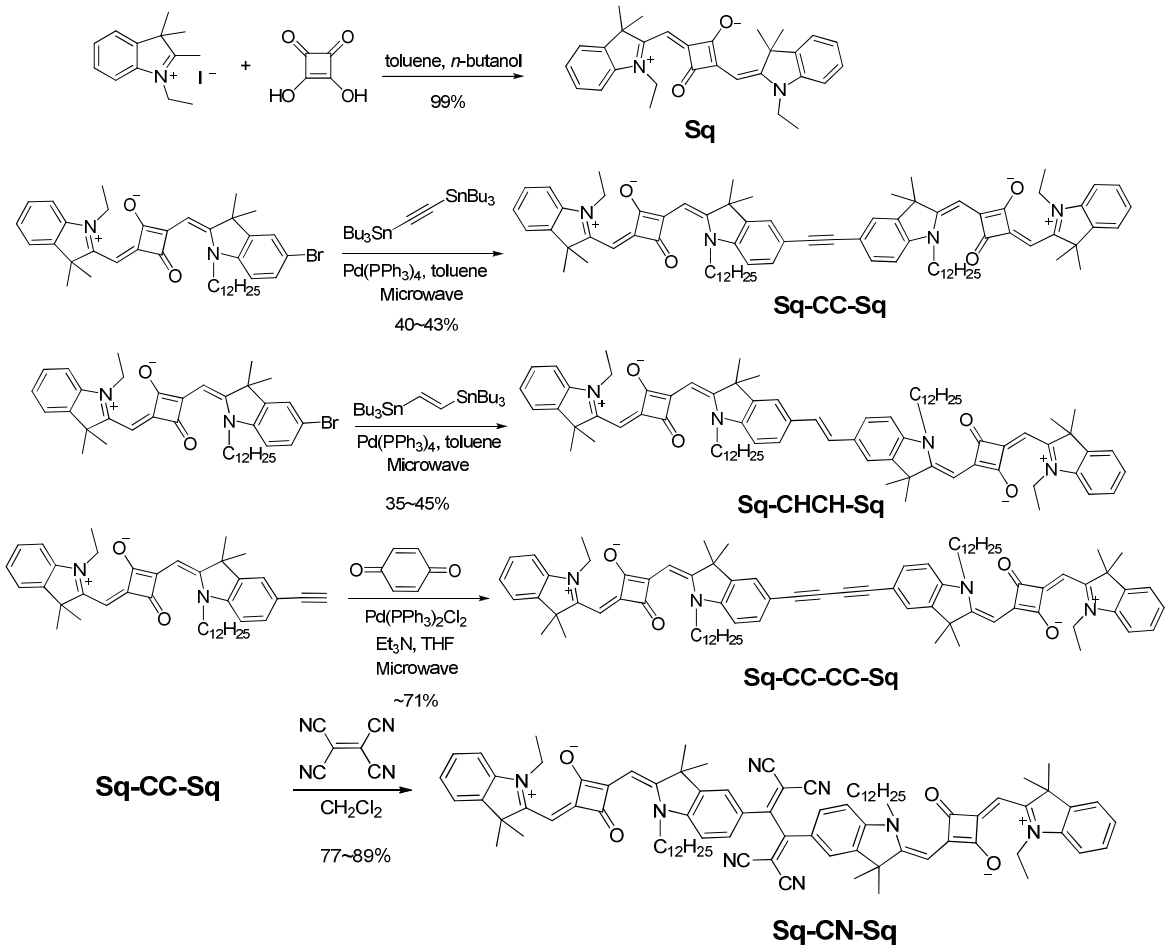

Scheme 3.4: The synthesis of squaraine dimers with different linkers.

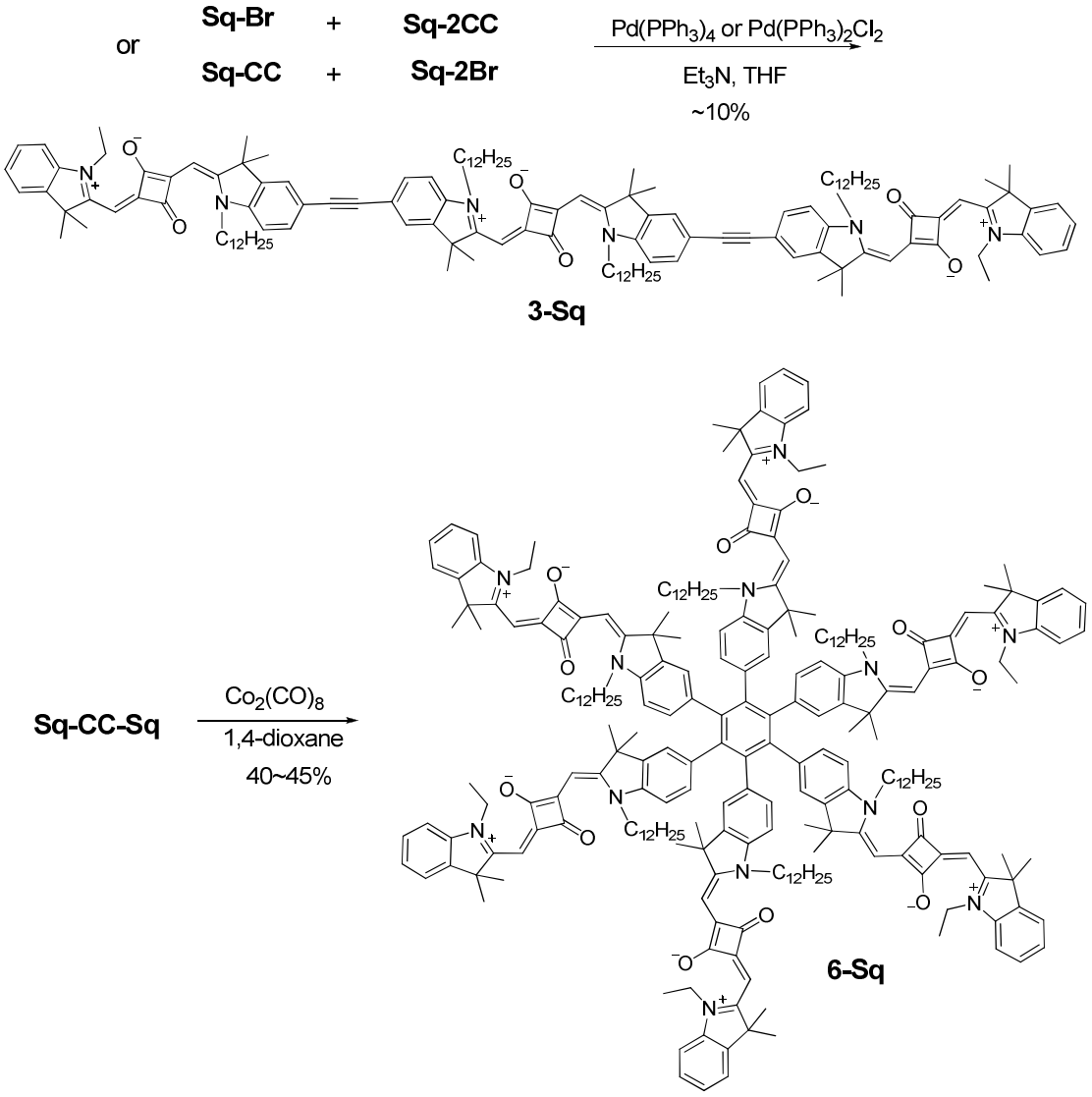

Scheme 3.5: The synthesis of 3-Sq and 6-Sq.

3.4 Optical properties of the squaraine oligomers

3.4.1 Absorption and fluorescence of the squaraine oligomers

UV-Vis. absorption spectra of the squaraines were taken in chloroform as shown in Figure 3.4. In general, the dimers and **3-Sq** showed much broader bathochromically-shifted absorption bands compared to **Sq,** which was similar to what Scherer and coworkers

observed.[27] Moving from monomeric squaraine, **Sq**, to dimer, **Sq-CC-Sq**, and trimer, **3-Sq**, the absorption maximum red shifts from 634 nm to 704 nm, corresponding to 0.19 eV difference in energy. The broad shoulder absorption at higher energy to the maximum in dimers and **3-Sq** might be explained by a manifold of vibronic side bands with additional rotamers which might present due to the unhindered C–C single bonds rotation. The hexamer, **6-Sq**, has extremely large extinction coefficient (ca. 1.2×10^6 $M^{-1}cm^{-1}$at 651 nm) with the oscillator strength calculated from the spectra as large as 6 times of **Sq**, indicating each squaraine unit contributes individually to the absorption, which may suggest weak interaction between each squaraine arm. Among all the dimers, the one with the vinylene linkage, **Sq-CHCH-Sq**, was found to possess the most bathochromically-shifted peak (~0.18 eV difference in absorption maxima) compared with **Sq**, but it still exhibits a sharp absorption band. The absorption band of the dimer with a butadiyne linker, **Sq-CC-CC-Sq**, is slightly blue-shifted with respect to **Sq-CC-Sq**, despite of the longer π-bridge, which is probably due to the torsion angle between each squaraine acetylene unit. The optical bandgaps for the dimers and trimer are in the range of 1.68 to 1.55 eV, estimated from the onsets of the lower energy bands in the solution absorption spectra according to $E_{gap}(optical) = 1240/\lambda_{onset}$ (where λ_{onset} is expressed in nm and E_{gap} in eV). The transition dipole moments of the first electronic transition were calculated. Comparable values to Scherer's work[27] were obtained for monomer and dimer, but there is no further increase as go from the dimers to **3-Sq**. The optical properties of these oligomers are summarized in Table 3.2

Table 3.2: Optical properties of the squaraine oligomers.

Compound	**Sq**	**Sq-CC-Sq**	**Sq-CC-CC-Sq**	**Sq-CHCH-Sq**	**3-Sq**	**6-Sq**
$\lambda_{max}{}^{a}$ (nm)	634	682	672	697	704	651
ε^{a} (10^5 $M^{-1}cm^{-1}$)	3.04	4.55	4.63	4.06	3.18	11.8
M_{ge} (D)	12.4	18.9	17.8	20.3	17.7	31.2
$\Phi_F{}^{b}$	0.49	0.79	0.77	0.66	0.56	0.48

[a]in chloroform; [b]in toluene

A broad non-cyanine like absorption band between 500 nm and 900 nm was observed for **Sq-CN-Sq** where the peak around 700 nm becomes slightly more pronounced and bathochromically-shifted with concentration increases (the molar absorptivity shown in Figure 3.4 is measured and averaged in the concentration range between 1.3×10^{-6} and 2.3×10^{-5} mol/L). A very small optical bandgap of ca. 1.24 eV was obtained as estimated from the absorption onset. The absorption maximum shows hypsochromic shift when increasing solvent polarity, where in methanol the peak is narrower while in toluene it absorbs more into the red.

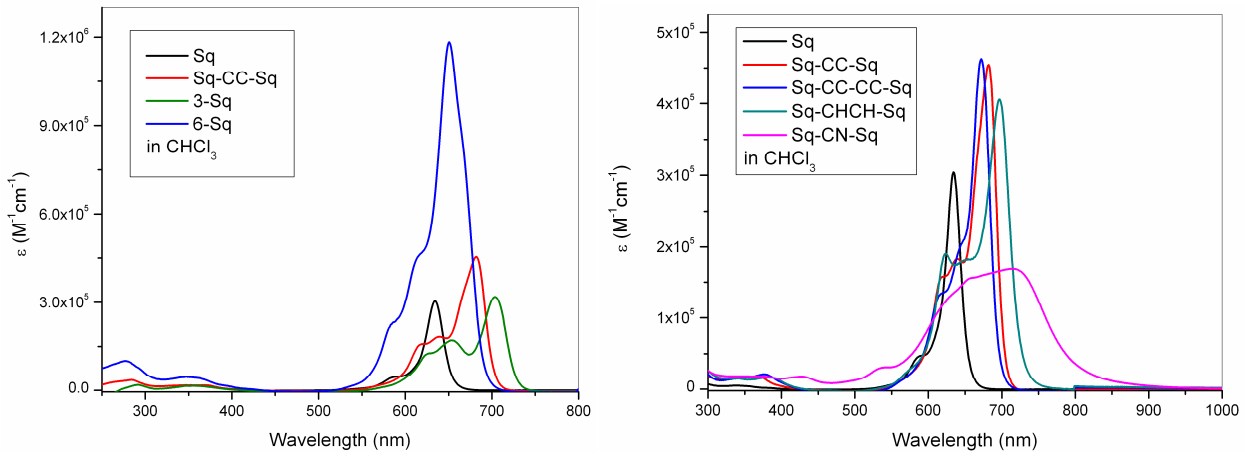

Figure 3.4: Molar absorptivities of squaraine oligomers.

The fluorescence spectra have similar shape for all the oligomers, despite the different vibrational features in the absorption spectra. The Stokes shift for monomer **Sq** is very small, ca. 10 nm, with the fluorescence spectrum appearing as a mirror image (Figure 3.5), which is quite typical for squaraine dyes. Larger Stokes shifts were observed in

oligomers with relatively red-shifted emission. The fluorescence quantum yields (Φ_F) of the squaraine oligomers in toluene solution were determined by Dr. Jochen Campo in the Perry group using meso-tetraphenylporphine (H2TPP, Φ_F = 0.073 in toluene[37]) as reference, and are summarized in Table 3.2. Relatively high fluorescence quantum yields were measured, especially for the dimer series.

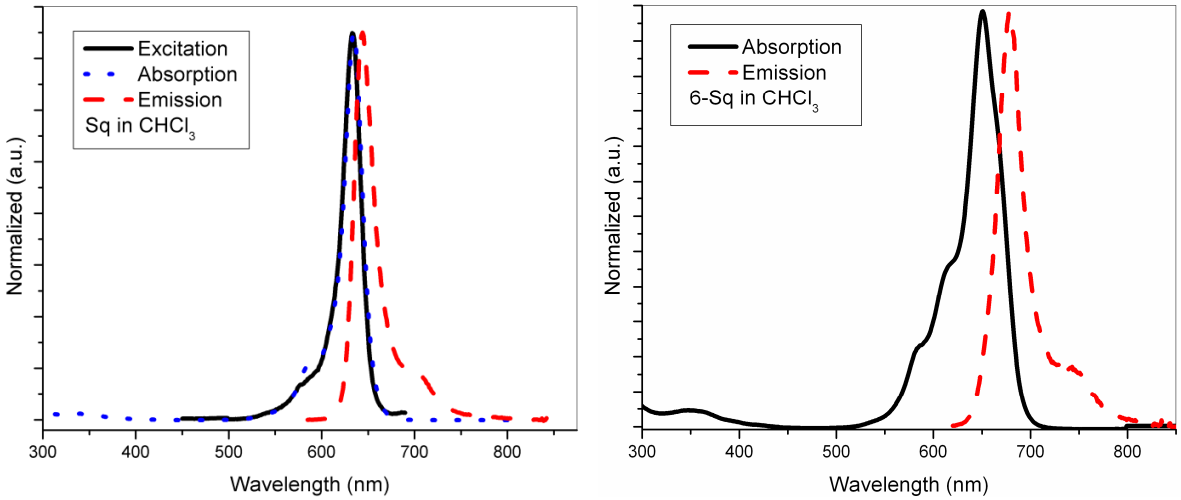

Figure 3.5: Fluorescence spectra of Sq (left) and 6-Sq (right) with their absorption spectra.

3.4.2 Femtosecond transient spectra of the squaraine oligomers

Transient absorption spectra of these oligomers were collected by Dr. Jochen Campo in the Perry group. All squaraines were measured in toluene solution at optical density (OD) of about 1 in a cuvette with a 2 mm path length, and were excited at a slightly longer wavelength than their absorption maxima. Signals in Figure 3.6 were generated upon excitation of **6-Sq** at 675 nm and using a probe in the visible and near-IR range. In the visible region, the transient spectra shortly (< 1 ps) after the photo-excitation with femtosecond laser pulses show the excited-state absorption (ESA) spectrum of **6-Sq** centered at around 500 nm along with the ground-state absorption bleaching. The signals in the near-IR region show a broad band over the entire measurable window (800 – 1600 nm)

with a peak around 900 nm. The lifetime of the excited-state of **6-Sq** was estimated to be ~1.8 ns. Except for **Sq-CN-Sq**, the transient spectra of **3-Sq** and all the dimers are quite similar to **6-Sq** discussed above, with lifetimes between 1.1 – 1.5 ns. Only unstructured transient signals were observed on **Sq-CN-Sq** with fairly short lifetime of ca. ~4 ps. The fairly long excited-state life time and strong ESA in near-IR make these materials possible optical-power limiting (OPL) candidates in this wavelength range, considering squaraine dyes in general also exhibit strong 2PA in these wavelengths, as discussed in the next section.

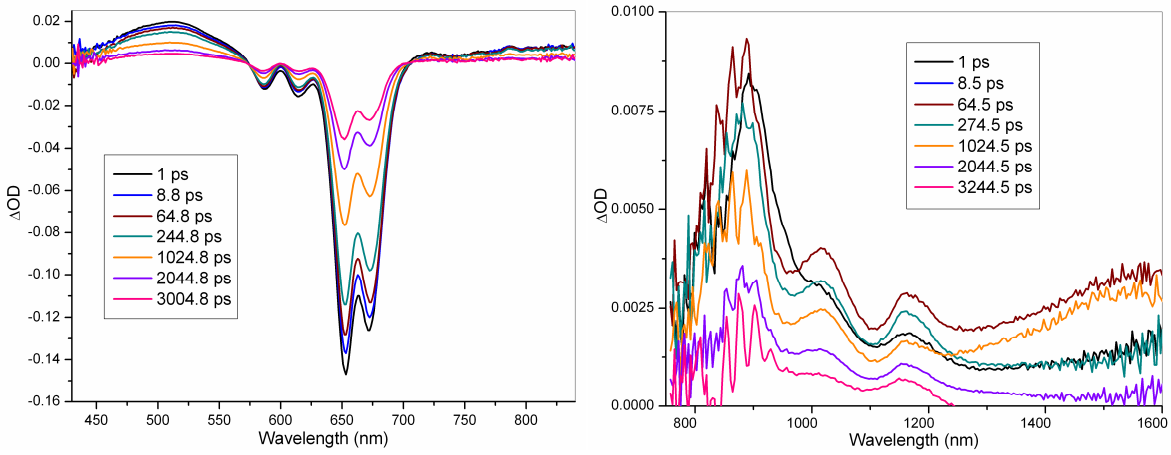

Figure 3.6: Femtosecond transient absorption spectra of 6-Sq in toluene. Left: collected by visible probe; right: collected by near-IR probe. (Figure adapted from Dr. Jochen Campo in the Perry group)

3.4.3 Two-photon absorption of the squaraine oligomers

The two-photon absorption behavior of **Sq**, **Sq-CC-CC-Sq** and **6-Sq** was studied using femtosecond two-photon induced fluorescence (TPIF) and z-scan measurements by Dr. Jochen Campo in the Perry group. As shown in Figure 3.7, there are at least two 2PA transitions for **Sq** in the wavelength range investigated, one resides close to the 1PA

transition, which was attributed to excitation of the molecule to a vibrational sublevel of the lowest-energy one-photon allowed state[27,28] The maximum 2PA cross-section δ around 250 GM at photon wavelength of ca. 1180 nm from both TPIF and z-scan measurements is comparable with literature values.[27,38] The peak with higher transition energy around photon wavelength of 800 nm was not fully resolved as observed in Webster's work[38] due to the limitation of measurement window. This transition can be assigned to excitation of the molecule to a 2PA-allowed higher electronic excited-state.

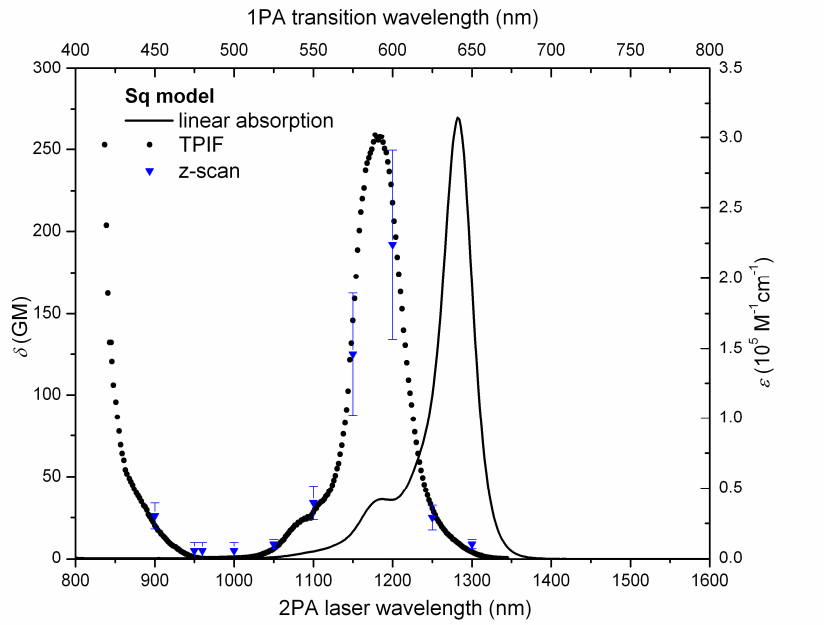

Figure 3.7: 1PA in toluene (line), two-photon induced fluorescence (TPIF) excitation spectra in CCl_4 (black dots) and degenerate (z-scan) 2PA spectra (blue data points) of Sq in THF solution. (Figure adapted from Dr. Jochen Campo in the Perry group)

There are four experimentally observed 2PA bands for **Sq-CC-CC-Sq**: a relatively weak band with $\delta \approx 600$ GM (two-photon excitation at 1200 nm) corresponding to the 2PA excitation into the vibrational sublevel of the lowest-energy one-photon allowed state[27,28] as also observed for **Sq**. Much enhanced 2PA bands at two-photon wavelength of 920 nm and 870 nm were observed which are assigned to the 2PA-allowed electronic excited-states. The 2PA cross-section maximum over 10 000 GM (Figure 3.8) is at least over 15 times of the

corresponding peak observed in **Sq** as reported in Webster's work (750 GM at photon wavelength of 820 nm).[38] The large 2PA cross-section could be attributed to electronic coupling between each squaraine unit in the dimer. Again, unresolved band with 2PA cross-section up to at least 19 000 GM was revealed close to the measurement limit at 800 nm.

The 2PA spectra of **6-Sq** is quite similar to **Sq,** exhibiting a 2PA band with comparable cross-sections to **Sq** close to its 1PA resonance. The unresolved peak of several thousand GM at photon energy around 1.4 eV was observed for **6-Sq**. Single wavelength z-scan measurements on the other dimers and **3-Sq** at 950 nm reveal 2PA cross-sections comparable to **Sq-CC-CC-Sq**, on the order of several thousand GM. The full spectra will be further explored using TPIF method in the Perry group.

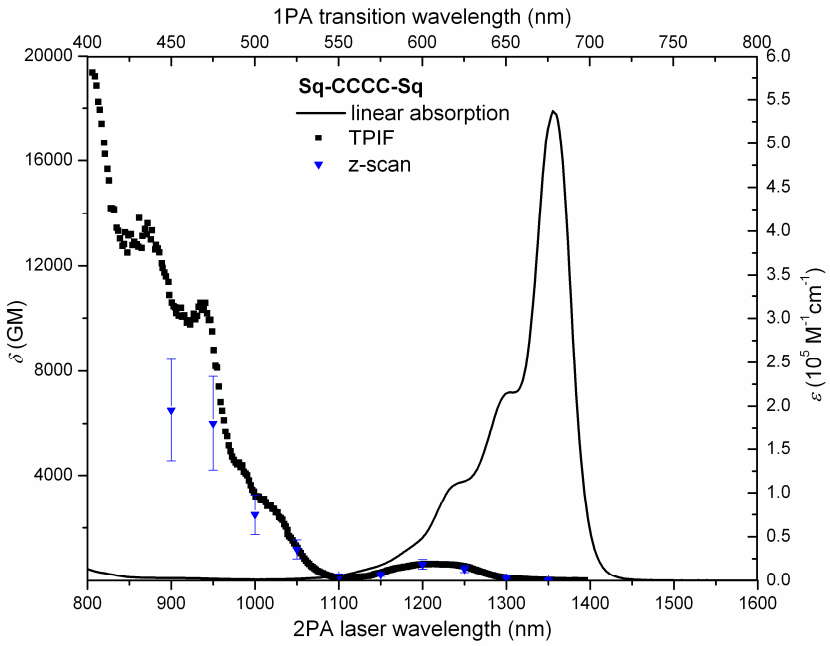

Figure 3.8: 1PA in toluene (line), TPIF excitation spectra in CCl_4 (black dots) and degenerate (z-scan) 2PA spectra (blue data points) of Sq-CC-CC-Sq in THF solution. (Figure adapted from Dr. Jochen Campo in the Perry group)

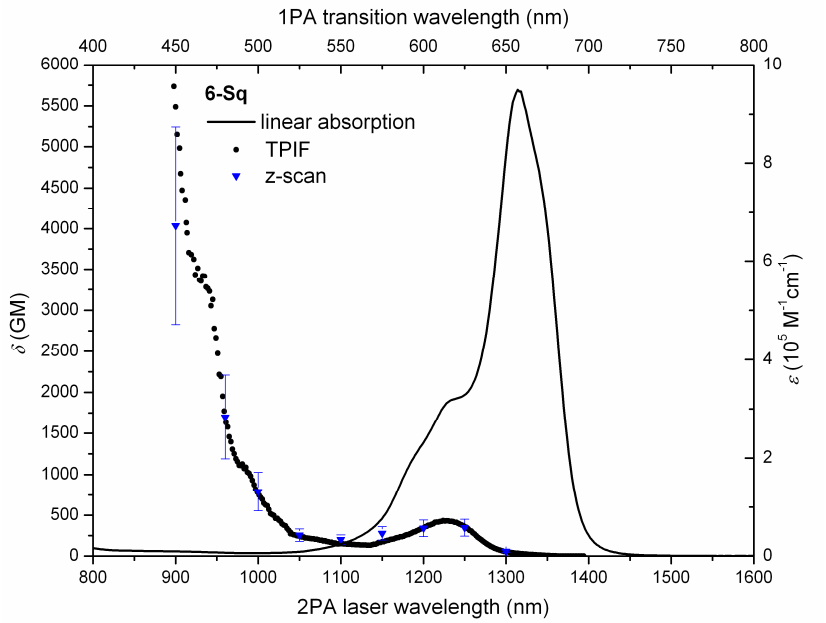

Figure 3.9: 1PA in toluene (line), TPIF excitation spectra in CCl_4 (black dots) and degenerate (z-scan) 2PA spectra (blue data points) of 6-Sq in toluene solution. (Figure adapted from Dr. Jochen Campo in the Perry group)

3.5 Electronic properties of the squaraine oligomers

3.5.1 Electrochemistry of the squaraine oligomers

Cyclic voltammetry measurements of the squaraine oligomers were conducted in 0.1 M anhydrous dichloromethane solution of $^{n}Bu_4NPF_6$ with bis(pentamethylcyclopentadienyl) iron(II) as internal reference at a scan rate of 50 mV s^{-1}. The half-wave potential ($E_{1/2}$) values (defined as (E_{pa} + E_{pc})/2, where E_{pa} and E_{pc} are peak oxidation and reduction potentials, respectively) are summarized in Table 3.3. In general, the squaraine oligomers are readily oxidized and difficult to reduce. It is worth noting that each squaraine unit undergoes a one-electron redox process at the same potential as calculated from the integration of peaks in *differential* pulse voltammetry (DPV). The redox potentials of dimers and **3-Sq** are slightly lower compared to **Sq** with the most

distinguishable change in **Sq-CC-Sq**. The redox potential of **6-Sq** remains almost the same as **Sq** which might indicate there is no strong interaction between each squaraine arm and the observation is consistent with that from absorption spectra. The electron affinity (EA) was estimated from the first electrochemical half-wave reduction potentials $E_{1/2}^{0/-}$ with EA = -e ($E_{1/2}^{0/-}$ + 4.8 V) based on the ionization potentials (IP) value of 4.8 eV for solid state ferrocene with respect to zero vacuum level.[39] Except for **Sq-CC-Sq**, which has an EA of ca. -3.24 eV, the EAs for the other oligomers are around -3.1 eV. The first oxidation potentials were used to estimate the IPs of the compounds, which were found to be around -4.7 eV. The "electrochemical gap" estimated from the redox potential for the compounds list here are almost identical of ca. 1.74 ± 0.04 eV despite the structure and absorption spectra difference.

Table 3.3: Cyclic voltammetry data of squaraine oligomers

$E_{1/2}$ *vs* $FeCp_2^{+/0}$ *(V)*	*2n+ / +**	*n+ / 0**	*0 / n–**
Sq	0.52	0.04	–1.71
Sq-CC-Sq	0.65	0.18	–1.56
Sq-CC-CC-Sq	0.55	0.09	–1.65
Sq-CHCH-Sq	0.52	0.03	–1.69
3-Sq	0.55	0.08	–1.66
6-Sq	0.54	0.06	–1.72

**n* = number of squaraine unit

There are two additional peaks at −0.82 eV and −1.12 eV vs. ferrocene observed for **Sq-CN-Sq** (Figure 3.10), and these peaks could be assigned to the two sets of cyano-groups on the bridge acquiring or losing one electron at each reduction and oxidation process, respectively. Because of the effect of the electron withdrawing substituents, the first oxidation potential of **Sq-CN-Sq** is increased by 0.16 eV with respect to **Sq**.

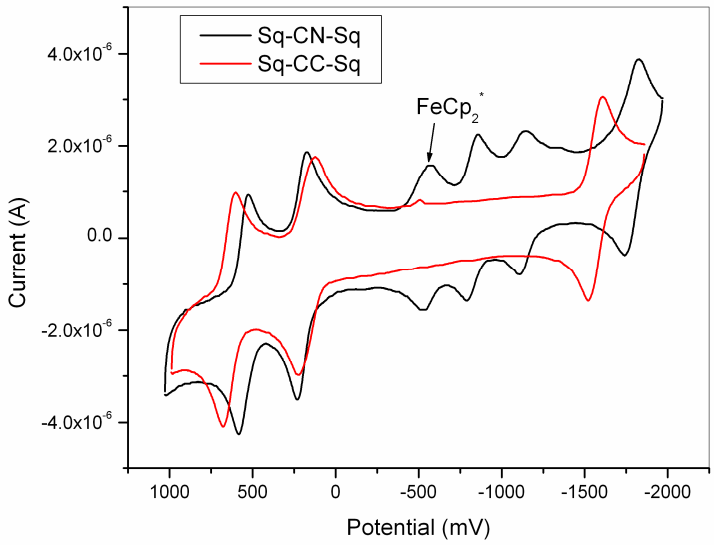

Figure 3.10: Cyclic voltammetry curve of Sq-CN-Sq and Sq-CC-Sq with bis(pentamethylcyclopentadienyl) iron(II) ($FeCp_2^*$) as internal standard; the potential is referenced to ferrocene.

3.5.2 Photovoltaic characterization

Because of the good light-harvesting ability and their good electron donating ability, some of the oligomers have been tested in organic solar cell devices as the donor component of the active layer, in a blend with soluble fullerene derivative PCBM at different weight ratios by Dr. Yinhua Zhou in the Kippelen group. The device configuration used for this investigation is illustrated in Figure 3.11. The weight ratios of squaraine/PCBM in the solution used to spin-coat the active layers were 1 : 1 and 1: 3. The incident photon-to-current conversion efficiency (IPCE) for squaraine/PCBM = 1 : 3 blends was found to be significantly higher over the whole spectral region, even at the squaraine absorption peak, than for the other blend ratio (Figure 3.12), although the IPCE values are still relatively low (~10%) as compared to other squaraine-based systems in literature.[40-43] As a result, higher short-circuit currents (J_{SC}) were measured for 1:3 blends, leading to a higher power conversion efficiency (PCE) for this

composition. One possible explanation for the observed trend is the lack of high energy absorption by the squaraine portion and a relatively low charge transport mobility of squaraine donor, which is on the order of 10^{-4} $cm^2V^{-1}s^{-1}$ for **6-Sq** in transistor devices.

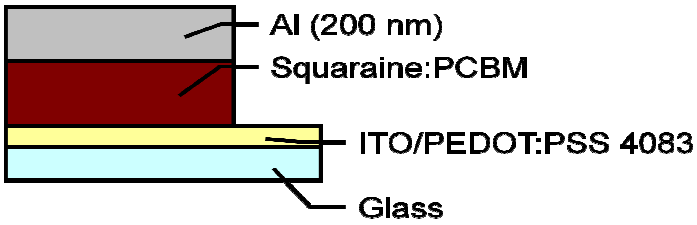

Figure 3.11: General solar cell structure for squaraine/PCBM blends. (Figure adapted from Dr. Yinhua Zhou from the Kippelen group)

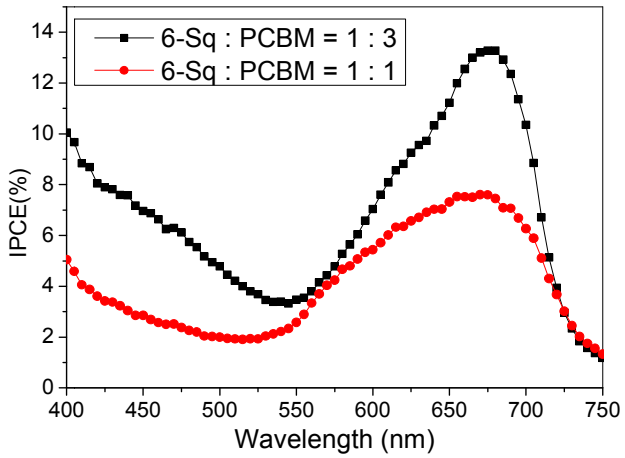

Figure 3.12: IPCE curves for the 6-Sq /PCBM blends. (Figure adapted from Dr. Yinhua Zhou from the Kippelen group)

The monomer **Sq** was found only to give a PCE of ca. (0.056 ± 0.004)% with relatively low J_{SC} of ca. 0.47 ± 0.01 mA/cm^2 and open-circuit voltage (V_{OC}) of ca. 0.36 ± 0.01 V. The PCE increases going from **Sq** to the dimers and a further increase was observed for **6-Sq**. The highest device performance among those oligomers with a PCE of (0.42 ± 0.01)% for the average of four devices, were achieved using **6-Sq** : PCBM = 1:3 weight ratio (Table 3.4). A much smoother film as observed from atomic force microscopy (AFM) images and more coverage of the solar spectrum might be responsible for the better performance of the devices incorporating larger oligomers.

The dimer with cyano-groups on the bridge, **Sq-CN-Sq**, only shows little improvement in PCEs as compared to **Sq-CC-Sq**, despite it has a much broader absorption spectrum compared to the other oligomers.

Table 3.4: Summary of solar cell performances using squaraine/PCBM blends

Device	V_{OC} *(V)*	J_{SC} *(mA/cm^2)*	*FF*	η *(%)*
Sq[a]	0.36 ± 0.01	0.47 ± 0.01	0.34 ± 0.02	0.056 ± 0.004
Sq-CC-Sq[a]	0.51 ± 0.01	0.82 ± 0.01	0.369 ± 0.006	0.154 ± 0.004
Sq-CC-CC-Sq[a]	0.53 ± 0.01	0.84 ± 0.02	0.356 ± 0.010	0.158 ± 0.033
Sq-CN-Sq[b]	0.51 ± 0.03	0.74 ± 0.02	0.324 ± 0.028	0.183 ± 0.027
6-Sq[b]	0.482 ± 0.006	1.56 ± 0.06	0.38 ± 0.01	0.42 ± 0.01

[a]under illumination of Oriel lamp, 100 mW/cm^2; [b]under illumination of oriel lamp, 67 mW/cm^2

3.6 Conclusions

Bis(indolinylenemethyl)squaraine-based dimers with various π-bridges, a trimer, and a hexamer were designed and synthesized. The absorption bands of the oligomers show bathochromic shift compared with the **Sq** model. The fluorescence quantum yields of the dimers are fairly high in toluene with similar emission spectra despite of the different vibrational structure of their absorption spectra. Except for **Sq-CN-Sq**, which has very short excited-state lifetime, all the other oligomers possess similar transient spectra, characterized by an excited-state absorption band around 500 nm and broad transient absorption in the region of 800–1600 nm with lifetimes around 1.1–1.8 ns. A large enhancement in 2PA cross-sections of **Sq-CC-CC-Sq**, was observed with peak performance at laser wavelengths of 800–900 nm. The other oligomers also show a 2PA cross-section on the order of several thousand GM at 950 nm determined by z-scan. These oligomers have been investigated as light harvesting donors in organic solar cells as blends

with PCBM. Moderate efficiencies were achieved but with significant improvement in PCEs from **Sq** to dimers and **6-Sq**, which could be attributed to more coverage of solar spectrum by the oligomers and morphology changes.

3.7 Experimental Section

General: All the chemicals were purchased from commercial sources and used without further purification, unless otherwise indicated. Where necessary, dichloromethane, THF, and toluene were dried using a MBraun solvent purification system. The ^{1}H, and ^{13}C NMR spectra were collected on a Bruker 400 MHz or 500 MHz or a Varian 300 MHz spectrometer. Mass spectra were measured on a VG Instruments 70-SE using the electron impact (EI) or fast-atom bombardment (FAB) mode and on an Applied Biosystems 4700 Proteomics Analyzer using MALDI mode. Elemental analyses were carried out by Atlantic Microlab using a LECO 932 CHNS elemental analyzer. Solution and thin film UV-Vis absorption spectra were recorded on a Varian Cary 5E UV-Vis-near-IR spectrophotometer while solution emission spectra were recorded with a Shimadzu FP-5301PC spectrofluorometer. Electrochemical measurements were carried out under nitrogen in deoxygenated 0.1 M solutions of tetra-*n*-butylammonium hexafluorophosphate in anhydrous dichloromethane using a computer-controlled BAS 100B electrochemical analyzer, a glassy-carbon working electrode, a platinum-wire auxiliary electrode, and an Ag wire anodized with AgCl as a pseudo-reference electrode at a scan rate of 50 mV/s. The potentials were referenced to the ferrocene ($FeCp_2^{+/0}$)

redox couple by using bis(pentamethylcyclopentadienyl)iron(II) as an internal standard (-0.55 V vs. ferrocene).

Femtosecond transient absorption measurements: The experiments were performed on a commercially available transient absorption spectroscopy system (Helios, Newport), by Dr. Jochen Campo in the Perry group. The excitation source was generated by an optical parametric amplifier (TOPAS, Newport) pumped by a Ti:Sapphire regenerative amplifier (Spitfire, Newport), operating at 500 Hz repetition rate. Approximately 5% of the 800 nm Spitfire output was used to generate the white-light continuum probe beam in a proprietary nonlinear optical crystal, at the wavelengths of 440 – 850 nm using a Ti:Sapphire crystal and 800 – 1600 nm using Nd:YAG crystal in a sapphire plate. All squaraines were measured in toluene solution (OD of about 1 in a 2 mm path length cuvette), and were excited at a slightly longer wavelength than their absorption maxima.

Femtosecond z-scan:[44] The experiments were performed by Dr. Jochen Campo in the Perry group at multiple wavelengths for **Sq, Sq-CC-CC-Sq**, and **6-Sq**, selected wavelength for other oligomers. **Sq-CC-Sq**, **Sq-CHCH-Sq**, **Sq-CC-CC-Sq** and **Sq** were measured in THF while toluene was used for all other squaraines. A computer tunable ultrafast optical parametric amplifier (TOPAS, Newport), which is pumped in turn by a Ti:Sapphire regenerative amplifier (Spitfire, Newport) was used, at a repetition rate of 1 kHz. The reference, open-aperture and closed-aperture signals are detected simultaneously using large area germanium photoreceivers (2033, New Focus) and are integrated using Boxcar integrators (SR250, Stanford Research Systems). The integrated signals are acquired using a data acquisition card (6025E, National Instruments) and an

in-house developed Labview program. The final result was obtained by careful extrapolation to zero irradiance.

Two-photon induced fluorescence measurements: The two-photon absorption spectrum of **Sq, Sq-CC-CC-Sq**, and **6-Sq** were measured by Dr. Jochen Campo in carbon tetrachloride (for IR transparency), using a modified two-arm referenced two-photon fluorescence technique.[45] The output beam of the computer controlled TOPAS is weakly focused between the sample and reference (both of them being liquids in a 1 cm path length cuvette). A small portion of the beam is split off before the focusing lens and is directed into a monochromator (MicroHR, Horiba) coupled to a sandwich diode photo-detector (DSD2, ThorLabs) to monitor the TOPAS output wavelength during the two-photon fluorescence measurements, as well as the relative excitation power during measurements of the fluorescence power dependence. The two-photon fluorescence is collected by two aspheric lenses and is sent into an optical fiber (BFB-455-7, Princeton Instruments) connected to a monochromator (SpectraPro-150, Acton). The fluorescence spectra of the sample and reference are then detected as two rows on a CCD (ST-133, Roper Scientific). The measurements are performed by scanning the laser wavelength and simultaneously collecting the two-photon absorption induced fluorescence signals from the two channels. Setting of the excitation wavelength and collection of the fluorescence data are computer controlled through custom-designed LabView VIs. The different collection geometry and efficiency in the two channels is taken into account by placing the sample in channel one and the reference in channel two, and then exchanging the positions. The complete spectrum is scaled by measuring the two-photon absorption cross section at a single wavelength. [2-[2-[2[9dimethylamino]phenyl]-1,3-butadienyl]-1-

ethylpyridinum monoperchlorate (LDS698) in chloroform was used as reference for **6-Sq** and **Sq**. **Sq-CC-CC-Sq** was measured relative to **6-Sq** in carbon tetrachloride.

Organic solar cell fabrication: Solar cells were fabricated by Dr. Yinhua Zhou in the Kippelen group. The squaraines were used as donor materials and blended with the acceptor [6,6]-phenyl C_{61} butyric acid methyl ester (Nano-C, $PC_{60}BM$). Squaraine/$PC_{60}BM$ solutions were made in chlorobenzene with weight ratios of 1:1 and 1:3 and a total concentration of 20 mg/mL. ITO-coated glass (Colorado Concept Coatings LLC) with a sheet resistivity of ~15 Ω/sq was used as the substrates for the solar cells. The substrates were patterned by kapton® tape and etched by the vapor from acid solution (1:3, HNO_3: HCl) at 60 °C for 5 min. The substrates were cleaned in an ultrasonic bath of detergent water, rinsed with deionized water, and then cleaned in sequential ultrasonic baths of deionized water, acetone, and isopropanol. Nitrogen was used to dry the substrates after each of the last three baths. A layer of PEDOT:PSS (CLEVIOS P VP AI 4083, H. C. Starck, 30 nm) was filtered through a 0.45-μm-pore PVDF filter and spin coated on the substrates at 5,000 rpm for 1 min, and the substrates were annealed at 120 ºC for 10 min in atmosphere. After loading into a nitrogen-filled glove box, films of the active layers were deposited on the substrates by spin coating for 1 min at speeds of 1,000 rpm or 2000 rpm. The solutions were filtered through 0.2-μm-pore PTFE filters prior to spin coating. The substrates were then loaded into a vacuum thermal evaporation system (SPECTROS, Kurt J. Lesker) connected to the glove box, and 200 nm of Al was deposited through a shadow mask at a rate of 1 – 3 Å/s and a base pressure of ~2×10^{-7} Torr to define the cathodes. The completed devices were transferred in a sealed container to another nitrogen-filled glove box for electrical measurements.

Current-voltage characteristics were measured using a source meter (2400, Keithley) controlled by a LabVIEW program. When testing the solar cells under illumination, filtered light from a 175 W Xenon lamp (ASB-XE-175EX, CVI) with an irradiance of ~68 mW/cm^2 or Oriel lamp with an irradiance of 100 mW/cm^2 was used as a broadband light source.

Synthesis:

A: 4-Bromophenyl hydrazine hydrochloride (22.3 g, 100 mmol) and 3-methyl-2-butanone (8.6 g, 0.10 mol) were added to a round-bottomed flask. Acetic acid (300 mL) was added and the mixture was heated to 100 ºC overnight. After the reaction mixture was cooled down to room temperature, the solvent was removed. The residue was worked up with water and dichloromethane. The solvent was removed to give **A** as a brown oil (22.6 g, 95%). ^{1}H NMR (300 MHz, $CDCl_3$): δ 7.38 (m, 3H), 2.24 (s, 3H), 1.27 (s, 6H). The ^{1}H NMR spectrum is consistent with that reported in the literature.[46]

B: A (10 g, 43 mmol) and 1-iodododecane (25 g, 86 mmol) were refluxed in CH_3CN (30 mL) for 5 d. After the reaction mixture was cooled down to room temperature, diethyl ether was added and stored at -10 ºC for 1 h. The solid precipitated out was filtered and washed with diethyl ether. It was then dried under vacuum to give **B** as an off-white solid (18 g, 78%). ^{1}H NMR (400 MHz, $CDCl_3$): δ 7.68 (m, 2H), 7.51 (m, 1H), 4.64 (t, J = 7.6 Hz, 2H), 3.06 (s, 3H), 1.88 (quintet, J = 7.2 Hz, 2H), 1.66 (s, 6H), 1.22 (m, 18H), 0.85 (t, J = 6.4 Hz, 3H). ^{13}C{^{1}H} NMR (100 MHz, $CDCl_3$): δ 195.67, 143.48, 140.04, 132.71, 126.76, 124.49, 117.05, 54.75, 50.56, 31.82, 29.49, 29.39, 29.24, 29.07, 27.83, 26.76, 23.11, 22.61, 17.28, 14.06 (Two aliphatic peaks missing probably due to overlap of near coincidental resonances). HRMS (EI) Calcd. for $C_{23}H_{36}BrN$ (M-HI$^+$): 405.2031. Found:

405.2032. Anal. Calcd. for $C_{23}H_{37}BrIN$: C, 51.70; H, 6.98; N, 2.62. Found: C, 51.74; H, 7.01; N, 2.72.

D: 2,3,3-Trimethylindolinene (15.4 g, 97 mmol) and iodoethane (45.0 g, 290 mmol) were refluxed in CH_3CN (30 mL) overnight. After the reaction mixture was cooled to room temperature, the solid was filtered out and washed with diethyl ether. It was dried under vacuum to give **D** as a light pink solid (28.3 g, 93%). ^{1}H NMR (300 MHz, $CDCl_3$): δ 7.57 (m, 4H), 4.75 (q, J = 7.5 Hz, 2H), 3.14 (s, 3H), 1.62 (s, 6H), 1.60 (t, J = 7.8 Hz, 3H). The ^{1}H NMR spectrum is consistent with that reported in the literature.[32]

E: An equimolar amount of **D** (7.28 g, 38.9 mmol) was added to a solution of diethyl squarate[32] (6.62 g, 38.9 mmol) and triethylamine (3.93 g, 38.9 mmol) in ethanol (100 mL). After the mixture was refluxed overnight and cooled down, the solvent was removed under vacuum and the residue was passed through a silica gel column twice with dichloromethane/ethyl acetate (20 : 1) to give **E** as an orange solid (9.56 g, 75%). ^{1}H NMR (500 MHz, $CDCl_3$): δ 7.26 (m, 2H), 7.06 (t, J = 7.5 Hz, 1H), 6.86 (d, J = 8.0 Hz, 1H), 5.38 (s, 1H), 4.88 (q, J = 7.0 Hz, 2H), 3.87 (q, J = 7.5 Hz, 2H), 1.60 (s, 6H), 1.50 (t, J = 7.5 Hz, 3H), 1.32 (t, J = 7.5 Hz, 3H). HRMS (EI) Calcd. for $C_{19}H_{21}NO_3$ (M^+): 311.1521. Found: 311.1491. ^{1}H NMR spectrum is consistent with that reported in the literature.[32]

F: E (5.20 g, 15.9 mmol) was refluxed in ethanol (100 mL) and NaOH (15 mL, 40% wt) was added and kept refluxing for 30 min. After it was cooled to room temperature, 2M HCl aqueous solution was added to adjust the pH to ~ 3. After removal of the solvent, the residue was dissolved in dichloromethane and washed with water, dried over Na_2SO_4. The solvent was removed to give **F** as a brown solid (4.9 g, ~100%) which was used in

the next step without further purification. ^{1}H NMR (300 MHz, $CDCl_3$): δ 7.29 (m, 2H), 7.11 (t, J = 7.5 Hz, 1H), 6.93 (d, J = 7.8 Hz, 1H), 5.64 (s, 1H), 3.96 (m, 2H), 1.64 (s, 6H), 1.35 (t, J = 7.2 Hz, 3H). ^{1}H NMR spectrum is consistent with that reported in the literature.[32]

Sq-Br: F (283 mg, 1.00 mmol) and **B** (533 mg, 1.00 mmol) were added to a dried two-neck round-bottomed flask. It was evacuated/filled with nitrogen three times. Anhydrous toluene (20 mL) and *n*-butanol (10 mL) were added and the mixture was heated to reflux, during which period of time water was removed by Dean-Stark trap. After the solvent was removed, the residue was purified by silica gel chromatography with chloroform/ethyl acetate (10 : 1 to 5 : 1) to give **Sq-Br** as a blue solid with metallic luster (389 mg, 58%). ^{1}H NMR (400 MHz, $CDCl_3$): δ 7.38 (m, 4H), 7.15 (t, J = 7.2 Hz, 1H), 7.00 (d, J = 7.6 Hz, 1H), 6.78 (d, J = 8.4 Hz, 1H), 5.96 (s, 1H), 5.90 (s, 1H), 4.07 (m, 2H), 3.87 (m, 2H), 1.76 (m, 12H), 1.38–1.22 (m, 23H), 0.85 (t, J = 6.8 Hz, 3H). ^{13}C{^{1}H} NMR (100 MHz, $CDCl_3$): δ 182.25, 180.90, 178.83, 170.52, 168.53, 144.19, 142.36, 141.82, 141.71, 130.56, 127.85, 125.63, 124.04, 122.39, 116.10, 110.38, 109.36, 86.80, 86.55, 49.53, 49.10, 43.72, 38.55, 31.89, 29.68, 29.57, 29.50, 29.45, 29.34, 29.31, 27.12, 27.04, 26.87, 22.67, 14.11, 12.06. (One aliphatic peak missing probably due to overlap of near coincidental resonances). HRMS (FAB) Calcd. for $C_{40}H_{51}BrN_2O_2$ (M^+): 670.3134. Found: 670.3149. Anal. Calcd. for $C_{40}H_{51}BrN_2O_2$: C, 71.52; H, 7.65; N, 4.17. Found: C, 71.16; H, 7.88; N, 3.98.

Sq-2Br: **B** (1.12 g, 2.10 mmol) and squaric acid (119 mg, 1.05 mmol) were added to a dried two-neck round-bottomed flask. It was evacuated/filled with nitrogen three times. Anhydrous toluene (20 mL) and *n*-butanol (10 mL) were added and the mixture was

heated to reflux, during which period of time water was removed by Dean-Stark trap. After the solvent was removed, the residue was purified by a silica gel plug with chloroform to give **Sq-2Br** as a blue solid with metallic luster (1.01 g, 99%). ^{1}H NMR (400 MHz, $CDCl_3$): δ 7.40 (m, 4H), 6.82 (d, J = 8.0 Hz, 2H), 5.92 (s, 2H), 3.91 (m, 4H), 1.75 (m, 12H), 1.23 (m, 40H), 0.85 (t, J = 6.8 Hz, 6H). ^{13}C{^{1}H} NMR (100 MHz, $CDCl_3$): δ 180.29, 169.44, 141.56, 130.68, 125.72, 116.57, 110.67, 87.08, 49.35, 43.88, 31.90, 29.58, 29.51, 29.46, 29.32, 27.05, 26.97, 22.68, 14.12. (Two aromatic and three aliphatic peaks missing probably due to overlap of near coincidental resonances). HRMS (ESI) Calcd. for $C_{50}H_{70}Br_2N_2O_2$ (MH^+): calcd: 889.3882. Found: 889.3483. Anal. Calcd. for $C_{50}H_{70}Br_2N_2O_2$: C, 67.41; H, 7.92; N, 3.14. Found: C, 67.17; H, 8.08; N, 3.12.

G: Sq-Br (2.24 g, 3.34 mmol) was dissolved in anhydrous THF (15 mL) and fresh distilled Et_3N (10 mL). The solution was deoxygenated with nitrogen flow for 10 min. CuI (19 mg, 0.10 mmol), and $Pd(PPh_3)_2Cl_2$ (231 mg, 0.20 mmol) were added quickly. The solution was then deoxygenated with nitrogen flow for another 10 min. Trimethylsilyl acetylene (2 mL) was added and the whole was heated at 80 ºC overnight. The solvent was removed, and the residue was purified by flash silica gel column chromatography with chloroform, followed by size-exclusion column chromatography (S-X1, Biobeads, THF) to give **G** as a blue solid (1.88 g, 81%). ^{1}H NMR (400 MHz, $CDCl_3$): δ 7.34 (m, 4H), 7.15 (t, J = 7.6 Hz, 1H), 6.00 (d, J = 8.0 Hz, 1H), 6.84 (d, J = 8.0 Hz, 1H), 5.97 (s, 1H), 5.92 (s, 1H), 4.09 (m, 2H), 3.89 (m, 2H), 1.77 (m, 12H), 1.40–1.23 (m, 23H), 0.85 (t, J = 6.8 Hz, 3H), 0.24 (s, 9H). ^{13}C{^{1}H} NMR(100 MHz, $CDCl_3$): δ 182.30, 181.03, 178.95, 170.52, 169.04, 142.69, 142.43, 142.12, 141.80, 132.11, 127.89, 125.96, 124.11, 122.49, 117.82, 109.46, 109.02, 105.24, 94.14, 87.18, 86.66, 49.59,

48.92, 43.91, 38.63, 31.90, 29.59, 29.50, 29.47, 29.34, 29.32, 27.11, 27.05, 26.97, 26.90, 22.68, 14.12, 12.07, 0.02. (One aliphatic peak missing probably due to overlap of near coincidental resonances). HRMS (MALDI) Calcd. for $C_{45}H_{60}N_2O_2Si$ (M^+): 688.4424. Found: 688.4424. Anal. Calcd. for $C_{45}H_{60}N_2O_2Si$: C, 78.44; H, 8.78; N, 4.07. Found: C, 78.04; H, 9.07; N, 3.91.

Sq-CC from **G**: **G** (1.88 g, 2.73 mmol) was added to a dried round-bottomed flask and dissolved in the mixture of THF (20 mL) and methanol (20 mL) under nitrogen. The mixture was deoxygenated with nitrogen flow for 10 min. Potassium carbonate (3.78 g, 27.3 mmol) was added quickly and mixture was stirred at room temperature overnight. The crude product was purified by a plug of silica gel (chloroform/ethyl acetate = 15 : 1) and size-exclusion column chromatography (S-X1, Biobeads, THF) to give **Sq-CC** as a blue solid (1.12 g, 66%). ^{1}H NMR (400 MHz, $CDCl_3$): δ 7.40 (m, 2H), 7.31 (m, 2H), 7.15 (t, J = 7.2 Hz, 1H), 7.00 (d, J = 7.8 Hz, 1H), 6.86 (d, J = 8.4 Hz, 1H), 5.97 (s, 1H), 5.92 (s, 1H), 4.08 (m, 2H), 3.90 (m, 2H), 3.07 (s, 1H), 1.76 (m, 12H), 1.41–1.22 (m, 23H), 0.85 (t, J = 6.8 Hz, 3H). ^{13}C{^{1}H} NMR(100 MHz, $CDCl_3$): δ 182.22, 181.15, 178.72, 170.67, 168.77, 142.94, 142.38, 142.21, 141.77, 132.18, 127.85, 125.97, 124.10, 122.39, 116.55, 109.40, 108.89, 87.11, 86.64, 83.74, 49.55, 48.77, 43.68, 38.57, 31.87, 29.56, 29.48, 29.45, 29.32, 29.29, 27.10, 27.03, 26.94, 26.85, 22.65, 14.09, 12.06. (One aromatic and one aliphatic peaks missing probably due to overlap of near coincidental resonances). HRMS (ESI) Calcd. for $C_{42}H_{52}N_2O_2$ (MH^+): 616.4107. Found: 616.4129. Anal. Calcd. for $C_{42}H_{52}N_2O_2$: C, 81.78; H, 8.50; N, 4.54. Found: C, 81.54; H, 8.67; N, 4.49.

C: **Sq-2Br** (3.19 g, 3.60 mmol) was dissolved in anhydrous THF (15 mL) and fresh distilled Et_3N (10 mL). The solution was deoxygenated with nitrogen flow for 10 min.

CuI (20 mg, 0.10 mmol), and $Pd(PPh_3)_2Cl_2$ (151 mg, 0.21 mmol) were added quickly. The solution was then deoxygenated with nitrogen flow for another 10 min. Trimethylsilyl acetylene (3 mL) was added and the whole was heated at 70 ºC overnight. The solvent was removed, and the residue was purified by flash silica gel chromatography with chloroform, followed by size-exclusion column chromatography (S-X1, Biobeads, THF) to give **C** as a blue solid (2.34 g, 70%). ^{1}H NMR (400 MHz, $CDCl_3$): δ 7.41 (m, 4H), 6.87 (d, J = 8.4 Hz, 2H), 5.95 (s, 2H), 3.92 (m, 4H), 1.75 (m, 12H), 1.23 (m, 40H), 0.86 (t, J = 6.8 Hz, 6H), 0.24 (s, 18H). $^{13}C\{^1H\}$ NMR (100 MHz, $CDCl_3$): δ 180.29, 169.80, 142.51, 132.11, 125.93, 118.15, 109.14, 105.04, 94.31, 87.40, 49.08, 43.87, 31.90, 29.58, 29.50, 29.47, 29.33, 27.04, 22.69, 14.13, 0.01 (Two aromatic and four aliphatic peaks missing probably due to overlap of near coincidental resonances). HRMS (MALDI) Calcd. for $C_{60}H_{88}N_2O_2Si_2$ (M^+): 924.6384. Found: 924.6382. Anal. Calcd. for $C_{60}H_{88}N_2O_2Si_2$: C, 77.86; H, 9.58; N, 3.03. Found: C, 77.79; H, 9.62; N, 3.04.

Sq-2CC from **C**: **C** (2.34 g, 2.53 mmol) was added to a dried round-bottom flask and dissolved in the mixture of THF (15 mL) and methanol (15 mL) under nitrogen. It was deoxygenated with nitrogen flow for 10 min. Potassium carbonate (3.49 g) was added quickly and the mixture was stirred at room temperature overnight. The compound was purified by silica gel column chromatography with chloroform/ethyl acetate (20 : 1) and size-exclusion column chromatography (S-X1, Biobeads, THF) to give **Sq-2CC** as a blue solid (1.16 g, 59%). ^{1}H NMR (300 MHz, $CDCl_3$): δ 7.42 (m, 4H), 6.89 (d, J = 8.7 Hz, 2H), 5.96 (s, 2H), 3.94 (m, 4H), 3.09 (s, 2H), 1.75 (m, 12H), 1.23 (m, 40H), 0.85 (t, J = 6.9 Hz, 6H). $^{13}C\{^1H\}$ NMR (100 MHz, $CDCl_3$): δ 180.59, 169.87, 142.77, 142.33,

132.26, 126.06, 117.08, 109.24, 87.46, 83.62, 49.09, 43.88, 31.90, 29.58, 29.51, 29.47, 29.32, 27.05, 22.68, 14.12 (Two aromatic and four aliphatic peaks missing probably due to overlap of near coincidental resonances). HRMS (ESI) Calcd. for $C_{54}H_{72}N_2O_2$ (MH^+): 781.5672. Found: 781.5578. Anal. Calcd. for $C_{54}H_{72}N_2O_2$: C, 83.03; H, 9.29; N, 3.59. Found: C, 82.92; H, 9.38; N, 3.61.

Sq-CC-Sq: **Sq-Br** (200 mg, 0.290 mmol) and $Pd(PPh)_4$ (17 mg, 0.030 mmol) were added to a dried microwave tube. Anhydrous toluene (3 mL) was added and the solution was freeze-pumped for 3 times. Bistributylstannylacetylene (79 μL, 0.145 mmol) was added. The microwave (CEM, Discover) was set to standard mode: Power = 100 watt, T = 100 °C, run time = 10 min, hold time = 30 min. Four batches of reactions were combined together for purification. After the solvent was removed, the residue was passed through a pad of silica gel eluting with dichloromethane (3% methanol) and then a size-exclusion column chromatography (S-X1, Biobeads, THF). After solvent was removed, the residue was refluxed in heptane for 2 hours and the solid was filtered out. After washed with hexane and dried under vacuum, **Sq-CC-Sq** was obtained as a blue solid (320 mg, 45%). ^{1}H NMR (400 MHz, $CDCl_3$): δ 7.46 (m, 4H), 7.35 (m, 2H), 7.31 (m, 2H), 7.15 (t, J = 7.6 Hz, 2H), 7.00 (d, J = 8.0 Hz, 2H), 6.90 (d, J = 8.0 Hz, 2H), 5.98 (s, 2H), 5.94 (s, 2H), 4.08 (m, 4H), 3.92 (m, 4H), 1.75 (br, 24H), 1.41–1.23 (m, 46H), 0.85 (t, J = 7.2 Hz, 6H). ^{13}C{^{1}H} NMR (100 MHz, $CDCl_3$): δ 182.32, 180.78, 178.78, 170.42, 168.82, 142.38, 141.84, 131.48, 127.85, 125.38, 124.02, 122.40, 118.01, 109.34, 109.09, 89.75, 87.14, 86.59, 49.51, 48.89, 43.77, 38.55, 31.90, 29.59, 29.51, 29.48, 29.36, 29.32, 27.15, 27.07, 27.02, 26.90, 22.68, 14.12, 12.07 (Two aromatic and one aliphatic peaks missing probably due to overlap of near coincidental resonances). HRMS (MALDI) Calcd. for

$C_{82}H_{102}N_4O_4$ (M^+): 1206.790; Found: 1206.783. Anal. Calcd. for $C_{82}H_{102}N_4O_4$: C, 81.55; H, 8.51; N, 4.64. Found: C, 81.29; H, 8.57; N, 4.59.

Sq-CHCH-Sq: **Sq-Br** (198 mg, 0.295 mmol) and $Pd(PPh)_4$ (17 mg, 0.030 mmol) were added to a dried microwave tube. Anhydrous toluene (3 mL) was added and the solution was freeze-pumped for 3 times. Bistributylstannylvinylene (78 μL, 0.145 mmol) was added. The microwave (CEM, Discover) was set to standard mode: Power = 100 watt, T = 100 °C, run time = 10 min, hold time = 45 min. Three batches of reactions were combined together for purification. After the solvent was removed, the residue was passed through a pad of silica gel with dichloromethane (3% methanol) and then a size-exclusion column (S-X1, Biobeads, THF). The compound was purified by silica gel column chromatography (chloroform/methanol = 30 : 1) to get rid of trace squaraine tin compound. After solvent was removed, the residue was then refluxed in heptane for 2 hours and the solid was filtered out. After washed with hexane and dried under vacuum, **Sq-CHCH-Sq** was obtained as a green solid (232 mg, 31%). ^{1}H NMR (400 MHz, $CDCl_3$): δ 7.52 (s, 2H), 7.41 (m, 2H), 7.35 (m, 2H), 7.30 (m, 2H), 7.14 (t, J = 7.6 Hz, 2H), 7.10 (s, 2H), 6.98 (d, J = 8.0 Hz, 2H), 6.93 (d, J = 8.4 Hz, 2H), 5.95 (s, 4H), 4.06 (m, 4H), 3.96 (m, 4H), 1.79 (m, 24H), 1.41–1.23 (m, 46H), 0.85 (t, J = 7.2 Hz, 6H). ^{13}C{^{1}H} NMR (100 MHz, $CDCl_3$): δ 182.61, 179.67, 179.03, 169.73, 169.31, 142.88, 142.22, 142.08, 141.97, 133.36, 127.80, 127.16, 126.75, 123.75, 122.37, 119.64, 109.47, 109.15, 87.00, 86.37, 49.35, 49.09, 43.86, 38.43, 31.90, 29.59, 29.52, 29.48, 29.36, 29.32, 27.17, 27.09, 26.97, 22.68, 14.12, 12.03 (Two aliphatic peaks missing probably due to overlap of near coincidental resonances). HRMS (MALDI) Calcd. for $C_{82}H_{104}N_4O_4$ (M^+):

1208.7276. Found: 1208.7976. Anal. Calcd. for $C_{82}H_{104}N_4O_4 \cdot H_2O$: C, 80.22; H, 8.70; N, 4.56. Found: C, 80.40; H, 8.66; N, 4.50.

Sq-CC-CC-Sq: **Sq-CC** (150 mg, 0.244 mmol), $Pd(PPh)_2Cl_2$ (8.5 mg, 0.012 mmol), CuI (2.3 mg, 0.012 mmol), and 1,4-benzoquinone (26.3 mg, 0.244 mmol) were added to a dried microwave tube. Anhydrous THF (2 mL) and freshly distilled Et_3N (2 mL) were added and the solution was freeze-pumped for 3 times. The microwave (CEM, Discover) was set to standard mode: Power = 80 watt, T = 60 °C, run time = 10 min, hold time = 30 min. After the solvent was removed, the residue was passed through a pad of silica gel with chloroform (2% methanol) and then a size-exclusion column (S-X1, Biobeads, THF). After solvent was removed, the residue was refluxed in heptane for 2 hours and the solid was filtered out. After washed with hexane and dried under vacuum, **Sq-CC-CC-Sq** was obtained as a blue solid (107 mg, 71%). ^{1}H NMR (400 MHz, $CDCl_3$): δ 7.46 (m, 4H), 7.35 (m, 2H), 7.31 (m, 2H), 7.17 (t, J = 7.6 Hz, 2H), 7.02 (d, J = 7.6 Hz, 2H), 6.87 (d, J = 8.4 Hz, 2H), 5.99 (s, 2H), 5.94 (s, 2H), 4.10 (m, 4H), 3.90 (m, 4H), 1.77 (br, 24H), 1.41–1.23 (m, 46H), 0.85 (t, J = 7.2 Hz, 6H). ^{13}C{^{1}H} NMR (100 MHz, $CDCl_3$): δ 182.26, 181.65, 178.47, 170.94, 168.27, 143.28, 142.44, 141.74, 132.76, 127.88, 126.22, 124.23, 122.42, 116.11, 109.49, 109.00, 87.38, 86.79, 82.34, 74.23, 49.65, 48.66, 43.68, 38.64, 31.89, 29.57, 29.50, 29.46, 29.34, 29.31, 27.16, 27.05, 26.97, 26.83, 22.67, 14.11, 12.11 (One aromatic and one aliphatic peaks missing probably due to overlap of near coincidental resonances). HRMS (MALDI) Calcd. for $C_{84}H_{102}N_4O_4$ (M^+): 1230.7901. Found: 1230.7815. Anal. Calcd. for $C_{84}H_{102}N_4O_4 \cdot 0.5H_2O$: C, 81.31; H, 8.37; N, 4.52. Found: C, 81.25; H, 8.43; N, 4.40.

Sq-CN-Sq: **Sq-CC-Sq** (197 mg, 0.163 mmol) and tetracyanoethylene (104 mg, 0.82 mmol) were stirred in dichloromethane (8 mL) under nitrogen overnight. After the solvent was removed, the residue was passed through a pad of silica gel with chloroform (4% methanol) and then a size-exclusion column (S-X1, Biobeads, THF). After solvent was removed, the residue was refluxed in heptane for 2 hours and the solid was filtered out. After washed with hexane and dried under vacuum, **Sq-CN-Sq** was obtained as a green solid (193 mg, 89%). ^{1}H NMR (400 MHz, $CDCl_3$): δ 7.78 (d, J = 2.0 Hz, 2H), 7.63 (m, 2H), 7.41 (m, 2H), 7.35 (m, 2H), 7.26 (t, J = 7.6 Hz, 2H), 7.13 (d, J = 8 Hz, 2H), 6.92 (d, J = 8.8 Hz, 2H), 6.12 (s, 2H), 6.00 (s, 2H), 4.19 (q, J = 7.2 Hz, 4H), 3.87 (t, J = 7.6 Hz, 4H), 1.78 (m, 24H), 1.45–1.23 (m, 46H), 0.85 (t, J = 7.2 Hz, 6H). ^{13}C{^{1}H} NMR (100 MHz, $CDCl_3$): δ 186.02, 182.61, 181.32, 175.29, 173.94, 165.70, 164.41, 148.83, 143.53, 142.89, 141.18, 132.02, 128.18, 125.61, 125.05, 123.00, 122.62, 113.40, 112.36, 110.47, 109.14, 89.72, 88.24, 80.82, 50.53, 47.68, 43.75, 39.30, 31.88, 29.57, 29.52, 29.47, 29.33, 29.30, 27.35, 27.10, 27.00, 26.43, 22.66, 14.10, 12.41 (One aliphatic peak missing probably due to overlap of near coincidental resonances). HRMS (MALDI) Calcd. for $C_{84}H_{102}N_8O_4$ (M^+): 1334.8024. Found: 1334.7881. Anal. Calcd. for $C_{84}H_{102}N_8O_4 \cdot 0.5H_2O$: C, 78.59; H, 7.72; N, 8.33. Found: C, 78.52; H, 7.70; N, 8.31.

3-Sq: **Sq-2CC** (80 mg, 0.103 mmol), **Sq-Br** (206 mg, 0.308 mmol), $Pd(PPh)_4$ (11.9 mg, 0.0103 mmol), and CuI (2.0 mg, 0.010 mmol) were added to a dried microwave tube. Anhydrous THF (2 mL) and freshly distilled Et_3N (2 mL) were added and the solution was freeze-pumped for 3 times. The microwave (CEM, Discover) was set to standard mode: Power = 80 watt, T = 80 °C, run time = 10 min, hold time = 25 min. After the solvent was removed, the residue was passed through a pad of silica gel with chloroform

(2% methanol) and then a size-exclusion column (S-X1, Biobeads, THF). After solvent was removed, the residue was refluxed in heptane for 2 hours and the solid was filtered out. After washed with hexane and dried under vacuum, **3-Sq** was obtained as a blue solid (20 mg, 10%). ^{1}H NMR (400 MHz, $CDCl_3$): δ 7.47 (m, 8H), 7.35 (m, 2H), 7.31 (m, 2H), 7.15 (t, J = 7.6 Hz, 2H), 7.01 (d, J = 8.0 Hz, 2H), 6.92 (m, 4H), 5.96 (m, 6H), 4.08 (m, 4H), 3.93 (m, 8H), 1.78 (m, 36H), 1.41–1.23 (m, 86H), 0.85 (t, J = 7.2 Hz, 12H). ^{13}C{^{1}H} NMR (100 MHz, $CDCl_3$): δ 182.25, 180.86, 180.03, 178.77, 170.46, 169.61, 168.78, 142.39, 141.84, 131.52, 127.86, 125.41, 124.04, 122.41, 118.42, 117.92, 109.36, 109.09, 89.97, 89.65, 87.46, 87.16, 86.62, 49.53, 49.12, 48.89, 43.88, 43.76, 38.56, 31.90, 29.59, 29.52, 29.49, 29.36, 29.32, 27.16, 27.09, 26.90, 22.68, 14.12, 12.08 (Eight aromatic and fourteen aliphatic peaks missing probably due to overlap of near coincidental resonances). HRMS (MALDI) Calcd. for $C_{134}H_{172}N_6O_6$ (M^+): 1961.3338. Found: 1961.3208. Anal. Calcd. for $C_{134}H_{172}N_6O_6 \cdot H_2O$: C, 81.25; H, 8.85; N, 4.24. Found: C, 81.10; H, 8.87; N, 4.21.

6-Sq: **Sq-CC-Sq** (322 mg, 0.267 mmol) was added to a dried round-bottomed flask. It was evacuated/filled with nitrogen 3 times. Anhydrous *p*-dioxane (6 mL) was added. A catalytic amount of $Co_2(CO)_8$ was added quickly under nitrogen. The solution was deoxygenated with nitrogen flow for 5 min before heated to reflux overnight. After the reaction mixture was cooled to room temperature, the solvent was removed and the residue was passed through a pad of silica gel with chloroform and methanol. The crude product was then purified by size-exclusion column chromatography (S-X1, Biobeads, THF). The first band was collected to give **6-Sq** as a purple blue solid (156 mg, 47%). ^{1}H NMR (400 MHz, CD_2Cl_2): δ 7.30 (m, 12H), 7.12 (m, 6H), 6.99 (m, 6H), 6.75 (m, 12H),

6.58 (m, 6H), 5.84 (s, 6H), 5.74 (s, 6H), 4.04 (m, 12H), 3.76 (m, 12H), 1.75 (s, 72H), 1.41–1.23 (m, 138H), 0.83 (t, 18H). $^{13}C\{^{1}H\}$ NMR (125 MHz, $CDCl_3$): δ 182.21, 182.11, 179.27, 169.63, 169.04, 142.69, 142.39, 141.98, 141.57, 140.51, 140.04, 135.95, 130.92, 127.75, 126.10, 123.57, 122.34, 107.99, 107.63, 86.75, 86.40, 49.29, 48.52, 43.64, 38.35, 32.00, 29.61, 29.35, 27.00, 22.64, 14.12, 12.00 (Seven aliphatic peaks missing probably due to overlap). Anal. Calcd for $C_{246}H_{306}N_{12}O_{12}\cdot 6H_2O$: C, 79.19; H, 8.59; N, 4.50. Found: C, 79.03; H, 8.35; N, 4.47.

3.8 References

(1) Pawlicki, M.; Collins, H. A.; Denning, R. G.; Anderson, H. L. *Angew. Chem. Int. Ed.* **2009**, *48*, 3244.

(2) Rumi, M.; Barlow, S.; Wang, J.; Perry, J. W.; Marder, S. R. *Adv. Polym. Sci.* **2008**, *213*, 1.

(3) He, G. S.; Tan, L.-S.; Zheng, Q.; Prasad, P. N. *Chem. Rev.* **2008**, *108*, 1245.

(4) Albota, M.; Beljonne, D.; Brédas, J.-L.; Ehrlich, J. E.; Fu, J.-Y.; Heikal, A. A.; Hess, S. E.; Kogej, T.; Levin, M. D.; Marder, S. R.; McCord-Maughon, D.; Perry, J. W.; Röckel, H.; Rumi, M.; Subramaniam, G.; Webb, W. W.; Wu, X.-L.; Xu, C. *Science* **1998**, *281*, 1653.

(5) Kogej, T.; Beljonne, D.; Meyers, F.; Perry, J. W.; Marder, S. R.; Brédas, J.-L. *Chem. Phys. Lett.* **1998**, *298*, 1.

(6) Rumi, M.; Ehrlich, J. E.; Heikal, A. A.; Perry, J. W.; Barlow, S.; Hu, Z.; McCord-Maughon, D.; Parker, T. C.; Röckel, H.; Thayumanavan, S.; Marder, S. R.; Beljonne, D.; Brédas, J.-L. *J. Am. Chem. Soc.* **2000**, *122*, 9500.

(7) Song, J.; Aratani, N.; Kim, P.; Kim, D.; Shinokubo, H.; Osuka, A. *Angew. Chem. Int. Ed.* **2010**, *49*, 3617.

(8) She, C.; Easwaramoorthi, S.; Kim, P.; Hiroto, S.; Hisaki, I.; Shinokubo, H.; Osuka, A.; Kim, D.; Hupp, J. T. *J. Phys. Chem. A* **2010**, *114*, 3384.

(9) Yoon, M.-C.; Noh, S. B.; Tsuda, A.; Nakamura, Y.; Osuka, A.; Kim, D. *J. Am. Chem. Soc.* **2007**, *129*, 10080.

(10) Hisaki, I.; Hiroto, S.; Kim, K. S.; Noh, S. B.; Kim, D.; Shinokubo, H.; Osuka, A. *Angew. Chem. Int. Ed.* **2007**, *46*, 5125.

(11) Drobizhev, M.; Stepanenko, Y.; Rebane, A.; Wilson, C. J.; Screen, T. E. O.; Anderson, H. L. *J. Am. Chem. Soc.* **2006**, *128*, 12432.

(12) Ahn, T. K.; Kim, K. S.; Kim, D. Y.; Noh, S. B.; Aratani, N.; Ikeda, C.; Osuka, A.; Kim, D. *J. Am. Chem. Soc.* **2006**, *128*, 1700.

(13) Inokuma, Y.; Ono, N.; Uno, H.; Kim, D. Y.; Noh, S. B.; Kim, D.; Osuka, A. *Chem. Commun.* **2005**, 3782.

(14) Frampton, M. J.; Akdas, H.; Cowley, A. R.; Rogers, J. E.; Slagle, J. E.; Fleitz, P. A.; Drobizhev, M.; Rebane, A.; Anderson, H. L. *Org. Lett.* **2005**, *7*, 5365.

(15) Drobizhev, M.; Stepanenko, Y.; Dzenis, Y.; Karotki, A.; Rebane, A.; Taylor, P. N.; Anderson, H. L. *J. Phys. Chem. B* **2005**, *109*, 7223.

(16) Kim, D.; Osuka, A. *Acc. Chem. Res.* **2004**, *37*, 735.

(17) Drobizhev, M.; Stepanenko, Y.; Dzenis, Y.; Karotki, A.; Rebane, A.; Taylor, P. N.; Anderson, H. L. *J. Am. Chem. Soc.* **2004**, *126*, 15352.

(18) Ogawa, K.; Ohashi, A.; Kobuke, Y.; Kamada, K.; Ohta, K. *J. Am. Chem. Soc.* **2003**, *125*, 13356.

(19) Screen, T. E. O.; Thorne, J. R. G.; Denning, R. G.; Bucknall, D. G.; Anderson, H. L. *J. Am. Chem. Soc.* **2002**, *124*, 9712.

(20) Taylor, P. N.; Wylie, A. P.; Huuskonen, J.; Anderson, H. L. *Angew. Chem. Int. Ed.* **1998**, *37*, 986.

(21) Lin, V. S.-Y.; DiMagno, S. G.; Therien, M. J. *Science* **1994**, *264*, 1105.

(22) Anderson, H. L. *Chem. Commun.* **1999**, 2323.

(23) Thorne, J. R. G.; Kuebler, S. M.; Denning, R. G.; Blake, I. M.; Taylor, P. N.; Anderson, H. L. *Chem. Phys.* **1999**, *248*, 181.

(24) Screen, T. E. O.; Lawton, K. B.; Wilson, G. S.; Dolney, N.; Ispasoiu, R.; Goodson III, T.; Martin, S. J.; Bradley, D. D. C.; Anderson, H. L. *J. Mater. Chem.* **2001**, *11*, 312.

(25) Song, J.; Jang, S. Y.; Yamaguchi, S.; Sankar, J.; Hiroto, S.; Aratani, N.; Shin, J.-Y.; Easwaramoorthi, S.; Kim, K. S.; Kim, D.; Shinokubo, H.; Osuka, A. *Angew. Chem. Int. Ed.* **2008**, *47*, 6004.

(26) Wilson, G. S.; Anderson, H. L. *Chem. Commun.* **1999**, 1539.

(27) Scherer, D.; Dorfler, R.; Feldner, A.; Vogtmann, T.; Schwoerer, M.; Lawrentz, U.; Grahn, W.; Lambert, C. *Chem. Phys.* **2002**, 179.

(28) Ohira, S.; Rudra, I.; Schmidt, K.; Barlow, S.; Chung, S.-J.; Zhang, Q.; Matichak, J.; Marder, S. R.; Brédas, J.-L. *Chem. Eur. J.* **2008**, *14*, 11082.

(29) Andrews, J. H.; Khaydarov, J. D. V.; Singer, K. D.; Hull, D. L.; Chuang, K. C. *J. Opt. Soc. Am. B* **1995**, *12*, 2360.

(30) Kato, S.-I.; Diederich, F. *Chem. Commun.* **2010**, *46*, 1994.

(31) Fischer, E.; Jourdan, F. *Ber. Dtsch. Chem. Ges.* **1883**, *16*, 2241.

(32) Yum, J.-H.; Walter, P.; Huber, S.; Rentsch, D.; Geiger, T.; Nüesch, F.; Angelis, F. D.; Grätzel, M.; Nazeeruddin, M. K. *J. Am. Chem. Soc.* **2007**, *129*, 10320.

(33) Miguel, L. S.; Matzger, A. J. *Macromolecules* **2007**, *40*, 9233.

(34) Yan, Q.; Zhao, D. *Org. Lett.* **2009**, *11*, 3426.

(35) Kivala, M.; Boudon, C.; Gisselbrecht, J.-P.; Enko, B.; Seiler, P.; Müller, I. B.; Langer, N.; Jarowski, P. D.; Gescheidt, G.; Diederich, F. *Chem. Eur. J.* **2009**, *15*, 4111.

(36) Fechtenkötter, A.; Tchebotareva, N.; Watson, M.; Müllen, K. *Tetrahedron* **2001**, *57*, 3769.

(37) Gratz, H.; Penzkofer, A. *Chem. Phys.* **2000**, *254*, 363.

(38) Webster, S.; Odom, S. A.; Padilha, L. A.; Przhonska, O. V.; Peceli, D.; Hu, H.; Nootz, G.; Kachkovski, A. D.; Matichak, J.; Barlow, S.; Anderson, H. L.; Marder, S. R.; Hagan, D. J.; Van Stryland, E. W. *J. Phys. Chem. B* **2009**, *113*, 14854.

(39) Thelakkat, M.; Schmidt, H.-W. *Adv. Mater.* **1998**, *10*, 219.

(40) Wei, G.; Wang, S.; Renshaw, K.; Thompson, M. E.; Forrest, S. R. *ACS Nano* **2010**, *4*, 1927.

(41) Silvestri, F.; Irwin, M. D.; Beverina, L.; Facchetti, A.; Pagani, G. A.; Marks, T. J. *J. Am. Chem. Soc.* **2008**, *130*, 17640.

(42) Bagnis, D.; Beverina, L.; Huang, H.; Silvestri, F.; Yao, Y.; Yan, H.; Pagani, G. A.; Marks, T. J.; Facchetti, A. *J. Am. Chem. Soc.* **2010**, *132*, 4074.

(43) Mayerhöffer, U.; Deing, K.; Gruß, K.; Braunschweig, H.; Meerholz, K.; Würthner, F. *Angew. Chem. Int. Ed.* **2009**, *48*, 8776.

(44) Sheik-Bahae, M. *IEEE J. Quant. Electr.* **1990**, *26*, 760.

(45) Makarov, N. S.; Drobizhev, M.; Rebane, A. *Opt. Express* **2008**, *16*, 4029.

(46) Zimmermann, T.; Hennig, L. *J. Heterocyclic Chem.* **2002**, *39*, 263.

Chapter 4: Synthesis, Photophysical and Organic Photovoltaic Properties of Phthalocyanine- and Squaraine-based Platinum and Gold Complexes

4.1 Introduction to reverse saturable absorption-based optical-power limiting

The rapid development of laser technology has driven a lot of research interest in effective optical limiters for protecting human eyes, optical sensors and sensitive optical components. In the late 1960s, nonlinear absorption of light was first experimentally observed by Guiliano and Hess.[1] They observed that some dyes did not bleach to transparency (saturable absorbers) but darkened under intense illumination. This could be considered as the first description of reverse saturable absorption (RSA), which is one of the main mechanisms for optical-power limiting (OPL), as already discussed in Chapter 2.[2-4] RSA generally occurs in materials in which the excited-state absorption cross-section σ_{ex} is significantly greater than the corresponding ground-state value σ_g over the spectral region of interest.

Absorption of a photon of appropriate energy can excite a molecule from its ground singlet-state (S_0) to its first excited singlet-state (S_1). It can be further excited from S_1 to higher excited singlet-states (S_n) with absorption cross-section σ_S. The molecule initially follows the Beer's law. As the molecule absorbs, the S_1 state could become populated and contributes more to the overall absorption. When the S_1 state becomes substantially populated at a high fluence, if σ_S is smaller than σ_g, the molecule will become less strongly absorbing or "bleached", i.e. it is a saturable absorber. However, in the case when $\sigma_S \gg \sigma_g$, the transmittance will be smaller at high fluence and

such a material is considered as a reverse saturable absorber. To describe such a photo-induced process, a three level diagram involving S_0, S_1, and S_n can only be applied for short pulses (subnanosecond) and in the case that higher excited-state absorption are negligible. In general, S_1 has relatively a short lifetime[5] and decays rapidly; hence less significant pulse attenuation is observed for longer timescales (i.e. microseconds). However, in some systems, in which strong spin-orbit coupling is present, the molecule may undergo intersystem crossing (ISC) from S_1 to the lower energy triplet state, T_1. Triplet states often possess lifetimes of microseconds timescale or even longer; such states can, therefore, accumulate significant population during the laser pulse. If the excited triple-state absorption cross-section (σ_T) is larger than that of the ground state, significant optical-power suppression can be achieved for lasers with pulse widths of nanosecond or longer. The process is illustrated in Figure 4.1 using a five level diagram.

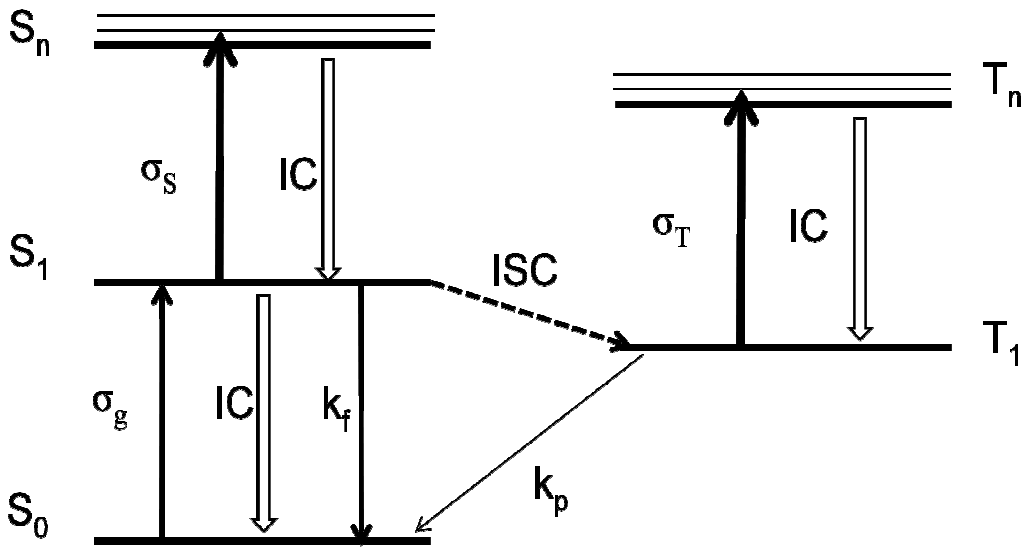

Figure 4.1: Five level model for reverse saturable absorption. Shown are the ground- state absorption coefficient (σ_g), excited singlet-state absorption coefficient (σ_S), excited triplet-state absorption coefficient (σ_T), fluorescence rate constant (k_f) and phosphorescence rate constant (k_p), internal conversion (IC), and intersystem crossing (ISC).

The vast majority of studies of RSA, using dyes such as metallophorphyrins and metallophthalocyanines (MPc),[3,6,7] have focused on achieving efficient intersystem crossing from S_1 to T_1 which results in a large triplet-state population following irradiation. The heavy-atom effect gives greater access to highly absorbing triplet manifold by facilitating the spin–orbit coupling to enhance the ISC from S_1 to T_1, and significantly enhances the optical limiting response. Perry and co-workers[6] studied the group IIIA and group IVA MPcs and found that as the atomic number increases, the first singlet excited-state lifetime (τ_S) decrease and the triplet quantum yield (Φ_T) increase. Due to an enhanced triplet contribution, the nonlinear absorption of the MPcs increased with an increasing atomic number of the center metals, using 532-nm 8-ns laser pulses.

Platinum with the atomic number of 78 is a fairly "heavy" atom and its coordination chemistry has been widely studied. Platinum(II) acetylides coordinated with terpyridyl[7,8] or phosphine ligands[9,10] are known to be promising chromophores with strong excited-state absorptions. Recently, some monomeric, oligomeric and polymeric Pt(II) bis(acetylide) complexes and Au(I) triphenylphosphine acetylides have been reported to possess excellent optical-power limiting responses to nanosecond lasers at 532 nm with very impressive figure of merit σ_{ex}/σ_g and low thresholds.[11-13] The distinctive OPL response was attributed to mixing of the metal d orbitals with the ligand π orbitals which resulted in strong spin-orbital coupling.

4.2 Motivation and molecular design

Phthalocyanine (Pc) and squaraine (Sq) dyes, with their wide transparency

window and large π-electron conjugation systems, can be a potential building unit for platinum and gold containing architectures as optical-power limiters. As showing in Figure 4.4,[6] the linear absorption of phthalocyanines feature a high energy B-band absorption and a low energy Q-band absorption. The strong transient absorption obtained after 100 ns following photo-excitation could be assigned to triplet excited-state absorption, which extends over the window of ground-state transparency between 400 nm and 600 nm. Hence, MPcs are promising candidates for OPL over this wavelength range, especially to the widely used 532 nm laser. The heavy atom effects in Pc core have been extensively studied and efficient optical limiters have been achieved.[3,14] A new triad assembly (**Pc-Pt-Pc**), in which two zinc phthalocyanines (ZnPc) are linked together through platinum acetylides, was designed. The platinum atom conjugated linked to Pc rings are expected to increase the intersystem crossing rate than ZnPc to generate sufficient Pc triplet-state subsequent to photo-excitation. Another possible advantage for such a system is the attached ligands on the platinum atom might significantly increase the solubility of this compound and help to prevent the π–π stacking between the Pc moieties as well, especially in solid state, which may reduce excited-state quenching from dye aggregates.

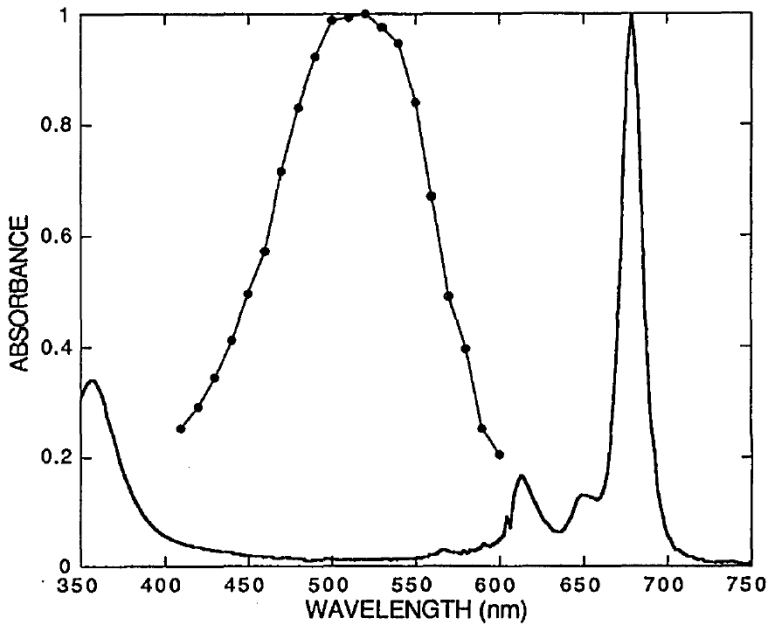

Figure 4.2: Electronic absorption spectrum of bis[tri-(nhexyl)siloxy]SnPc in toluene solution. Also shown (curve with circles) is the transient absorption spectrum (arbitrary units) of SnPc in toluene obtained 100 ns after excitation at 355 nm.[6] Reprinted with permission from Ref 6. Copyright 1994 Optical Society of America.

Squaraine dyes are also conjugated molecules with extended π-electron delocalization and a wide wavelength window of ground-state transparency, which can be potentially utilized for OPL at certain wavelengths, adapting the idea applied for the **Pc-Pt-Pc** discussed above. Furthermore, squaraines are known to be strong two-photon absorbing dyes in the near infrared region, which could also be a merit for optical limiting application using such dyes, as discussed in Chapter 2,[15] to have a wide spectral response to high intensity irradiation depending on the spectral position of any $T_1 \rightarrow T_n$ absorption. Here, a squaraine triad (**Sq-Pt-Sq**) and its polymer analog ($[\mathbf{Sq\text{-}Pt}]_n$) were designed as possible OPL materials exploiting the possible squaraine triplet-state absorption with the presence of heavy atoms, perhaps helping in increasing intersystem crossing rate of these dyes. The mono-squaraine-based gold- and platinum-containing metallo-sqauraines were synthesized for comparison purpose with the aim in better

understanding the structure-property relationships. The chemical structures of the new metallo-phthalocyanine and squaraines are summarized in Figure 4.3.

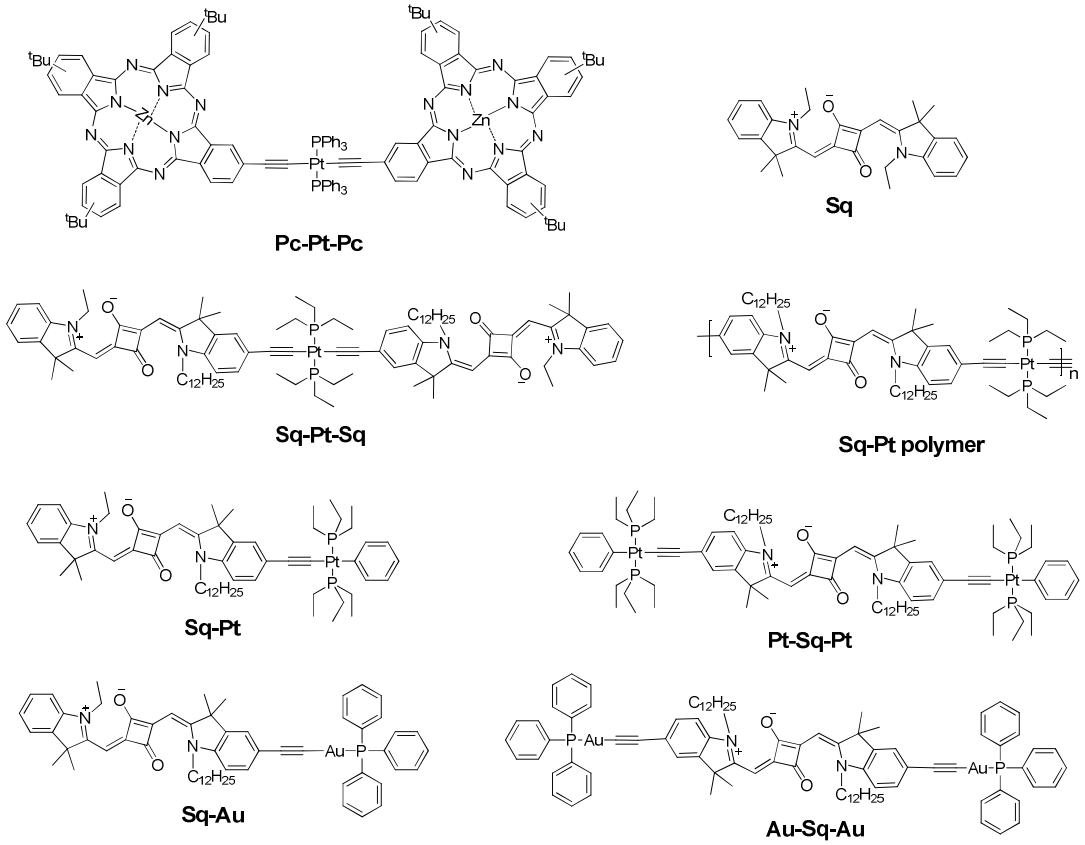

Figure 4.3: Chemical structures of Sq (referred in the discussion, see Chapter 3 for detail), metallo-phthalocyanine and squaraines.

4.3 Synthesis of phthalocyanine- and squaraine-based complexes

The synthesis of phthalocyanine acetylide coordinated Pt(II) complex (**Pc-Pt-Pc**) followed the procedure shown in Scheme 4.1. 2-Methylbut-3-yn-2-ol was chosen as the protecting group for the triple bond due to its higher polarity compared with the unprotected forms, which could help in purification using silica gel column chromatography.[16,17] The protected phthalonitrile acetylene (A) was cyclized together with *tert*-butylphthalonitrile (B) to give a statistical mixture of A_mB_{4-m} type products with

zinc core. The AB_3 and A_2B_2 type compounds were isolated using silica gel column chromatography. Refluxing the AB_3 compound with catalytic amount of NaOH powder in toluene afforded the corresponding phthalocyanine zinc (II) ligand with acetylene functionality, **Pc-CC**. The platinum complexes with triphenylphosphine (PPh_3) ligands were made under similar conditions to those for other platinum acetylides described in the literature.[18] The pure product was isolated in reasonably high yield following silica gel column chromatography and size-exclusion column chromatography.

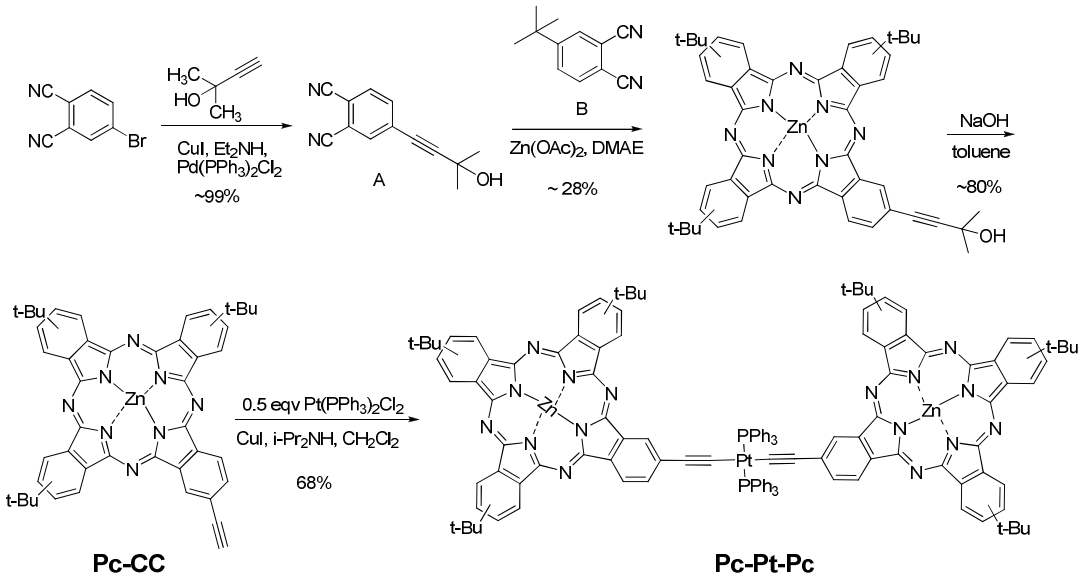

Scheme 4.1: The synthesis of phthalocyanine-based platinum complex (Pc-Pt-Pc).

The squaraine-based platinum triad (**Sq-Pt-Sq**) and polymer (**[Sq-Pt]$_n$**) were obtained by reacting the squaraine-based ligands with *trans*-dichlorobis(triethylphosphine)Pt(II) under basic conditions in relatively high yields (Scheme 4.2). Gel permeation chromatography (GPC) data in THF suggested the polymer has a reasonable molecular weight and polydispersity (M_w = 36k, M_n = 17k, estimated using polyester standards). The ^{31}P NMR spectra of both the phthalocyanine- and squaraine-based complexes show large coupling constants between phosphorus and

platinum nuclei (ea. $J_{P\text{-}Pt}$ = 2366 Hz in **Sq-Pt-Sq**). The absence of a peak at 540 cm^{-1} in the IR spectra suggests *trans*- conformation of these complexes.[19,20]

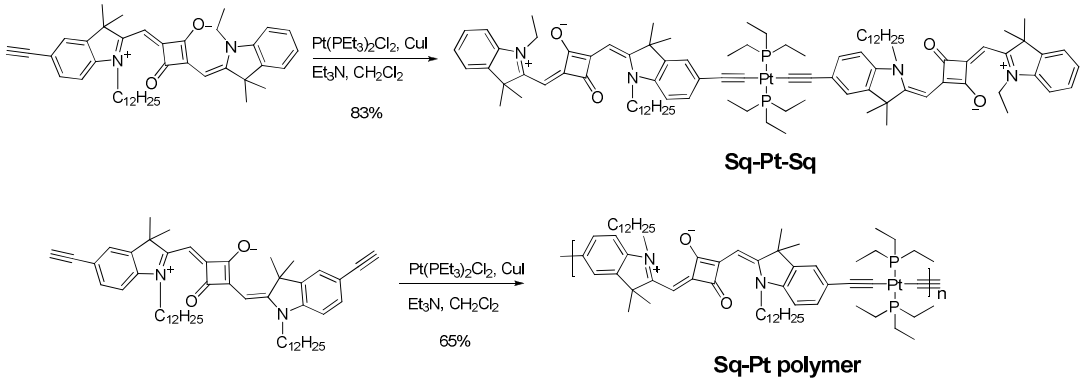

Scheme 4.2: The synthesis of squaraine-platinum triad and polymer.

In order to obtain squaraine mono- (**Sq-Pt**) and di-platinum (**Pt-Sq-Pt**) complexes, *trans*-Pt$(PEt_3)_2$PhCl was made following literature procedure[21,22] from *cis*-dichlorobis(triethylphoshine) platinum (II) by first converting it to the corresponding trifluoromethanesulfonate complex and further reacting with sodium tetraphenylborate and lithium chloride. **Sq-Pt** and **Pt-Sq-Pt** complexes were obtained under similar conditions as these used to make **Sq-Pt-Sq**. By comparison, the squaraine mono- (**Sq-Au**) and di-gold (**Au-Sq-Au**) containing analogues were made following literature procedures for other gold acetylides with modified purification processes.[21] The mono-substituted **Sq-Au** and **Sq-Pt** were synthesized in high yields and using simple chromatographic purification. However, the di-substituted squaraines (**Pt-Sq-Pt** and **Au-Sq-Au**) required careful size-exclusion chromatography to be performed at least twice to remove the mono-substituted products which were always found in the reaction mixture even at longer reaction time in the presence of excess platinum or gold reagents.

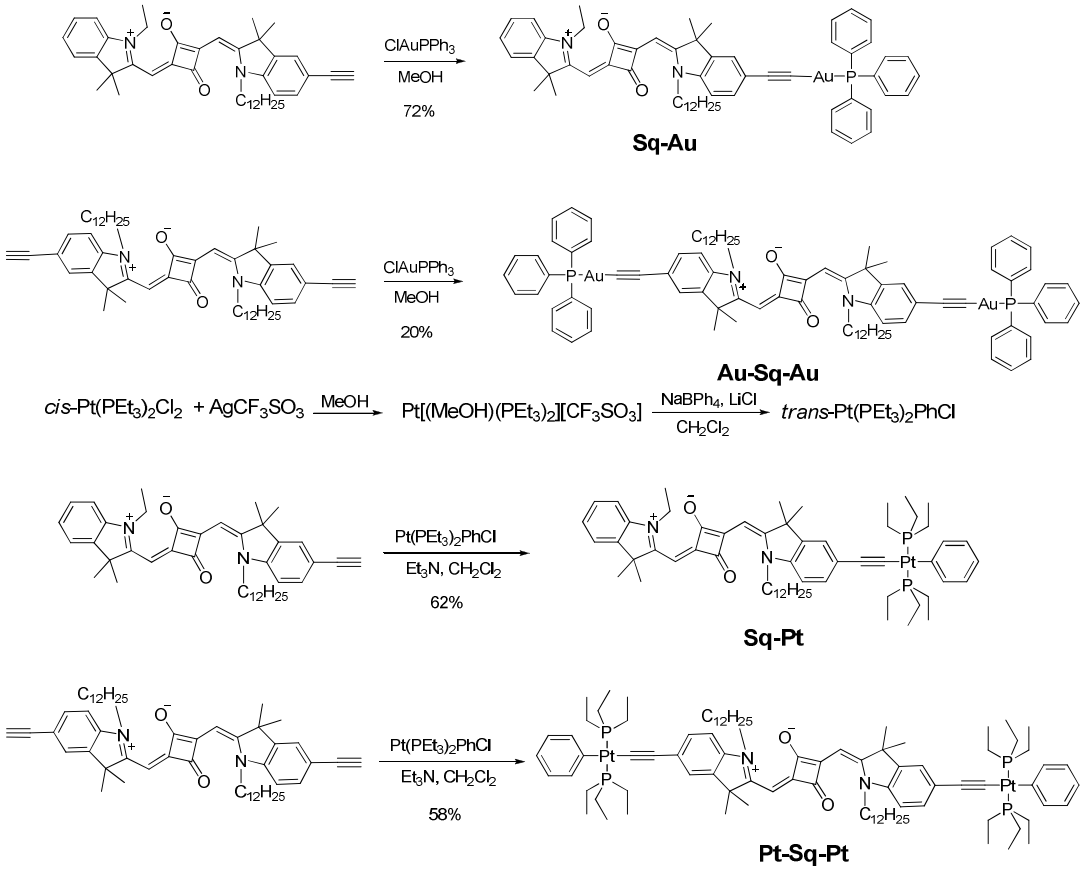

Scheme 4.3: The synthesis of squaraine mono- and di-platinum or gold complexes.

4.4 Optical properties of the metal complexes

4.4.1 Absorption and photo-stability of the metal complexes

The absorption spectra of **Pc-Pt-Pc** were taken in different solvents. Compared to the ligand precursor, **Pc-CC**, the Q-band (the low energy band) of **Pc-Pt-Pc** slightly bathochromically shifted and there is an additional shoulder absorption in the region between 400 – 500 nm which could be assigned to the metal (Pt) to ligand (**Pc-CC**) charge transfer absorption. The absorption spectrum of **Pc-Pt-Pc** is much narrower with larger peak extinction coefficient in THF, which is probably due to the coordination effect of THF to the zinc core.

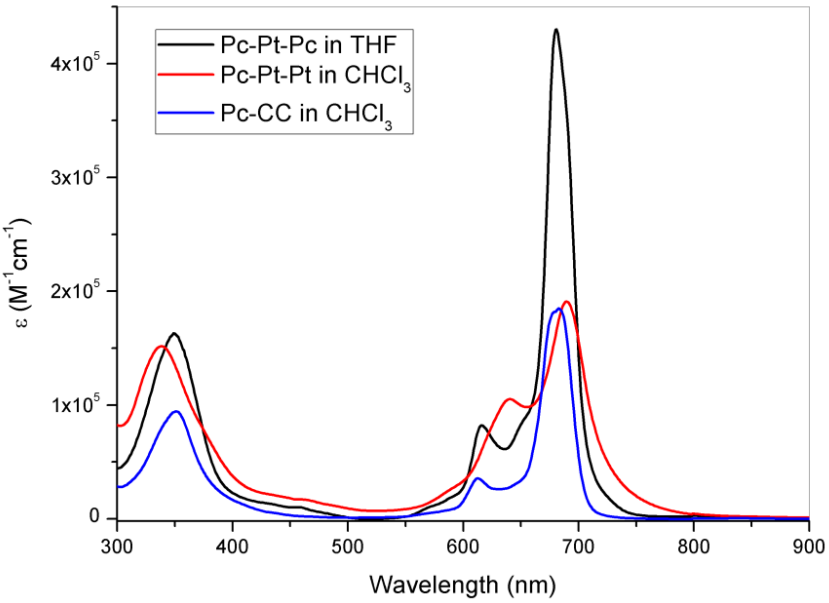

Figure 4.4: Molar absorptivities of Pc-Pt-Pc in THF and $CHCl_3$.

The photo-stability of these metal complexes in solution was studied in different solvents under various conditions. Solution samples were added to a capped cuvette and the absorption spectra were recorded at certain time interval, between which the cuvette was stored under ambient light. As one example shown in Figure 4.5, the peak absorbance of **Pc-Pt-Pc** toluene solution decreased to 60% of its original value after 18 hours. While it was kept in dark, the absorbance stayed the same and continued to decrease when explored to light again. However, in THF, the solution sample is quite stable even with the presence of water.

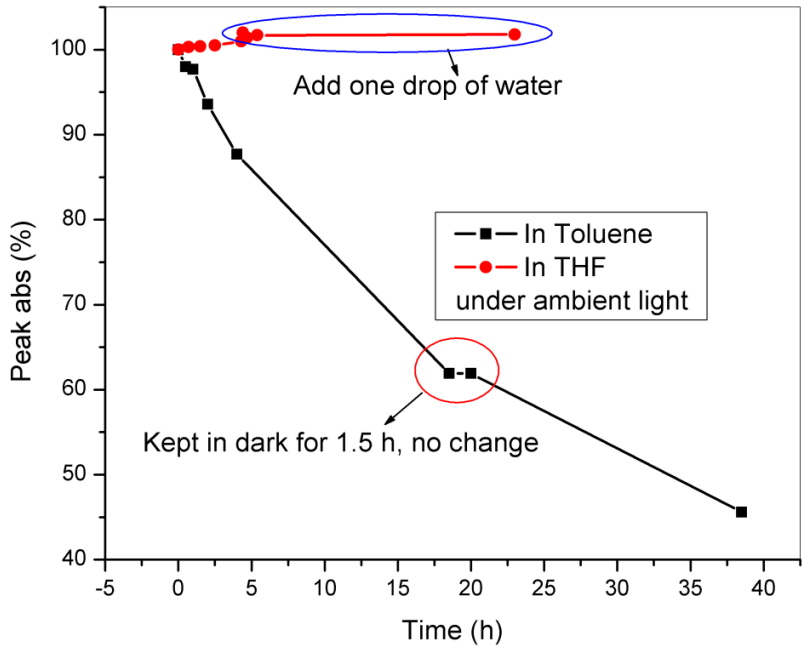

Figure 4.5: Photostability study of Pc-Pt-Pc in THF and toluene.

The absorption spectra of these squaraine complexes show bathochromically-shifted peaks as more metal centers were incorporated. A large extinction coefficient of ca. 6.0 × 10^5 $M^{-1}cm^{-1}$ in chloroform at the absorption maximum for **Sq-Pt-Sq**, along with red shift compared with **Sq** model compound (Figure 4.3) was recorded. The **[Sq-Pt]$_n$** polymer absorbs further to the near-IR with slightly broader peak which is probably due to a small degree of aggregation between squaraine units in polymer chains. The optical gaps for **Sq-Pt-Sq** and **[Sq-Pt]$_n$** are 1.70 and 1.63 eV, respectively, estimated from the onsets of the lower energy bands in the solution absorption spectra according to E_{gap}(optical) = 1240/λ_{onset}. Photo-stability test of the squaraine-based complexes revealed that toluene is a good solvent for such materials and no significant degradation was observed, at least after two days, for most of the compounds.

Table 4.1: Optical properties of squaraine-platinum and gold complexes

Compound	solvent	**Sq**	**Sq-Pt-Sq**	**[Sq-Pt]$_{nn}$**	**Sq-Pt**	**Pt-Sq-Pt**	**Sq-Au**	**Au-Sq-Au**
λ_{max} (nm)	$CHCl_3$	634	672	703	–	–	654	672
	toluene	–	676	706	669	693	–	–
ε (10^5 $M^{-1}cm^{-1}$)	$CHCl_3$	3.04	6.04	1.83	–	–	3.24	3.18
	toluene		4.57	2.31	2.85	3.46	–	–
Φ_F	$CHCl_3$	0.29	0.15	0	–	–	–	–
	toluene	–	–	–	0.54	0.58	0.43	0.49

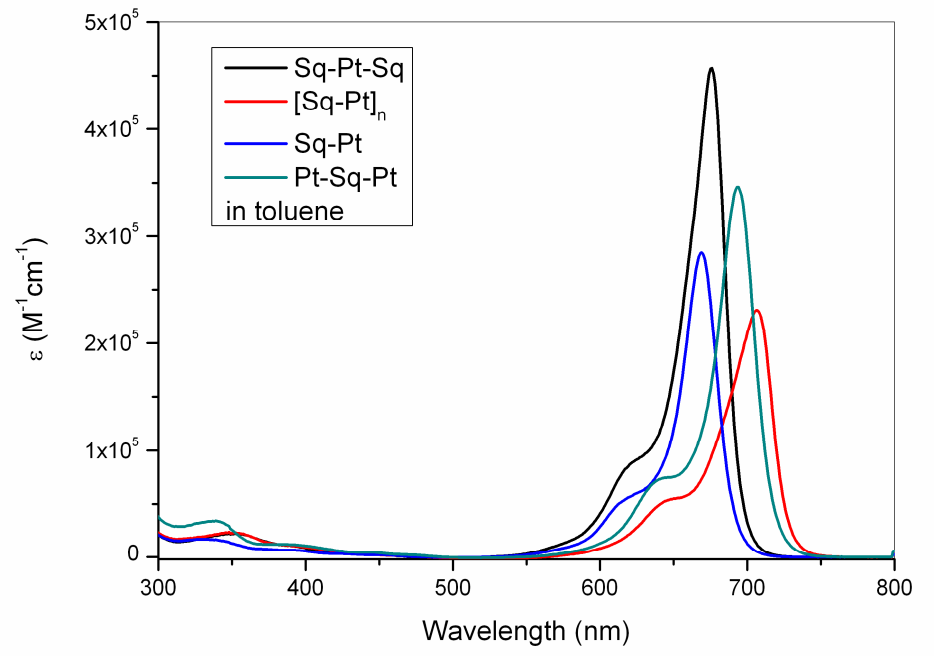

Figure 4.6: UV-Vis absorption spectra of Sq-Pt-Sq and [Sq-Pt]$_n$ in toluene.

The gold-containing squaraines followed a similar trend, where the complexes are bathochromically shifted compared to the corresponding terminal alkyne (0.06 eV for **Sq-Au**, and 0.11 eV for **Au-Sq-Au**), but the molar absorptivities remain almost the same. Furthermore, the gold containing compounds (**Sq-Au** and **Au-Sq-Au**) showed lower photo-stability and smaller red-shift in the absorption spectra in solution than the corresponding platinum compounds. The optical properties of these complexes are summarized in Table 4.1.

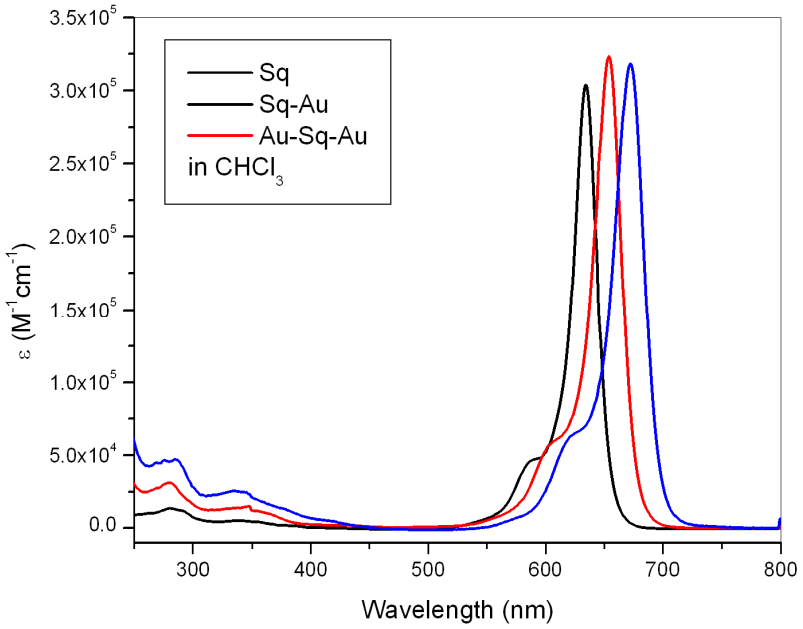

Figure 4.7: UV-Vis absorption spectra of squaraine-gold complexes in $CHCl_3$.

4.4.2 Emission of the metal complexes

All complexes showed small Stokes shifts of a few nanometers (less than 0.03 eV), and the fluorescence spectra closely resemble the mirror images of the lower band of the absorption spectra. The fluorescence quantum yield (Q.Y.) of **Pc-Pt-Pc** was determined to be <0.1% in chloroform (using a cyanine dye G40, Q.Y. = 0.52 in acetonitrile, as reference), which is highly quenched compared with ZnPc (30% in pyridine[23]). **Sq-Pt-Sq** has a quantum yield about 15% and **Sq-Pt polymer** has no measurable emission. The fluorescence quantum yields of monomeric squaraine-based complexes were measured in toluene using Cresyl Violet as the reference (FL Q.Y. = 0.54 in methanol[24]). It is suprising to see that much higher fluorescence quantum yield (Table 4.1) were obtained, giving that it is only 29% for the squaraine model compound **Sq**,[25] despite of the presence of heavy atoms. The reason is still not clear yet.

4.4.3 Pump-probe and double pump-probe measurements on Pc-Pt-Pc

The photophysical properties of some of the complexes have been studied in the Van Stryland group at the University of Central Florida. In pump-probe measurements, a strong linearly polarized pump pulse excites the molecules and creates a population distribution in the excited-state. The excited-state behavior of the molecule can be monitored by using a less intense probe pulse with different time delays. A femtosecond laser was used to pump the sample of **Pc-Pt-Pc** in THF with a pulse width of 150 fs; signals recorded after a 24 ns delay, as shown in Figure 4.8, indicate there is a transient absorption peak at around 532 nm, at which wavelength the ground-state absorption of **Pc-Pt-Pc** is negligible. This absorption was assigned to the $T_1 \rightarrow T_n$ absorption due to the long-lived lifetime. The excited singlet and triplet absorption cross-sections extracted from fitting the data for multiple transient spectra acquired at different delay times, are $\sigma_S = 8 \times 10^{-18}$ cm^2 and $\sigma_T = 18 \times 10^{-18}$ cm^2 at 532 nm, respectively.

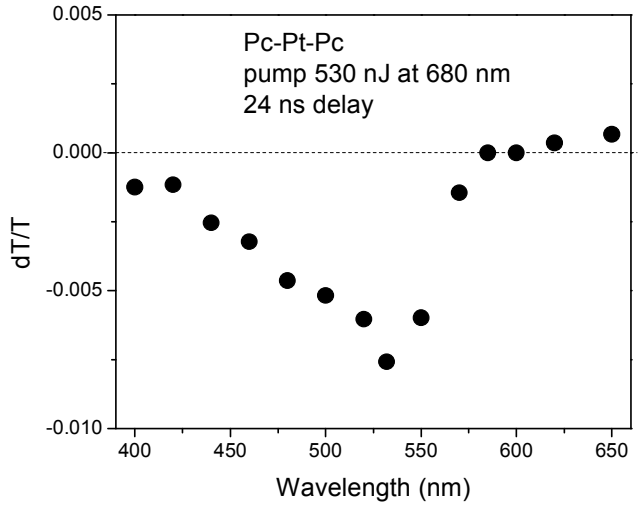

Figure 4.8: Femtosecond pump-probe results for Pc-Pt-Pc in THF, probed at 24 ns delay. (Figure was adapted from Dr. Lazaro Padilha in the Van Stryland group)

Further studies involved a picosecond double pump-probe (DPP) measurement (Figure 4.9), which consisted of the standard pump-probe but modified by including a second pump at a fixed delay of ~6 ns. As illustrated in Figure 4.1, after the first pump pulses, the molecule is excited to S_1, which will either decay to the ground-state or undergo intersystem crossing to the triplet-state, T_1. The second pump interacts with a set of modified populations that the transmittance change induced by the second pump is depended on the population distribution in both the ground-state and the triplet-state. The DPP method allows collection of excited singlet and triplet absorption cross-sections, the lifetime of the excited singlet-state, and the triplet quantum yield in one measurement.[26] DPP spectra on **Pc-Pt-Pc** were taken in THF at 680 nm near the ground-state absorption peak using low irradiance pulses (0.5μJ), given concerns about the stability of the compound. Data fitting of the curve gave the triplet quantum yield of ~0.50, which is almost identical to that reported for zinc phthalocyanine (0.50) in the literature.[27] This suggests no strong mixing between the platinum d-orbital and the phthalocyanine π-orbitals. Other approaches of metallophthalocyanines by core metallation using heavy atoms,[6,28-30] exhibit much higher the triplet quantum yield than **Pc-Pt-Pc**. However, this architecture with additional triphenylphosphine ligands can provide good solubility and make the compound more processable.

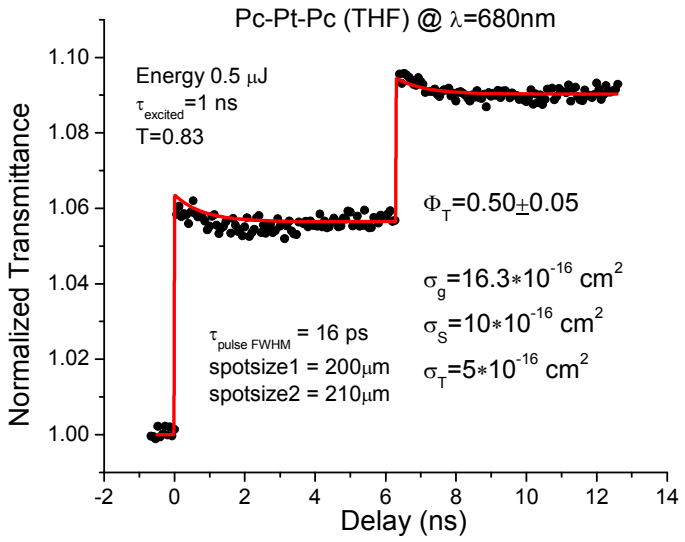

Figure 4.9: Picosecond double pump-probe results for Pc-Pt-Pc at 680 nm (Figure was adapted from Mr. Davorin Peceli in the Van Stryland group)

4.4.3 Pump-probe and double pump-probe measurements on squaraine metal complexes

Similar studies have been performed on squaraine-metal complexes. The transient peak of **Sq-Pt-Sq** after 24 ns delay is around 585 nm when pumped by a femtosecond laser at 675 nm as shown in Figure 4.10. Further data fitting from picosecond double pump-probe at 675 nm gave a estimated triplet-quantum yield of roughly 10% (Figure 4.11). These results suggested that there might be very weak electronic coupling through the indolium unit of squaraine to the metal center, meaning the heavy atom(s) do not substantially enhance the intersystem crossing rate. No measurable triplet signal for **Sq-Pt polymer** was obtained, although its fluorescence quantum yield is close to zero. There might be some other processes associated with its polymeric architecture, aggregation for example, which plays a role in quenching the excited-state. Consistent with the higher

fluroescence quantium yields of the **Sq-Au** and **Au-Sq-Au**, no long-lived (longer than several nanosecond timescale) excited-state signal was observed.

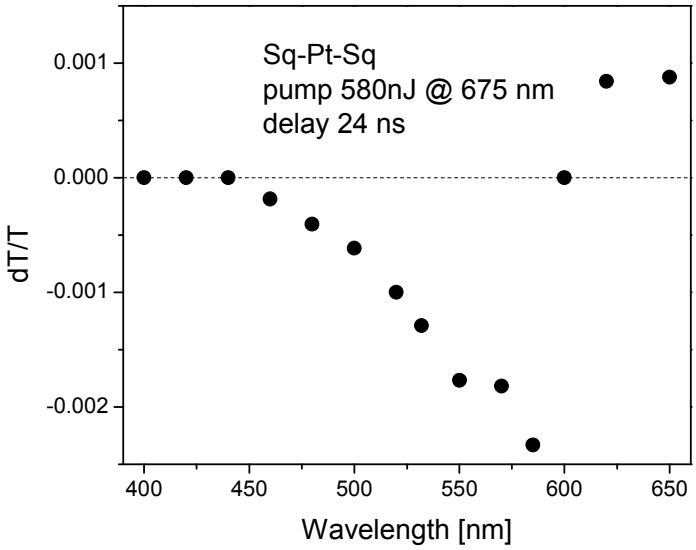

Figure 4.10: Femtosecond pump-probe results for Sq-Pt-Sq in $CHCl_3$, probed at 24 ns delay. (Figure was adapted from Dr. Lazaro Padilha in the Van Stryland group)

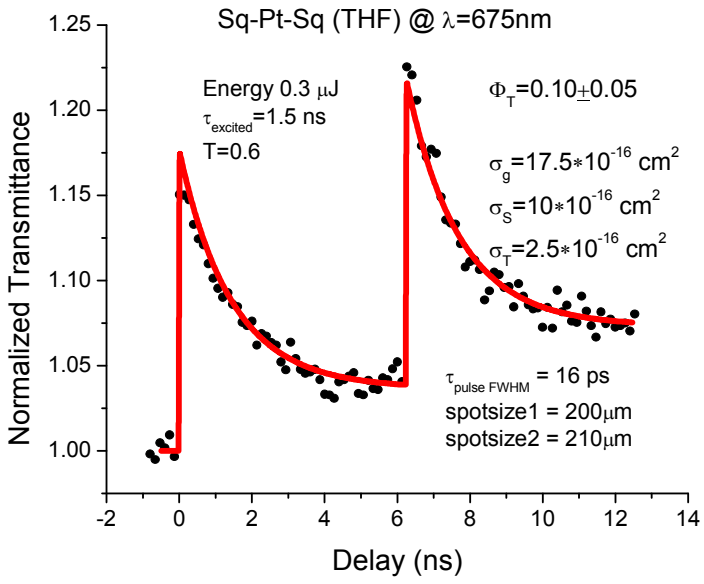

Figure 4.11: Picosecond double pump-probe results for Sq-Pt-Sq in THF at 675 nm. (Figure was adapted from Mr. Davorin Peceli in the Van Stryland group)

4.5 Electronic properties and photovoltaic performance of the metal complexes

4.5.1 Use of metallopolymers for solar cells

As discussed earlier, these newly developed phthalocyanine- and squaraine-based complexes exhibit good light harvesting ability in the near-IR which is attractive for photovoltaic applications. Research is emerging on using metalated conjugated polymers or oligomers as alternative donors to all-organic congeners in organic solar cells with their combined advantages of metal complexes and polymers.[31-33] In principle, polymers or oligomers possess the feature of low-cost and easy fabrication of thin-film devices by solution casting or printing technologies while metal complexes can provide easily tunable electronic structures and, in many cases, intrinsically low ionization energies. Among these metallopolymers, platinum(II)-based poly(arylene ethynylene)s are outstanding building blocks, where the d-orbitals of platinum can overlap with the p-orbitals of the alkyne unit,[34] hence, the electron delocalization can be enhanced. Furthermore, additional ligands (usually triaryl or trialkyl phosphines) can provide good solubility and film forming properties, which are important for device fabrication. In order to capture more of sun light, low gap Pt-polyynes have been investigated, specifically those obtained as condensation products with donor moieties such as fluorene, thiophene, thienothiophene, and phenothiazine, and acceptor groups such as benzothiadiazole, thienopyrazine, pyridopyrazine and dithiophenone. Power conversion efficiencies (PCE) of ca. 2% – 4% were achieved using these materials blending with soluble fullerene derivative, [6,6]-phenyl C_{61} butyric acid methyl ester (PCBM).[35-40] Adopting these ideas, solar cells using the blends of the newly developed squaraine-based complexes with PCBM were investigated.

4.5.2 Electrochemistry of the metal complexes

Cyclic voltamotry measurements on these complexes were conducted in 0.1 M $^{n}Bu_4NPF_6$ in dry dichloromethane with bis(pentamethylcyclopentadienyl)iron(II) ($Cp^*_2Fe^{+/0}$) as internal reference at a scan rate of 50 mV s^{-1}. The half-wave potentials ($E_{1/2}$) values (defined as (E_{pa} + E_{pc})/2, where E_{pa} and E_{pc} are peak oxidation and reduction potentials, respectively), are summarized in Table 4.2. Incorporation of metals does not have much influence on the redox potentials, suggesting that the electronic coupling between the metal and squaraine core is limited. Compared with the model compound **Sq**, the complexes become slightly easier to oxidize and harder to reduce as more platinum atoms are incoporated, while opposite trend was observed for gold complexes, although the differences are small. The first electrochemical half-wave reduction potentials $E_{1/2}^{0/-}$ were used to estimate the ionization potential (IP) and electron affinity (EA) with EA = -e ($E_{1/2}^{0/-}$ + 4.8 V) based on assuming a value of 4.8 eV for the solid state IP of ferrocene with respect to zero vacuum level.[41] Here, the EAs for **Sq-Pt-Sq** and **[Sq-Pt]$_n$** are around -3.1 eV. Their IPs are estimated from the first oxidation potential of the dyes to be 4.8 eV in each case. The "electrochemical gap" estimated from the redox potential for **Sq-Pt-Sq** and **[Sq-Pt]$_n$** (~1.7 eV) are rather close to their optical gap. This suggests that the energetic stabilization of these complexes by strong solvation of ionic species in the CV measurements (at least in 0.1 M solutions of $^{n}Bu_4NPF_6$ in anhydrous dichloromethane) is similar to that of the "exciton-binding energy" of their excited-state.

Table 4.2: Cyclic voltammetry data of squaraine-metal complexes

$E_{1/2}$ vs $FeCp_2^{+/0}$ (V)	2+/+	+/0	0/–
Sq	0.52	0.04	–1.71
Sq-Pt-Sq*	0.50	0	–1.72
Sq-Pt polymer	0.48	–0.04	–1.72
Sq-Pt	0.50	–0.01	–1.72
Pt-Sq-Pt	0.46	–0.08	–1.76
Sq-Au	0.53	0.02	–1.69
Au-Sq-Au	0.55	0.02	–1.67

*The oxidation state should be 4+/2+, 2+/0, 0/2–, 2–/4–

4.5.3 Photovoltaic cell characterization

Bulk heterojunction organic photovoltaic devices were constructed using blends of **Sq-Pt-Sq** or **[Sq-Pt]$_n$** with PCBM in the Kippelen group using the same device configuration, Al/Sq:PCBM/PEDOT:PSS/ITO, as described in Chapter 3. Weight ratios of 1:1 and 1:3 in squaraine/PCBM blends were tested. The spin-coated squaraine/PCBM blends formed smooth films which gave quite reproducible device performance. Here a higher PCBM ratio in the blends resulted in relatively higher short-circuit current (J_{SC}) and fill factor (*FF*), which corresponding to cells with higher PCEs. According to the incident photon-to-current conversion efficiency (IPCE, Figure 4.12) of devices using **[Sq-Pt]$_n$**/PCBM blends, the PCBM rich cells give higher IPCEs in the high energy wavelengths (400 −550 nm) presumably due to the PCBM light-harvesting in this region. The lower IPCEs in the region of 550 nm to 750 nm could come from the low ratio of the **[Sq-Pt]$_n$** materials. The higher device PCEs using **[Sq-Pt]$_n$**/PCBM blend in 1:3 weight ratio could be attributable to the morphology difference as change of donor/PCBM ratio, which could affect the charge mobility in the blends as well as the exciton dissociation efficiencies. The best device performance with an

average J_{SC} of 1.27 ± 0.02 mA/cm^2, a open-circuit voltage (V_{OC}) of 0.474 ± 0.007, and a *FF* of 0.44 ± 0.02, which corresponding to a overall PCE of 0.39± 0.01 %, were achieved using the blend [**Sq-Pt**]$_n$: PCBM in 1:3 weight ratio.

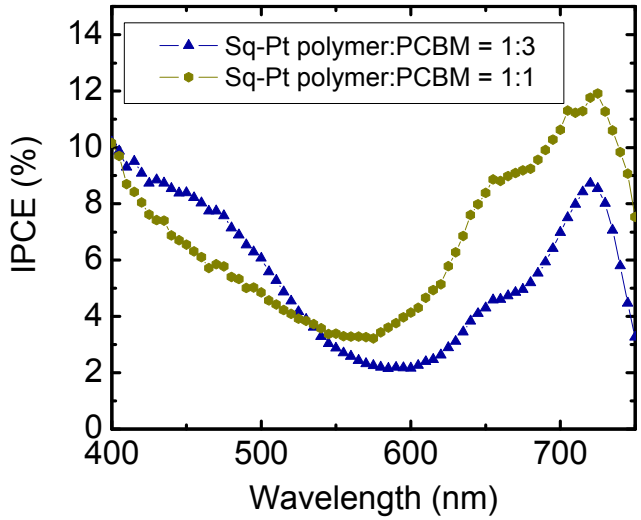

Figure 4.12: IPCE curves for the [Sq-Pt]$_n$/PCBM blends. (Adapted from Dr. Yinhua Zhou in the Kippelen group)

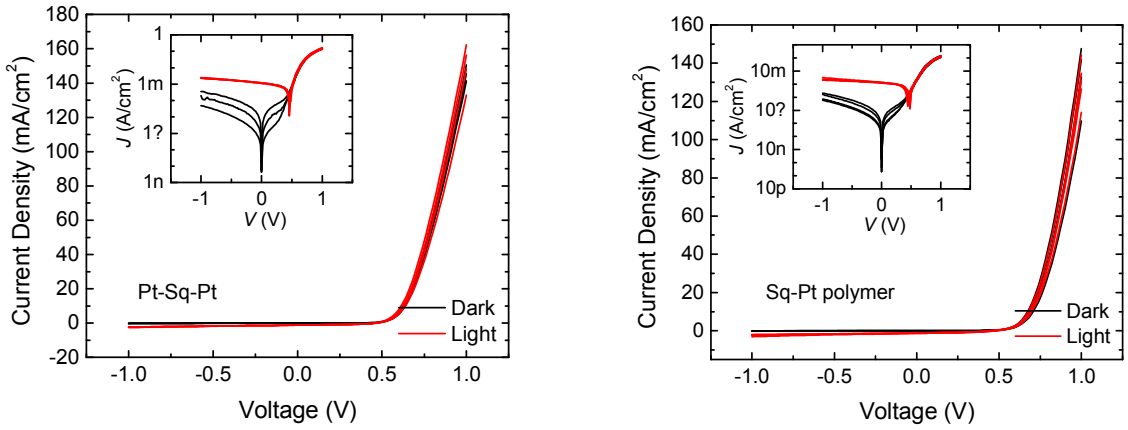

Figure 4.13: *I-V* characteristics of the solar cells for squaraine donor/PCBM blends. (Adapted from Dr. Yinhua Zhou in the Kippelen group)

The device using active layer of [**Sq-Pt**]$_n$/PCBM blends were annealed at 110 °C for 15 min.[42] Much lower J_{SC}, V_{OC} and *FF* were observed for all the cases, which caused the PCE decreased almost to 50% of the original value. The overall

performances of these platinum containing squaraine donors in solar cells are moderate compared to device based on other squaraine dyes,[42-45] which could be due to the unbalanced charge transport mobility and unfavorable morphologies. However, compared with the metal-free squaraine dimer analogues (see Chapter 3 for structure and synthesis detail), higher J_{SC} and PCEs were obtained as summarized in Table 4.3. The PCE increases with relatively more platinum component in the squaraine donor which indicates the platinum atoms might facilitate charge transport which led to higher current in solar cells.

Table 4.3: Summary of solar cell performance of squaraine donor/PCBM blends

Device	V_{OC} *(V)*	J_{SC} *(mA/cm^2)*	*FF*	η *(%)*
Sq-CC-CC-Sq[a]	0.53 ± 0.01	0.84 ± 0.02	0.356 ± 0.010	0.158 ± 0.033
Sq-Pt-Sq[a]	0.46 ± 0.01	1.15 ± 0.03	0.436 ± 0.017	0.231 ± 0.015
[Sq-Pt]$_n$[b]	0.474 ± 0.007	1.27 ± 0.02	0.44 ± 0.02	0.39± 0.01
After annealing[b]	0.316 ± 0.001	1.07 ± 0.01	0.36 ± 0.01	0.20± 0.01

[a]Under illumination of Oriel lamp, 100 mW/cm^2; [b]Under illumination of Oriel lamp, 68 mW/cm^2

4.6 Conclusions

In this chapter, a series of phthalocyanine- and squaraine-based metal complexes have been synthesized through coordination of corresponding acetylide ligands to platinum or gold. Photophysical properties including photo-stabilities, fluorescence, excited-state absorption and triplet quantum yields of these complexes were studied. These complexes showed red-shifted absorption compared with the ligand molecule and reasonable photo-stability in certain solvents. In general, the platinum complexes have advantages over the gold analogues in terms of photo-stability and triplet quantum yields,

although the "heavy atom" effect does not significantly influence the intersystem crossing rate in these systems, which might due to weak coupling between the conjugation core and the metal. The triplet quantum yield (Φ_T) of **Pc-Pt-Pc** is ~0.5, which is almost identical as ZnPc, while Φ_T = 0.1 was obtained for **Sq-Pt-Sq** from data fitting of double pump-probe measurements. **Sq-Pt-Sq** and **[Sq-Pt]$_n$** were also characterized in photovoltaic cells as donors in blends with PCBM. Although, only moderate power conversation efficiencies have been achieved, there are significant improvements compared with the metal-free squaraine oligomers described in Chapter 3, which provides a promising design strategy for future material developments.

4.7 Experimental Section

General: All the chemicals were purchased from commercial sources and used without further purification, unless otherwise indicated. Where necessary, THF and toluene, dichloromethane were dried using MBraun solvent purification system. The synthesis of **Sq-CC** and **Sq-2CC** has been reported in Chapter 3. The ^{1}H, ^{13}C, and ^{31}P NMR spectra were collected on a Bruker 400 MHz or 500 MHz spectrometer. Mass spectra were measured on a VG Instruments 70-SE using the electron impact (EI) or fast-atom bombardment (FAB) mode and on an Applied Biosystems 4700 Proteomics Analyzer using MALDI mode. Elemental analyses were carried out by Atlantic Microlab using a LECO 932 CHNS elemental analyzer. GPC data was collected on a Waters 1515 isocratic HPLC pump with Styragel® HR 5E THF column of 4.6 × 300 mm equipped with a Waters 2489 UV/Visible detector using polystyrene as standard. Solution (chloroform,

toluene) UV-Vis absorption spectra were recorded on a Varian Cary 5E UV/Vis/near-IR spectrophotometer while solution (chloroform, toluene) emission spectra were recorded with a Shimadzu FP-5301PC spectrofluorometer. Electrochemical measurements were carried out under nitrogen in deoxygenated 0.1 M solutions of tetra-*n*-butylammonium hexafluorophosphate in dry dichloromethane using a computer-controlled BAS 100B electrochemical analyzer, a glassy-carbon working electrode, a platinum-wire auxiliary electrode, and an Ag wire anodized with AgCl as a pseudo-reference electrode in a scan rate of 50 mV/s. The potentials were referenced to $FeCp_2^{+/0}$ redox couple by using bis(pentamethylcyclopentadienyl)iron(II) as an internal standard (-0.55 V vs. ferrocene).

Pump-probe and double pump-probe measurements: The experiments were carried out by Lazaro Padilha and Davorin Peceli in the Van Stryland group at University of Central Florida. In pump-probe measurements, a femtosecond laser–Ti:Sapphire amplified system (CPA 2110, Clark-MXR) (τ_{FWHM} = 130 fs) which outputs 780 nm pulses at 1 kHz repetition rate with a pulse width 150 fs (FWHM) was used. The pump pulse was generated from an OPG/A (TOPAS-800, Light Conversion, LTD.), while the probe pulses were generated from focusing 780 nm pulses into a 1 cm water cell to create a white-light continuum. Narrow band-pass interference filters were used to select wavelengths for the probe pulses. The double pump-probe experiments were performed with a picosecond laser system: 10-Hz EKSPLA PL2143 Nd:YAG laser with an SPLAPG401/DFG optical parametric generator/amplifier (OPG/A) tunable from 0.42 to 2.3 μm (τ_{FWHM} = 16 ps). Beam waists of pump beams were measured with knife-edge scans. Solution samples were prepared with anhydrous solvent and deoxygenated with nitrogen flow, and were transferred to a 0.1 cm cuvette.

Solar cell fabrication: Solar cells were fabricated by Dr. Yinhua Zhou in the Kippelen group by blending the squaraine donor materials with the acceptor [6,6]-phenyl C_{61} butyric acid methyl ester (Nano-C, $PC_{60}BM$). Squaraine:$PC_{60}BM$ solutions were made in chlorobenzene with weight ratios of 1:1 and 1:3 and a total concentration of 20 mg/mL. ITO-coated glass (Colorado Concept Coatings LLC) with a sheet resistivity of ~15 Ω/sq was used as the substrates for the solar cells. The substrates were patterned by Kapton® tape and etched by the vapor from acid solution (1:3, HNO_3: HCl) at 60 °C for 5 min. The substrates were cleaned in an ultrasonic bath of detergent water, rinsed with deionized water, and then cleaned in sequential ultrasonic baths of deionized water, acetone, and isopropanol. Nitrogen was used to dry the substrates after each of the last three baths. A layer of PEDOT:PSS (CLEVIOS P VP AI 4083, H. C. Starck, 30 nm) was filtered through a 0.45-μm-pore PVDF filter and spin coated on the substrates at 5,000 rpm for 1 min, and the substrates were annealed at 120 ºC for 10 min in atmosphere. After loading into a nitrogen-filled glove box, films of the active layers were deposited on the substrates by spin coating for 1 min at speeds of 1,000 rpm. The solutions were filtered through 0.2-μm-pore PTFE filters prior to spin coating. The substrates were then loaded into a vacuum thermal evaporation system (SPECTROS, Kurt J. Lesker) connected to the glove box, and 200 nm of Al was deposited through a shadow mask at a rate of 1 – 3 Å/s and a base pressure of ~2×10^{-7} Torr to define the cathodes. The completed devices were transferred in a sealed container to another nitrogen-filled glove box for electrical measurements. Current-voltage characteristics were measured using a source meter (2400, Keithley) controlled by a LabVIEW program. When testing the solar cells of $[\mathbf{Sq\text{-}Pt}]_n$/PCBM under illumination, filtered light from a 175 W Xenon lamp

(ASB-XE-175EX, CVI) was used as a broadband light source with an irradiance of ~68 mW/cm^2. When testing the solar cells of **Sq-Pt-Sq/PCBM** under illumination, Oriel lamp was used as the white light source with an irradiance of 100 mW/cm^2. After first measurement, the devices were annealed at 110 ºC for 10 min and tested again to see the annealing effect on the performance of the devices.

Synthesis:

4-(3-Hydroxy-3-methylbut-1-ynyl)phthalonitrile:[16,17] 4-Bromophthalonitrile (1.03 g, 5.00 mmol), CuI (6.5 mg, 0.025 mmol) and $Pd(PPh_3)Cl_2$ (55 mg, 0.050 mmol) were added to a dried round-bottomed flask. It was evacuated/refilled with nitrogen 3 times. Anhydrous THF (8 mL), 2-methylbut-3-yn-2-ol (1.2 mL, 10 mmol) and deoxygenated diethylamine (16 mL) were added. The mixture was heated at 50 ºC for 2 h. The solvent was removed and the residue was worked up with dichloromethane and water. After the solvent of organic phase was removed, it was purified by chromatography (silica gel, chloroform/ethyl acetate = 5 : 1). The second fraction was removed solvent to give the desired product as a yellow solid (1.04 g, 99%). ^{1}H NMR (400 MHz, $CDCl_3$): δ 7.79 (s, 1H), 7.71 (m, 2H), 1.97 (s, 1H), 1.61 (s, 6H). The ^{1}H NMR spectrum is consistent with that reported in the literature.[16,17]

Tri-*tert*-butyl-(3-hydroxy-3-methylbut-1-ynyl)phthalocyaninato-zinc(II):[16,46] A mixture of 4-*tert*-butyl-phthalonitrile (2.50 g, 13.6 mmol), 4-(3-hydroxy-3-methylbut-1-ynyl)phthalonitrile (711 mg, 3.40 mmol) and anhydrous $Zn(AcO)_2$ (930 mg, 5.10 mmol) were added to a two-neck round-bottomed flask, which was then evacuated/refilled with nitrogen 3 times. Dimethylaminoethanol (30 mL) was deoxygenated and added to the mixture through a syringe. The mixture was refluxed for 24 h. The solvent was

evaporated under reduced pressure. The crude product was purified by column chromatography (silica gel, dichloromethane with 1~5% isopropanol). The third fraction was removed solvent to give the desired product as a blue solid with metallic luster (390 mg, 17%). ^{1}H NMR (400 MHz, d_5-pyridine): δ 9.97−9.66 (m, 8H), 8.36 (br, 4H), 2.01 (s, 6H), 1.70−1.61 (m, 27 H) (O*H* resonance not observed). The ^{1}H NMR spectrum is consistent with that reported in the literature.[16,46]

Tri-*tert*-butyl ethynyl phthalocyaninatozinc(II) (Pc-CC):[16,46] Tri-*tert*-butyl ethynyl phthalocyaninatozinc (101 mg, 0.120 mmol) and powder NaOH (4.9 mg, 0.12 mmol) were added to a dried round-bottomed flask. Anhydrous toluene (3 mL) was added and the mixture was heated up to reflux for 4 h. The reaction mixture was passed through a silica plug (chloroform/ethyl acetate = 15 : 1) to give **Pc-CC** as a blue solid (80 mg, 85%). ^{1}H NMR (400 MHz, d_5-pyridine): δ 9.93–9.57 (m, 8H), 8.41 (br, 4H), 4.58 (m, 1H), 1.70 (m, 27 H). The ^{1}H NMR spectrum is consistent with that reported in the literature.[16,46]

Pc-Pt-Pc: *cis*-Pt(PPh_3)$_2$$Cl_2$ (60 mg, 0.076 mmol) was dissolved in anhydrous dichloromethane (15 mL) and *i*-Pr_2NH (3 mL). The solution was deoxygenated for 30 min with nitrogen flow. **Pc-CC** (128 mg, 0.167 mmol) and CuI (catalytic amount, ca. 2~3 mg) were added quickly. The mixture was stirred at room temperature overnight under nitrogen. After the solvent was removed, the residue was passed through a pad of silica gel with dichloromethane (3% methanol) and then a size-exclusion column (S-X1, Biobeads THF) to give **Pc-Pt-Pc** as a green solid (116 mg, 68%). ^{1}H NMR (400 MHz, d_5-pyridine): δ 9.94−9.51 (m, 16H), 8.34 (m, 8H), 7.99 (t, J = 8.8 Hz, 12H), 7.49 (m, 6H), 7.41 (t, J = 6.4 Hz, 12H), 1.64 (m, 54H). ^{31}P{^{1}H} NMR (161.97 MHz, CD_2Cl_2): δ 17.05

($J_{P\text{-}Pt}$ = 2329 Hz). Anal. Calcd. for $C_{128}H_{108}N_{16}P_2PtZn_2 \bullet 4H_2O$: C, 65.97; H, 5.02; N, 9.62. Found: C, 66.01; H, 4.93; N, 9.52.

Sq-Pt-Sq: *trans*-$Pt(PPEt_3)_2Cl_2$ (88.4 mg, 0.170 mmol) and **Sq-CC** (241 mg, 0.390 mmol) were added to a vial and transferred into a nitrogen glove box. Oxygen-free triethylamine (4 mL) and dichloromethane (4 mL) were added to the mixture and catalystic amount (ca. 2~3 mg) of CuI was added quickly. The mixture was stirred at room temperature in the glove box for 3 days. After the solvent was removed, the residue was passed through a pad of silica gel eluting with dichloromethane (3% methanol) and then a size-exclusion column (S-X1, Biobeads THF). It was then refluxed in heptane for 2 h before it was allowed to cool down to room temperature. The product was recovered by filtration. After washing with hexane and drying under vacuum, **Sq-Pt-Sq** was obtained as a green solid (235 mg, 83%). ^{1}H NMR (400 MHz, $CDCl_3$): δ 7.32 (m, 2H), 7.28 (m, 2H), 7.31 (m, 4H), 7.11 (t, J = 7.6 Hz, 2H), 6.95 (d, J = 7.6 Hz, 2H), 6.81 (d, J = 8.4 Hz, 2H), 5.91 (s, 4H), 4.03 (m, 4H), 3.94 (m, 4H), 2.18 (m, 12H), 1.75 (br, 24H), 1.37 (t, J = 7.6 Hz, 18H), 1.23 (m, 46H), 0.86 (t, J = 7.2 Hz, 6H). ^{13}C{^{1}H} NMR (100 MHz, $CDCl_3$): δ 182.45, 179.33, 178.41, 169.88, 168.95, 142.09, 139.71, 130.45, 127.72, 124.62, 123.42, 122.30, 109.46, 109.13, 108.91, 108.54, 86.68, 86.15, 49.19, 49.15, 43.82, 38.27, 31.89, 29.57, 29.52, 29.47, 29.35, 29.31, 27.13, 27.06, 27.02, 26.98, 22.67, 16.41 (t, $J_{C\text{-}P}$ = 18 Hz), 14.11, 11.97, 8.39 (Three aromatic and one aliphatic peaks missing probably due to overlap of near coincidental resonances). ^{31}P{^{1}H} NMR (161.97 MHz, $CDCl_3$): δ 11.81 ($J_{P\text{-}Pt}$ = 2366 Hz). HRMS (MALDI) Calcd. for $C_{96}H_{132}N_4O_4P_2Pt$ (MH^+): 1662.9444; Found: 1662.9021. Anal. Calcd. for $C_{96}H_{132}N_4O_4P_2Pt$: C, 69.33; H, 8.00; N, 3.37. Found: C, 69.15; H, 7.89; N, 3.31.

[Sq-Pt]$_n$: *trans*-Pt(PPEt$_3$)$_2$Cl$_2$ (146.3 mg, 0.291 mmol) and **Sq-2CC** (230.8 mg, 0.291 mmol) were added to a vial and transferred into a nitrogen glove box. Oxygen-free triethylamine (3 mL) and dichloromethane (3 mL) were and catalytic amount (ca. 2~3 mg) of CuI was added quickly. The mixture was stirred at room temperature for 2 days. After the vial was taken out of the glove box, phenyl acetylene (0.6 mL) was added in quenching the reaction. The reaction mixture was passed through a pad of silica gel with chloroform and ethyl acetate and then a size-exclusion column (S-X1, Biobeads THF). The first and second band were collected and precipitated from methanol and refluxed in heptanes for 2 h before it was allowed to cool to room temperature. The batches of product was recovered by filtration as a green solid (a: 80 mg; b: 100 mg, total yield 50%). ^{1}H NMR (400 MHz, CDCl$_3$): δ 7.15 (4nH), 6.79 (2nH), 5.89 (2nH), 3.90 (4nH), 2.18 (12nH), 1.74 (12nH), 1.23 (58nH), 0.86 (6nH). ^{31}P{^{1}H} NMR (161.97 MHz, CDCl$_3$): δ 11.81 ($J_{P\text{-}Pt}$ = 2358 Hz). GPC (THF): a: M_w = 29.1k, M_n = 14.5k, PDI = 2.0; b: M_w = 35.8k, M_n = 17.0k, PDI = 2.1. Anal. Calcd. for [$C_{66}H_{100}N_2O_2P_2Pt\cdot1.5H_2O$]$_n$: C, 64.05; H, 8.39; N, 2.26. Found: C, 63.96; H, 8.19; N, 2.32.

Sq-Au: **Sq-CC** (198 mg, 0.32 mmol) and triphenylphosphine gold chloride (207 mg, 0.42 mmol) were dissolved in methanol (4 mL, HPLC grade) and deoxygenated with nitrogen flow for 5 min. Sodium methoxide (138 mg, 2.56 mmol) in methanol (4 mL, HPLC grade) was added dropwise to the mixture. The mixture was stirred at room temperature overnight. The resulting solid was filtered and dissolved in THF. The crude product was purified by size-exclusion column (S-X1, Biobeads THF). The compound was then dissolved in ~2 mL chloroform and precipitated from 100 mL cold hexane. After drying under vacuum, **Sq-Au** was obtained as a purple blue solid (250 mg, 72%). ^{1}H NMR (400

MHz, $CDCl_3$): δ 7.52–7.42 (m, 17H), 7.31 (m, 2H), 7.12 (t, J = 7.2 Hz, 1H), 6.96 (d, J = 8.0 Hz, 1H), 6.83 (d, J = 8.4 Hz, 1H), 5.92 (s, 1H), 5.91 (s, 1H), 4.04 (m, 2H), 3.91 (m, 2H), 1.76 (s, 6H), 1.73 (s, 6H), 1.23 (m, 23H), 0.85 (t, J = 7.2 Hz, 3H). $^{13}C\{^1H\}$ NMR (100 MHz, $CDCl_3$): δ 182.55, 179.53, 171.17, 169.86, 169.45, 142.36, 142.09, 141.20, 134.38, 135.24, 131.94, 131.56, 129.99, 129.40, 129.20, 129.10, 127.72, 126.56, 123.57, 122.32, 120.08, 108.99, 86.87, 86.30, 49.26, 49.08, 31.89, 29.57, 29.51, 29.34, 29.31, 27.06, 26.98, 26.92, 22.66, 14.10, 11.96 (One aromatic and five aliphatic peaks missing probably due to overlap of near coincidental resonances). $^{31}P\{^1H\}$ NMR (161.97 MHz, $CDCl_3$): δ 42.94. HRMS (MALDI) Calcd. for $C_{60}H_{66}AuN_2O_2P$ (M^+): 1074.4527; Found: 1074.4269. Anal. Calcd. for $C_{60}H_{66}AuN_2O_2P$: C, 67.03; H, 6.19; N, 2.61. Found: C, 67.06; H, 6.16; N, 2.62.

Au-Sq-Au: **Sq-2CC** (174 mg, 0.22 mmol) and triphenylphosphine gold chloride (265 mg, 0.535 mmol) were dissolved in methanol (7 mL, HPLC grade) and degassed with nitrogen flow for 5 min. Sodium methoxide (119 mg, 2.2 mmol) in methanol (3 mL, HPLC grade) was added dropwise to the mixture. The mixture was stirred at room temperature overnight. The resulting solid was filtered and dissolved in THF. The crude product was purified by size-exclusion column (S-X1, Biobeads THF) and the fractions were collected according to the absorption spectra. The compound was then dissolved in ~2 mL chloroform and precipitated from 100 mL cold hexane. After drying under vacuum, **Au-Sq-Au** was obtained as a blue green solid (70 mg, 19%). ^1H NMR (400 MHz, $CDCl_3$): δ 7.55–7.42 (m, 34H), 6.83 (d, J = 8.0 Hz, 2H), 5.90 (s, 2H), 3.91 (m, 4H), 1.73 (s, 12H), 1.23 (m, 40H), 0.85 (t, J = 7.2 Hz, 6H). $^{13}C\{^1H\}$ NMR (100 MHz, $CDCl_3$): δ 179.15, 169.61, 142.07, 141.21, 134.36, 134.22, 131.91, 131.57, 129.97, 129.41, 129.20,

129.09, 126.57, 119.99, 108.95, 86.94, 49.04, 43.82, 31.89, 29.57, 29.50, 29.33, 29.30, 27.07, 26.93, 22.66, 14.10 (Three aliphatic peaks missing probably due to overlap of near coincidental resonances). $^{31}P\{^{1}H\}$ NMR (161.97 MHz, $CDCl_3$): δ 42.95. HRMS (MALDI) Calcd. for $C_{90}H_{100}Au_2N_4O_4P_2$ (M^+): 1696.6591; Found: 1696.6368. Anal. Calcd. for $C_{90}H_{100}Au_2N_4O_4P_2$: C, 63.67; H, 5.94; N, 1.65. Found: C, 63.40; H, 5.94; N, 1.86.

***trans*-Pt(PEt$_3$)$_2$PhCl**:[22] *cis*-Pt$(PEt_3)_2Cl_2$ (244 mg, 0.49 mmol) and silver triflate (250 mg, 0.97 mmol) were dissolved in methanol (10 mL, 20 eqv. by volume) and stirred for 30 min. The resulting pink solid was filtered and dichloromethane (10 mL) was added to the filtrate. Sodium tetraphenylborate (166 mg, 0.49 mmol) was added to the solution and stirred for 30 min. Lithium chloride (41 mg, 0.97 mmol) was added and it was stirred for another 10 min. The reaction mixture was filtered through a pad of Celite. The solvent of the filtrate was removed and the residue was recrystallized from acetone and water. Pale yellow crystals were collected (180 mg, 71%). ^{1}H NMR (400 MHz, $CDCl_3$): δ 7.29 (d, J = 6.8 Hz, 2H), 6.86 (t, J = 7.2 Hz, 2H), 6.79 (d, J = 7.2 Hz, 1H), 1.61 (m, 12H), 1.06 (quintet, J = 8 Hz, 18H). ^{1}H NMR spectrum is consistent with that reported in the literature.[22]

Sq-Pt: **Sq-CC** (119 mg, 0.19 mmol) and *trans*-Pt$(PEt_3)_2$PhCl (126 mg, 0.23 mmol) were added to a dried round-bottomed flask. Anhydrous dichloromethane (10 mL) and triethylamine (10 mL) were added to dissolve the reactants and the solution was deoxygenated with nitrogen flow for 10 min. A catalytic amount (ca. 2~3 mg) of CuI was added quickly and the reaction mixture was stirred under nitrogen at room temperature overnight. After the reaction mixture was passed through a pad of silica gel, the solvent

was removed and the residue was purified with size-exclusion chromatography (S-X1, Biobeads THF) to give **Sq-Pt** as a blue solid (133 mg, 62%). ^{1}H NMR (400 MHz, $CDCl_3$): δ 7.34 (m, 4H), 7.22 (m, 2H), 7.13 (d, J = 7.2 Hz, 1H), 7.00 (d, J = 8.0 Hz, 1H), 6.95 (t, J = 7.2 Hz, 2H), 6.68 (d, J = 8.0 Hz, 1H), 6.77 (t, J = 7.2 Hz, 1H), 5.89 (m, 2H), 4.05 (m, 2H), 4.00 (m, 2H), 1.77 (m, 24H), 1.39–1.26 (m, 23H), 1.10 (quintet, J = 8.0 Hz, 18H), 0.87 (t, J = 7.2 Hz, 3H). ^{13}C{^{1}H} NMR (100 MHz, $CDCl_3$): δ 182.14, 180.44, 179.05, 170.19, 168.86, 156.56 (t, $J_{C\text{-}P}$ = 10 Hz), 142.55, 139.81 139.58, 130.60, 128.08, 127.65, 125.83, 124.75, 123.58, 122.54, 121.61, 115.13 (t, $J_{C\text{-}P}$ = 15 Hz), 110.20, 109.70, 109.34, 86.94, 86.33, 49.55, 49.38, 44.16, 38.64, 32.29, 30.06, 29.98, 29.93, 29.87, 29.75, 29.71, 27.50, 27.40, 27.14, 27.08, 23.06, 15.48 (t, $J_{C\text{-}P}$ = 17 Hz), 14.26, 12.10, 8.17 (Two aromatic and peaks missing probably due to overlap of near coincidental resonances). ^{31}P{^{1}H} NMR (161.97 MHz, $CDCl_3$): δ 10.55 ($J_{P\text{-}Pt}$ = 2640 Hz). HRMS (MALDI) Calcd. for $C_{60}H_{86}N_2O_2P_2Pt$ (M^+): 1123.5812; Found: 1123.5644. Anal. Calcd. for $C_{60}H_{86}N_2O_2P_2Pt$: C, 64.09; H, 7.71; N, 2.49. Found: C, 64.30; H, 7.77; N, 2.43.

Pt-Sq-Pt: **Sq-2CC** (121 mg, 0.154 mmol) and *trans*-Pt(PEt_3)$_2$PhCl (185 mg, 0.34 mmol) were added to a dried round-bottomed flask. Anhydrous dichloromethane (10 mL) and triethyl amine (10 mL) were added to dissolve the reactants and the solution was deoxygenated with nitrogen flow for 10 min. Catalytic amount (ca. 2~3 mg) of CuI was added quickly and the reaction mixture was stirred under nitrogen at room temperature for 2 days. After the reaction mixture was passed through a pad of silica gel, the solvent was removed and the residue was purified with size-exclusion chromatography (S-X1, Biobeads THF) to give **Pt-Sq-Pt** as a blue solid (160 mg, 58%). ^{1}H NMR (400 MHz, $CDCl_3$): δ 7.32 (m, 4H), 7.20 (m, 4H), 6.95 (t, J = 7.2 Hz, 4H), 6.79 (m, 4H), 5.88 (s, 2H),

3.91 (m, 4H), 1.74 (m, 36H), 1.39–1.24 (m, 40H), 1.08 (quintet, J = 8 Hz, 36H), 0.86 (t, J = 7.2 Hz, 6H). $^{13}C\{^{1}H\}$ NMR (100 MHz, $CDCl_3$): δ 182.20, 178.96, 169.35, 156.61 (t, $J_{C\text{-}P}$ = 10 Hz), 142.46, 139.99, 139.60, 130.57, 127.64, 125.50, 124.74, 121.60, 114.80 (t, $J_{C\text{-}P}$ = 15 Hz), 110.23, 109.46, 86.77, 49.36, 44.05, 32.30, 29.99, 29.94, 29.89, 29.77, 29.72, 27.46, 27.42, 27.15, 23.07, 15.49 (t, $J_{C\text{-}P}$ = 17 Hz), 14.27, 8.18 (one aliphatic peak missing probably due to overlap of near coincidental resonances). $^{31}P\{^{1}H\}$ NMR (161.97 MHz, $CDCl_3$): δ 10.54 ($J_{P\text{-}Pt}$ = 2637 Hz). HRMS (MALDI) Calcd. for $C_{90}H_{140}N_2O_2P_4Pt_2$ (M^+): 1794.9161; Found: 1794.9154. Anal. Calcd. for $C_{90}H_{140}N_2O_2P_4Pt_2$: C, 60.18; H, 7.86; N, 1.56. Found: C, 60.12; H, 7.92; N, 1.60.

4.8 References

(1) Giuliano, C. R. H., L. D. *IEEE J. Quantum Electron* **1967**, *QE 3*, 358.

(2) Spangler, C. W. *J. Mater. Chem.* **1999**, *9*, 2013.

(3) de la Torre, G.; Vázquez, P.; Agulló-López, F.; Torres, T. *Chem. Rev.* **2004**, *104*, 3723.

(4) Tutt, L. W. B., T. F. *Prog. Quant. Electr.* **1993**, *17*, 299.

(5) Anslyn, E. V.; Dougherty, D. A. *Modern Physical Organic Chemistry*; University Science Books, 2004.

(6) Perry, J. W. M., K.; Marder, S. R.; Perry, K. J.; Daniel Alvarez, J.; Choong, I. *Opt. Lett.* **1994**, *19*, 625.

(7) Guo, F. S., W.; Liu, Y.; Schanze, K. *Inorg. Chem.* **2005**, *44*, 4055.

(8) Sun, W. Z., H.; Barron, P. M. *Chem. Mater.* **2006**, *18*, 2602.

(9) Vestberg, R. W., R.; Eriksson, A.; Lopes, C.; Carlsson, M.; Eliasson, B.; Glimsdal, E.; Lindgren, M.; Malmström, E. *Macromolecules* **2006**, *39*, 2238.

(10) Westlund, R. G., E.; Lindgren, M.; Vestberg, R.; Hawker, C.; Lopesd, C.; Malmström, E. *J. Mater. Chem.* **2008**, *18*, 166.

(11) Zhou, G.-J. W., W.-Y.; Cui, D.; Ye, C. *Chem. Mater.* **2005**, *17*, 5209.

(12) Zhou, G.-J. W., W.-Y.; Ye, C.; Lin, Z. *Adv. Funct. Mater.* **2007**, *17*, 963.

(13) Zhou, G. W., W.-Y.; Poon, S.-Y.; Ye, C.; Lin, Z. *Adv. Funct. Mater.* **2009**, *19*, 531.

(14) Zhang, L. W., L. *J. Mater. Sci.* **2008**, *43*, 5692.

(15) Beverina, L.; Salice, P. *Eur. J. Org. Chem.* **2010**, 1207.

(16) Maya, E. M.; Vázquez, P.; Torres, T. *Chem. Commun.* **1997**, 1175.

(17) Maya, E. M.; Haisch, P.; Vázquez, P.; Torres, T. *Tetrahedron* **1998**, *54*, 4397.
(18) Rachford, A. A.; Goeb, S.; Castellano, F. N. *J. Am. Chem. Soc.* **2008**, *130*, 2766.
(19) Lee, T. W.; Staufer., R. C. *J. Am. Chem. Soc* **1975**, *97*, 195.
(20) Furlani, A.; Carusi, P.; Russo, M. V. *J. Organomet. Chem.* **1976**, *116*, 113.
(21) Wong, W.-Y.; Guo, Y.; Ho, C.-L. *J Inorg Organomet Polym* **2009**, *19*, 46.
(22) Siegmann, K.; Pregosin, P. S.; Venanzi, L. M. *Organometallics* **1989**, *8*, 2659.
(23) Seybold, P. G.; Gouterman, M. *J. Mol. Spec.* **1969**, *31*, 1.
(24) Isak, S. J.; Eyring, E. M. *J. Phys. Chem.* **1992**, *96*, 1738.
(25) Webster, S.; Odom, S. A.; Padilha, L. A.; Przhonska, O. V.; Peceli, D.; Hu, H.; Nootz, G.; Kachkovski, A. D.; Matichak, J.; Barlow, S.; Anderson, H. L.; Marder, S. R.; Hagan, D. J.; Van Stryland, E. W. *J. Phys. Chem. B* **2009**, *113*, 14854.
(26) Swatton, S. N. R.; Welford, K. R.; Hollins, R. C.; Sambles, J. R. *Appl. Phys. Lett.* **1997**, *71*, 10.
(27) Zhang, X.-F.; Xu, H. *J. Chem. Soc. Faraday Trans.* **1993**, *89*, 3347.
(28) Nalwa, H. S.; Kakuta, A.; Mukoh, A. *Chem. Phys. Lett.* **1993**, *203*, 109.
(29) Nalwa, H. S.; Kakuta, A.; Mukoh, A. *J. Phys. Chem.* **1993**, *97*, 1097.
(30) Diaz-Garcia, M. A.; Ledoux, I.; Duro, J. A.; Torres, T.; Agulló-López, F.; Zyss, J. *J. Phys. Chem.* **1994**, *98*, 8761.
(31) Eloi, J.-C.; Chabanne, L.; Whittell, G. R.; Manners, I. *Materials Today* **2008**, *11*, 28.
(32) Wong, W.-Y.; Harvey, P. D. *Macromol. Rapid Commun.* **2010**, *31*, 671.
(33) Wong, W.-Y.; Ho, C.-L. *Acc. Chem. Res.* **2010**, *43*, 1246.
(34) Louwen, J. N.; Hengelmolen, R.; Grove, D. M.; Oksam, A. *Organometallics* **1984**, *3*, 908.
(35) Wong, W.-Y.; Wang, X.-Z.; He, Z.; Chan, K.-K.; Djurišić, A. B.; Cheung, K.-Y.; Yip, C.-T.; Ng, A. M.-C.; Xi, Y. Y.; Mak, C. S. K.; Chan, W.-K. *J. Am. Chem. Soc* **2007**, *129*, 14372.
(36) Liu, L.; Ho, C.-L.; Wong, W.-Y.; Cheung, K.-Y.; Fung, M.-K.; Lam, W.-T.; Djurišić, A. B.; Chan, W.-K. *Adv. Funct. Mater.* **2008**, *18*, 2824.
(37) Wong, W.-Y.; Wang, X.-Z.; He, Z.; Djurišić, A. B.; Yip, C.-T.; Cheung, K.-Y.; Wang, H.; Mak, C. S. K.; Chan, W.-K. *Nat. Mater.* **2007**, *6*, 521.
(38) Wu, P.-T.; Bull, T.; Kim, F. S.; Luscombe, C. K.; Jenekhe, S. A. *Macromolecules* **2009**, *42*, 671.
(39) Wong, W.-Y.; Chow, W.-C.; Cheung, K.-Y.; Fung, M.-K.; Djurišić, A. B.; Chan, W.-K. *J. Organomet. Chem.* **2009**, *694*, 2717.
(40) Wong, W.-Y.; Wang, X.; Zhang, H.-L.; Cheung, K.-Y.; Man-Kin Fung; Djurišić, A. B.; Chan, W.-K. *J. Organomet. Chem.* **2008**, *693*, 3603.
(41) Thelakkat, M.; Schmidt, H.-W. *Adv. Mater.* **1998**, *10*, 219.
(42) Mayerhöffer, U.; Deing, K.; Gruß, K.; Braunschweig, H.; Meerholz, K.; Würthner, F. *Angew. Chem. Int. Ed.* **2009**, *48*, 8776.
(43) Silvestri, F.; Irwin, M. D.; Beverina, L.; Facchetti, A.; Pagani, G. A.; Marks, T. J. *J. Am. Chem. Soc.* **2008**, *130*, 17640.

(44) Bagnis, D.; Beverina, L.; Huang, H.; Silvestri, F.; Yao, Y.; Yan, H.; Pagani, G. A.; Marks, T. J.; Facchetti, A. *J. Am. Chem. Soc.* **2010**, *132*, 4074.
(45) Wei, G.; Wang, S.; Renshaw, K.; Thompson, M. E.; Forrest, S. R. *ACS Nano* **2010**, *4*, 1927.
(46) Maya, E. M.; Vázquez, P.; Torres, T. *Chem. Eur. J.* **1999**, 2004.

Chapter 5: Squaraine Chromophores for Dye-sensitized Solar Cells

5.1 Introduction

Clean renewable energy resources are highly demanded globally due to the depletion of fossil fuels and to environmental concerns. Since the pioneering work by Grätzel and O'Reagan published on dye-sensitized nanocrystalline semiconductors in 1991,[1] dye-sensitized solar cells (DSSCs) have attracted great research interest from scientists around the world as promising candidates for low-cost alternatives to conventional solid-state photovoltaic devices.[2-5] The most efficient DSSC devices to date give solar-light-to-electric power conversion efficiencies (PCEs) of up to 12%.[5-8] In chapter one, the working principle of DSSCs and some squaraine sensitizers have been discussed. The lack of absorption in the red and near-infrared (IR) region of the spectrum and their low molar absorption coefficients ($\varepsilon \leq 20000$ $M^{-1}cm^{-1}$) are limiting further improvement in efficiency of current explored ruthenium complexes. One way to potentially further improve DSSC performance is to develop sensitizers showing increased light-harvesting ability in the near-IR to capture more solar radiation.

Squaraine dyes are promising candidates for near-IR sensitization due to their strong absorption in this region.[9-11] A bis(indolinylenemethyl)squaraine-based sensitizer (**SQ1**) with carboxylic docking group directly bound to the π-conjugated backbone has achieved PCEs up to 4.5% under 1.5 AM.[12] This efficiency was further increased to 5.4% by additional benzannulation of one of the indolium unit.[13] It has been demonstrated from previous research on squaraines that an electronically unsymmetrical design for efficient

electron injection[12] and an increase in π-conjugation to bathochromically shift the main low-energy absorption band[13] are efficient approaches to enhance performance.

Recent research on squaraine-based sensitizers for DSSCs mainly focused on two aspects to obtain improved solar-light-harvesting: a) shifting the absorption further into near-IR region; b) pursuing panchromatic absorption to cover more of the solar spectrum. Based on a previous reported bis(indolinylenemethyl)-based squaraine bearing a carboxylic acid anchor group,[12] derivatives of **SQ1** have been developed through modification of the "donor" part. One of the indolium units is replaced by a triarylamine-type donor in **JK-64H**,[14] **JK-216**[15] and **JYL-SQ5**[16] (Figure 5.1) linked to the squaraine core through various bridges. These dyes have significant *incident photon*-to-current conversion efficiencies (*IPCEs*) across the entire visible widow and some extend out to wavelengths as long as 900 nm (shown for the example of **JYL-SQ5** in Figure 5.2).

In the device using **JK-64H** with a 20 μm thick TiO_2 layer, a short-circuit photocurrent density (J_{SC}) of 13.60 mA cm^{-2}, an open-circuit voltage (V_{OC}) of 490 mV, and a fill factor (*FF*) of 0.70 were obtained, corresponding to an overall efficiency (η) of 4.70%, under AM 1.5.[14] Devices with higher *V*oc of 510 mV were achieved using **JK-64Hx** sensitizer with a hexyl group on the fluorene donor. The improved efficiency was attributed to the suppressed charge recombination resulting from the blocking effect of the larger substituents.[17] More recently, the same group developed new panchromatic squaraines by extending the conjugation on donor end with additional thiophene and pyrrole units.[15] The more markedly unsymmetrical mixed pyrrole / indoline squaraine **JK-216,** which exhibits a red shift of its main absorption peak relative to that of **SQ 1**, set a record for squaraine-sensitized DSSCs with PCEs up to 6.29% on a 20 nm TiO_2 layer.

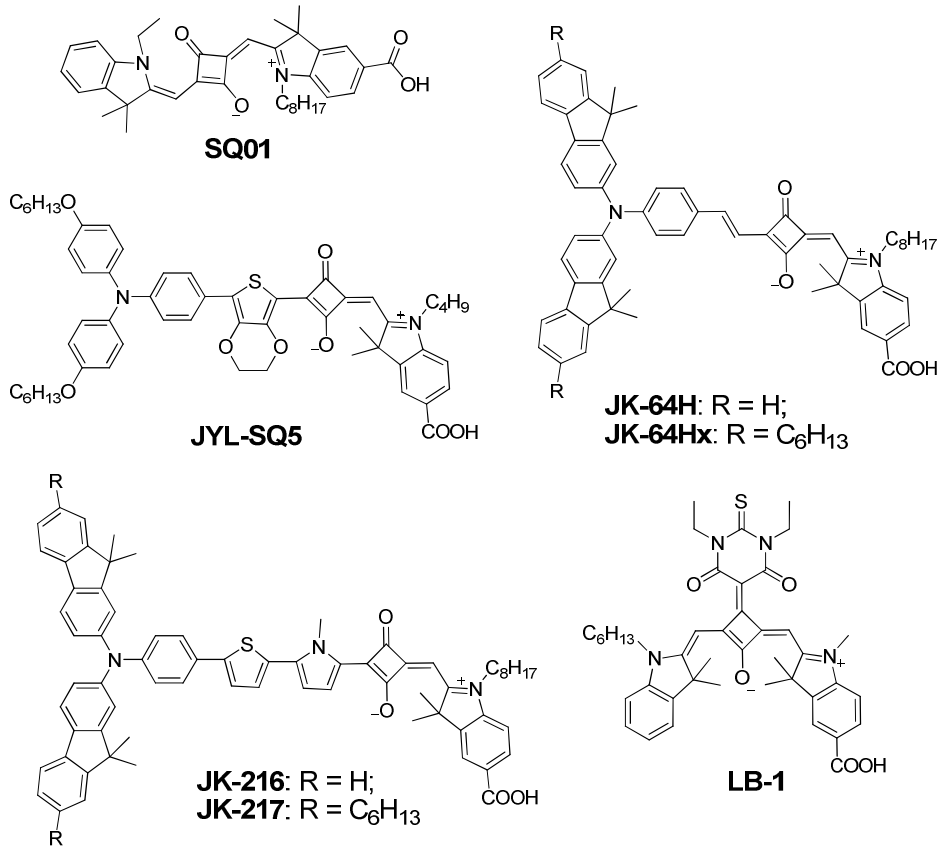

Figure 5.1: Structures of squaraine-based sensitizers.

Recently, **JYL-SQ5** with a promising absorption band centered at 691 nm in ethanol solution, bathochromically shifted compared to the parent squaraine, which possesses a electron rich 3,4-ethylene-dioxythiophene (EDOT) bridge between the di(4-hexoxylphenyl)aminophenyl donor and the squaraine core was reported.[16] Despite its promising light-harvesting ability, only a moderate PEC of 2.61% were obtained in **JYL-SQ5** sensitized device, associated with relatively low V_{OC} of 422 mV, and *FF* of 0.557.

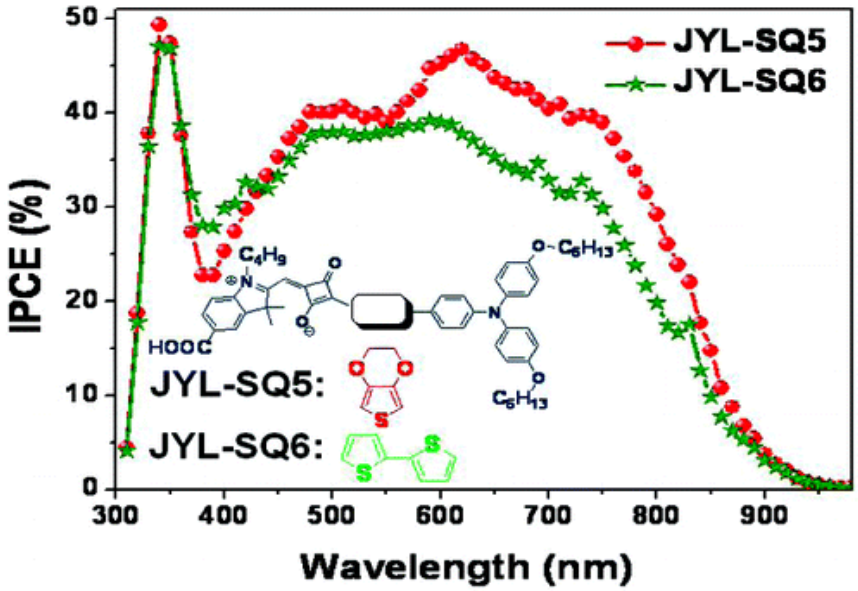

Figure 5.2: IPCE spectra of the devices sensitized by JYL-SQ5 or JYL-SQ6 and a blank device (without dye).[16] Reprinted with permission from ref. 16. Copyright 2010 American Chemical Society.

A core-modified squaraine with diethylthiobarbiturate group (**LB-1** in Figure 5.1) was found to show an additional band at higher energy than the main absorption band and broad IPCE spectra with an efficiency of ca. 4.7%.[18] Although encouragingly panchromatic absorption were observed with these unsymmetrical squaraines as described above, efficiencies were comparable or even lower than that for **SQ1**. A relatively low extinction coefficient (< 1×10^5 $M^{-1}cm^{-1}$) and low *V*oc were revealed compared with the bis(indolinylenemethyl)squaraine **SQ1** (J_{SC} of ca. 10.50 mA cm^{-2}, V_{OC} of ca. 603 mV, and *FF* of ca. 0.71, corresponding to a PCE of 4.5%).[12]

5.2 Motivation and molecule design

As discussed above, the bis(indolinylenemethyl)-based squaraines are promising candidates for DSSC application and there is still room to further increase the PCE. In order to reach higher efficiency, higher J_{SC} and V_{OC} are desired, as PCE is given by the

equation $\eta = J_{sc} \times V_{oc} \times FF$, where J_{SC} is correlated with the light harvesting capability of the sensitizer and the electron injection efficiency, while V_{OC} are more affected by charge injection efficiency and charge recombination degree.[17] Hence, near-IR absorption and significant high-energy absorption to cover more of the solar spectrum are desirable. Efficient charge transfer from the dye to the conduction band of TiO_2 and reduced charge recombination are also crucial points for achieving efficient devices. Moreover, relatively simple synthesis and purification for producing cost-effective materials are highly desirable.

In this chapter, a series of bis(indolinylenemethyl)squaraine-based sensitizers (as shown in Figure 5.3) with various surface anchoring groups and bridges have been synthesized and characterized to examine their solar cell performance in DSSCs. Additional π-bridges, such as ethynyl, phenyl, and thiophenyl were used to examine their role in contributing to higher energy absorption as well as to spatially localize the HOMO of the dye away from the end docking to TiO_2 surface in order to reduce charge recombination. Due to the strong hydrophilic interaction of the carboxylic acid with silica gel, the chromatography purification of carboxylic acid based-sensitizers is generally tedious and inefficient. Some anhydride-based dyes have been proven to successfully sensitize TiO_2 film with reasonable performance in DSSCs,[19,20] and are much more easily purified than corresponding acids. **S1** and **S2** with naphthalic anhydride and phthalic anhydride were designed for this purpose. Furthermore, the cyanoacrylic acid anchor group has been proven to be more efficient in charge injection from the LUMO of the dye to TiO_2 conduction band and reducing the degree of charge recombination degree, which contributes to higher V_{OC}, than carboxylic acid, probably due to the stronger π-electron-

withdrawing ability of -C=C(CN)(COOH) vs. -COOH. **S3** to **S6** with a cyanoarylic acid acceptor and extended conjugation through ethynylaryl, phenyl or thiophenyl have been synthesized to study the role of the bridging group. The structures of these squaraines are listed in Figure 5.3.

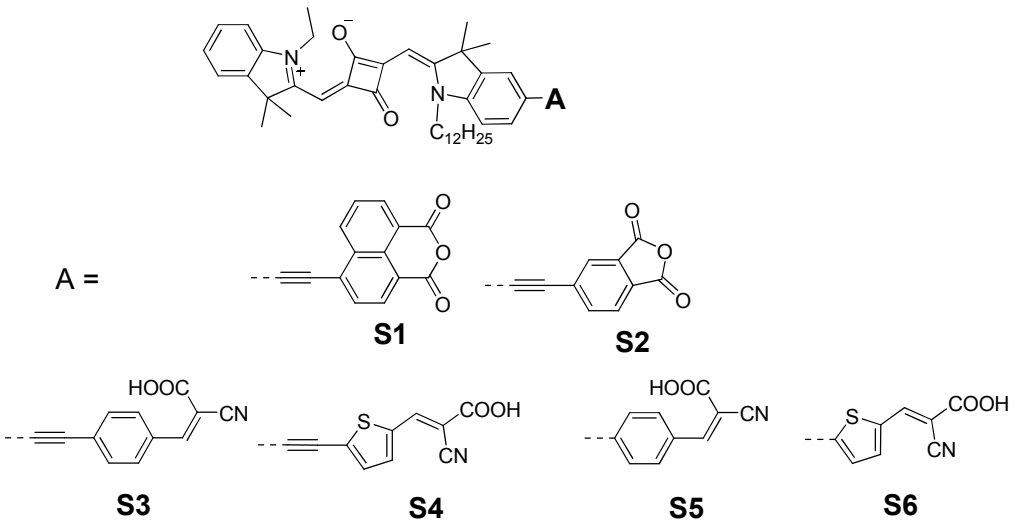

Figure 5.3: Structures of the squaraines for DSSCs

5.3 Synthesis of squaraine-based sensitizers

Extending the conjugation from the squaraine core utilized a Sonogashira coupling reaction[21] for the triple-bond linked anchor groups and a microwave-assisted Suzuki coupling reaction[22] for the non-triple-bond linked anchor groups. The synthetic procedures are illustrated in Scheme 5.1.

S1 and **S2** were obtained through the Sonogashira couplings between squaraine acetylenes (**Sq-CC**), 4-bromo-1,8-naphthalic anhydride and 4-bromo-phthalic anhydride, respectively. The coupling reactions were tried using both **Sq-Br** with arylacetylene and arylbromide with **Sq-CC**, but only worked in the latter case as Sonogashira coupling is more favorable using organic halide with electron-poor substitutes[23] (see Chapter 3 for

detailed synthesis of **Sq-CC** and **Sq-Br**). It was found that oxidative homo-coupling of **Sq-CC** could lead to low yields for the cross-coupling reactions to make the squaraine oligomers as discussed in Chapter 3. However, under copper-free conditions[21] with carefully elimination of oxygen from the reaction flask, the reactions worked well. During the course of phthalic anhydride modified squaraine synthesis, the preliminary results obtained from naphthalic anhydride sensitized solar cell device test revealed the relatively low short-circuit current which might suggest that the anhydride group may not bind sufficiently strongly to allow saturated dye adsorption onto TiO_2, which resulted in a relatively low J_{SC} and PCE. Therefore, the phthalic anhydride was converted to di-acid during column chromatography purification in the presence of acetic acid for better binding on TiO_2. The attempts to obtain pure naphthalic di-acid failed since the naphthalic anhydride is appears to be more stable than the di-acid.[24]

The sensitizers **S3** to **S6**, with cyanoacrylic acid groups, were obtained through straightforward synthetic procedures. The Sonogashira and microwave-assisted Suzuki cross-coupling reaction afforded the corresponding aldehydes in high isolated yield starting from **Sq-CC** and **Sq-Br**. The respective aldehydes were further condensed with cyanoacetic acid to form the sensitizers **S3** to **S6**; the aldehydes with thiophene (**S4** and **S6**) bridges were found to be more reactive than those with phenyl bridges in general. Flash silica gel column chromatography and several size-exclusion columns were utilized to purify the products.

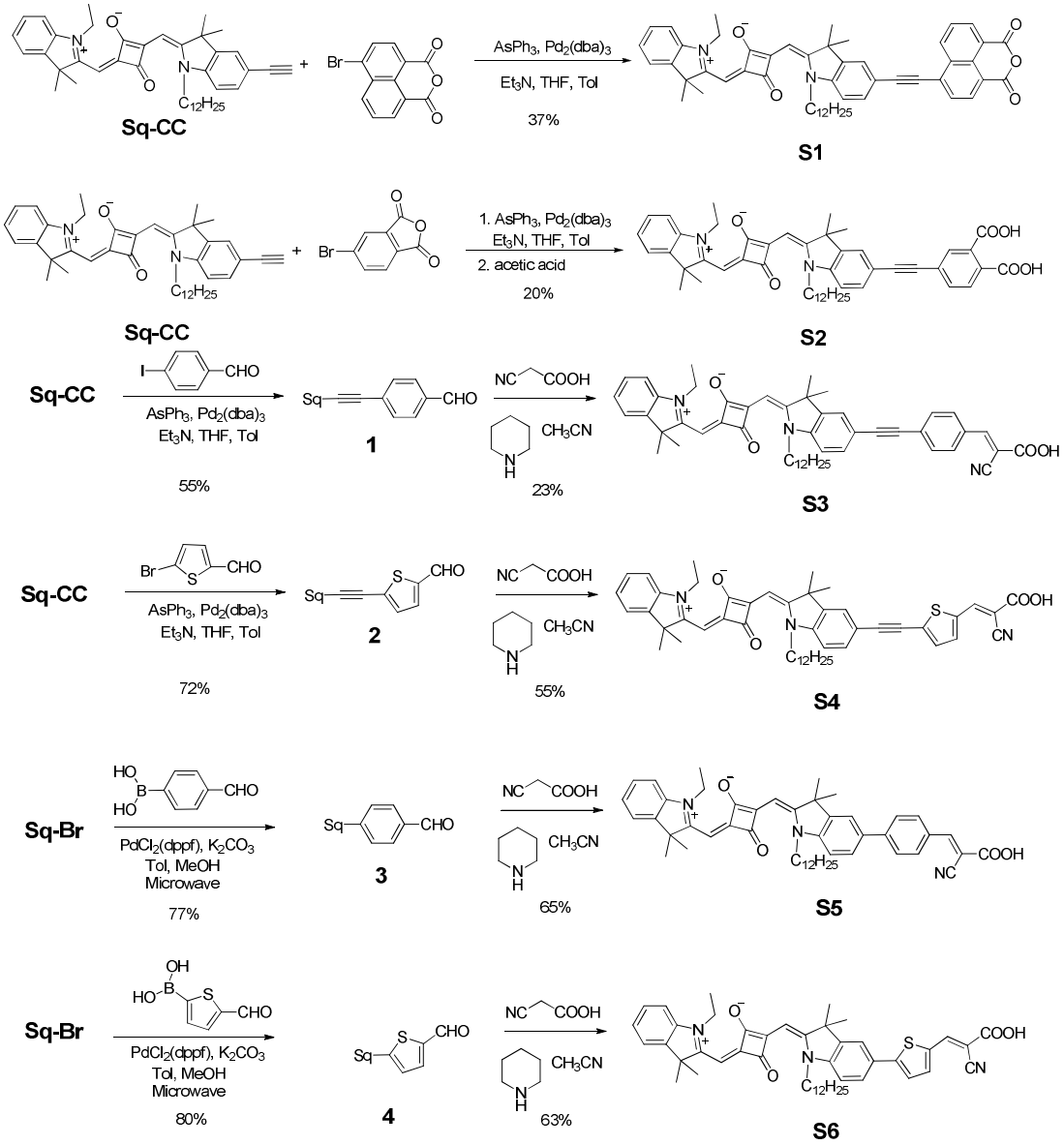

Scheme 5.1: The synthesis of squaraine-based sensitizers.

5.4 Absorption and electrochemistry of squaraine-based sensitizers

The extended conjugation and presence of strong electron withdrawing groups led to significantly bathochromically-shifted absorption in these sensitizers relative to the **Sq** model squaraine (see Chapter 3 for detail), but with similar molar absorptivities. The absorption maxima of the sensitizers are around 653–671 nm (1.85–1.90 eV) in

chloroform as shown in Figure 5.4 with **S6** having the most bathochromically shifted absorption. It is worth noting that, comparing with **Sq**, there are quite noticeable absorption in the high energy region between 300–450 nm with extinction coefficient from 3 000 to 28 000 $M^{-1}cm^{-1}$.

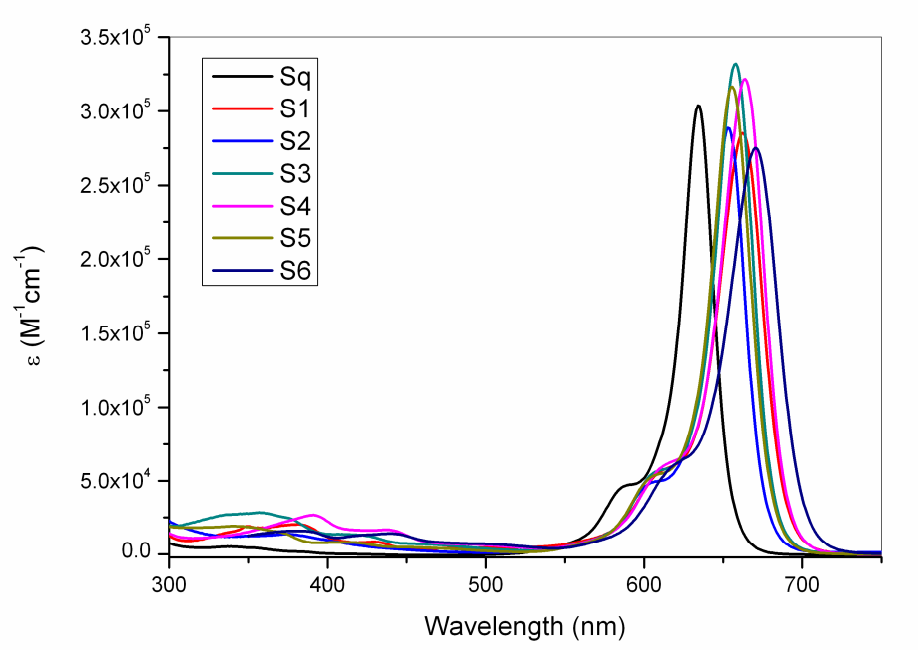

Figure 5.4: Absorption spectra of the new squaraine-based sensitizers and squaraine model compound Sq (structure and synthesis detail see Chapter 3).

The UV-vis.-NIR absorption spectrum of the most bathochromically-shifted example, **S6**, was studied in ethanol which is the solvent used to fabricate the DSSC devices and in order to make fair comparisons with **SQ1**. A moderate hypsochromic shift of the absorption maximum to 659 nm (1.88 eV) and the high peak molar absorptivity of 279 000 M^{-1} cm^{-1} was observed in highly polar ethanol solution. Compared with **SQ1**, which has an absorption maximum at 636 nm (1.95 eV), the 23 nm (0.07 eV) red shift is consistent with the expected effect of extending the conjugation. There is significant absorption of **S6** at shorter wavelengths compared to that of **SQ1**, which shows negligible

absorption in the 350-450 nm range, while the molar absorptivity of **S6** in EtOH varies from 6 000 to 17 000 $M^{-1}cm^{-1}$ in this region. When the dye is adsorbed onto a 2.8 µm nanocrystalline TiO_2 film (performed by Rebecca M. Hill in the Grätzel group), there is a considerable broadening and a splitting of the low-energy peak (maxima at 624 and 663 nm on TiO_2 vs. 659 nm in EtOH), presumably largely due to dye-dye interactions. In addition, the absorption on the high-energy side of the absorption maximum, between 350 nm to 500 nm, is observed.

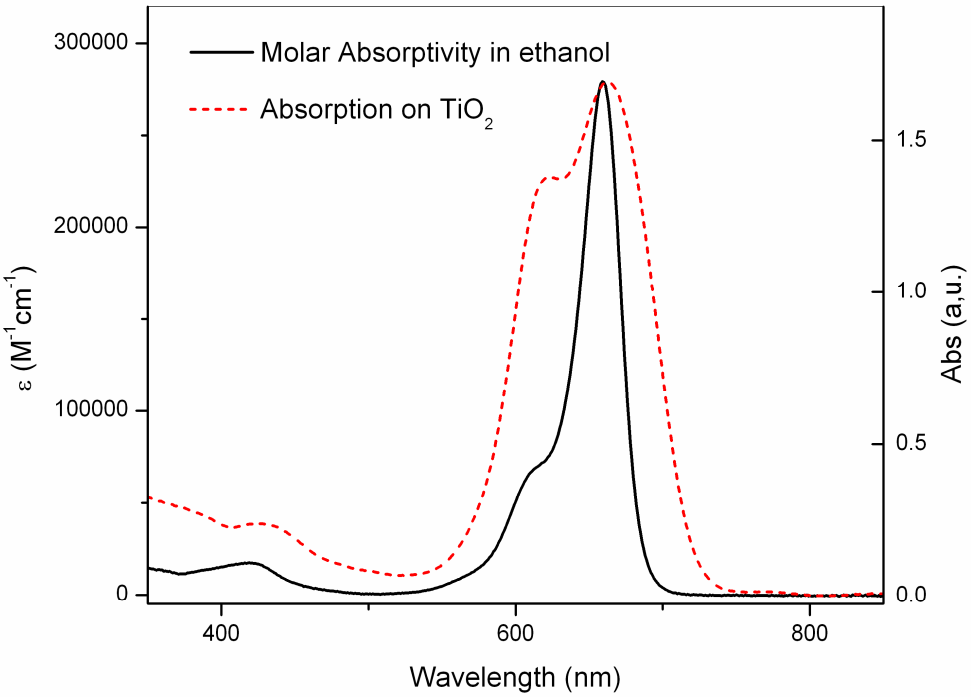

Figure 5.5: Absorption spectra of S6 in ethanol (black solid line) and on a 2.8 µm TiO_2 film (red dotted line) using an identical nanocrystalline TiO_2 film as a baseline. (Measurements performed by Rebecca M. Hill in the Grätzel group)

The electrochemical properties of these sensitizers have been studied by cyclic voltammetry in dichloromethane with a 0.1 M tetra-*n*-butylammonium hexafluorophosphate as the electrolyte. Except the naphthalic anhydride **S1** which showed two reduction peaks within the measurement window, the other sensitizers have

similar reduction and oxidation potential. The extra process observed for **S1**, at reduction potential of ca. –0.98 V vs. NHE,[25,26] could be attributed to the reduction of the naphthalene anhydride moiety. Compared with the squaraine model compounds **Sq**, these sensitizers have slightly lower reduction potentials as the electron withdrawing groups attached. The half-wave potentials corresponding to molecular oxidation and reduction are around +0.8 V and –0.94 V vs. NHE, respectively.[25,26] The redox potential for the electrolyte I_3^-/I^- couple is ca. +0.44 V vs. NHE,[27] so the oxidation potential of these sensitizers are appropriate for regeneration from their radical cations by an I_3^-/I^- electrolyte. In order to have sufficient driving force to efficiently inject electrons into the TiO_2 conduction band, the excited-state oxidation potential of the dye should be at least as reducing as –0.66 V vs. NHE.[25,28] The excited-state energy, $E^{(0,0)}$, for **S1** to **S6** were estimated to be in the range of 1.83–1.76 eV from the absorption spectra in chloroform using the wavelength on the low-energy side of the maxima at which the absorbance is 10% of that at the maxima. The value of $E^{(0,0)}$ indicates that the excited-state oxidation potentials are around –1.0 V vs. NHE, which should be sufficient for electron injection into the conduction band of TiO_2. The optical and electrochemical properties of **S1** to **S6** are summarized in Table 5.1.

Table 5.1: Optical and electrochemical properties of S1 to S6.

Dye	λ_{max} [nm (eV)]	ε_{max} [$M^{-1}cm^{-1}$]	λ_{onset} [nm]	$E(S^+/S)^a$ [V v. NHE]	$E^{(0-0)}$ [V]	$E(S^+/S^*)^a$ [V v. NHE]
S1	662 (1.87)	285 000	692	0.80	1.79	-0.99
S2	653 (1.90)	289 000	679	0.81	1.83	-1.02
S3	658 (1.88)	332 000	684	0.79	1.81	-1.02
S4	664 (1.87)	322 000	692	0.80	1.79	-0.99
S5	656 (1.89)	316 000	683	0.78	1.82	-1.04
S6	671 (1.85)	275,000	703	0.80	1.76	-0.96

[a]estimated using a value of +0.46 V for $FeCp_2^{+/0}$ in CH_2Cl_2 vs. SCE[26] and +0.24 V for SCE vs. NHE[25]

5.5 Photovoltaic performance

The photovoltaic characteristics of **S1** to **S6** sensitized solar cells with standard I_3^- /I^- based liquid electrolyte were investigated by Dr. Jun-Ho Yum in the Grätzel group at École Polytechnique Fédérale de Lausanne in Switzerland. The solar cell performance under standard global AM 1.5 simulated solar conditions, are summarized in Table 5.2. With a double layer of 6 μm thick TiO_2 and 5 μm thick scattering TiO_2 layer, a dye solution of 5×10^{-5} M in ethanol containing 5 mM 3*a*,7*a*-dihydroxy-5*b*-cholic acid (chenodeoxycholic acid, CDCA) were employed. The co-adsorbent CDCA was used to reduce dye aggregation. Devices sensitized by **S1** and **S2** revealed relatively low PCEs at ~1%. There is very little current produced by these dyes, even at the wavelength of the absorption maximum, the IPCE is no more than 20%, compared to the 40-60% IPCE seen in the other dyes (Figure 5.6). The inefficient electron injection into TiO_2 is most likely to be the problem for **S1** and **S2**, in which the anchoring and bridging group may lead to different LUMO electron delocalization. **S3**, **S4**, and **S5** sensitized devices showed moderate PECs with comparable values which have a plateau of over 30% in 550–700 nm regions in the IPCE curves. IPCEs are around 25–30% in the high energy region between 350 nm and 500 nm, which indicates the high energy absorption of these dyes is an important contribution to the photocurrent and there might be strong dye-dye interaction on the TiO_2 films.

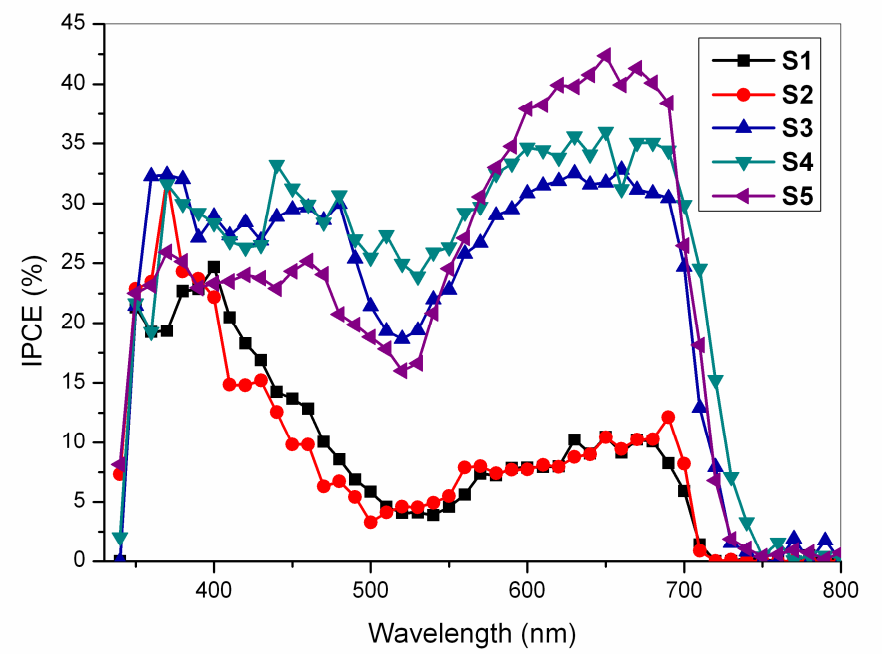

Figure 5.6: IPCEs of a liquid DSSC with an active area of 0.2 cm^2 (mask area) in which a nanocrystalline TiO_2 film, supported on a conducting glass sheet, is derivatized with a monolayer of S1 to S5 in the presence of chenodeoxycholic acid and using the JH34 redox electrolyte (see Experimental Section).

When comparing **S3** with **S5** and **S4** with **S6**, the acetylene linked dyes do not function as well as their counterparts without alkyne linkage, although **S3** and **S5** perform quite similarly in efficiency. The higher IPCE of **S3** than that of **S5** in the range of 350 – 500 nm is consistent with the superior light harvesting ability of **S3** relative to **S5,** as can be seen from their absorption spectra. However, at the wavelengths where the main absorption bands of squaraines reside, significantly higher IPCEs were obtained for **S5** than **S3**, which may be attributed to the more efficient electron injection from **S5**. The alkyne linkage may result in weak electronic coupling between the squaraine core and the anchor group, as it was found in the some mixed-valence systems linked by diarylacetylene vs. diaryl, weaker electronic coupling was observed in the former case.[29,30]

Table 5.2: Photovoltaic characteristics of S1 to S6.

Dye	J_{SC} [mA/cm^2]	V_{OC} [mV]	*FF*	η
S1	2.88	524	0.69	1.0%
S2	2.77	563	0.73	1.1%
S3	7.26	604	0.74	3.3%
S4	8.53	613	0.74	3.8%
S5	7.80	605	0.74	3.5%
S6	14.1	632	0.70	6.2%

Dye **S6**, which has the most bathochromicaly-shifted absorption, stands out of this series with PCE up to 6.21%. This efficiency further increased with optimization using 1 $\times$ 10^{-4} M dye solution in ethanol containing 10 mM CDCA to give a J_{SC} of 14.8 mA/cm^2, V_{OC} of 642 mV, and a fill factor (*FF*) of 0.71, corresponding to an overall PCE, η, of 6.7%. This efficiency stands out among the previously published squaraine-sensitized cells, as does the very broad range over wavelengths over which high IPCE are obtained (Figure 5.7). It is worth noting that its closest rival – the mixed pyrrole / indoline squaraine dye of ref. [15] – only gave a PCE of 6.29% when a much thicker layer of TiO_2 was used; using thicknesses comparable to that used here (6 μm), the PCE was significantly lower (4.48%). The plateau of IPCE is around 60% in the high energy region and close to 70% at the wavelengths around the main absorption band. As seen for a previous sensitizer,[18] the high-energy absorption contributes to the sensitizer's overall photovoltaic performance. Other factors such as aggregation may play a role in the panchromatic response, since when adsorbed onto TiO_2, the dye spectrum is significantly broadened from the solution spectrum. A major factor in the increased overall efficiency might be the red-shifted absorption, although each of these aforementioned factors contributes. The low-energy absorption maximum is at 663 nm for **S6** on TiO_2 and the absorbance at 700 nm is still 40% of that at the maximum, while the absorption

maximum of **SQ1** adsorbed on TiO_2 is at 651 nm, with very little absorption at wavelengths in excess of 700 nm.[12] These differences in absorption spectra account for the distinguishable near-IR response of the corresponding devices. The IPCE curve of DSSCs using **S6** display a measurable response extending to ca. 770 nm, with an IPCE of over 20% seen to wavelengths as long as 740 nm, while for cells using the previous **SQ1** sensitizer an IPCE of below 20% is seen for wavelengths longer than 700 nm.

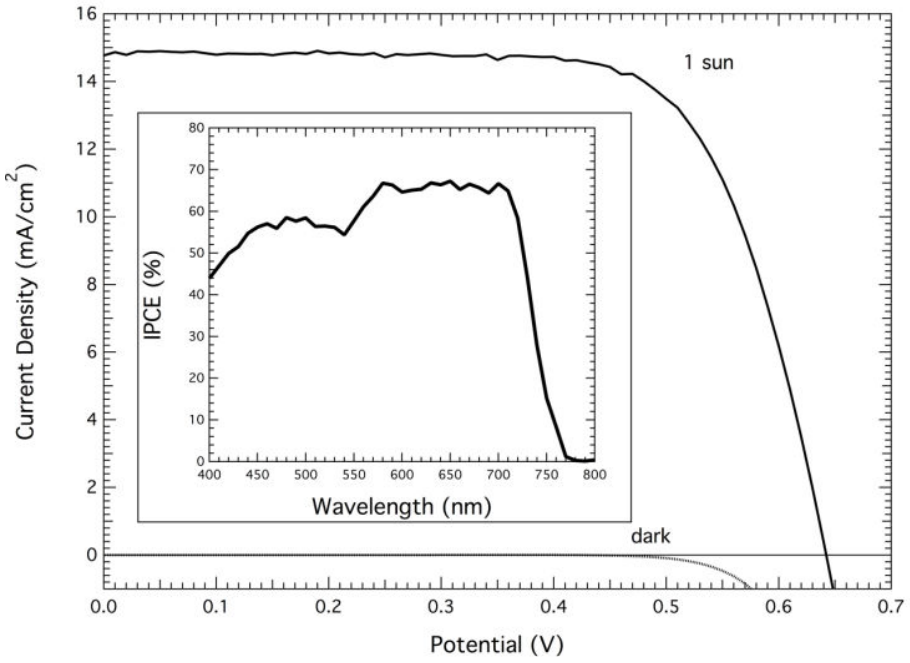

Figure 5.7: Current–voltage characteristics and IPCE (inset) of a liquid DSSC with an active area of 0.2 cm^2 (mask area) in which a nanocrystalline TiO_2 film, supported on a conducting glass sheet, is derivatized with a monolayer of S6 in the presence of chenodeoxycholic acid and using the JH34 redox electrolyte (see Experimental Section). (Figure adapted from Jun-Ho Yum in the Grätzel group)

The solid-state dye-sensitized solar cells (ssDSSC) were investigeated by Amalie Dualeh using **S6** and an organic hole-transport material, 2,2',7,7'-tetrakis-(*N,N*-di-*p*-methoxyphenyl-amino)-9,9'-spiro-bifluorene (spiro-OMeTAD) in place of the liquid electrolyte and a TiO_2 film thickness of 2 µm, a J_{SC} of 6.61 mA/cm^2, lower than in the

liquid cell is observed, with some difference in the IPCE plot. The current-voltage characteristics and IPCE curves are shown in Figure 5.8. Although the J_{SC} of the ssDSSC device was lower, the V_{OC} (706 mV) was higher, as is characteristic for solid-state cells using this hole transport material,[13] and the ssDSSC performed well with an overall efficiency of 2.7% under AM 1.5. This is an improvement upon the current top-performing squaraine-sensitized ssDSSC (2.15% for the dye of ref. [13]). The high performance of the dye can be attributed to the efficient light-harvesting capability as well as the factors discussed for the liquid cells.

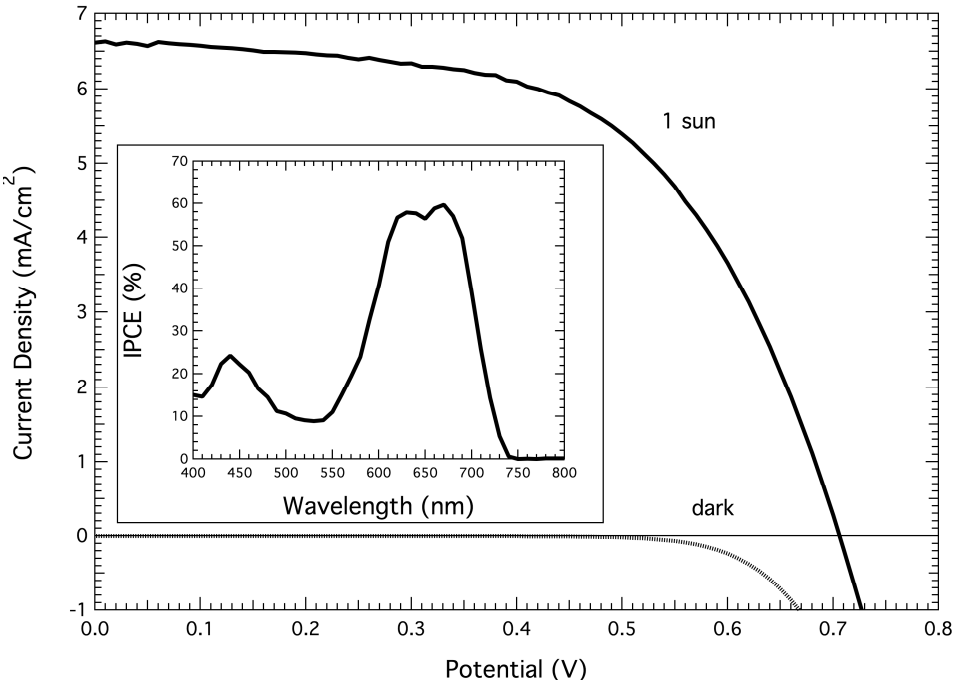

Figure 5.8: Current–voltage characteristics and IPCE spectrum (inset) of a solid-state DSC with an active area of 0.29 cm^2 in which a nanocrystalline TiO_2 film, supported on a conducting glass sheet, is derivatized with a monolayer of S6 and uses a hole-transporting material (see Experimental Section). (Figure adapted from Amalie Dualeh in the Grätzel group)

5.6 Conclusions

In conclusion, the squaraine sensitizers **S1** to **S6** have been investigated in mesoscopic solar cell devices. Bathochromic shift were achieved through extending conjugation from the squaraine core with different bridges. The redox potential and excited-state energy of the dyes are suitable for electron injection from the excited-state of the dyes into TiO_2 conduction band and regeneration of the dyes by I_3^-/I^- electrolyte as estimated from the electrochemistry and optical data. The distinguishable performances utilizing this series of sensitizers reveal their intrinsic differences arising from the anchor groups and conjugation bridges. Among these dyes, **S6** displays an outstanding PCE of 6.7% in liquid DSSCs and 2.7% in ssDSSCs under standard global AM 1.5 solar conditions. The high efficiencies are related to both the red-shifted absorption of **S6** compared to previous squaraine sensitizers, as well as to its high absorptivity (>10 000 $M^{-1}cm^{-1}$ in solution) over much of the visible spectrum and into the near-IR.

This **S6** sensitizer opens up many possibilities for squaraine sensitizer development, where squaraines may be designed with functionalities that lead to both a red-shifted absorption maximum as well as panchromatic absorption for increased solar power conversion efficiency. Promising further avenues to explore these (indolinylenemethyl)squaraine-based sensitizers including three basic approaches:

1. Other π-bridges such as 3-hexylthiophene, 3,4-ethylene-dioxythiophene, dithienopyrrole, dithienosilole are expected not only to bathochromically shift the absorption further into the near-IR region with more extended conjugation but also reduce aggregation between dye molecules. As one can conclude from the device performance of **S6** that with higher concentration of aggregation breaking agents, CDCA,

higher PCE was achieved, which might indicate strong aggregation formed on nanocrystalline TiO_2. The dye aggregates may lead to strong intermolecular quenching of the excited-states of the dyes and lower electron injection efficiency which prevent the dyes to functionally attached to TiO_2 surface thus acting as filters. As a result, lower J_{SC} and consequently poor photovoltaic performance are observed.[4,17,31] The alkyl group incorporated in these donor bridges could reduce aggregation, facilitate the formation of compact sensitizer layers to block the approach of redox couple and reduce charge recombination.[32,33] The new bridges might also increase the hole-electron separation in the dye excited states and to provide additional absorption in the higher energy part for better solar light harvesting as well.

2. Squaraines with benzothiazole, benzoselenazole, quinoline as endgroups were shown to absorb further at longer wavelengths than that of bis(indolinylene)squaraine.[34,35] Replace the indolium unit of **S6** with the more π-donating moieties could push the light harvesting to cover more solar spectrum.

3. Molecular engineering of the unsymmetrical squaraine utilizing triaryl-amine type donor and extending the donor bridge have been proven to be successful achieving panchromatic absorption as already discussed above for ref [14-16]. Modification of the current system through more extended conjugation at the donor end along with bulky substituents may help to tune the redox potential, increase the light harvesting ability over the whole spectrum, and block the electrolyte approaching the semiconductor surface to reduce charge recombination, and thus to give an overall high efficiency.

5.7 Experimental section

General: All the chemicals were purchased from commercial sources and used without further purification, unless otherwise indicated. The synthesis of **Sq-CC** and **Sq-Br** are reported in Chapter 3. Where necessary, THF and toluene were dried using a MBraun solvent purification system. ^{1}H and ^{13}C NMR spectra were collected on a Bruker 400 MHz spectrometer. Mass spectra were measured on a VG Instruments 70-SE using the electron impact (EI) or fast-atom bombardment (FAB) mode and on an Applied Biosystems 4700 Proteomics Analyzer using MALDI mode. Elemental analyses were carried out by Atlantic Microlab using a LECO 932 CHNS elemental analyzer. UV-Vis-NIR absorption spectra were recorded on a Varian Cary 5E spectrophotometer. The absorption spectrum of a film on titania was recorded using an identical nanocrystalline titania film as a baseline. Cyclic voltammetry was performed using a Electrochemical measurements (cyclic voltammetry at 50 mVs^{-1}) were performed using a CH Instruments 620D potentiostat in 0.1 M $^{n}BuNPF_6$ in CH_2Cl_2 using a glassy carbon working electrode, a platinum wire auxillary electrode, and, as a pseudo-reference electrode, a silver wire anodized in 1 M aqueous potassium chloride solution. Bis(pentamethylcyclopentadienyl)-iron(II) was used as an internal reference (-0.55 V vs. ferrocene)

Liquid solar cell fabrication and characterization: A double layer TiO_2 film of 6 μm transparent and 5 μm scattering layers was prepared by screen-printing and treated with a 0.05 M titanium tetrachloride solution as previously reported.[36,37] The films were heated to 500 °C in air for 30 min before use, then dipped in 5×10^{-5} M dye solutions in ethanol containing 5 mM 3*a*,7*a*-dihydroxy-5*b*-cholic acid (chenodeoxycholic acid) for 15 h at room temperature. A quick rinse with acetonitrile was performed before fabrication of the solar cells, which was done using the procedure, testing conditions and equipment

previously reported.[36] The liquid electrolyte consisted of 0.6 M 1,3-dimethylimidazolium iodide, 0.03 M iodine, 0.05 M LiI, 0.05 M guanidinium thiocyanate, and 0.25 M *tert*-butylpyridine in 15/85 (v/v) mixture of valeronitrile and acetonitrile.

Solid-state solar cell fabrication and characterization: The detailed procedure for the fabrication of solid-state cells has been described previously.[36,37] A compact layer of approx. 100 nm TiO_2 was deposited by spray pyrolysis on cleaned fluorine-doped tin oxide (FTO) glass sheets. The substrates were treated with a 20 mM solution of $TiCl_4$ for 6 h at ambient temperature in the dark and sintered at 500 °C for 30 min before and after the deposition of a homemade TiO_2 nanoparticle paste by screen printing to give 2 μm thick layers. The films were heated to 500 °C for 30 min and after cooling to approximately 80 °C were immersed in the dye solution (0.1 mM) for 1 h. The hole transporting material used, 2,2',7,7'-tetrakis-(*N,N*-di-*p*-methoxyphenyl-amino)-9,9'-spiro-bifluorene (spiro- OMeTAD), was dissolved in chlorobenzene to give a concentration of 0.15 M. Solutions of *tert*-butylpyridine (0.12 M) and lithium bis(trifluoromethylsulfonyl)-imide salt (predissolved in acetonitrile) (22.2 mM) were added as additives. 40 μL of spiro-OMeTAD solution was deposited onto the dye-coated substrates and allowed to penetrate for 30 s and subsequently spin coated for 30 s at 2000 rpm. The device fabrication was finished by depositing a 200 nm-thick silver electrode by evaporation.

Synthesis:

S1: **Sq-CC** (182 mg, 0.29 mmol), 4-bromonaphthalic anhydride (245 mg, 0.89 mmol), triphenylarsine (45 mg, 0.15 mmol), and $Pd_2(dba)_3$ (27 mg, 0.030 mmol) were added in anhydrous toluene (10 mL) and THF (3 mL) in a dried round-bottomed flask. Freshly

distilled triethylamine (3 mL) was deoxygenated and added. The mixture was degassed with nitrogen flow for another 15 min. The reaction was stirred at room temperature for 4 h. The crude product was purified by flash silica gel column eluting with dichloromethane/ethyl acetate (5:1 to 3:1) and 1% acetic acid, and then with size-exclusion column (S-X1, Biobeads, THF). The fraction from the column was dried and precipitated from hexane to give **S1** as a blue solid (110 mg, 46%). ^{1}H NMR (400 MHz, $CDCl_3$): δ 8.84 (d, J = 8.4 Hz, 1H), 8.67 (d, J = 7.2 Hz, 1H), 8.57 (d, J = 7.6 Hz, 1H), 7.98 (d, J = 7.6 Hz, 1H), 7.92 (t, J = 8.0 Hz, 1H), 7.60 (m, 2H), 7.33 (m, 2H), 7.19 (t, J = 7.2 Hz, 1H), 7.04 (d, J = 8.0 Hz, 1H), 6.96 (d, J = 8.0 Hz, 1H), 6.03 (s, 1H), 5.97 (s, 1H), 4.11 (m, 2H), 3.92 (m, 2H), 1.83 (s, 6H), 1.79 (s, 6H), 1.41–1.23 (m, 23H), 0.85 (t, J = 7.2 Hz, 3H). ^{13}C{^{1}H} NMR (100 MHz, $CDCl_3$): δ 182.19, 177.88, 171.54, 167.80, 160.48, 160.19, 144.05, 142.66, 142.52, 141.65, 133.96, 133.79, 132.63, 132.50, 131.66, 130.78, 130.35, 129.61, 127.97, 127.82, 125.76, 124.52, 122.47, 119.17, 117.55, 115.82, 109.70, 109.10 ,101.61, 87.60, 87.01, 86.11, 49.82, 48.61, 43.71, 38.77, 31.89, 29.68, 29.58, 29.51, 29.48, 29.37, 29.31, 27.32, 27.08, 26.99, 26.79, 22.67, 14.10, 12.14. HRMS (EI) Calcd. for $C_{54}H_{56}N_2O_5$ (M^+): 812.4189. Found: 812.4207. Anal. Calcd. for $C_{54}H_{56}N_2O_5 \cdot 2H_2O$: C, 76.39; H, 7.12; N, 3.30. Found: C, 76.39; H, 7.08; N, 3.11.

S2: **Sq-CC** (180 mg, 0.29 mmol), 4-bromophthalic anhydride (199 mg, 0.88 mmol), triphenylarsine (45 mg, 0.15 mmol), and $Pd_2(dba)_3$ (26 mg, 0.029 mmol) were added in anhydrous toluene (15 mL) and THF (5 mL) in a dried round-bottomed flask. Freshly distilled triethylamine (5 mL) was deoxygenated and added. The mixture was degassed with nitrogen flow for another 15 min. The reaction was stirred at room temperature for 2 h. The crude product was purified by flash silica gel column with ethyl acetate and acetic

acid, and then with size-exclusion column (S-X1, Biobeads, THF). The fraction from the column was dried and precipitated from hexane to give **S2** as a blue solid (28 mg (12%). ^{1}H NMR (400 MHz, $CDCl_3$): δ 8.03 (s, 1H), 7.87 (m, 1H), 7.55 (m, 1H), 7.43–7.30 (m, 4H), 7.15 (m, 1H), 6.99 (d, J = 7.6 Hz, 1H), 6.86 (d, J = 8.0 Hz, 1H), 6.06 (s, 1H), 5.93 (s, 1H), 4.10 (m, 2H), 3.90 (m, 2H), 1.74 (m, 12H), 1.41–1.23 (m, 23H), 0.82 (t, J = 7.2 Hz, 3H) (CO_2H resonance not observed). ^{13}C{^{1}H} NMR (100 MHz, $CDCl_3$): δ 171.08, 168.98, 142.89, 142.46, 141.68, 133.15, 132.03, 127.89, 125.50, 124.31, 122.35, 117.21, 109.64, 109.30, 92.73, 88.29, 87.24, 86.92, 49.61, 48.80, 43.78, 40.78, 38.73, 31.87, 29.67, 29.57, 29.52, 29.47, 29.37, 29.30, 27.06, 26.73, 22.65, 14.10, 12.08. (Eighteen aromatic and one aliphatic peaks missing probably due to overlap of near coincidental resonances. Also, the solubility of the compound is not very good, which gave rise to weak signals.) HRMS (MALDI) Calcd. for $C_{50}H_{56}N_2O_6$ (M^+): 780.4138. Found: 780.3988. Anal. Calcd. for $C_{50}H_{56}N_2O_6$•$3H_2O$: C, 71.92; H, 7.48; N, 3.35. Found: C, 71.62; H, 7.49; N, 3.05.

1: **Sq-CC** (200 mg, 0.325 mmol), 4-iodobenzaldehyde (376 mg, 1.62 mmol), triphenylarsine (49.6 mg, 0.162 mmol), and $Pd_2(dba)_3$ (29.8 mg, 0.0325 mmol) were added in anhydrous toluene (15 mL) and THF (5 mL) in a dried round-bottomed flask. Freshly distilled triethylamine (5 mL) was deoxygenated and added. The mixture was degassed with nitrogen flow for another 15 min. The reaction was stirred at room temperature for 4 h. The crude product was purified by silica gel column with dichloromethane and methanol and then with size-exclusion column (S-X1, Biobeads, THF). The fraction from the column was dried and precipitated from hexane to give **1** as a blue solid (150 mg, 66%). ^{1}H NMR (400 MHz, $CDCl_3$): δ 10.00 (s, 1H), 7.85 (d, J = 8.0

Hz, 2H), 7.65 (d, J = 8.0 Hz, 2H), 7.48 (m, 2H), 7.33 (m, 2H), 7.17 (t, J = 7.2 Hz, 1H), 7.01 (d, J = 8.0 Hz, 1H), 6.91 (d, J = 8.8 Hz, 1H), 5.99 (s, 1H), 5.94 (s, 1H), 4.09 (m, 2H), 3.91 (m, 2H), 1.78 (m, 12H), 1.41–1.23 (m, 23H), 0.85 (t, J = 7.2 Hz, 3H). $^{13}C\{^{1}H\}$ NMR (100 MHz, $CDCl_3$): δ 191.35, 182.28, 181.64, 178.62, 170.94, 168.43, 143.24, 142.46, 141.78, 135.27, 131.92, 129.76, 129.62, 127.90, 125.67, 124.24, 122.44, 116.88, 109.50, 109.04, 93.98, 88.72, 87.35, 86.78, 49.67, 48.77, 43.76, 38.65, 31.90, 29.59, 29.50, 29.32, 27.23, 27.08, 27.01, 26.87, 22.68, 14.10, 12.11 (Two aromatic and three aliphatic peaks missing probably due to overlap of near coincidental resonances). HRMS (EI) Calcd. for $C_{49}H_{56}N_2O_3$ (M^+): 720.4291. Found: 720.4280. Anal. Calcd. for $C_{49}H_{56}N_2O_3$: C, 81.63; H, 7.83; N, 3.89. Found: C, 81.52; H, 7.84; N, 3.98

S3: 1 (80 mg, 0.11 mmol) and cyanoacetic acid (19 mg, 0.22 mmol) were added to a dried round-bottomed flask with condenser, which was then evacuated and filled with nitrogen 3 times. Anhydrous acetonitrile (8 mL) was added to dissolve the reactants. The reaction mixture was heated to reflux for 4 h after the addition of piperidine (20 μL). The solvent was evaporated and the residue was passed through a pad of silica gel with dichloromethane and methanol (15:1). The crude product was dissolved in chloroform and washed with acetic acid aqueous solution and then water. The organic layer was dried over Na_2SO_4 and the solvent was removed. The residue was purified by size-exclusion column (S-X1, Biobeads, THF). The blue green fraction from the column was dried and precipitated from hexane to give **S3** as a blue solid (20 mg, 23%). ^{1}H NMR (400 MHz, $CDCl_3$): δ 8.25 (s, 1H), 7.98 (d, J = 8.0 Hz, 2H), 7.61 (d, J = 8.0 Hz, 2H), 7.49 (m, 2H), 7.37 (m, 2H), 7.18 (t, J = 7.2 Hz, 1H), 7.03 (d, J = 7.6 Hz, 1H), 6.93 (d, J = 9.2 Hz, 1H), 6.05 (s, 1H), 5.97 (s, 1H), 4.13 (m, 2H), 3.97 (m, 2H), 1.78 (m, 12H), 1.43–

1.22 (m, 23H), 0.85 (t, J = 6.8 Hz, 3H) (CO_2H resonance not observed). $^{13}C\{^1H\}$ NMR (100 MHz, $CDCl_3$): δ 182.80, 178.13, 175.23, 171.56, 169.19, 164.22, 153.52, 143.13, 142.55, 141.65, 132.02, 130.97, 128.28, 127.98, 125.66, 124.51, 122.43, 117.20, 116.21, 109.76, 109.35, 94.07, 89.12, 87.34, 87.05, 49.74, 48.88, 43.84, 38.90, 31.90, 29.59, 29.53, 29.50, 29.39, 29.32, 27.11, 27.04, 26.71, 22.68, 14.12, 12.15 (Four aromatic and two aliphatic peaks missing probably due to overlap of near coincidental resonances). HRMS (MALDI) Calcd. for $C_{52}H_{57}N_3O_4$ (M^+): 787.4349; Found: 787.4263. Anal. Calcd. for $C_{52}H_{57}N_3O_4 \bullet 1.5H_2O$: C, 76.63; H, 7.42; N, 5.16. Found: C, 76.25; H, 7.41; N, 4.84.

2: **Sq-CC** (330 mg, 0.53 mmol), 5-bromothiophene-2-carbaldehyde (307 mg, 1.61 mmol), triphenylarsine (82 mg, 0.27 mmol), and $Pd_2(dba)_3$ (45 mg, 0.05 mmol) were added in anhydrous toluene (15 mL) and THF (5 mL) in a dried round-bottomed flask. Freshly distilled triethylamine (5 mL) was deoxygenated and added. The mixture was degassed with nitrogen flow for another 15 min. The reaction was stirred at 60 °C for 2.5 h. The crude product was purified by silica gel column with dichloromethane and ethyl acetate (2:1 first, then 1:1) and then with size-exclusion column (S-X1, Biobeads, THF). The fraction from the column was dried and precipitated from hexane to give **2** as a green solid (280 mg, 71%). ^1H NMR (400 MHz, $CDCl_3$): δ 9.85 (s, 1H), 7.65 (d, J = 4.0 Hz, 1H), 7.46 (m, 2H), 7.36 (m, 1H), 7.32 (m, 2H), 7.17 (t, J = 7.2 Hz, 1H), 7.02 (d, J = 8.0 Hz, 1H), 6.90 (d, J = 8.8 Hz, 1H), 6.00 (s, 1H), 5.94 (s, 1H), 4.10 (m, 2H), 3.91 (m, 2H), 1.78 (m, 12H), 1.41–1.23 (m, 23H), 0.85 (t, J = 7.2 Hz, 3H). $^{13}C\{^1H\}$ NMR (100 MHz, $CDCl_3$): δ 182.33, 181.83, 178.35, 171.10, 168.14, 143.59, 143.53, 142.45, 141.71, 136.16, 133.17, 132.16, 131.97, 127.91, 125.47, 124.31, 122.44, 116.06, 109.55, 109.03, 87.42, 86.83, 82.15, 49.70, 48.67, 43.70, 38.68, 31.89, 29.58, 29.51, 29.48, 29.35, 29.31,

27.21, 27.06, 26.97, 26.82, 22.67, 14.12, 12.12 (Three aromatic and one aliphatic peaks missing probably due to overlap of near coincidental resonances). HRMS (MALDI) Calcd. for $C_{47}H_{54}N_2O_3S$ (M^+): 726.3855; Found: 726.3747. Anal. Calcd. for $C_{47}H_{54}N_2O_3S$: C, 77.65; H, 7.49; N, 3.85. Found: C, 77.46; H, 7.71; N, 3.92.

S4: **2** (150 mg, 0.21 mmol) and cyanoacetic acid (35 mg, 0.42 mmol) were added to a dried round-bottomed flask with condenser, which was then evacuated and filled with nitrogen 3 times. Anhydrous acetonitrile (10 mL) was added to dissolve the reactants. The reaction mixture was heated to reflux for 5 h after the addition of piperidine (30 μL). The solvent was evaporated and the residue was passed through a pad of silica gel with ethyl acetate first and then with dichloromethane and methanol (6:1). The solvent was removed and the residue was dissolved in chloroform and washed with dilute HCl aqueous solution and water. The organic layer was dried over Na_2SO_4 and removed solvent to give S4 as a blue solid (90 mg, 55%). ^{1}H NMR (400 MHz, $CDCl_3$): δ 8.31 (s, 1H), 7.68 (d, J = 4.0 Hz, 1H), 7.47 (m, 2H), 7.36 (m, 3H), 7.19 (t, J = 7.2 Hz, 1H), 7.05 (d, J = 7.6 Hz, 1H), 6.94 (d, J = 8.8 Hz, 1H), 6.08 (s, 1H), 5.99 (s, 1H), 4.15 (m, 2H), 3.98 (m, 2H), 1.78 (m, 12H), 1.43–1.21 (m, 23H), 0.84 (t, J = 6.8 Hz, 3H) (CO_2H resonance not observed). ^{13}C{^{1}H} NMR (100 MHz, $CDCl_3$): δ 178.57, 175.15, 171.75, 168.85, 164.38, 145.76, 143.51, 142.59, 141.62, 137.22, 136.54, 132.86, 132.11, 132.02, 127.99, 125.46, 124.58, 122.44, 116.45, 116.38, 109.82, 109.39, 100.12, 99.71, 87.49, 87.17, 82.51, 49.80, 48.78, 43.84, 38.95, 31.90, 29.60, 29.54, 29.51, 29.41, 29.33, 27.13, 27.05, 26.69, 22.68, 14.13, 12.18 (Two aromatic and two aliphatic peaks missing probably due to overlap of near coincidental resonances). HRMS (MALDI) Calcd. for

$C_{50}H_{55}N_3O_4S$ (M^+): 793.3913; Found: 793.3731. Anal. Calcd. for $C_{50}H_{55}N_3O_4S$•1.5H_2O: C, 73.14; H, 7.12; N, 5.12. Found: C, 73.37; H, 6.91; N, 5.08.

3:[22] **Sq-Br** (100 mg, 0.15 mmol) and 4-formylphenylboronic acid (67.5 mg, 0.45 mmol), $PdCl_2$(dppf) (12 mg, 0.015 mmol), and potassium carbonate (103 mg, 0.75 mmol) were added to a dried microwave tube. It was flushed with nitrogen in a glove box for 30 min and, under nitrogen, toluene (2 mL) and methanol (2 mL) were added and the tube was capped. The microwave reactor (CEM, Discover) was set to standard mode: T = 70 °C, Power = 60 watt, hold time = 30 min. Three batches of the reaction mixture were combined and passed through a pad of silica gel with dichloromethane and ethyl acetate. The crude product was purified by size-exclusion column (S-X1, Biobeads, THF) and precipitated from hexane to give **3** as a green solid (240 mg, 77%). ^{1}H NMR (400 MHz, $CDCl_3$): δ 10.04 (s, 1H), 7.94 (d, J = 8.0 Hz, 2H), 7.74 (d, J = 8.0 Hz, 2H), 7.57 (m, 2H), 7.33 (m, 2H), 7.16 (t, J = 7.2 Hz, 1H), 7.01 (m, 2H), 5.98 (s, 1H), 5.97 (s, 1H), 4.08 (m, 2H), 3.97 (m, 2H), 1.80 (m, 12H), 1.41–1.23 (m, 23H), 0.85 (t, J = 7.2 Hz, 3H). ^{13}C{^{1}H} NMR (100 MHz, $CDCl_3$): δ 191.79, 182.34, 180.83, 178.84, 170.48, 169.02, 146.71, 143.13, 142.37, 141.84, 135.00, 134.96, 130.38, 127.87, 127.32, 127.20, 124.05, 122.41, 121.17, 109.54, 109.36, 87.14, 86.58, 49.54, 49.10, 43.82, 38.56, 31.90, 29.59, 29.53, 29.48, 29.38, 29.32, 27.27, 27.09, 27.05, 26.90, 22.67, 14.11, 12.07 (One aromatic and one aliphatic peaks missing probably due to overlap of near coincidental resonances). HRMS (EI) Calcd. for $C_{47}H_{56}N_2O_3$ (M^+): 696.4291; Found: 696.4288. Anal. Calcd. for $C_{47}H_{56}N_2O_3$•H_2O: C, 78.95; H, 8.18; N, 3.92. Found: C, 79.23; H, 7.92; N, 3.87.

S5: **3** (150 mg, 0.22 mmol) and cyanoacetic acid (55 mg, 0.65 mmol) were added to a dried round-bottomed flask with condenser, which was then evacuated and filled with

nitrogen 3 times. Anhydrous acetonitrile (15 mL) was added to dissolve the reactants. The reaction mixture was heated to reflux for 4 h after the addition of piperidine (40 μL). The solvent was removed and the residue was passed through a pad of silica gel with ethyl acetate first and then with dichloromethane and methanol (6:1). The solvent was evaporated and the residue was dissolved in chloroform and washed with dilute HCl aqueous solution and water. The organic layer was dried over Na_2SO_4 and removed solvent to give **S5** as a blue solid (107 mg. 65%). ^{1}H NMR (400 MHz, $CDCl_3$): δ 8.33 (s, 1H), 8.09 (d, J = 8.0 Hz, 2H), 7.72 (d, J = 8.0 Hz, 2H), 7.59 (m, 2H), 7.34 (m, 2H), 7.17 (t, J = 7.2 Hz, 1H), 7.04 (m, 2H), 6.07 (s, 1H), 6.03 (s, 1H), 4.13 (m, 2H), 4.06 (m, 2H), 1.80 (m, 12H), 1.43–1.22 (m, 23H), 0.83 (t, J = 6.8 Hz, 3H) (CO_2H resonance not observed). ^{13}C{^{1}H} NMR (100 MHz, $CDCl_3$): δ 183.03, 177.02, 175.07, 171.23, 169.86, 164.37, 153.98, 145.10, 143.21, 143.05, 142.51, 141.71, 135.06, 131.73, 130.44, 127.93, 127.73, 127.32, 127.11, 124.34, 122.38, 120.95, 116.36, 109.93, 109.65, 103.32, 87.21, 86.87, 49.63, 49.21, 43.95, 38.84, 31.86, 29.57, 29.56, 29.52, 29.47, 29.40, 29.28, 27.14, 27.04, 26.74, 22.68, 14.07, 12.10 (One aliphatic peak missing probably due to overlap of near coincidental resonances). HRMS (MALDI) Calcd. for $C_{50}H_{57}N_3O_4$ (M^+): 763.4349; Found: 763.4315. Anal. Calcd. for $C_{50}H_{57}N_3O_4$•0.5H_2O: C, 77.69; H, 7.56; N, 5.44. Found: C, 77.55; H, 7.65; N, 5.41.

4:[22] **Sq-Br** (100 mg, 0.15 mmol) and 5-formylthiophen-2-ylboronic acid (70 mg, 0.45 mmol), $PdCl_2$(dppf)·CH_2Cl_2 (12 mg, 0.015 mmol), and potassium carbonate (103 mg, 0.75 mmol) were added to a dried microwave tube. It was flushed with nitrogen in a glove box for 30 min and, under nitrogen, toluene (2 mL) and methanol (2 mL) were added and the tube was capped. The microwave reactor (CEM, Discover) was set to

standard mode: T = 70 °C, Power = 60 watt, hold time = 15 min. Three batches of the reaction mixture were combined and passed through a pad of silica gel with dichloromethane and ethyl acetate. The crude product was purified by size-exclusion column (S-X1, Biobeads, THF) and precipitated from hexane to give **4** as a green solid (250 mg, 80%). ^{1}H NMR (400 MHz, $CDCl_3$): δ 9.86 (s, 1H), 7.72 (d, J = 4.0 Hz, 1H), 7.58 (m, 2H), 7.36 (m, 2H), 7.31 (t, J = 7.2 Hz, 1H), 7.16 (t, J = 7.2 Hz, 1H), 7.01 (d, J = 8.0 Hz, 1H), 6.95 (d, J = 8.0 Hz, 1H), 6.00 (s, 1H), 5.95 (s, 1H), 4.09 (m, 2H), 3.92 (m, 2H), 1.80 (m, 12H), 1.41–1.23 (m, 23H), 0.85 (t, J = 7.2 Hz, 3H). ^{13}C{^{1}H} NMR (100 MHz, $CDCl_3$): δ 182.57, 182.26, 181.48, 178.33, 170.94, 168.23, 154.22, 143.79, 143.15, 142.41, 141.77, 141.72, 137.60, 128.22, 127.89, 126.53, 124.24, 123.44, 122.41, 120.17, 109.50, 87.37, 86.76, 49.64, 48.82, 43.74, 38.64, 31.87, 29.56, 29.50, 29.45, 29.34, 29.29, 27.25, 27.05, 26.99, 26.81, 22.65, 14.10, 12.10 (One aromatic and one aliphatic peaks missing probably due to overlap of near coincidental resonances). HRMS (EI) Calcd. for $C_{45}H_{54}N_2O_3S$ (M^+): 702.3855; Found: 702.3850. Anal. Calcd. for $C_{45}H_{54}N_2O_3S{\bullet}H_2O$: C, 74.96; H, 7.83; N, 3.89. Found: C, 75.20; H, 7.60; N, 3.81.

S6: Formylthiophenyl squaraine (130 mg, 0.18 mmol) and cyanoacetic acid (32 mg, 0.37 mmol) were added to a dried round-bottomed flask with condenser, which was then evacuated and filled with nitrogen 3 times. Anhydrous acetonitrile (10 mL) was added to dissolve the reactants. The reaction mixture was heated to reflux for 4 h after the addition of piperidine (20 μL). The solvent was removed and the residue was passed through size-exclusion column (S-X1, Biobeads, THF). The crude product, obtained from the major fraction, was dissolved in dichloromethane and washed with aqueous acetic acid and water. The organic layer was dried over Na_2SO_4 and removed the solvent to give **S6** as a

blue solid (90 mg, 63%). ^{1}H NMR (400 MHz, $CDCl_3$): δ 8.33 (s, 1H), 7.69 (d, J = 2.8 Hz, 1H), 7.62 (d, J = 6.4 Hz, 1H), 7.58 (m, 1H), 7.36 (m, 2H), 7.31 (t, J = 6.4 Hz, 1H), 7.18 (t, J = 6.0 Hz, 1H), 7.03 (d, J = 6.4 Hz, 1H), 6.95 (d, J = 6.8 Hz, 1H), 6.04 (s, 1H), 5.97 (s, 1H), 4.13 (m, 2H), 3.96 (m, 2H), 1.79 (m, 12H), 1.43–1.22 (m, 23H), 0.84 (t, J = 6.4 Hz, 3H) (CO_2H resonance not observed). $^{13}C\{^{1}H\}$ NMR (100 MHz, $CDCl_3$): δ 182.77, 178.77, 175.51, 171.59, 168.82, 164.90, 154.24, 146.49, 143.92, 143.23, 142.57, 141.66, 139.06, 134.60, 128.18, 127.97, 126.74, 124.51, 123.77, 122.43, 120.15, 116.67, 109.77, 98.29, 87.49, 87.11, 49.77, 48.96, 43.89, 38.92, 31.88, 29.59, 29.54, 29.50, 29.41, 29.31, 27.22, 27.09, 27.05, 26.72, 22.66, 14.10, 12.18 (One aromatic and one aliphatic peaks missing probably due to overlap of near coincidental resonances). HRMS (MALDI) Calcd. for $C_{48}H_{55}N_3O_4S$ (M^+): 769.3913; Found: 769.3920. Anal. Calcd. for $C_{48}H_{55}N_3O_4S \bullet H_2O$: C, 73.16; H, 7.29; N, 5.33. Found: C, 72.82; H, 7.11; N, 5.15.

5.8 References

(1) O'Regan, B.; Grätzel, M. *Nature* **1991**, *353*, 737.
(2) Grätzel, M. *Curr. Opin. Colloid Interface Sci.* **1999**, *4*, 314.
(3) Grätzel, M. *J. Photochem. Photobiol. C: Photochem. Rev.* **2003**, *4*, 145.
(4) Grätzel, M. *Acc. Chem. Res.* **2009**, *42*, 1788.
(5) Hagfeldt, A.; Boschloo, G.; Sun, L.; Kloo, L.; Pettersson, H. *Chem. Rev.* **2010**, *110*, 6595.
(6) Zeng, W.; Cao, Y.; Bai, Y.; Wang, Y.; Shi, Y.; Zhang, M.; Wang, F.; Pan, C.; Wang, P. *Chem. Mater.* **2010**, *22*, 1915.
(7) Cao, Y.; Bai, Y.; Yu, Q.; Cheng, Y.; Liu, S.; Shi, D.; Gao, F.; Wang, P. *J. Phys. Chem. C* **2009**, *113*, 6290.
(8) Chiba, Y.; Islam, A.; Wanatabe, Y.; Komiya, R.; Koide, N.; Han, L. *Jpn. J. Appl. Phys.* **2006**, *45*, 638.
(9) Beverina, L.; Salice, P. *Eur. J. Org. Chem.* **2010**, 1207.
(10) Sreejith, S.; Carol, P.; Chithra, P.; Ajayaghosh, A. *J. Mater. Chem.* **2008**, *18*, 264.
(11) Ajayaghosh, A. *Acc. Chem. Res.* **2005**, *38*, 449.

(12) Yum, J.-H.; Walter, P.; Huber, S.; Rentsch, D.; Geiger, T.; Nüesch, F.; Angelis, F. D.; Grätzel, M.; Nazeeruddin, M. K. *J. Am. Chem. Soc.* **2007**, *129*, 10320.

(13) Geiger, T.; Kuster, S.; Yum, J.-H.; Moon, S.-J.; Nazeeruddin, M. K.; Grätzel, M.; Nüesch, F. *Adv. Funct. Mater.* **2009**, *19*, 2720.

(14) Choi, H.; Kim, J.-J.; Song, K.; Ko, J.; Nazeeruddin, M. K.; Grätzel, M. *J. Mater. Chem.* **2010**, *20*, 3280.

(15) Paek, S.; Choi, H.; Kim, C.; Cho, N.; So, S.; Song, K.; Nazeeruddin, M. K.; Ko, J. *Chem. Commun.* **2011**, *ASAP*.

(16) Li, J.-Y.; Chen, C.-Y.; Lee, C.-P.; Chen, S.-C.; Lin, T.-H.; Tsai, H.-H.; Ho, K.-C.; Wu, C.-G. *Org. Lett.* **2010**, *12*, 5454.

(17) Ning, Z.; Fu, Y.; Tian, H. *Energy Environ. Sci.* **2010**, *3*, 1170.

(18) Beverina, L.; Ruffo, R.; Mari, C. M.; Pagani, G. A.; Sassi, M.; Angelis, F. D.; Fantacci, S.; Yum, J.-H.; Grätzel, M.; Nazeeruddin, M. K. *ChemSusChem* **2009**, *2*, 621.

(19) Westlund, R.; Glimsdal, E.; Lindgren, M.; Vestberg, R.; Hawker, C.; Lopesd, C.; Malmström, E. *J. Mater. Chem.* **2008**, *18*, 166.

(20) Li, C.; Liu, Z.; Schöoneboom, J.; Eickemeyer, F.; Pschirer, N. G.; Erk, P.; Herrmann, A.; Müllen, K. *J. Mater. Chem.* **2009**, *19*, 5405.

(21) Ljungdahl, T.; Pettersson, K.; Albinsson, B.; Mårtensson, J. *J. Org. Chem* **2006**, *71*, 1677.

(22) Moon, S.-J.; Yum, J.-H.; Humphry-Baker, R.; Karlsson, K. M.; Hagberg, D. P.; Marinado, T.; Hagfeldt, A.; Sun, L.; Grätzel, M.; Nazeeruddin, M. K. *J. Phys. Chem. C* **2009**, *38*, 16816.

(23) Chinchilla, R.; Nájera, C. *Chem. Rev.* **2007**, *107*, 874.

(24) Barros, T. C.; Yunes, S.; Menegon, G.; Nome, F.; Chaimovich, H.; Politi, M. J.; Dias, L. G.; Cuccovia, I. M. *J. Chem. Soc., Perkin Trans. 2* **2001**, 2342.

(25) *Handbook of Physics and Chemistry*; 63rd ed.; CRC Press: Boca Raton, FL, 1982.

(26) Connelly, N. G.; Geiger, W. E. *Chem. Rev.* **1996**, *96*, 877.

(27) Hagfeldt, A.; Grätzel, M. *Chem. Rev.* **1995**, *95*, 49.

(28) Nazeeruddin, M. K.; Grätzel, M. *Encyclopedia of Electrochemistry: Semiconductor Electrodes and Photoelectrochemistry*; Wieley-VCH: Germany, 2002.

(29) Sutton, J. E.; Taube, H. *Inorg. Chem.* **1981**, *20*, 3125.

(30) Lambert, C.; Nöll, G. *J. Am. Chem. Soc.* **1999**, *121*, 8434.

(31) Mishra, A.; Fischer, M. K. R.; Bäuerle, P. *Angew. Chem. Int. Ed.* **2009**, *48*, 2474.

(32) Miyashita, M.; Sunahara, K.; Nishikawa, T.; Uemura, Y.; Koumura, N.; Hara, K.; Mori, A.; Abe, T.; Suzuki, E.; Mori, S. *J. Am. Chem. Soc.* **2008**, *130*, 17874.

(33) Koumura, N.; Wang, Z.-S.; Mori, S.; Miyashita, M.; Suzuki, E.; Hara, K. *J. Am. Chem. Soc.* **2006**, *128*, 14256.

(34) Sprenger, H. E.; Ziegenbein, W. *Angew. Chem. Int. Ed.* **1967**, *6*, 553.

(35) Terpetschnig, E.; Lakowicz, J. R. *Dyes and Pigments* **1993**, *21*, 227.

(36) Nazeeruddin, M. K.; De Angelis, F.; Fantacci, S.; Selloni, A.; Viscardi, G.; Liska, P.; Ito, S.; Takeru, B.; Grätzel, M. *J. Am. Chem. Soc.* **2005**, *127*, 16835.

(37) Snaith, H. J.; Humphry-Baker, R.; Chen, P.; Cesar, I.; Zakeeruddin, S. M.; Grätzel, M. *Nanotechnology* **2008**, *19*, 424003.

Chapter 6: Conclusions and Outlook

6.1 Conclusions and outlook

This dissertation described the synthesis and characterization of new squaraine-based materials and their applications in non-linear optics and organic electronics. Chapter 1 provided an overview on the synthesis and the optical and electrochemical properties of squaraine-based materials and their applications in two-photon absorption (2PA), bulk-heterojuction organic photovoltaics (OPVs), dye-sensitized solar cells (DSSC), and some other related research fields. In Chapter 2, the main goal was to develop squaraines with extended π-conjugation for high 2PA efficiency in the near-infrared (IR) region, and 2PA related applications, particularly for optical-power limiting (OPL) in solution and films. Chapter 3 described oligomer approaches to enhance 2PA: the synthesis and properties of squaraine dimers with various linkages, a trimer, and a hexamer. Chapter 4 discussed the synthesis and photophysical properties of phthalocyanine- and squaraine-containing metal complexes and using the squaraine-platinum triad and polymer as light-harvesting donors for organic solar cells. Chapter 5 focused on developing squaraine sensitizers with various anchor groups and π-bridges for DSSCs.

The first research part of this thesis, including Chapters 2 and 3, was concerned with developing π-conjugated squaraines to achieve high 2PA efficiency. In Chapter 2, a series of π-extended bis(donor)-substituted squaraines have been synthesized,

characterized, and investigated on their photophysical properties. Thiophene and pyrrole moieties with branched alkyl chains were incorporated into the bridge with diaryl or dialkyl amino-donors to tune the absorption spectra and the film forming properties of the squaraines. With extended conjugation, these squaraines were found to absorb into the near-IR region with large transition dipole moments between the ground state and the first electronic excited-state. The 2PA behavior of **Sq1-4** was investigated using two-photon induced fluorescence (TPIF) and z-scan techniques. Large 2PA cross-sections (δ) with peak performance at around 920 nm and δ_{max} over 50 000 GM (1 GM = 10^{-50} cm^4 s $photon^{-1}$) for **Sq1**, and δ_{max} over 30 000 GM at around 1100 nm for **Sq2-4** were revealed. It is worth noting that the 2PA spectra of **Sq3** and **Sq4** cover a broad range in the near-IR (1000–1400 nm) with δ over 10 000 GM. A four-fold power suppression of nanosecond pulses at 850 nm using **Sq1** toluene solution was observed and a suppression of more than 10 times of 1550 nm femtosecond pulses was achieved using **Sq2** neat films and toluene solutions. The nonlinear transmittance measurements along with the strong transient signal of **Sq2** suggested excited-state absorption (ESA) is contributing to the OPL response at 1550 nm. **G2Sq1**, a dendronized version of **Sq1**, has also been synthesized by incorporating a Fréchet type polyether dendron into the pyrrole moieties. Smoother and higher optical quality films were achieved using **G2Sq1** with narrower solid-state absorption and a larger transparency window in the near-IR than seen for **Sq1**.

Chapter 3 focused on extending conjugation of bis(indolinylenemethyl)-based squaraines by forming oligomers through different linkages at the 5- position of indoline. The linear absorption spectra of the dimers and trimer significantly bathochromically shift in comparison to the monomeric model compound **Sq**. Considerably enhanced 2PA

into the higher two-photon allowed electronic excited-state was revealed by TPIF and z-scan of the dimers. The electrochemistry of the oligomers remain similar to that of **Sq**, but organic solar cell devices using these squaraines as donors, blended with the soluble fullerene derivative PCBM, showed significant improvement from **Sq** to dimers and **6-Sq**, which could be attributed to improved absorption of solar spectrum by the oligomers, formation of smoother films by the oligomers, and the possible morphology difference in devices active layer.

Future research for such π-extended squaraine could include studies of the following.

1) Optical-power limiting properties at multiple wavelengths in near-IR region using **Sq3** and **Sq4** by utilizing their large 2PA cross-sections over a broad spectrum range and strong excited-state absorption to achieve wide-band optical limiters. The high quality optical films formed by **G2Sq1** may allow realizing its practical applications in thick films on sensor protectors.

2) Exploring the high 2PA efficiency in the near-IR region of these squaraines along with the good film forming properties for other 2PA induced applications such as all optical switching induced by non-degenerate 2PA loss upon applying a control beam to the optical fibers.

3) Improving the electronic coupling between squaraine oligomers or polymers by linking the monomeric unit through more conjugated moieties and stronger electronic coupling site. The possible structures are illustrated in Figure 6.1

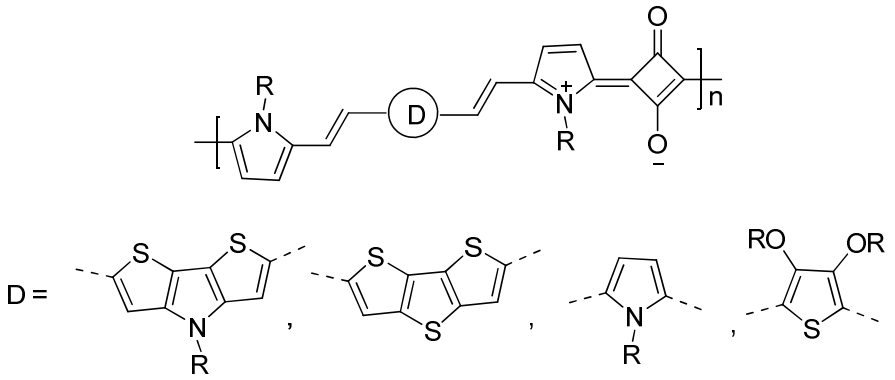

Figure 6.1: Proposed structures of squaraine oligomers and polymers.

Chapter 4 extended the study for OPL incorporating heavy atoms into squaraine and phthalocyanine (Pc) architectures to examine the impact on the triplet quantum yield. The fluorescence quantum yield of **Pc-Pt-Pc** triad is less than 0.1%; however, the triplet quantum yield of this compound was determined to be 0.5, which is almost identical with the monomeric zinc phthalocyanine, indicating only minor Pt contributions to the Pc frontier orbitals. Among these platinum- and gold-containing squaraines, triplet-state absorption was only observed in the case of **Sq-Pt-Sq** triad with triplet quantum yield of ca. 0.1. No triplet-state signal and surprisingly high fluorescence quantum yields were recorded for the monomeric squaraine-platinum or gold complexes. The photovoltaic performances of the **[Sq-Pt]$_n$** polymer and **Sq-Pt-Sq** reveal significant improvements compared with the corresponding metal-free dimers which could be attributed to the better mediation of charge transport and possible morphology change in the presence of platinum.

Future directions for research on squaraine heavy-atom(s) containing materials could include the following.

1) The singlet oxygen generation quantum yield was shown to significantly increase of bis(benzoselenazole)-based squaraine than that of the bis(benzothiazole) and bis(indoline)-based squaraine,[1,2] indicating considerably more rapid intersystem crossing in this class of squaraines. Integration of heavy atom(s) directly into the π-conjugation of squaraines may allow the π-electron of the conjugation backbone strongly mixed with the heavy-atom(s) orbitals which could enhance the heavy-atom facilitated intersystem crossing. Such an approach can include introducing bromine and iodine atoms as substituents of the aromatic rings or by condensation with heavy-atom-rich moieties to form conjugated systems. These possible designs could include the structures shown in Figure 6.1 with the "D" as heavy-atom rich moieties.

2) Extending the conjugation through condensation at the squarylium core with heavy-atom rich moieties or the ligands to heavy metal may allow the tuning of the excited-state energy and make the intersystem crossing more rapidly.

The last part of this thesis, Chapter 5, explored the use of bis(indolinylenemethyl)squaraine-based sensitizers with various anchor groups and linkages for DSSCs. Naphthalic anhydride, dicarboxylic acid, and cyanoacrylic acid surface docking groups were linked to the squaraine core through ethynyl, phenyl or thiophenyl π-bridges. Bathochromic shifts and significant high energy absorption were observed in these sensitizers, compared with the squaraine model compound **Sq**. **S6,** incorporating more extended conjugation beyond the squaraine core through a slightly electron-rich thiophene ring along with the more strongly π-accepting carboxycyanovinyl

group, gave the champion cell performance among these dyes. Its power conversion efficiencies (PCEs) of up to 6.74% in liquid cells and 2.69% in solid-state DSSCs stand out of previous published squaraine-sensitized cells. It was worth noting that high incident-photon-to-current efficiencies (IPCE) covering very broad range wavelengths are obtained indicating that the high solar cell efficiencies based on **S6** are not only attributable to its intense absorption in the near-IR region, but also to the panchromatic response over the whole visible spectrum.

Further research on squaraine-based sensitizers could include the following.

1) The absorption spectra of the squaraine sensitizers could be bathochromically shifted by using approaches such as replacing indoline by benzothiazole, benzoselenazole, and quinoline[3,4] or utilizing longer conjugation bridge with long branched alkyl substituents which could also help to reduce aggregation.
2) The high-energy region absorption could be increased by incorporating fused ring π-bridges or modifying the "donor" part by using a triaryl amine-type donor with extended conjugation, in which the bulky substituents of the triaryl amine may provide blocking effect to prevent the electrolytes approaching the semiconductor surface, thus reducing charge recombination.

The possible design of structures is shown in Figure 6.2.

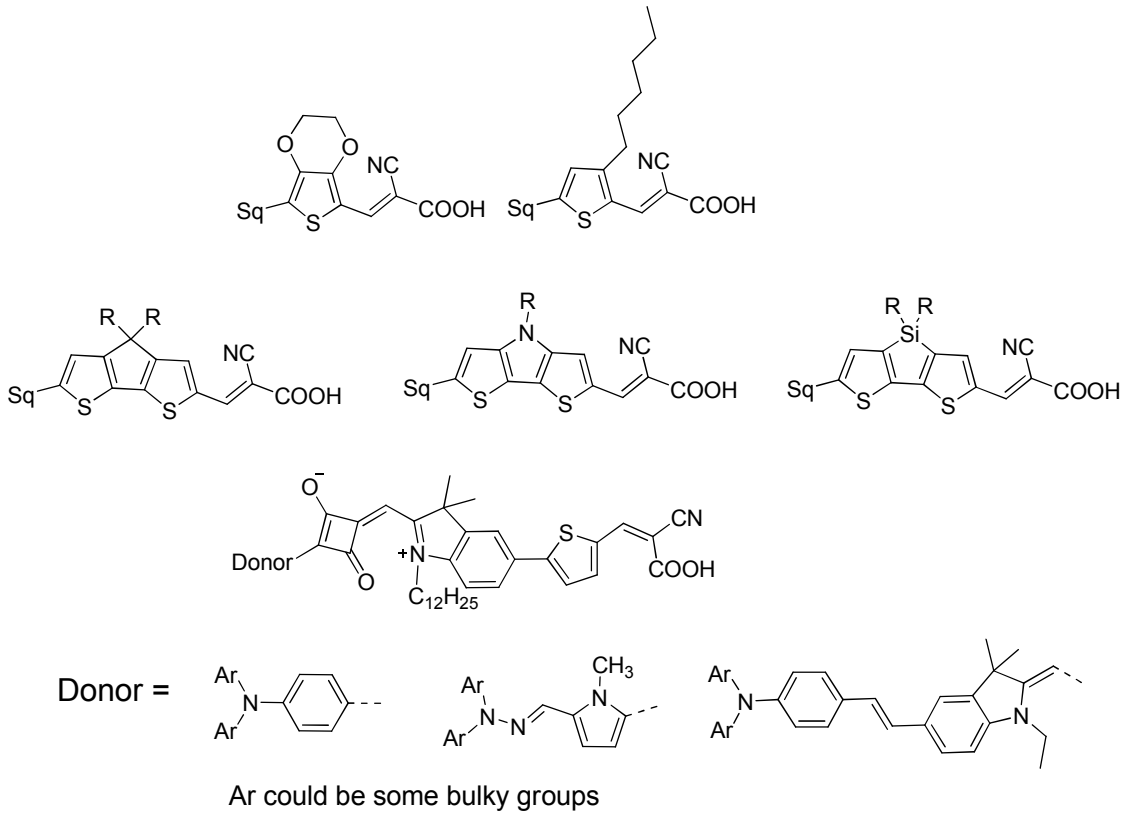

Figure 6.2: Possible structures for new squaraine sensitizers.

In conclusion, this thesis provided insight into structure-property relationships in squaraine materials and their use in optical-power limiting and solar cells. From what has been observed, π-extended squaraines are promising candidates possessing very large 2PA cross-sections that can be future investigated for other 2PA-induced processes. Although the squaraine-metal complexes approach might not be successful for OPL and high efficient donor in OPV, the studies could offer guide research in designing other heavy-atom containing system and organometallic materials for solar cells. The combination of possible squaraine excited triplet-state absorption in the visible spectrum and strong 2PA in the near-IR may allow achieving wide-band OPL utilizing different mechanisms. Moreover, the use of a π-bridge and a more accepting cyanoacrylic acid

anchor group significantly increase the solar-cell performance in squaraine-based sensitizers which opens up many possibilities for squaraine sensitizer development, including incorporation of other donor and acceptor moieties on the indoline termini to increase the hole-electron separation in the excited-state and to provide additional absorption in the high energy part of the spectrum to increase solar power-conversion efficiency.

6.2 References

(1) Santos, P. F.; Reis, L. V.; Almeida, P.; Serrano, J. P.; Oliveira, A. S.; Vieira Ferreira, L. F. *J. Photochem. Photobiol., A* **2004**, *163*, 267.

(2) Santos, P. F.; Reis, L. V.; Duarte, I.; Serrano, J. P.; Almeida, P.; Oliveira, A. S.; Ferreira, L. F. V. *HeIv. Chim. Acta* **2005**, *88*, 1135.

(3) Sprenger, H. E.; Ziegenbein, W. *Angew. Chem. Int. Ed.* **1967**, *6*, 553.

(4) Terpetschnig, E.; Lakowicz, J. R. *Dyes and Pigments* **1993**, *21*, 227.